UNIVERSITÀ
DEGLI STUDI
DI PADOVA

Sede Amministrativa: Università degli Studi di Padova

Dipartimento di Scienze Chimiche

CORSO DI DOTTORATO DI RICERCA IN: Scienze Molecolari
CURRICOLO: Scienze Farmaceutiche
CICLO: XXX

DEVELOPMENT OF MULTIFUNCTIONAL ANTICANCER AGENTS: DESIGN, SYNTHESIS AND EVALUATION OF HYBRID COMPOUNDS CONTAINING KINASE INHIBITOR MOIETIES

Tesi redatta con il contributo finanziario della Fondazione Cariparo

Coordinatore: Ch.mo Prof. Leonard Prins
Supervisore: Ch.mo Prof. Giovanni Marzaro
Co-Supervisore: Ch.mo Prof. Diego Montagner

Dottoranda: Martina Dalla Via

INDEX

FIGURES

SCHEMES

TABLES

ABBREVIATIONS

Abl	*Abelson* kinase
ACN	Acetonitrile
Arg	Arginine
Asp	Aspartate
ATP	Adenosine triphosphate
BCR	Breakpoint cluster region gene
Boc_2O	Di-*tert*-butyl-dicarbonate
BOP	(Benzotriazol-1-yloxy)tris(dimethylamino)phosphonium hexafluorophosphate
BP	Hydrophobic binding pocket
c-KIT	Mast/stem cell growth factor receptor
CML	Chronic Myeloid Leukemia
CSF1R	Colony stimulating factor 1 receptor
DMF	Dimethylformamide
DMF-DMA	Dimethylformamide dimethyl acetal
DMSO	Dimethyl sulfoxide
DNA	Deoxyribonucleic Acid
EGF	Epidermal growth factor
EGFR	Epidermal growth factor receptor
EtOH	Ethanol
FGFR	Fibroblast growth factor receptor
FLT3	Fms-like tyrosine kinase 3
Gly	Glycine

HAT	Histone acetyl transferase
HDAC	Histone deacetylases
HDACI	Histone deacetylases inhibitor
HEPES	4-(2-hydroxyethyl)-1-piperazineethanesulfonic acid
HGFR	Hepatocyte growth factor receptor
His	Histidine
HSC	Hematological stem cell
IGFR	Insulin like growth factor receptor
KOtBu	Potassium *tert*-butoxide
MAPK	Mitogen activated protein kinase
MeOH	Methanol
MW	Microwave
NMP	*N*-methyl-2-pyrrolidone
NMR	Nuclear Magnetic Resonance
NRTK	Non-receptor tyrosine kinase
Phe	Phenilalanine
PKC	Protein kinase C
PKs	Protein kinases
PDGFR	Platelet-derived growth factor receptor
RET	Rearranged during transfection receptor
ROS	Radical oxygen species
RT	Room temperature
RTK	Receptor Tyrosine Kinase
SAHA	Suberoyl anilide of hydroxamic acid
SAR	Structure activity relationship

Ser	Serine
SH2	Src homology 2
SH3	Src homology 3
SOD	Superoxide dismutase
STK	Serine-threonine kinase
TEA	Triethylamine
TFA	Trifluoroacetic acid
THF	Tetrahydrofuran
TK	Tyrosine kinase
TKI	Tyrosine kinase inhibitor
TPP	Triphenylphosphine
Tyr	Tyrosine
VEGFR	Vascular endothelial growth factor receptor
d	Doublet
dd	Doublet of doublets
ddd	Doublet of doublet of doublets
dt	Doublet of triplets
m	Multiplet
s	Singlet
t	Triplet
td	Triplet od doublets
q	Quartet

1. ABSTRACT

Cancer is a complex and a multiple-genes involved disease; for this reason it can not be treated or cured with a single drug modulating the biological function of a single target. The innovation related to multi-targeted drugs, combining the activity of different cancer progression relevant targets, became a burgeoning research topic. Drugs that act on multiple targets can enhance efficacy and reduce chemo-resistance that causes disease relapse and metastasis and remains the main obstacle to cancer therapy. One of the main target nowadays are tyrosine kinases (TKs); since most protein kinases stimulate cell growth and proliferation, cell survival and migration, they can, if overexpressed, amplified or constitutively active, assume oncogenic properties. Other ideal biological targets are enzymes as histone deacetylases (HDAC) and mitochondrial functions. Herein we present the development and the preliminary evaluation of new Abl/HDAC inhibitors bearing the pyrido-pyrimidine main scaffold; the functionalization of the most active compounds with metal ions (*i.e.* Zn^{2+}, Cu^{2+} and Fe^{3+}); the development of novel multi-kinase inhibitors bearing the 4-anilinopyrimidine scaffold; the development of novel cKIT/^{wt}RET/^{V804M}RET inhibitors bearing the 4-anilinopyridine scaffold. Besides, the development of multi-kinase inhibitors endowed with antifibrotic properties as well as novel topoisomerase inhibitors are reported.

The structures of the novel still unpublished compounds are reported in Figure 1.

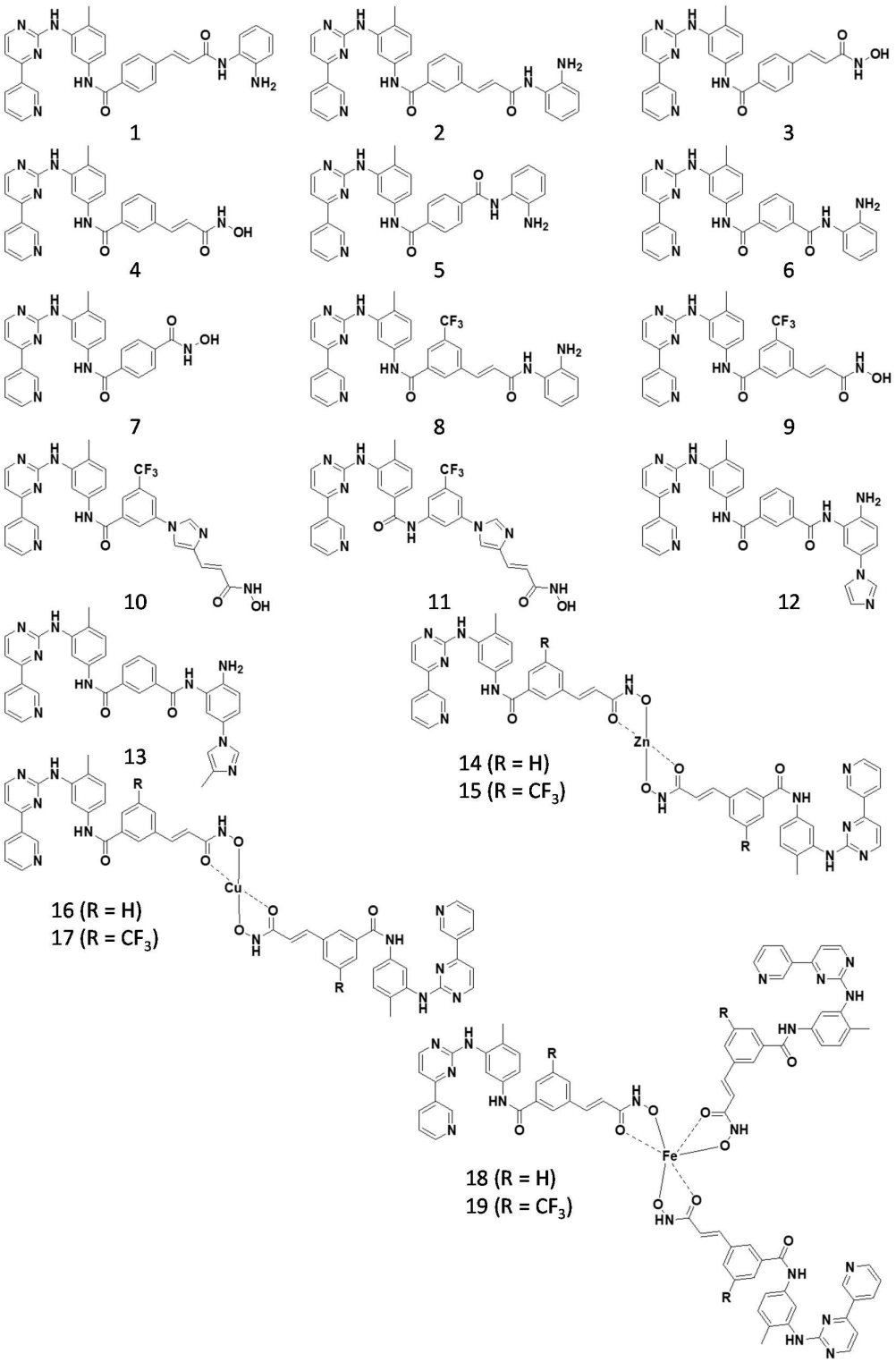

Figure 1. *Structures of potential dual TK/HDAC inhibitors.*

2. INTRODUCTION

The anti-cancer drugs research is constantly moving from the study of drugs with a nonspecific mechanism of action to the so called targeted therapy. This novel approach relies on inhibiting specific biomolecules fundamental for cancer growth and for the maintenance of an adequate microenvironment for cell hyper-proliferation.[1] Hence, most drugs have emerged from the current 'one molecule - one target - one disease' philosophy, and it will undoubtedly remain dominant in medicinal chemistry research for many years to come.[2]

The aim of this strategy is to discover small molecules that are able to modulate the biological function of a single target that is fully responsible for a disease in order to reduce the risk of related side effects (off- target effects). However, the evidences that drugs designed to act on single molecular targets are usually insufficient for multigene diseases such as cancer are constantly increasing. Recent findings have highlighted the importance of a multi-target approach: the simultaneous blockade of different pathways involved in the cancer growth leads to a more effective therapy over the mono-therapies, with reduced drug resistance phenomena onset.[3]

Multi-target therapeutics can be achieved through two different strategies, the combination of single targeted drugs or the administration of a multi-targeted agent.

The co-administration of two or more drugs to target cancer-inducing or cell-sustaining pathways is a fundamental principle of cancer therapy; certain cancers have been effectively treated with such combinatorial approach.[4] Tyrosine kinases (TK) and the histone deacetylases (HDACs) are among the most interesting targets. Indeed, the co-administration of a TKI and of an HDACI is largely more effective than the administration of the single drug.[5,6]

Nevertheless, the co-administration of multiple agents is often limited by drug-drug interactions and dose limiting toxicities.

2.1 MULTIFUNCTIONAL ANTICANCER AGENTS

The multi-target approach can be pursued also through a single agent endowed with multiple potency, *i.e.* a single compound able to simultaneously modulate the biological function of multiple targets. The multifunctional agent shows many advantages:

- The avoidance of different bioavailabilities, pharmacokinetics and metabolism of each component within the combination regimen;
- The lack of possible drug-drug interactions;
- The dosing regimen would be greatly simplified to enhance compliance and therapeutic efficacy;
- The cost of a single agent could be less than two separate agents;
- The administration of multi-target compounds leads to higher potency and lower side effects compared to the action of a mono-targeted agent but also then the co-administration of different target-selective agents.[7]

Positive clinical and preclinical data suggest that the multi-targeted agents are a burgeoning approach of treatments in cancer therapy.[8,9]

However, the molecular basis of the enhanced potency for dual inhibitors is far to be fully investigated.

2.2 PROTEIN KINASES

Protein kinases (PKs) are among the most investigated targets for cancer therapy, since they play a predominant regulatory role in almost every aspect of cell biology. PKs control metabolism, transcription, cell division and movement, programmed cell death and participate in the immune response and nervous system function.[10]

This class of enzymes regulates all the cellular events by transferring the γ-phosphate group of ATP to the target protein substrate that usually contain a tyrosine, a serine or a threonine residue.[11]

Protein phosphorylation involves the balanced action of protein kinases and phosphoprotein phosphatases, making phosphorylation-dephosphorylation an overall reversible process. The protein kinase family is about the second largest enzyme family and the fifth largest gene family in humans. It was revealed by chromosomal mapping that nearly half of protein kinase genes are involved in typical genetic alteration in cancer. Considering that cancer develops through the alteration of multiple genes, gene amplification is an effective acceleration machinery to promote tumorigenesis.[12] This result further emphasizes the importance of protein kinase inhibitors as potential drug targets.

The human kinome comprises 518 members, grouped in families, subfamilies, and classes, according to structural and functional similarities. Based on the phosphorylated amino acid residue PKs can be classify in two main classes: tyrosine kinases (TKs) and serine-threonine kinases (STKs).[13]

Protein kinases typically share a conserved arrangement of secondary structure elements that are arranged into 12 subdomains that fold into a bilobed catalytic core structure with ATP binding in a deep cleft located between the lobes (Figure 2).

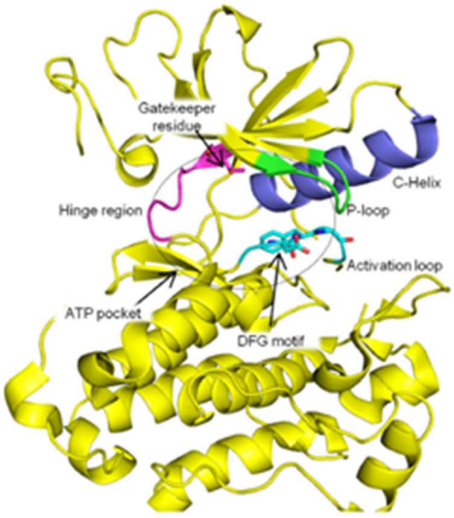

Figure 2. *Main elements in kinase structure.*

The catalytic cleft is between the N-terminal lobe (N-lobe) and a larger C-terminal lobe. The N-lobe mainly consists of 5 β-strands, which form the upper limit of the cleft, and one α-helix; differently, the C-lobe is mainly constituted of α-helixes. As shown in figure 3 the two lobes are connected with a linker including a hinge region and a convex-shaped motif (E_0). The N-lobe contains a highly flexible glycine-rich loop (G-loop) that can adopt various conformations, depending on the conformational state of the PK and on the presence of a ligand.[14]

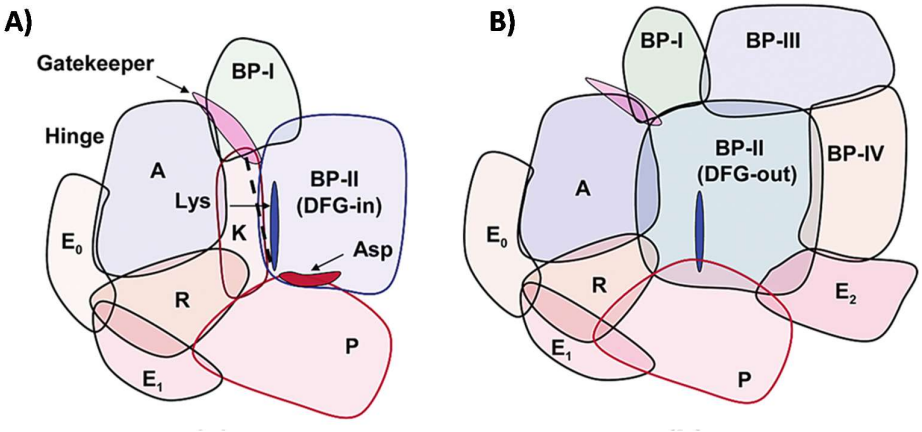

Figure 3*. Topological distribution of the binding pockets in the catalytic cleft with (A) a DFG-in conformation and (B) a DFG-out conformation.*

The catalytic cleft consists of two regions: the front cleft and the back cleft. The front cleft contains predominantly the ATP-binding site and the back cleft comprises elements important for the kinase catalysis regulation. These two regions share the N-terminus of the activation segment (A-segment) including the DFG (Asp-Phe-Gly) motif and are divided by a gatekeeper residue. The gatekeeper controls the access of small molecules into the back cleft: a small amino acid (threonine or alanine) at this position allows the back cleft to be accessible; a bulky gatekeeper (phenylalanine, leucine, or methionine) blocks the entry.

The A-segment in the C-lobe and α-helix in the N-lobe are two key elements for regulation of the kinase enzymatic activity. The A-segment consists of the DFG motif, the activation loop (A-loop), the P-loop, and other secondary structural elements.

In a fully active state (DFG-in conformation) the A-segment adopts an open conformation in order to move away the A-loop from the catalytic center, allowing the substrate binding. In the DFG-in conformation the side chain of the DFG Asp is directed into the ATP binding site and the aromatic ring of the Phe is positioned in the back cleft. The Asp is required to chelate Mg^{2+} and orient the ATP γ-phosphate for its transfer. Importantly, while the DFG-in conformation is required for the catalysis of an active protein kinase this motif can be present as well in inactive kinases.

In the DFG-out conformation the side chains of Asp and Phe exchange their position so that Asp is directed far from the ATP binding site. In this conformation these amino acids are oriented in order to avoid the transfer of phosphate and the activation loop blocks the access of both ATP and substrate to the enzyme.

The front cleft contains mainly the ATP binding site and relatively small non-ATP contact regions. The ATP binding site comprises the adenine (A), ribose (R), and phosphate (P) binding pockets.

The adenine binding pocket is highly hydrophobic, providing a major scaffold for ATP or inhibitor binding.

The back cleft comprises elements important for regulation of kinase catalysis (ATP-contactless). There exists hydrophobic binding pockets: BP-I (this pocket has often been used in the design of inhibitors to gain selectivity for kinase targets with a small-sized gatekeeper) and BP-II. In DFG-out conformation the movement of the activation loop exposes an additional hydrophobic binding sites directly adjacent to the ATP binding cleft, BP-III and BP-IV.

2.2.1 TYROSINE KINASES

The protein kinase family includes 385 serine/threonine kinases, 90 protein-tyrosine kinases, and 43 tyrosine-kinase like proteins. Of the 90 protein-tyrosine kinases, 58 are receptors with extracellular, transmembrane, and intracellular domains and 32 are non-receptors occurring intracellularly.

The family of TKs is of particular interest; their deregulation, through mutation or overexpression, is often related to cancer onset and progression.[13]

In the last two decades, a number of ATP-mimic TK inhibitors (TKIs) have been developed. TKIs share some common pharmacophore features, like a nitrogen-containing heterocycle (for the interaction with the kinase hinge region), a lipophilic moiety (for interaction with a hydrophobic region not exploited by ATP) and a bridge connecting the two. According to the bound kinase conformation, TKIs are classified as type I, I $^1/_2$, II, III, IV, V and VI inhibitors.[15]

Type I, I½, and type II inhibitors occupy part of the adenine binding pocket and form hydrogen bonds with the hinge region connecting the small and large lobes of the enzyme. Type III and IV inhibitors are allosteric in nature.

In particular:

- Type I binds the active kinase conformation (DFG-in). Type I inhibitors typically consist of a heterocyclic ring system that occupies the purine binding site, where it serves as a scaffold for side chains that occupy the adjacent hydrophobic regions I and II.
- Type I½ inhibitors bind to a DFG-in inactive conformation.
- Type II inhibitors bind to a DFG-out inactive kinase conformation, which bears a larger lipophilic cleft. Accordingly, type II inhibitors have a larger lipophilic moiety than type I inhibitors.
- Type III inhibitors bind next to the ATP-binding pocket, they are not ATP competitors.
- Type IV inhibitors do not bind to the ATP or peptide substrate binding sites.

- Type V inhibitors bind to two different regions of the protein kinase domain and are therefore bivalent inhibitors.
- Type VI inhibitors bind covalently to their target enzyme, they are capable of forming an irreversible bond, usually, by reacting with a nucleophilic cysteine residue

Receptor tyrosine kinases

The receptor TKs (RTKs) are cell-surface receptors that are sensitive to extracellular levels of growth factors, such as epidermal growth factor (EGF), chemokines or other ligands including those belonging to the insulin.

RTKs can be grouped into subfamilies according to their ligand affinity, amino acid sequences and structural homology. The RTK subfamilies include, among others, epidermal growth factor receptors (EGFRs), fibroblast growth factor receptors (FGFRs), insulin and insulin-like growth factor receptors (IR and IGFR), platelet-derived growth factor receptors (PDGFRs), vascular endothelial growth factor receptors (VEGFRs), hepatocyte growth factor receptors (HGFRs), and proto-oncogene c-KIT.[16]

All RTKs possess a glycosylated extracellular ligand binding domain, a short transmembrane segment and a cytoplasmic region containing the kinase domain.

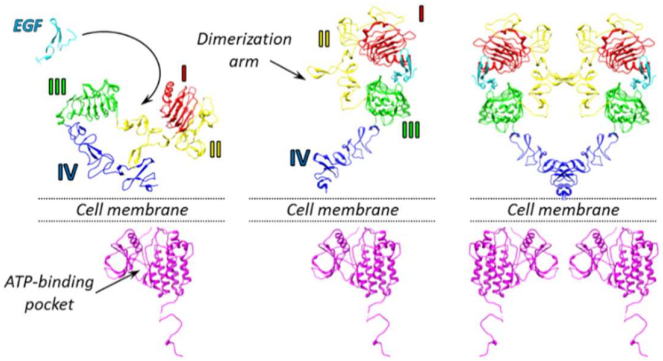

***Figure 4**. Mechanism of RTK activation.*

The intracellular signal transduction originates with RTKs ligand interaction, promoting receptor dimerization and tyrosine auto-phosphorylation within the RTK intracellular domains.

RTK phosphorylation stimulates the association of effector proteins and adaptor proteins, including phospholipase C-γ, mitogen-activated protein kinases and phosphatidylinositol 3-kinase, propagating the signal transduction cascade (Figure 4).

A hyperactivation of these downstream effector signaling networks promotes cellular growth, proliferation, migration, survival, metabolism, and other biological processes that are frequently associated with transformation and oncogenesis.[17]

Cytoplasmic tyrosine kinases

Cytoplasmic tyrosine kinases, or non-receptor tyrosine kinases (NRTK), mainly differ from the RTKs for the absence of the extracellular domain (Figure 5).

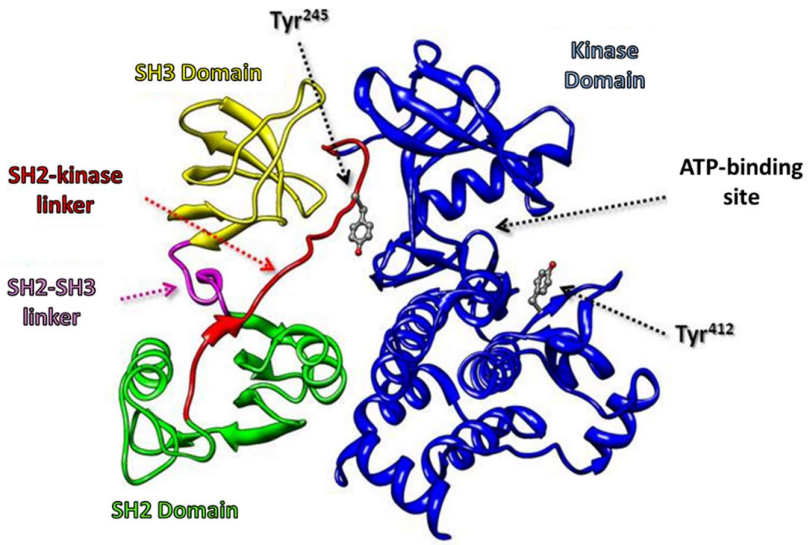

Figure 5. *Cytoplasmic TK structure.*

The majority of NRTKs are in the cytoplasm, although few of them are linked to the cellular membrane. Some NRTKs are anchored to the cell membrane through myristoylated or palmytoylated amino terminus.[18]

NRTKs are part of the signal cascade controlled by RTKs: upon interaction with activated RTKs, the NRTKs undergo a spatial rearrangement that leads to the active conformation (Figure 6). The active conformation is able to phosphorylate the protein substrate, thus causing the signal transduction.[19]

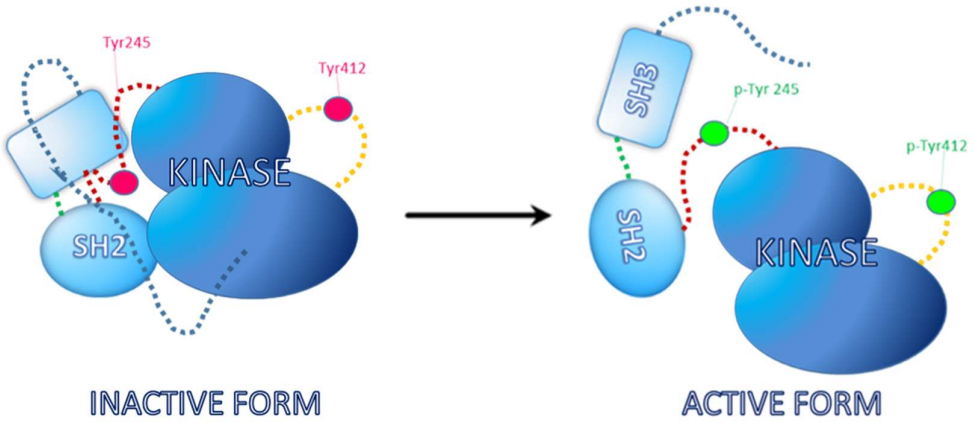

Figure 6. *TK activation mechanism*

NRTKs possess domains that mediate protein-protein, protein-lipid and protein-DNA interactions.

The most commonly protein-protein interaction domains are the Src homology 2 (SH2) and 3 (SH3) domains. The SH2 domain is a compact domain of about 100 residues that binds phosphotyrosine residues in a sequence-specific manner. The smaller SH3 domain (around 60 residues) binds sequences containing proline. Some NRTKs possess other interaction domains: for example Abl contains a F-actin and a DNA binding domain in addition to SH2 and SH3.[18, 20]

Usually, the activation of NRTKs is tightly regulated. However, a NRTKs deregulation can cause a hyper-stimulation of cell growth. One of the main NRTK example in clinical medicine is Abl (*Abelson kinase*).

2.3 DUAL TYROSINE KINASES-HDAC INHIBITORS

2.3.1 Abl TYROSINE KINASE AND INHIBITORS [21-23]

ABL was discovered over 30 years ago as the oncogene in the Abelson murine leukemia virus and later identified as an oncogene associated with chromosome translocations in human leukemia. These ABL fusion genes encode constitutively activated forms of the Abl tyrosine kinase required for cellular transformation.[21] The Abl family of protein kinases connect several extracellular stimuli to signaling pathways causing cell growth, survival, invasion, adhesion, and migration.

The SH2 and SH3 domains, the TK domain (containing the N-lobes and the C-lobe) and the portion called N-cap containing a myristic acid residue structurally characterize Abl (Figure 7).

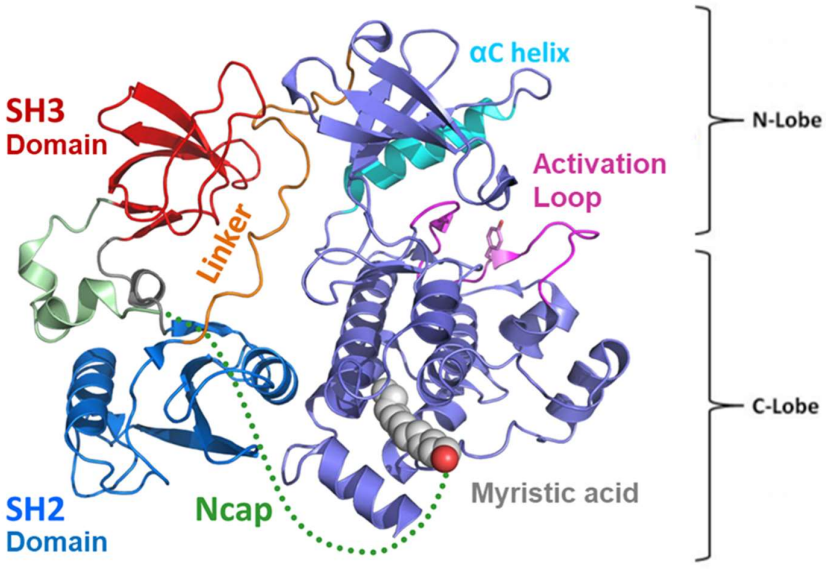

Figure 7. *Abl structure*

The interactions among the Abl domains are fundamental for the enzyme down-regulation: mutations or deletions within the different domains lead, in fact, to an increase kinase activity.

Examples of Abl domains interactions:

- The myristic acid binds to a hydrophobic region of the C-lobe, allowing the formation of hydrogen bonds between Tyr^{158} (of SH2 domain) and Tyr^{136} (of C-lobe) that hide the TK active site.
- The Ser^{69} phosphorylated amino acid (in the N-cap) interacts with the linker between SH3 and SH2 domains, regulating the kinase inhibition.
- The SH2 domain is able to modify its spatial orientation by interacting to the N-lobe stabilizing the kinase active form.
- The C-lobe contributes to the kinase activity through the activation loop. The activation loop contains a Tyr residue that, once phosphorylated, establish electrostatic interactions with an Arg. These interactions stabilize the open active site conformation allowing the substrate peptide access.

Chronic myeloid leukemia and imatinib

Chronic myeloid leukemia (CML) results from a gene defect in hematological stem cell (HSCs). ABL gene moves from chromosome 9 to chromosome 22 under the BCR gene leading to the formation of Philadelphia chromosome (Figure 8). The obtained oncogene is called BCR-ABL (Breakpoint Cluster Region - Abelson Leukemia) and codifies for the Bcr-Abl protein that contains the Abl kinase domain.[22]

In contrast to the tightly regulated c-Abl kinase, an auto-regulatory domain in the oncoprotein is truncated, leading to constitutive activation of the tyrosine kinase activity. The resulting unregulated phosphorylation of intracellular proteins in HSCs leads to the uncontrolled growth and survival of the leukemic cells.[24]

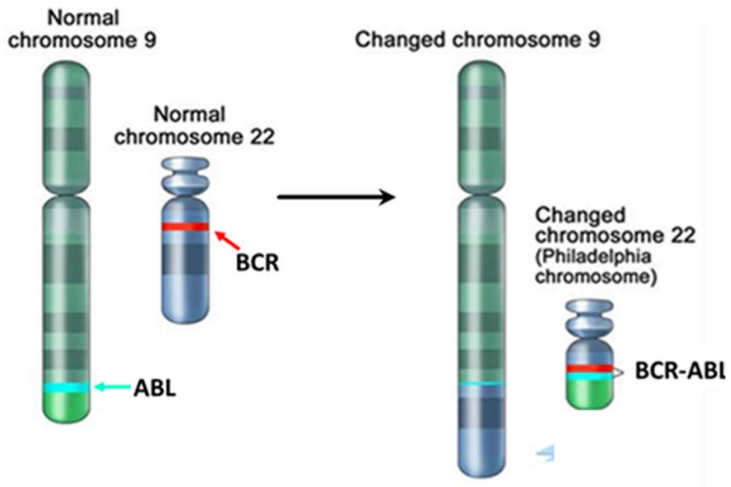

***Figure 8**. Philadelphia chromosome formation.*

Imatinib (Figure 9, **e**) inhibits Bcr-Abl protein and was the first FDA approved small molecule protein-kinase inhibitor. It was initially used for the treatment of CML.[23] Imatinib is a type II multi-TK inhibitor: besides Bcr-Abl, it is active against PDGFRβ and c-KIT. The chemical precursor of imatinib was discovered by the time-consuming process of testing a large number of compounds for inhibition of Protein kinase C (PKC) in vitro. PKC is a serine/threonine kinase that participates in many cellular processes and is implicated in tumor formation. Calcium and diacylglycerol second messengers regulate PKC activity.

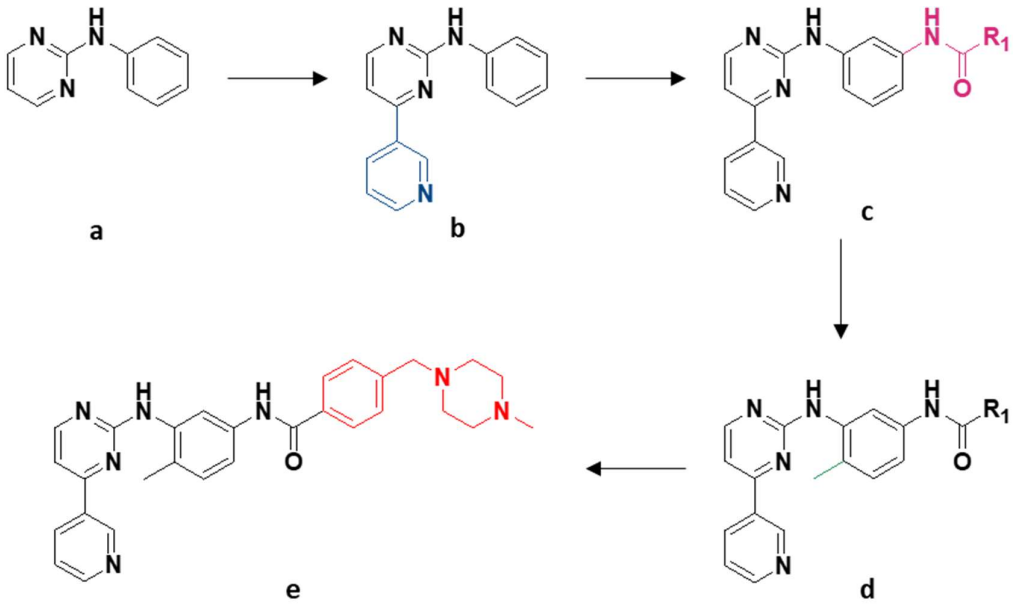

***Figure 9**. Imatinib optimization steps.*

The imatinib lead compound optimization (Figure 9) began from a phenylaminopyrimidine scaffold that inhibited serine/threonine protein kinases (compound **a**). The addition of a pyridine ring increased the PKC inhibitory potency (compound **b**), the addition of an amide group on the phenyl ring provided inhibitory activity against tyrosine kinases such as Bcr-Abl and PDGFR (compound **c**). A subsequent substitution at position 6 of the diaminophenyl ring abolished its PKC inhibitory activity (compound **d**). However, the first library of inhibitors based on **d** showed poor oral bioavailability and water solubility. The problem was solved through the additional attachment of a highly polar side chain (N-methylpiperazine) leading to imatinib (compound **e**).[13, 25]

Imatinib resistance and nilotinib

A rapid drug resistance onset often impairs the use of imatinib in therapy. The mechanisms of resistance can be described as Bcr-Abl dependent (amplification or overexpression of Bcr-Abl and point mutations in the Abl protein kinase

domain, including the gatekeeper T315I mutation) or independent (decreased drug uptake, increased drug efflux, upregulation of signaling pathways).

Thus, new potent Bcr-Abl inhibitors have been developed as, for example, nilotinib (Figure xB), that is a Abl, c-Kit, PDGFR, MAPK, ZAK inhibitor.[26]

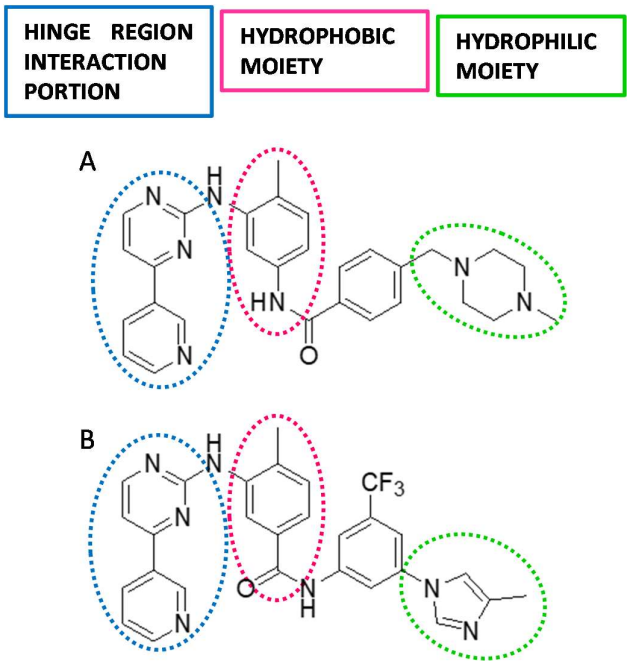

***Figure 10**. Structures of imatinib (A) and nilotinib (B).*

Imatinib and nilotinib are structurally related as they share three common features: a pyridine-pyrimidine portion interacting to the TK hinge region; an aniline hydrophobic moiety; a hydrophilic moiety (Figure 10).

Imatinib and nilotinib show highly comparable binding modes (Figure 11).

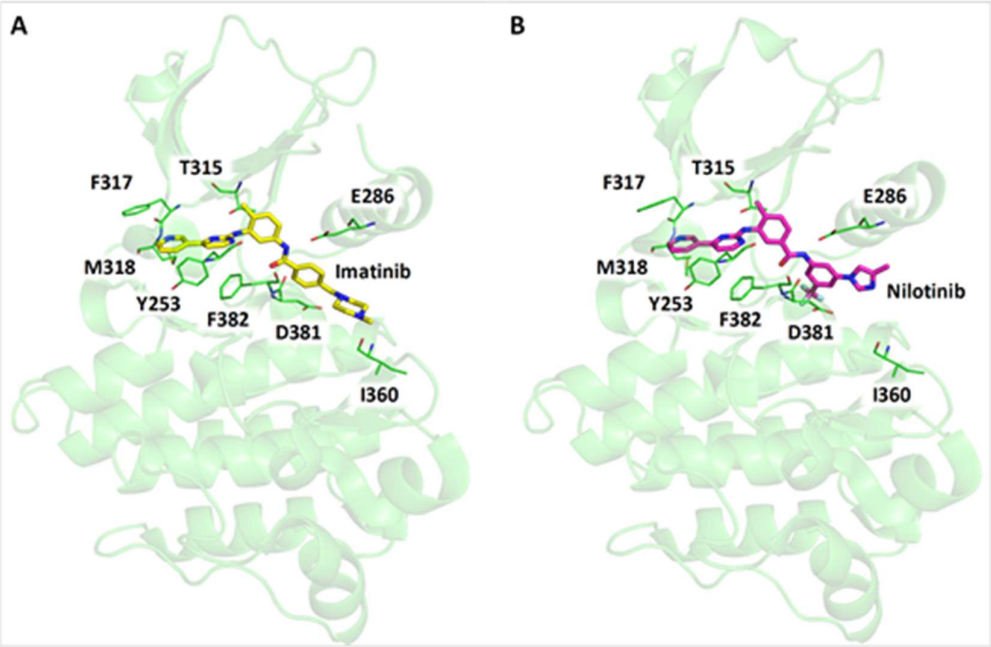

Figure 11. *Crystal structures of Abl-Imatinib (A) and Abl-Nilotinib (B) complexes.*

Nilotinib presents a reversed amidic function compared to imatinib, allowing for a better interaction with the amino acid of the catalytic pocket. Furthermore, the trifluoromethyl function increase the steric complementarity between the drug and the target. Nevertheless, also nilotinib can undergo to rapid onset of drug resistance phenomena.[26]

2.3.2 HISTONE DEACETYLASES AND INHIBITORS

The DNA is contained in the cell nucleus in a high organized and compact structure, called chromatin.[27] The structural entity of chromatin is the nucleosome, which is constituted by an octamer of histone proteins around which the double helix is enveloped (Figure 12).

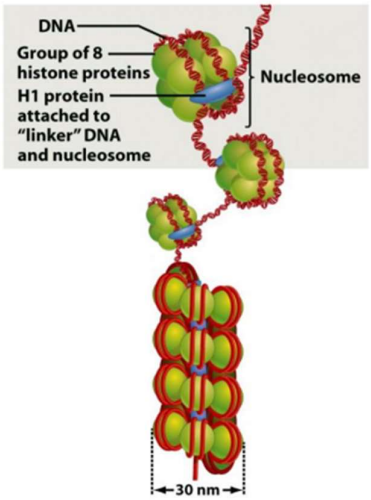

Figure 12. *Chromatin structure.*

Histones are small basic proteins characterized by a central hydrophobic domain, with a globular structure, and by *N*-terminal and *C*-terminal regions containing a high amount of basic amino acids, such as lysine and arginine. The histone terminal residues are directed outside the nucleosome and are accessible to proteases, thus undergoing to post-translational modifications such as acetylation and de-acetylation. These modifications regulate the chromatin structure, regulating the gene transcription. Histone acetylation state is regulated by the activity of two families of enzymes:[28] the histone acetyltransferases (HATs) and the histone deacetylases (HDACs). Usually, a highly acetylated histone core corresponds to a transcriptional activation, while a low acetylation causes a transcriptional repression. In fact, the positive charges of

low acetylated histones interact with the negatively charged DNA phosphate groups, maintaining a compact silent structure of chromatin (heterochromatin). The lysine acetylation neutralizes this histone positive charge, leading to a relaxed chromatin (euchromatin), which is accessible to the transcriptional factors and to the RNA polymerases (Figure 13).

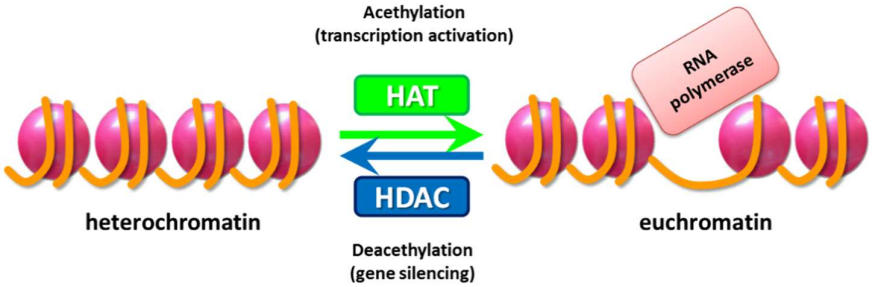

Figure 13. *Heterochromatin/euchromatin regulation equilibria by HATs and HDACs.*

The HDACs are grouped in two different classes, on the basis of the catalytic mechanism:[29]

1. Zinc dependent enzymes:
    - Class I: HDAC1, HDAC2, HDAC3, HDAC8;
    - Class II: HDAC4, HDAC5, HDAC6, HDAC7, HDAC9, HDAC10;
2. NAD dependent enzymes.

Class I and II HDACs are emerging therapeutic targets for cancer treatment. *In vivo* studies have demonstrated that HDACIs impair the cancer growth.

Different HDAC isoforms have been crystallized, allowing for the tridimensional characterization of the enzymes (Figure 14).[29]

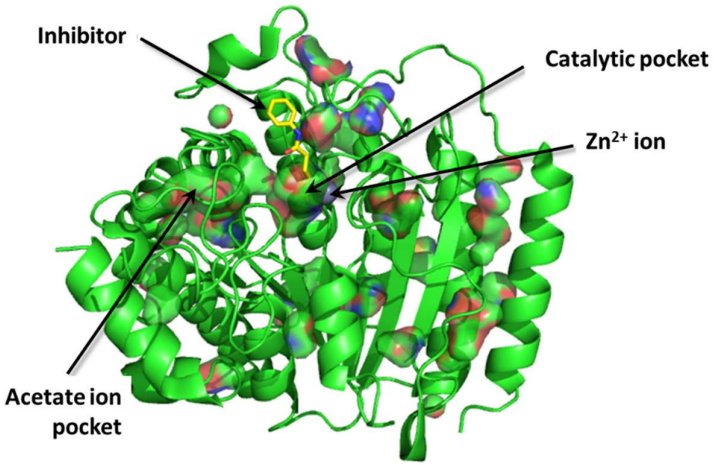

***Figure 14**. Example of HDAC structure.*

The catalytic pocket of zinc-dependent HDACs is constituted by a deep channel of about 11Å length, containing the zinc ion. Besides the metal ion, the bottom of the channel presents a further cavity for the acetate ion. The zinc ion is coordinated by two aspartates, one histidine and one water molecule.

As previously mentioned, histone deacetylases remove the acetyl group from lysine side chains in histone proteins. Class I/II HDACs have homologous active sites and are thought to proceed through a catalytic mechanism in which the His-Asp dyad work as a general acid-base catalytic pair. The proposed chemical mechanism is illustrated in figure 15.

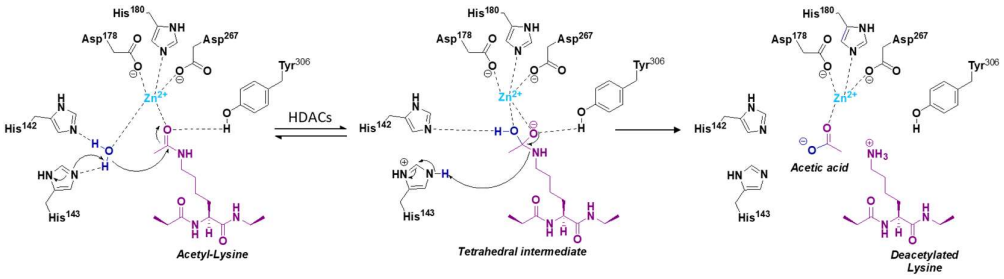

***Figure 15.** Proposed chemical mechanism of class I/II histone deacetylases (HDACs).*

The Zn^{2+} and Tyr^{306} polarize the carboxyl by coordinating to the acetyl oxygen. Asp^{178}, His^{180} and Asp^{267} (numbering from HDAC8 taken as representative

example) and a molecule of water coordinates the metal ion. The metal ion, His^{142} and His^{143} activate the water molecule for the nucleophilic attack to the acetyl carboxyl carbon. Subsequently, the tetrahedral intermediate collapses to form acetate and release the positively charged lysine products.[30]

HDACIs obstruct the substrate access directly binding the catalytic site, thus causing an accumulation of acetylated histone.

These inhibitors show several biological effects that concern the differentiation, the growth arrest and the apoptosis of transformed cells thus resulting in inhibitory growth of the tumor mass.

HDACIs can be grouped in hydroxamic acids, carboxylic acids, electrophilic ketones, *orto*-aminobenzamides and cyclic peptides, according to their chemical structures.[29] The suberoyl anilide of hydroxamic acid (SAHA) is the first FDA-approved HDACI to enter the clinic as a treatment for cutaneous T-cell lymphoma. Hydroxamic acids and *orto*-aminobenzamides (*e.g.* entinostat) are the most studied classes of HDACIs.

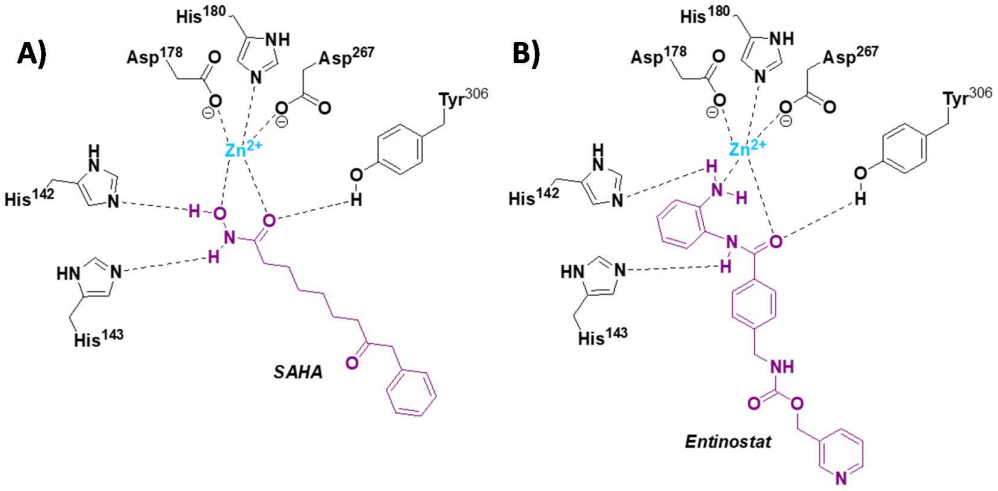

Figure 16. *Structures of SAHA (A) and entinostat (B) complexed with HDAC8.*

In figure 16 are described the structures of the complexes of SAHA (A) and entinostat (B) with HDAC8 and it is visible that the alkyl chain and the pyridine-

carbamate extend out of the lipophilic channel similarly to the side chain of a lysine residue.[31]

All the HDACIs share three common features: a zinc-chelating motif; an enzyme surface recognition portion; a linker between the first two portions (Figure 17).

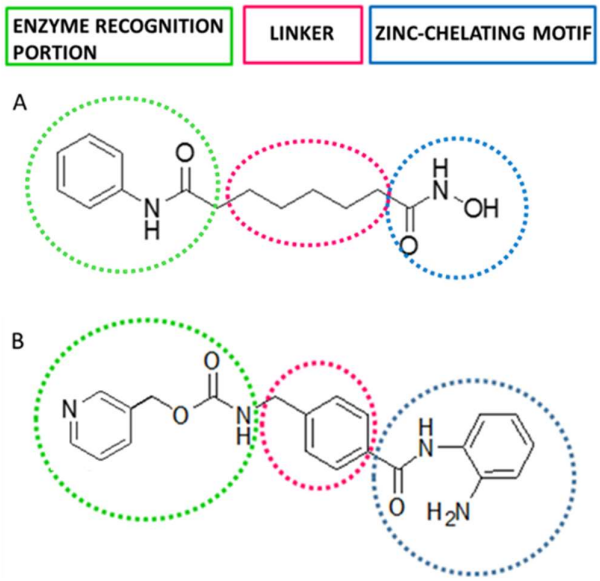

***Figure 17**. Structural features of SAHA (A) entinostat (B).*

Recent studies have shown that the association of Abl and HDAC inhibitors increases the efficacy of the anticancer therapy when compared to single agent treatment.[5] Moreover, the use of chimeric molecules bearing erlotinib and SAHA substructures have shown higher therapeutic efficacy when compared to the association therapy with the same drugs.[32] It is well known that the inhibition of HDAC influences the activity of different proteins (including TKs). However, it is not still clear why chimeric compounds lead to higher activity than the association of the same parent inhibitors. Therefore, these experimental evidences suggest the importance to identify new dual inhibitors of TK/HDAC and to study the mechanism of action.

2.3.3 METAL COMPLEXES

In the past, metal-based compounds were widely used in the treatment of disease conditions, but the lack of clear distinction between the therapeutic and toxic doses was a major challenge.

The milestone of metal-based anticancer therapy is cisplatin, that was discovered in 1960 by Barnett Rosenberg and founded the modern era of the metal-drugs.[33] However, platinum drugs can reveal many limitations such as severe side effects, toxicity and inherent and acquired resistance. Nowadays there is a growing interest in bio-metals (like copper, zinc and iron) as they are biocompatible and less toxic compared to non-endogenous heavy metals. Furthermore, metal complexes has gained much attention as their high anti-proliferative potency and their ability to preferentially accumulate in cancer cells.[34]

In nature, many biological systems make extensive use of metal ions, such as zinc and copper, which play critical roles in the normal functioning of organisms. Transition metals such as copper, iron, and manganese, among others, are involved in multiple biological processes, from electron transfer to catalysis to structural roles, and are frequently associated with active sites of proteins and enzymes. A dysregulation of some of these essential metals during normal biochemical processing can be implicated in the development of various pathological disorders, such as cancer. Therapeutic potential of metal complexes in cancer therapy has attracted a lot of interest mainly because metals exhibit unique characteristics, such as redox activity, variable coordination modes and reactivity toward the organic substrate.

Most metal ion complexes interfere with the DNA double helix differently than an uncoordinated drug. Complexes can bind to the nucleic acid structure in a covalent or noncovalent way and/or can function as a source of ROS which in turn causes DNA degradation.[35]

A large spectrum of transition metal complexes have been used as anticancer agents, although for many intercalation is not required for activity. For example:

- Zinc is an indispensable element that plays a critical role in cell proliferation, differentiation, and defense against free radicals. Zinc acts as a key structural component in many proteins and enzymes, including transcription factors, cellular signaling proteins, and DNA repair enzymes. Zinc is interesting in medicinal chemistry as DNA nucleases due to its natural abundance in humans and important roles in cellular functions.[36]
- Copper is an essential cellular element necessary for many biological pathways and it is a cofactor in enzyme catalytic processes. Copper complexes are known to mimic superoxide dismutase (SOD), an important antioxidant enzyme that protects cells from harmful radical superoxide through its dismutation to non-toxic molecules. Copper can undergo redox activity and competitively bind to the site that could otherwise be occupied by other metals.[33]
- Iron has been exploited in the development of anticancer agents as it is an essential component of various biological processes including erythropoiesis, electron transport and DNA synthesis. Additionally, iron most commonly exists in two oxidation states Fe(II) and Fe(III), which allows it to participate at important redox reactions.[36]

The huge variety of transition metal properties and ligand combinations has produced an extremely broad spectrum of metal-based compounds, each with a unique mechanism of action.

3. OBJECTIVE

The present project relies on the synthesis and the biological evaluation of novel anticancer multi-target compounds able to inhibit: 1) at least one tyrosine kinase and 2) another biomolecular target such as one of the HDAC.

Overall, the project aims at:

1. developing prototypes of novel potential anticancer agents, merging different molecular scaffolds endowed with known pharmacological properties;

2. characterizing the biological profile of the most interesting synthesized compounds, determining as much as possible the mechanism of action at molecular level.

The cytotoxicity of all the synthesized compounds will be determined on a panel of human cancer cell lines over-expressing and not-expressing the TKs of interest. The ability to inhibit the kinase activity of a panel of TKs (EGFR, CSF1-R, KIT, FLT3, PDGFRβ, VEGFR-2, RET, Abl and Src) will be assessed. Then, depending on the molecular structure of the compounds, the inhibitory activity against HDACs is also measured. Overall, the screening of the compounds will furnish a set of molecules on which more detailed biological assays will be performed. The selected compounds will be also evaluated on cell lines resistant to TKIs, HDACIs in order to investigate whether the dual inhibitors overcome the drug resistance phenomena. The molecular structure of the selected compounds will constitute the template for the design of novel and more active compounds that will be in turn synthesized and submitted to biological evaluation.

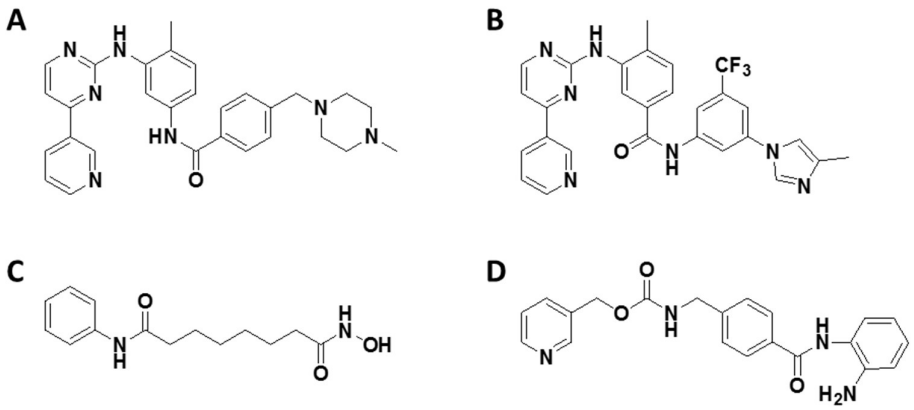

***Figure 18**. Structures of reference compounds.*

With the aim to develop novel potential dual HDAC/TK inhibitors, a set of imatinib (Figure 18A) and nilotinib (Figure 18B) analogues, bearing either a hydroxamic moiety (Figure 18C, SAHA) or an *o*-aminobenzamide moiety (Figure 18D, entinostat), have been designed.

The compounds of the library showing the most interesting activity will be subsequently functionalized with metal ions, as Zn^{2+}, Cu^{2+} and Fe^{3+}. The purpose of the functionalization is to investigate whether a metal could increase the cytotoxicity of these compounds by altering the redox cellular equilibrium and whether it could modulate the interaction with the cellular targets and the cellular uptake.

The main goal of the present PhD project is to synthesized and evaluate novel compounds endowed with multi-target properties. In particular, the research is focused on:

- Quinazolinone derivatives inhibiting EGFR and VEGFR2;
- Benzoquinoline derivatives as novel topoisomerase inhibitors;
- *N*-phenyl-*N'*-[4-(pyrimidin-4-ylamino)phenyl]urea derivatives inhibiting class III RTKs (CSF1R, FLT3, c-KIT, PDGFRα and PDGFRβ);
- *N*-(2-fluoro-5-trifluoromethylphenyl)-*N'*-[4-(pyrimidin-4-ylamino)phenyl]urea derivatives inhibiting c-KIT/ ^{wt}RET/ ^{V804M}RET;

- Pyrido-pyrimidine derivatives bearing either hydroxamate or aminobenzamide functions able to inhibit Abl kinase and HDAC;
- Metal complexes of pyrido-pyrimidine derivatives bearing hydroxamate function able to additionally modulate the redox balance.

The general structures of designed compounds are reported in Figure 19.

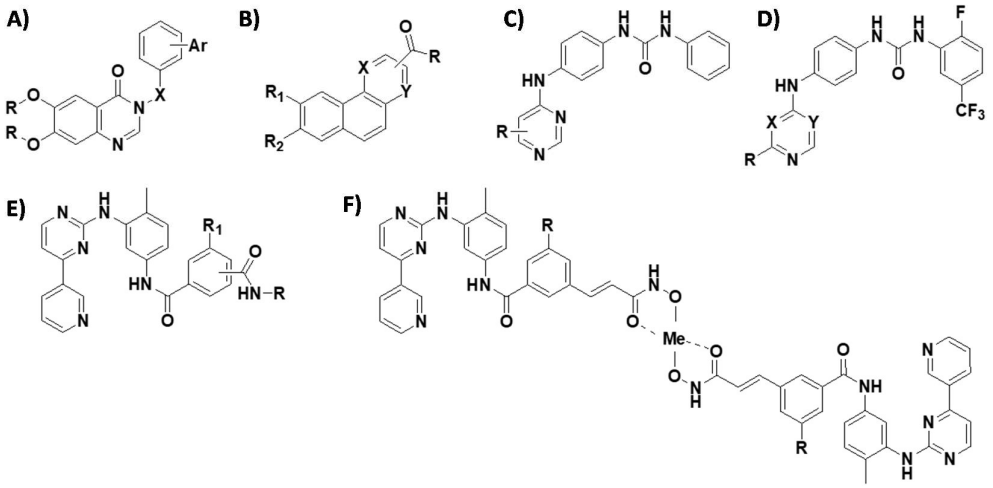

Figure 19. *General structures of A) Quinazolinone derivatives; B) Benzoquinoline derivatives; C) N-phenyl-N'-[4-(pyrimidin-4-ylamino)phenyl]urea derivatives; D) N-(2-fluoro-5-trifluoromethylphenyl)-N'-[4-(pyrimidin-4-ylamino)phenyl]urea derivatives; E) Pyrido-pyrimidine derivatives; F) Metal complexes of pyrido-pyrimidine derivatives.*

4. RESULTS AND DISCUSSION

4.1 SYNTHESIS OF DUAL TK-HDAC INHIBITORS

4.1.1 SYNTHESIS OF [4^{I}-(PYRIDIN-3^{II}-YL)PYRIMIDIN-2^{I}-YL]ANILINE MOIETIES

The synthesis of imatinib (**20**) and nilotinib (**21**) scaffolds (*i.e.* the portion of compound deputed to the interaction with the kinase *hinge region*; Scheme 1), started from 3-acetylpyridine (**24**) heated to reflux with *N*,*N*-dimethylformamide dimethyl acetal obtaining **25** with a good yield. At the same time, the two guanidine derivatives, *N*-(2-methyl-5-nitrophenyl)guanidine (**23**) and methyl 3-guanidino-4-methylbenzoate nitrate (**28**), were synthesized by reaction of the proper aniline derivative with cyanamide.

To obtain the imatinib scaffold 3-(*N,N*-dimethylamine)-1-(pyridin-3^{I}-yl)propen-1-one (**25**) was firstly condensed with **23** by microwave irradiation, affording the cyclization of the pyrimidine ring; the nitro group was subsequently reduced to amine **20**. Differently, nilotinib scaffold **21** was synthesized by classic heating, in the presence of sodium hydroxide, permitting both the cyclization of the pyrimidine ring and the hydrolysis of the methyl ester to obtain the acid function.

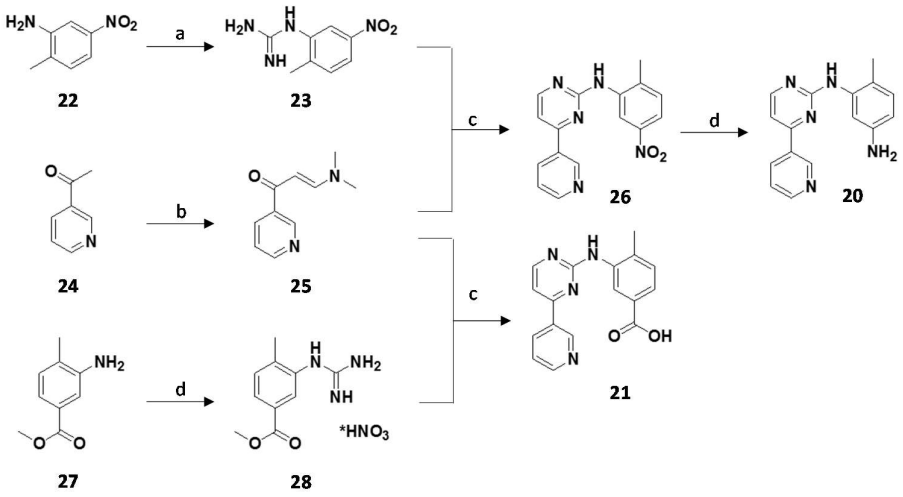

Scheme 1. *Synthesis of intermediates **20** and **21**. Reagents and conditions:*

a. 1) NH_2CN, HNO_3 15 M, EtOH, H_2O, reflux, 16 h; 2) NaOH, H_2O, RT, 1 h, 70% yield;

b. DMF-DMA, xylene, reflux, 16 h, 90% yield;

c. isopropanol, MW, 130°C, 10 min, 75% yield;

d. $SnCl_2 \cdot 2H_2O$, reflux, 1 h, 80% yield;

e. NH_2CN, HNO_3 15 M, EtOH, H_2O, reflux, 16 h, 75% yield;

f. EtOH, NaOH 2 M, reflux, 16 h, 54% yield.

4.1.2 SYNTHESIS OF *m*- OR *p*-VINYLBENZOIC ACID MOIETIES

The active function protection was required to synthesize the zinc chelating motif (both the *o*-aminobenzamide and the hydroxamic acid derivatives); in the first case the *o*-phenylenediamine (**33**) was mono-protected as *tert*-butoxycarbonyl amine (**34**; Scheme 2), stable under neutral or even basic conditions. Conversely, the protected hydroxylamine is commercially available as *O*-(tetrahydro-2*H*-pyran-2-yl)hydroxylamine.

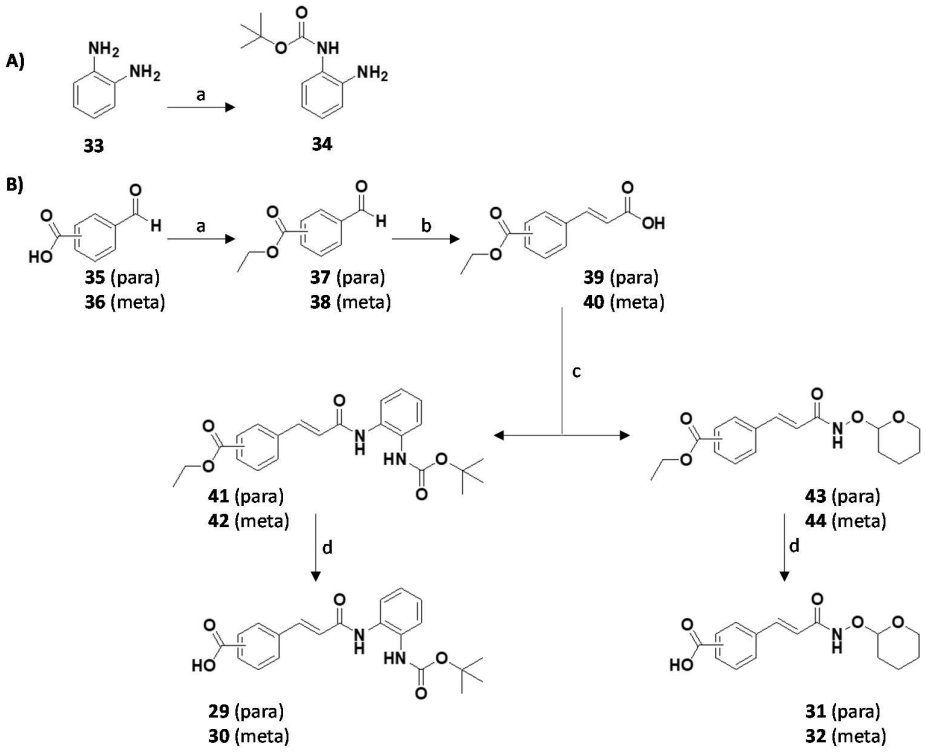

***Scheme 2**. Synthesis of intermediates **29-32**. Reagents and conditions:*

A) a. Boc_2O, THF, RT, 4 h, 69% yield;

B) a. 1) H_2SO_4 18 M, EtOH, reflux, 3.5 h; 2) I_2, acetone; RT, 5 min, quantitative yields;

b. malonic acid, piperidine, pyridine, reflux, 2.5 h, 63-70% yields;

c. protected amine derivative, BOP, TEA, DMF, RT, 16 h, 53-92% yields;

d. NaOH, H_2O, THF, RT, 16 h, 77-86% yields.

The synthesis of the *meta*- and *para*- vinylbenzoic acid moieties started from the esterification of the acid function of the proper formylbenzoic acid with ethanol

in the presence of sulfuric acid, to afford **37** and **38**. The subsequent step was the mixed aldol condensation between the aldehyde derivative and malonic acid in a basic medium to obtain the cinnamic acids (**39** and **40**). Then, the acid function was activated through the BOP method to afford the amide derivatives (**41**-**44**). The final step was the hydrolysis of the ester in alkaline medium.

4.1.3 SYNTHESIS OF *m*/*p*-{2^{IV}-CARBAMOYL-VINYL}-*N*-{4^{I}-METHYL-3^{I}-[4^{II}-(PYRIDIN-3^{III}-YL)PYRIMIDIN-2^{II}-YL]AMINOPHENYL}BENZAMIDE DERIVATIVES

The first library of compounds was synthesized through a convergent strategy by the condensation of the zinc-chelating moiety to the TKI scaffold, accordingly to scheme 3. The condensation of *meta*- and *para*-vinylbenzoic acids with imatinib scaffold **20** was carried out by BOP strategy. Finally the *o*-aminobenzamide was deprotected in trifluoroacetic acid and the hydroxamic acid in hydrochloric acid to obtain respectively compounds **1**, **2** and **3**, **4**.

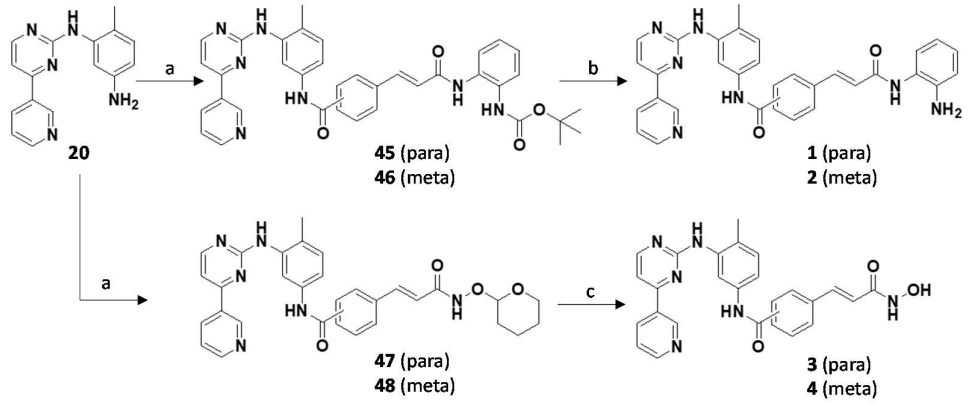

Scheme 3. *Synthesis of compounds **1**–**4**. Reagents and conditions:*
a. acid derivative, BOP, TEA, DMF, RT, 16 h, 40-100% yields;
b. TFA, RT, 2 h, 72-100% yields;
c. HCl 1M, MeOH, RT, 1.5 h, 33-55% yields.

4.1.4 SYNTHESIS OF PHTHALAMIC ACID MOIETIES

The first library of compounds included also the phthalamide derivatives synthesized starting from the terephthalic acid (**53**) or isophthalic acid (**54**) condensed to the protected *o*-phenylenediamine (**34**) and hydroxylamine through the BOP strategy and the subsequent hydrolysis to afford the phthalamic acid moiety (Scheme 4).

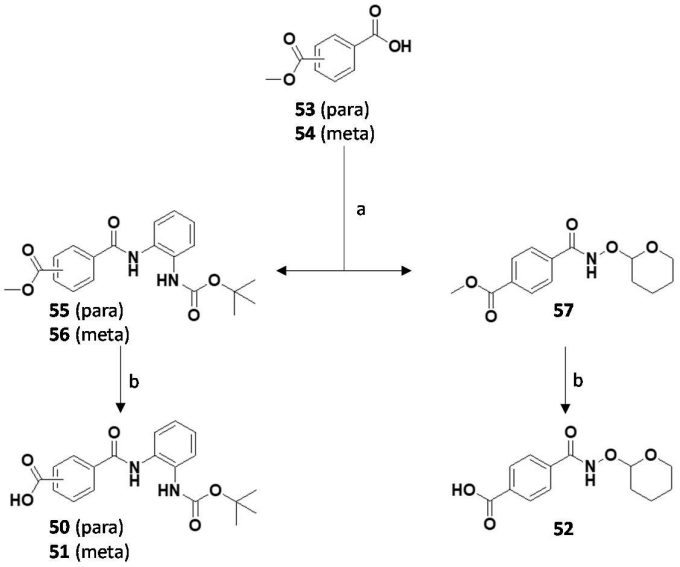

***Scheme 4**. Synthesis of intermediates **50-52**. Reagents and conditions:*
a. protected amine derivative, BOP, TEA, DMF, RT, 16 h, 80-100% yields;
b. NaOH, H_2O, THF, RT, 4 h, 58-76% yields.

4.1.5 SYNTHESIS OF *N*-{4^{I}-METHYL-3^{I}-[4^{II}-(PYRIDIN-3^{III}-YL)PYRIMIDIN-2^{II}-YL]AMINOPHENYL}PHTHALAMIDE DERIVATIVES

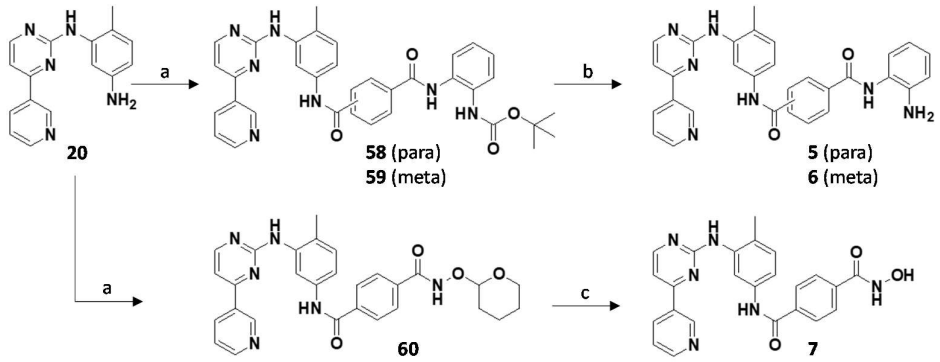

Scheme 5. *Synthesis of compounds **5**–**7**. Reagents and conditions:*
a. acid derivative, BOP, TEA, DMF, RT, 16 h, 95-100% yields;
b. TFA, RT, 2 h, 72-100% yields;
c. HCl 1M, MeOH, RT, 1.5 h, 20% yield.

The imatinib scaffold **20** was condensed to the proper phthalamic acid moiety activated through the BOP method to afford the amide derivatives (**58-60**) and finally the *o*-aminobenzamide and hydroxamic acid protection groups were treated with hydrochloric acid to release the final product active functions. (Scheme 5).

4.1.6 SYNTHESIS OF 3-{2^{IV}-CARBAMOYL-VINYL}-5-TRIFLUOROMETHYL-*N*-{4^{I}-METHYL-3^{I}-[4^{II}-(PYRIDIN-3^{III}-YL)PYRIMIDIN-2^{II}-YL]AMINOPHENYL}BENZAMIDE DERIVATIVES

Compounds in the second library of potential dual TK/HDAC inhibitors bear a trifluoromethyl and/or an imidazole function, while maintaining the *m*-vinylbenzamide and the isophthalamide moieties. Compounds **8** and **9** were synthesized accordingly to scheme 6 starting from the bromination of 3-trifluoromethylbenzoic acid (**61**) with *N*-bromosuccinimide.

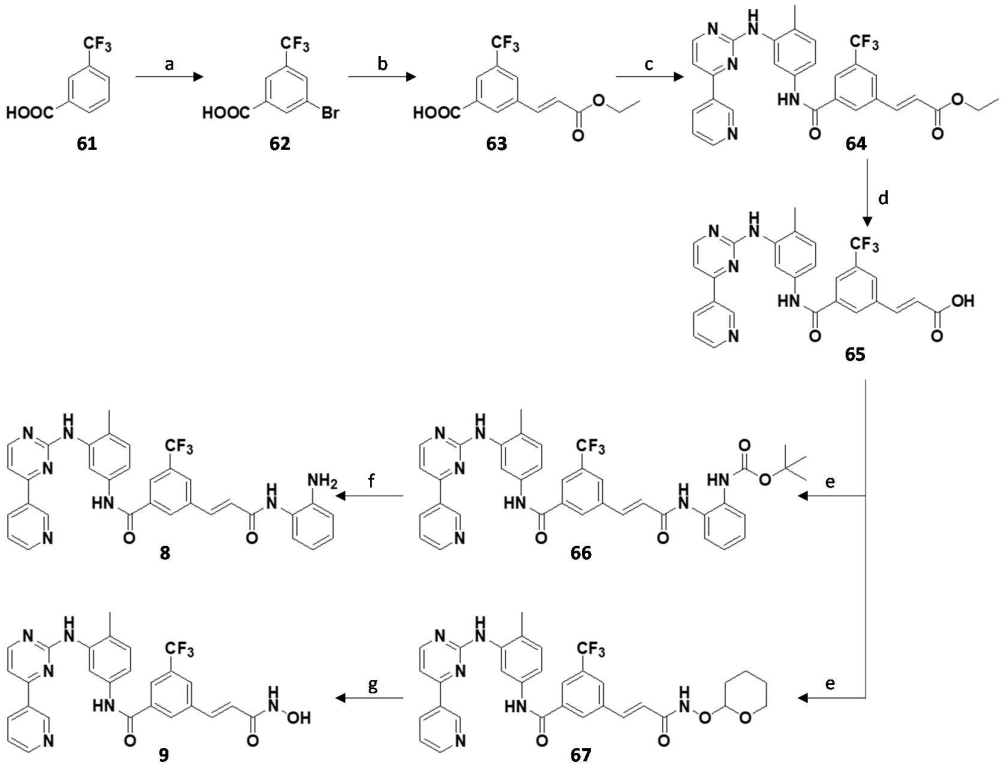

***Scheme 6**. Synthesis of compounds **8** and **9**. Reagents and conditions:*

a. N-bromosuccinimide, H_2SO_4 18 M, TFA, 40°C, 24 h, 91% yield;
b. ethyl acrylate, $Pd(OAc)_2$, TPP, TEA, 100°C (sealed tube), 16 h, 62% yield;
c. imatinib scaffold, BOP, TEA, DMF, RT, 16 h, quantitative yield;
d. NaOH, H_2O, THF, RT, 4 h, 92% yield;
e. protected amine derivative, BOP, TEA, DMF, RT, 16 h, quantitative yields;
f. TFA, RT, 2 h, 88% yield;
g. HCl 1M, MeOH, RT, 16 h, 75% yield.

The second step was the Heck's reaction between 3-bromo-5-trifluoromethylbenzoic acid (**62**) and ethyl acrylate, catalysed by palladium (II) acetate.

Compound **63** was condensed with imatinib scaffold **20** through BOP strategy and then was hydrolyzed to release the acid function (**65**). The acid was subsequently condensed to the (*tert*-butoxycarbonylamino)aniline (**34**) and the *O*-(tetrahydro-2*H*-pyran-2-yl)hydroxylamine; compound **66** was deprotected in trifluoroacetic acid, while compound **67** in methanol with hydrochloric acid.

4.1.7 SYNTHESIS OF 3-{4^{IV}-[(2^{V}-HYDROXYLAMINO)CARBONYL-VINYL]IMIDAZOL-1^{IV}-YL}-5-TRIFLUOROMETHYLBENZAMIDE DERIVATIVES

For the synthesis of compounds **68** and **69** two different strategies were applied, both starting with the esterification of urocanic acid (**70**) in ethanol (Scheme 7, A).

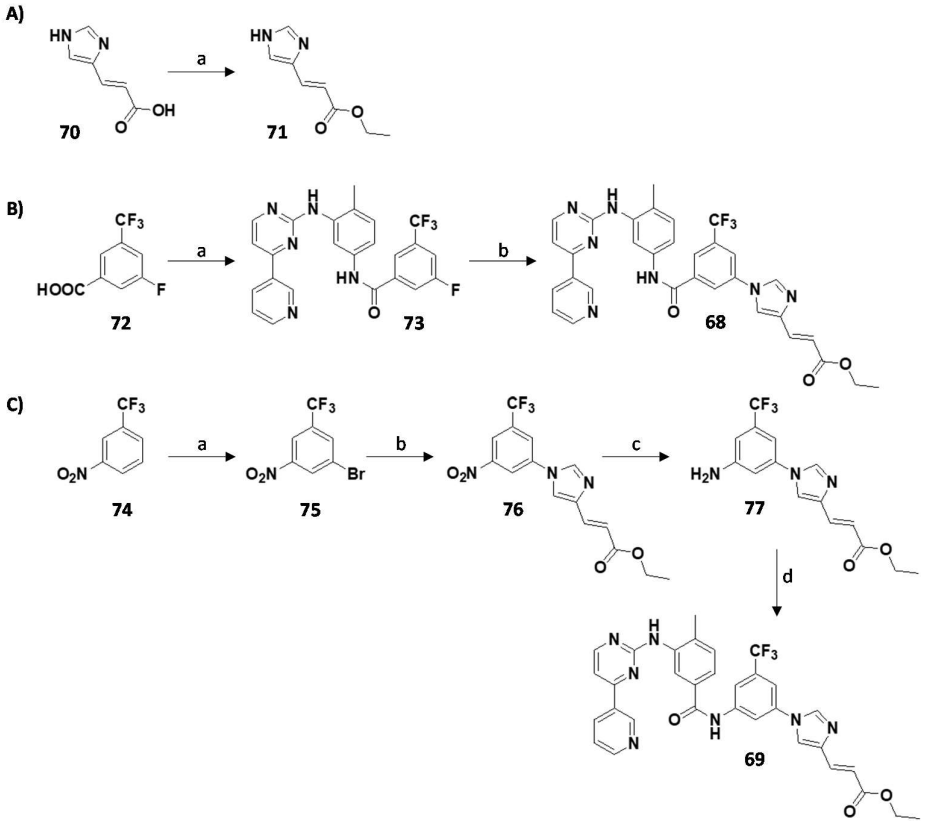

Scheme 7. *Synthesis of intermediates **68** and **69**. Reagents and conditions:*

A) a. H_2SO_4 18 M, EtOH, reflux, 3 h, quantitative yield;

B) a. imatinib scaffold, BOP, TEA, DMF, RT, 24 h, quantitative yield;
b. ethyl urocanate, K_2CO_3, DMF; 120°C (sealed tube), 10 h, 86% yield;

C) a. N-bromosuccinimide, H_2SO_4 18 M, 60°C, 2h, 87% yield;
b. ethyl urocanate, CuI, 8-OH-quinoline, K_2CO_3, DMSO, 100°C (sealed tube), 35% yield;
c. $SnCl_2$ x 2 H_2O, EtOH, 60°C, 1 h, 97% yield;
d. nilotinib scaffold, $SOCl_2$, NMP, 60°C, 1 h, 45% yield.

Compound **68** was synthesized trough a linear method, consisting 1) in the condensation of **20** with 3-fluoro-5-trifluoromethylbenzoic acid activated through BOP strategy, and 2) condensation of the so obtained **73** with ethyl urocanate (Scheme 7, B). Differently, compound **69** was synthesized starting from the bromination of 3-nitrobenzotrifluoride (**74**) with *N*-bromosuccinimide. Then compound **75** was condensed with ethyl urocanate trough an optimized Aza-Ullmann coupling. The nitro group of **76** was then reduced in ethanol with tin(II) chloride and condensed with compound **21** previously activated as acyl chloride (Scheme 7, C).

As aforementioned, the aza-Ullmann condensation needed optimization. Indeed, the generally accepted mechanism for this reaction involves the coordination of the nucleophile to the metal center, which then reacts with an aryl halide through oxidative addition, furnishing the final product after reductive elimination.[37]

The reaction mechanism is described in Figure 20.

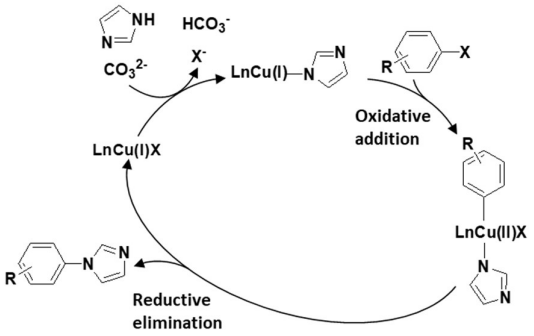

***Figure 20**. Aza-Ullman reaction mechanism.*

With this methodology catalytic amounts of copper (generally Cu(I)) can be used, but conversely a stoichiometric (or greater) amount of base is required.[38]

A mixture of ethyl urocanate (**71**) and 3-bromo-5-trifluoromethylnitrobenzene (**75**), in DMSO, employing copper iodide as catalyst and 8-hydroxyquinoline as ligand increasing the copper solubility and potassium carbonate as base was

initially heated at 120°C in a sealed tube under Ar_2 for 29 hours. Adopting this method the yield was very poor. Indeed, many products formed, prompting us to test other conditions.

Then ethylenediamine was used as ligand and *N*,*N*-dimethylformamide as solvent but also in this case it was not possible to obtain the conversion of starting materials.

We then performed a systematic search for the best reaction conditions, starting from the heating method in sealed tube, according to table 1.

Run	Solvent (5 ml x mmol Ar-Br)	Coordinating agent	Temp	time	CuI ratio	Yield (%)
1	DMSO	8-*OH*-quinoline	100°C	16h	10mol%	24
2	DMSO	8-*OH*-quinoline	100°C	16h	20mol%	35

Table 1. *Tested conditions (sealed tube).*

In both the cases, a double molar amount of both ethyl urocanate and base (potassium bicarbonate) was used.

The optimization through microwave assisted organic chemistry was also attempted as stated in table 2.

Run	Solvent (5 ml x mmol Ar-Br)	Coordinating agent	Temp	time	NOTE	Yield (%)
1	MeCN	8-*OH*-quinoline	100°C	10’	-	-
2	Dioxane	8-*OH*-quinoline	100°C	10’	-	-
3	MeCN	8-*OH*-quinoline	130°C	10’	-	25
4	Dioxane	8-*OH*-quinoline	130°C	10’	-	15
5	MeCN	Proline	130°C	10’	-	18
6	MeCN	Proline	130°C	10’	Ar-Br/imidazole ratio (1:1.5)	21
7	DMSO	Proline	130°C	10’	-	12
8	DMSO	Proline	120°C	10’	Complex mixture	-
9	DMSO	Proline	110°C	20’	Complex mixture	-
10	DMSO	Proline	100°C	20’	Complex mixture	-

Table 2. *Tested conditions (MW).*

In all the cases, a five times molar amount of ethyl urocanate and a double amount of base (potassium bicarbonate) were used. Remarkably, microwave irradiation did not improve the yield of the product.

The best reaction conditions are finally by heating in sealed tube with 20%mol of CuI.

Compounds **68** and **69** were then submitted to the same sequences of reaction to obtain **10** and **11** respectively (Scheme 8), *i.e.*:

1. ester hydrolysis in alkaline medium;
2. activation of acid function with BOP;
3. condensation with *O*-(tetrahydro-*2H*-pyran-2-yl)hydroxylamine;
4. de-protection in hydrochloric acid to release the hydroxamic acid (scheme xx).

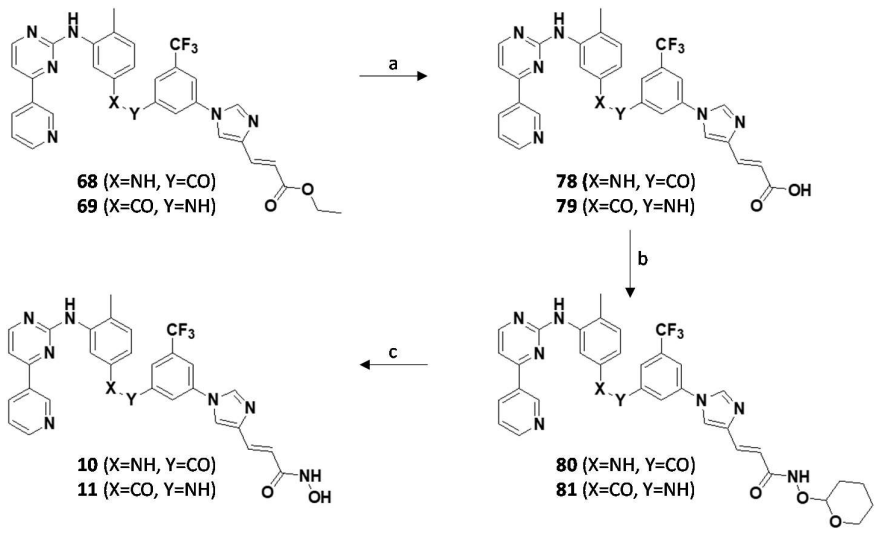

***Scheme 8**. Synthesis of compounds **10** and **11**. Reagents and conditions:*

a. NaOH, H_2O, THF, RT, 16 h, 47-55 yields;

b. O-(tetrahydro-2H-pyran-2-yl)hydroxylamine, BOP, TEA, DMF, RT, 16 h, 55% yields;

c. HCl 1 M, MeOH, RT, 16 h, 30% yields.

4.1.8 SYNTHESIS OF *N*^{I}-[5^{IV}-(IMIDAZOL-1^{V}-YL)-2^{IV}-AMINOPHENYL]-*N*-{4^{I}-METHYL-3^{I}-[4^{II}-(PYRIDIN-3^{III}-YL)PYRIMIDIN-2^{II}-YL]AMINOPHENYL}ISOPHTALAMIDE DERIVATIVES

Compounds **12** and **13** were synthesized through the same method (Scheme 9), starting from the aza-Ullmann coupling between 2-nitro-4-bromoaniline (**82**) and imidazole (**83**) or methylimidazole (**84**). The amino function was then protected with Boc_2O in a strong alkaline medium to give the *N*-boc derivatives **85** and **86**.

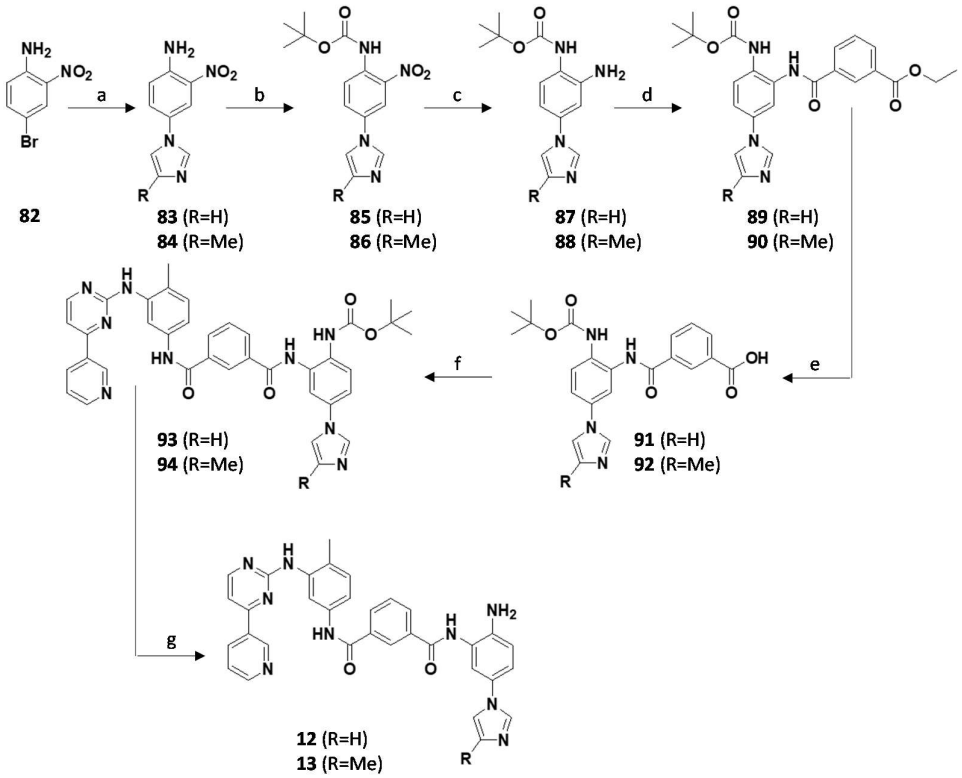

***Scheme 9**. Synthesis of compounds **12** and **13**. Reagents and conditions:*

a. imidazole derivative, CuI, 8-OH-quinoline, K_2CO_3, DMSO; 130°C, 48 h, 31-66% yields;

b. Boc_2O, KOtBu, DMSO, RT, 2 h, 45-73% yields;

c. $FeCl_3$, hydrazine, MeOH, reflux, 1.5 h, 50-70% yields;

d. mono-ethyl isophtalate , BOP, TEA, DMF, RT, 16 h, 50-*75% yields;*

e. NaOH, H_2O, THF, RT, 4 h, 22-31% yields;

f. imatinib scaffold, BOP, TEA, DMF, RT, 16 h, 56-65% yields;

g. TFA, RT, 2 h, 63-94% yields.

The nitro group was reduced with iron(III)chloride and hydrazine, and the amino derivatives were condensed with mono-ethyl isophtalate through the BOP method.

The esters **89** and **90** were dissolved in THF and hydrolyzed with aqueous sodium hydroxide to give the corresponding acids **91** and **92**. These intermediates were activated with BOP and condensed with compound **20**; finally the *o*-aminobenzamide moieties were deprotected by treatment with trifluoroacetic acid.

4.2 SYNTHESIS OF DUAL TYROSINE KINASES-HDAC INHIBITORS FUNCTIONALIZED

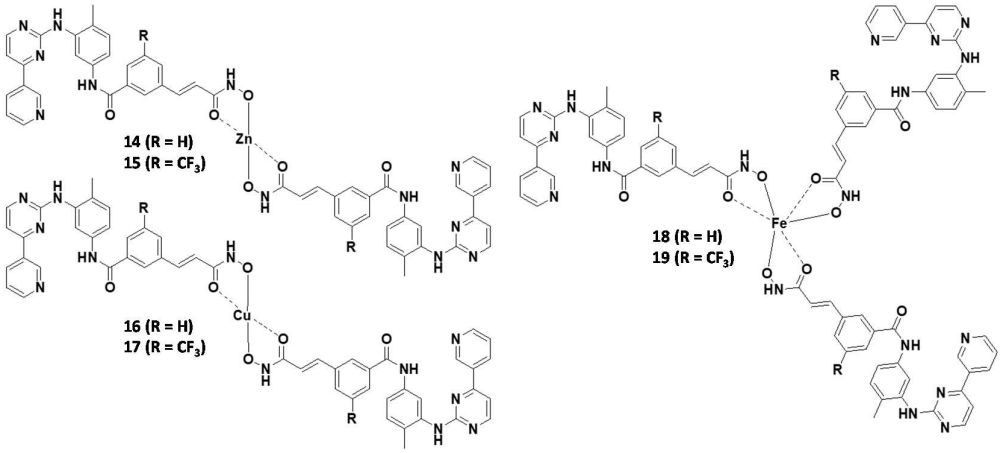

***Figure 21**. Structures of the zinc (II), copper (II) and iron(III) complexes.*

All the complexes (Figure 21) were synthesized following the same method: starting compounds (**4**, **9**) were dissolved in methanol and the solution was made alkaline with aqueous KOH 10% to allow the hydroxamate function to complex the respective metal. Then, an appropriate solution of the metal was added and the mixture was stirred overnight at room temperature.

Complexes **14-15, 16-17** were synthesized using the half amount of zinc acetate and copper chloride with respect to the starting compounds **4** and **9**.

To obtain compounds **18** and **19** one third molar amount of iron chloride was used.

The complexes were characterized by FT-IR spectrometry, elemental analysis and mass spectrometry. The Zinc derivatives were also analyzed by NMR (^{1}H and ^{13}C). The one week stability of the complexes was determined through NMR (only for the zinc derivatives) and subsequently the one month stability of frozen sample tubes in DMSO.

The HPLC stability analysis required that all the samples (compounds **4**; **9** and **14**) were diluted in ACN/Water solution (1:1) with 2 mM HEPES buffer at pH=7 to obtain a final concentration of 1 mM.

The mobile phase consisting of acetonitrile/water (80/20) + 2% TFA, at 0.75 ml/min flow rate was optimized which gave one sharp, well resolved peak with minimum tailing factor for each chromatogram. As described in table 3 the retention times were almost 3.4 minutes for all the eight samples but the presence of metals reduces the absorbance compared to the ligands. Compounds **4**, **9** and all the functionalized complexes shown to be stable in solution for at least five days.

Compound	Day	Retention time (min)	Area (μV*sec)
Ligand 4	**1**	3.37	29508706
	3	3.39	32122122
	5	3.36	30876055
14	**1**	3.38	1852581
	3	3.39	2064780
	5	3.38	2504862
16	**1**	3.38	2481464
	2	3.38	2956040
	6	3.38	2768632
	8	3.38	2922741
	10	3.38	2928927
18	**1**	3.40	686289
	3	3.40	587372
	5	3.41	718379

Compound	Day	Retention time (min)	Area (μV*sec)
Ligand 9	**1**	3.48	13758077
	3	3.45	13183865
	5	3.49	15466319
15	**1**	3.50	4360167
	3	3.40	4497950
	5	3.51	4551947
17	**1**	3.50	8147221
	3	3.41	8726998
	5	3.52	7781849
19	**1**	3.57	3552027
	2	3.57	3313327
	6	3.57	3539605
	8	3.57	3551614
	10	3.57	3522518

Table 3. *HPLC stability test results of ligands **4, 9** and their complexes.*

These compounds will be soon evaluated on isolated targets and against K562 cell line in collaboration with Prof. Soellner, Michigan University, and Dr. Gandin, University of Padua; the results will be compared to the metal-free compounds.

4.3 BIOLOGICAL RESULTS

Synthesized compounds were tested against isolated targets (*i.e.* Abl kinase and HDAC1). Besides, their ability to impair the viability of K562 cells (sensitive to HDACIs and TKIs) was measured.

The first set of compounds (**1**-**7**) showed high activity against isolated targets (Table 4).

Compound	Ki Abl WT (nM)	KiHDAC1 (nM)	GI_{50} (nM)
1	60 ± 20	>12400	>10000
2	6.1 ± 0.9	280 ± 40	5400
3	770 ± 90	15 ± 2	>10000
4	11.4 ± 0.2	5.4 ± 0.6	6800
5	230 ± 70	42 ± 10	>10000
6	60 ± 20	220 ± 50	>10000
7	1300 ± 200	55 ± 8	>10000
Imatinib	14 ± 4	/	650
Entinostat	/	60 ± 20	4300

***Table 4**. Results of biological evaluation for compounds **1-7**.*

Almost all the compounds showed nanomolar affinity towards at least one target. In particular, compound **2** had higher affinity than imatinib *vs* Abl, while compound **4** showed the best inhibitory activity against both the targets with inhibition constants lower than those of the reference compounds. Nevertheless, all the compounds showed poor cytotoxicity, probably as consequence of low cell permeability. Therefore, novel analogs of **2** and **4** were synthesized and submitted to biological evaluation (Table 5). Indeed, the second library of compounds (**8**-**13**) is characterized by the presence of a trifluoromethyl and/or an imidazole functions to improve the pharmacokinetic profile.

Compound	Ki Abl WT (nM)	KiHDAC1 (nM)	GI_{50} (nM)
8	<0.6	355 ± 75	19.4
9	2.6 ± 0.3	22 ± 1	28.2
10	<0.6	2400 ± 510	28.8
11	1.9 ± 0.6	420 ± 13	9.6
12	26 ± 14	30 ± 3	4000
13	7.5 ± 3.3	62 ± 25	3000
Imatinib	14 ± 4	/	650
Entinostat	/	60 ± 20	4300

***Table 5**. Results of biological evaluation for compounds **8-13**.*

Compounds **9**, **12** and **13** resulted as dual inhibitors of Abl and HDAC1 being almost equipotent against the two targets, whereas compounds **8**, **10** and **11** were certainly more active against the kinase. As expected, the trifluoromethyl group increased the affinity *vs* Abl. Indeed nilotinib was originally designed as an improved analog of imatinib: the CF_3 function was introduced to enhance the steric complementarity with the target.

All the compounds in the 2nd set showed a more interesting cytotoxicity than compounds in the 1st set. Taking together, the results indicated compound **9** as the most promising derivative, being a dual inhibitor endowed with nanomolar cytotoxicity.

The 2nd set of compounds was subsequently profiled against Ba/F3 cells (a murine interleukin-3 dependent pro-B cell lines) overexpressing the Bcr-Abl protein or the T315I Bcr-Abl mutant and against the parental line, to asses both the potency and downstream signaling of kinase oncogenes drawing the cell viability profile (Table 6).

Compound	WT Abl Ba/F3 GI_{50} (nM)	Parental Ba/F3 GI_{50} (nM)	T315I Abl Ba/F3 GI_{50} (nM)
8	2.5	>10000	4200
9	5.6	2500	4400
10	8.5	>10000	5200
11	29	>10000	17500
12	6700	4700	5700
13	885	24700	10400

Table 6. *Compounds **8-13** cell viability assays.*

Accordingly to the other biochemical and biological tests, compounds **8**, **9** and **10** showed promising growth inhibitory potency against the cell line overexpressing wild-type Abl.

The overall SARs against isolated targets are summarized in figure 22.

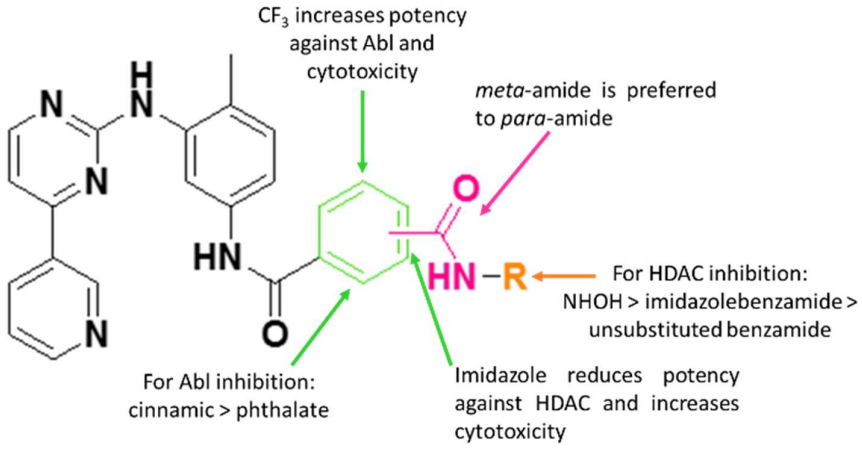

Figure 22*. SARs of synthesized compounds **1**-**13**.*

Briefly:

- Compounds **4**, **9**, **12** and **13** resulted dual inhibitors of Abl and HDAC1;
- Compounds **2**, **8**, **10** and **11** showed a better activity against the kinase;
- Compounds **8**, **9** and **10** showed a great growth inhibition against the cell line expressing wild-type Abl;
- All the compounds in the 2nd set showed a more interesting cytotoxicity;
- Accordingly to all the results compound **9** is the most promising derivative, being a dual inhibitor with nanomolar cytotoxicity.

5. EXPERIMENTAL PROCEDURES

5.1 MATERIALS

All commercial chemicals and solvents used (*Sigma Aldrich*, *Alfa Aesar* and *Carlo Erba*) were analytical grade and were used without further purifications.

Deuterated solvents for NMR analysis (*Aldrich*) show at least isotopic purity of 99.5%.

The thin layer chromatography was performed on pre-coated plates of silica gel 60 with fluorescent indicator UV_{254} (0.2 mm, *Macherey-Nagel*).

Flash chromatography was performed on a Biotage Isolera One using SNAP KP-Sil cartridges, eluting with the solvent specified for individual compounds.

Column chromatography was done with silica gel 60 (0.063-0.100 mm, *Merck*) each time by solvents elution.

An YMC-Pack Pro C_{18} column (5 µm particle size with a pore diameter of 120 Å, 25 cm length, 4.6 mm internal diameter) was used for stability analysis.

5.2 INSTRUMENTATION

Melting points were determined on open capillary, using the melting point apparatus Gallenkamp MFB-595-010M.

The ^{1}H-NMR spectra were recorded on a Bruker 300-AMX, 400-AMX and 500-AMX spectrometers with TMS as an internal standard. Coupling constants are given in Hz, and the relative area peaks agreed with all assignments.

Elemental analyses were performed on a Perkin-Elmer 2400 analyzer.

Mass spectra were performed on an Applied Biosystem Mariner System 5220 with direct injection of the sample.

IR spectra were recorded as KBr discs (4000-400 cm^{-1}) on a Perkin Elmer precisely Spectrum100 FT-IR spectrometer.

Microwave assisted reactions were performed on a CEM Discover® monomode reactor with the temperature monitored by a built-in infrared sensor and automatic control of power; all reactions were performed in closed devices with pressure control.

HPLC stability analysis were performed on a Waters Alliance 2695 separations module, with a detector at 254 nm (model W2487).

5.3 METHODS

5.3.1 SYNTHESIS OF DUAL TK-HDAC INHIBITORS

5.3.1.1 GENERAL METHODS

A) General method for the amide coupling reactions with BOP

(Benzotriazol-1-yloxy)tris(dimethylamino)phosphonium hexafluorophosphate (4.5 mmol), TEA (9.0 mmol) and the amino derivative (4.5 mmol) were in sequence added to a solution of acid derivative (4 mmol) in DMF (8 ml). The mixture was stirred at room temperature for 24 hours and then, drop to drop, poured into a saturated solution of NH_4Cl in H_2O (40 ml). The obtained precipitate was collected by filtration and washed with abundant H_2O to afford the amide derivative.

B) General method for the ester derivatives hydrolysis with NaOH

A solution of NaOH (0.1 g, 2.0 mmol) in H_2O (10 ml) was added to a solution of ester derivative (1 mmol) in MeOH or THF (10 ml). The mixture was heated at 45°C overnight. After cooling, the organic solvent was evaporated under vacuum and then the mixture was acidified with HCl 0.5M until complete precipitation of a solid. The solid precipitate was collected by filtration to obtain the acid derivative.

C) General method for the o-aminobenzamide derivatives deprotection

A solution of [(tert-butoxycarbonyl)aminophen-2-yl]benzamide derivative (0.5 mmol) in TFA (5 ml) was stirred at room temperature for 2 hours. The mixture was subsequently diluted with H_2O (100 ml) and alkalinized with NH_4OH 33% until complete precipitation of an insoluble residue. The precipitate was collected by filtration and washed with water to afford the *o*-aminobenzamide derivative.

D) General method for the hydroxamic acid derivatives deprotection

Starting from the [*O*-(tetrahydro-pyran-2-yl)hydroxylamino]carbonyl derivative (0.5 mmol) dissolved in MeOH (20 ml), HCl 1M (3.5 ml) was added. The mixture was stirred at room temperature for 2 hours and then part of the solvent was evaporated under vacuum. The solid precipitate was collected by filtration and was washed with water to give the hydroxamic acid derivative.

5.3.1.2 SYNTHESIS OF [4^{I}-(PYRIDIN-3^{II}-YL)PYRIMIDIN-2^{I}-YL]ANILINE MOIETIES

Synthesis of N-(2-methyl-5-nitrophenyl)guanidine

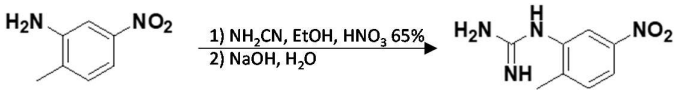

22 **23**

A solution of cianamide (1.3 g, 30.0 mmol) in water (3 ml) and HNO_3 65% (1.4 mL) were added to a suspension of 2-methyl-5-nitroaniline (3.0 g, 20.0 mmol) in EtOH (15 ml). The reaction mixture was refluxed for 16 hours (TLC: $CHCl_3$/MeOH 9/1). After cooling, a solution of cianamide (1.3 g, 30.0 mmol) in water (3 ml) and HNO_3 65% (1.4 ml) were again added to the mixture. The reaction mixture was refluxed for 16 hours. After cooling, diethyl ether (200 ml) was added to the mixture under stirring. The solid precipitate was collected by filtration and dissolved in H_2O (1 L). The solution was alkalized with NaOH (pH = 12). The mixture was stirred one hour in cooled bath to obtain a yellow precipitate. The solid residue was filtered to give ***N*-(2-methyl-5-nitrophenyl)guanidine** (2.7 g, 70% yield); mp 225°C.

^{1}H-NMR (300 MHz, DMSO-*d*$_6$): δ 7.59 (dd, J=8.3, J=2.5, 1H, 4-H); 7.50 (d, J=2.5, 1H, 6-H); 7.32 (d, J=8.3, 1H, 3-H); 5.28 (broad s, 4H, 2 x NH, NH_2); 2.15 (s, 3H, CH_3).

Synthesis of 3-(N,N-dimethylamine)-1-(pyridin-3^{I}-yl)propen-1-one

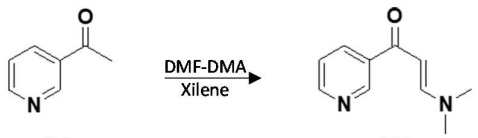

24 **25**

DMF-DMA (4.0 mL, 30.0 mmol) was added to a solution of 3-acetylpyridine (1.8 ml, 15.0 mmol) in xylene (6 ml). The mixture was heated at reflux for 16 hours (TLC: $CHCl_3$/MeOH 9/1). After cooling, the methanol formed was evaporated under reduced pressure. The oil residue was diluted with n-exane (3 ml) and stirred at room temperature. The resulting solid precipitate was collected by filtration to give **3-(*N,N*-dimethylamine)-1-(pyridin-3^{I}-yl)propen-1-one** (2.4 g, 90% yield); mp: 82°C.

^{1}H-NMR (300 MHz, $CDCl_3$-*d*): δ 9.08 (dd, J=2.0, J=0.8, 1H, 2^{I}-H); 8.67 (dd, J=4.9, J=2.0, 1H, 6^{I}-H); 8.19 (dt, J=8.0, J=2.0, 1H, 4^{I}-H); 7.86 (d, J=12.2, 1H, 2-H); 7.35 (ddd, J=8.0, J=4.9, J=0.8, 1H, 5^{I}-H); 5.68 (d; J=12.2, 1H, 3-H); 3.18 (s, 3H, CH_3), 2.95 (s, 3H, CH_3).

Synthesis of N^{I}-(2-methyl-5-nitrophenyl)-N-[4^{I}-(pyridin-3^{II}-yl)pyrimidin-2^{I}-yl]amine

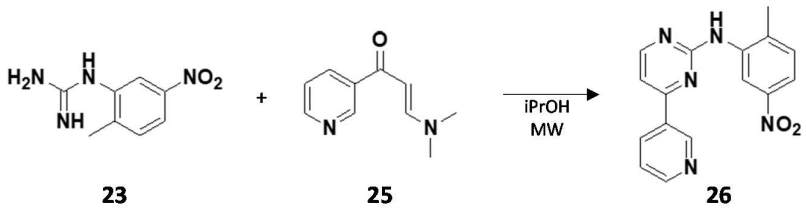

N-(2-methyl-5-nitrophenyl)guanidine (1.9 g, 10.0 mmol) was added to a solution of 3-(*N*,*N*-dimethylamine)-1-(pyridin-3^{I}-yl)propen-1-one (1.5 mg, 8.2 mmol) in isopropanol (16 ml). The mixture was microwave irradiated at 100°C for one minute (power set point 100W), subsequently at 130°C for 10 minutes (power set point 130W) and at 140°C for 10 minutes (power set point 150W), (TLC: $CHCl_3$/MeOH 9/1). After cooling the mixture was stirred at room temperature and *n*-hexane (20 ml) was added. The solid precipitate formed was collected by filtration to give **N^{I}-(2-methyl-5-nitrophenyl)-*N*-[4^{I}-(pyridin-3^{II}-yl)pyrimidin-2^{I}-yl]amine** (2.3 g, 75% yield); mp: 209°C.

^{1}H-NMR (300 MHz, $CDCl_3$-*d*): δ 9.50 (d, J=2.2, 1H, 6-H); 9.30 (dd, J=2.4, J=0.8, 1H, 2^{II}-H); 8.78 (dd, J=4.9, J=1.7, 1H, 6^{II}-H); 8.62 (d, J=5.20, 1H, 6^{I}-H); 8.57 (ddd, J=8.0, J=2.4, J=1.7, 1H, 4^{II}-H); 7.90 (dd, J=8.3, J=2.2, 1H, 4-H); 7.53 (d, J=8.3, 1H, 3-H); 7.35 (ddd, J=8.0, J=4.9, J=0.8, 1H, 5^{II}-H); 7.35 (d, J=5.2, 1H, 5^{I}-H); 2.48 (s, 3H, CH_3).

Synthesis of N^{I}-(2-methyl-5-aminophenyl)-N-[4^{I}-(pyridin-3^{II}-yl)pyrimidin-2^{I}-yl]amine

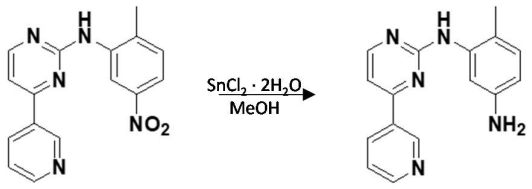

26 **20**

Tin(II) chloride dihydrate (6.2 g, 27.0 mmol) was added to a suspension of N^{I}-(2-methyl-5-nitrophenyl)-*N*-[4^{I}-(pyridin-3^{II}-yl)pyrimidin-2^{I}-yl]amine (1.4 g, 4.5 mmol) in MeOH (45 ml). The mixture was heated at reflux for 1 hour (TLC: $CHCl_3$/MeOH 9/1). After cooling, the methanol was evaporated under vacuum. The residue mixture was diluted in water (200 ml) and gently neutralized with $NaHCO_3$, the aqueous solution was extracted with EtOAc (3 x 40 ml). The organic phase was dried with Na_2SO_4 and concentrated to obtain compound **N^{I}-(2-methyl-5-aminophenyl)-*N*-[4^{I}-(pyridin-3^{II}-yl)pyrimidin-2^{I}-yl]amine** (1.0 g, 80% yield); mp: 135°C.

^{1}H-NMR (300 MHz, $CDCl_3$-*d*): δ 9.27 (dd, J=2.0, J=0.8, 1H, 2^{II}-H); 8.72 (dd, J=4.8, J=2.0, 1H, 6^{II}-H); 8.60 (d, J=5.20, 1H, 6^{I}-H); 8.35 (dt, J=8.0, J=2.0, 1H, 4^{II}-H); 7.62 (d, J=2.4, 1H, 6-H); 7.43 (ddd, J=8.0, J=4.8, J=0.8, 1H, 5^{II}-H); 7.16 (d, J=5.2, 1H, 5^{I}-H); 7.02 (d, J=8.1, 1H, 3-H); 6.94 (broad s, 1H, NH); 6.43 (dd, J=8.1, J=2.4, 1H, 4-H); 3.63 (broad s, 2H, NH_2); 2.25 (s, 3H, CH_3).

Synthesis of methyl 3-guanidino-4-methylbenzoate nitrate

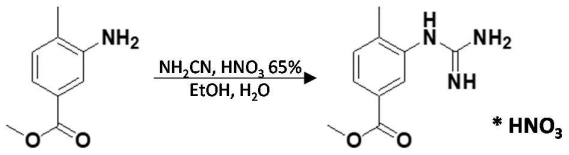

27 **28**

A solution of cianamide (0.9 g, 22.5 mmol) in H_2O (4.5 ml) and HNO_3 65% (1.0 ml, 14.3 mmol) were added to a suspension of 3-amino-4methylbeanzoate (2.5 g, 15.0 mmol) in Ethanol. The mixture was heated at reflux for 6 hours (TLC: $CHCl_3$/MeOH 9/1). After cooling, a solution of cianamide (0.9 g, 22.5 mmol) in H_2O (4.5 ml) and HNO_3 65% (1.0 ml, 14.3 mmol) were added again to the mixture. The mixture was heated at reflux for 16 hours. After cooling, the mixture was chilled in ice bath, diluted with diethyl ether (150 ml) and stirred to obtain a precipitate. The solid precipitate was collected by filtration to obtain **methyl 3-guanidino-4-methylbenzoate nitrate** (2.6 g, 75% yield), m.p. 206°C.

^{1}H-NMR (300 MHz, DMSO-d_6): δ 7.86 (dd, J=1.7, J=7.9, 1H, 6-H); 7.74 (d, 1H, J=1.7, 2-H); 7.50 (d, J=7.9, 1H, 5-H); 7.27 (broad s, 4H, 2 x NH, NH_2); 3.85 (s, 3H, CH_3); 2.27 (s, 3H, CH_3).

Synthesis of 4-methyl-3-{[4^{I}-(pyridin-3^{II}-yl)pyrimidin-2^{I}-yl]amino}benzoic acid

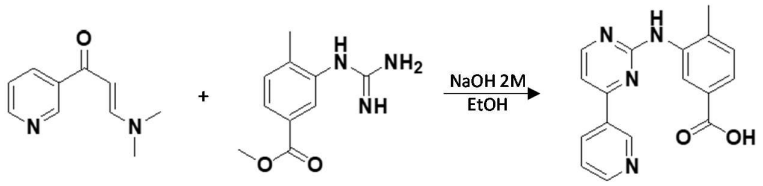

25 **28** **21**

Methyl 3-guanidino-4-methylbenzoate nitrate (1.8 g, 6.5 mmol) was added to a solution of 3-(*N*,*N*-dimethylamine)-1-(pyridin-3^{I}-yl)propen-1-one (1.3 g, 7.2 mmols) and NaOH (0.2 g, 6.3 mmol) in EtOH (20 ml). The mixture was heated to reflux for 16 hours (TLC: $CHCl_3$/MeOH 9/1). The solvent was subsequently evaporated and the obtained residue diluted with H_2O (150 ml) and extracted with EtOAc (3 x 60 ml). The organic phase was dried with anhydrous sodium sulphate and evaporated to obtain a solid residue. The residue was suspended in EtOH (20 ml) and H_2O (20 ml) and a NaOH 2M water solution (9 ml) was subsequently added. The mixture was heated to 45°C for 24 hours. After cooling, the mixture was acidified by addiction of HCl 1M until the formation of a precipitate. The precipitate was collected by filtration to give **4-methyl-3-{[4^{I}-(pyridin-3^{II}-yl)pyrimidin-2^{I}-yl]amino}benzoic acid** (1.1 g, 54% yield), m.p. 279°C.

^{1}H-NMR (300 MHz, DMSO-d_6): δ 9.27 (dd, J=2.0, J=0.7, 1H, 2^{II}-H); 9.06 (broad s, 1H, NH); 8.69 (dd, J=4.9, J=2.0, 1H, 6^{II}-H); 8.54 (d, J=5.2, 1H, 6^{I}H); 8.45 (dt, J=7.9, J=2.0, 1H, 4^{II}-H); 8.29 (d, J=1.7, 1H, 2-H); 7.63 (dd, J=7.9, J=1.7, 1H, 6-H); 7.53 (ddd, J=7.9, J=4.9, J=0.7, 1H, 5^{II}-H); 7.48 (d, J=5.2, 1H, 5^{I}-H); 7.36 (d, J=7.9, 1H, 5-H); 2.33 (s, 3H, CH_3).

5.3.1.3 SYNTHESIS OF *o*/*p*-VINYLBENZOIC ACID MOIETIES

Synthesis of 2-(tert-butoxycarbonyl)aminoaniline

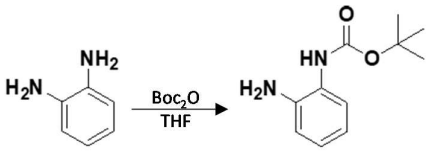

33 **34**

A solution of di Boc_2O (2.2 g, 10.0 mmol) in THF (3 ml) was added to a solution of *o*-phenylenediamine (1.1 g, 10 mmol) in THF (10 ml). The mixture was stirred at room temperature for 3 hours (TLC: $CHCl_3$/MeOH 9/1). The solvent was evaporated under vacuum and the solid residue was dissolved in EtOAc (1 ml) and precipitated by addition of petrol ether (4 ml). The solid obtained was collected by filtration obtaining **2-(tert-butyloxycarbonylamino)aniline** (1.4 g, 69% yield), m.p. 114 °C.

^{1}H-NMR (300 MHz, $CDCl_3$-*d*): δ 7.29-7.27 (m, 1H, 4-H); 6.99-6.97 (m, 2H, 3-H and 5-H); 6.88 (dd, J=6.4, J=1.8, 1H, 6-H); 4.50 (broad s, 2H, NH_2); 1.49 (s, 9H, CH_3).

Synthesis of 4-(ethoxycarbonyl)benzaldehyde

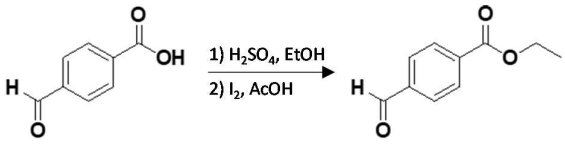

35 **37**

A solution of 4-formylbenzoic acid (5.5 g, 36.6 mmol) in EtOH (160 ml) and H_2SO_4 96% (0.9 ml) was heated at reflux for 16 hours (TLC: $CHCl_3$/MeOH 9/1). After cooling, the solvent was evaporated under vacuum obtaining a solid residue. The residue was dissolved in EtOAc (100 ml) and was washed with a $NaHCO_3$ water solution (3 x 50 ml). The organic phase was dried over anhydrous sodium sulfate and was then evaporated under vacuum. The obtained solid was dissolved in acetone (140 ml) and I_2 (0.9 g, 3.5 mmol) was added to the solution. The mixture was stirred at room temperature for 5 minutes; it was subsequently diluted with a water solution of sodium thiosulfate (150 ml). Acetone was removed under vacuum and the mixture extracted with EtOAc (3 x 50 ml). The organic phase was dried over anhydrous sodium sulfate and then evaporated under vacuum to afford **4-(ethoxycarbonyl)benzaldehyde** (6.5 g, quantitative yield), m.p. 158°C.

^{1}H-NMR (300 MHz, DMSO-d_6): δ 10.11 (s, 1H, CHO); 8.15 (d, J=8.4, 2H, 3-H and 5-H); 8.04 (d, J=8.4, 2H, 2-H and 6-H); 4.36 (q, J=7.0, 2H, $\underline{CH_2}CH_3$); 1.34 (t, J=7.0, 3H, $CH_2\underline{CH_3}$).

Synthesis of 3-(ethoxycarbonyl)benzaldehyde

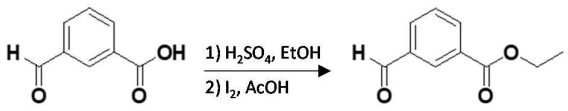

36 **38**

Compound **38** was obtained starting from 3-formylbenzoic acid (0.5 g, 3.0 mmol) with the same procedure as for compound **37** (0.5 g, quantitative yield).

^{1}H-NMR (400 MHz, DMSO-d_6): δ 10.10 (s, 1H, CHO); 8.45 (t, J=1.8, 1H, 2-H); 8.25 (dt, J=7.8, J=1.4, 1H, 4-H); 8.17 (dt, J=7.8, J=1.4, 1H, 6-H); 7.76 (t, J=7.8, 1H, 5-H); 4.37 (q, J=7.1, 2H, $\underline{CH_2}CH_3$); 1.35 (t, J=7.1, 3H, $CH_2\underline{CH_3}$).

Synthesis of 4-(ethoxycarbonyl)cinnamic acid

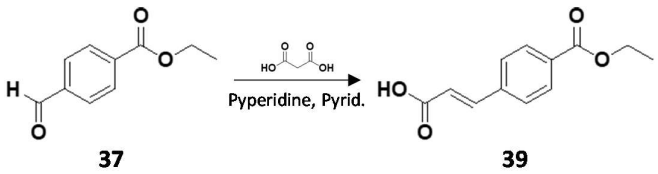

37 **39**

A mixture of 4-(ethoxycarbonyl)benzaldehyde (3.0 g, 16.8 mmol), malonic acid (3.5 g, 33.7 mmol) and pyridine (0.3 g, 3.4 mmol) in piperidine (8.4 ml) was heated to reflux for 2.5 hours (TLC: $CHCl_3$/MeOH 9/1). After cooling, the mixture was slowly poured into H_2O (70 ml) under stirring. The obtained precipitate was collected by filtration and purified by crystallization in EtOH to obtain **4-(ethoxycarbonyl)cinnamic acid** (2.3 g, 63% yield), m.p. 220°C.

^{1}H-NMR (300 MHz, DMSO-d_6): δ 12.56 (s, 1H, OH); 7.97 (d, J=8.3, 2H, 3-H and 5-H); 7.83 (d, J=8.3, 2H, 2-H and 6-H); 7.63 (d, J=16.0, 1H, 1^I-H); 6.66 (d, J=16.0, 1H, 2^I-H); 4.32 (q, J=7.1, 2H, $\underline{CH_2}CH_3$); 1.32 (t, J=7.1, 3H, $CH_2\underline{CH_3}$).

Synthesis of 3-(ethoxycarbonyl)cinnamic acid

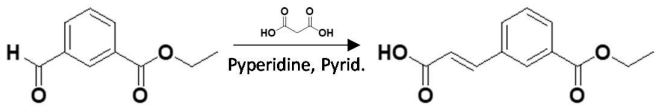

38 **40**

Compound **40** was obtained starting from 3-(ethoxycarbonyl)benzaldehyde (0.5 g, 3.0 mmol), with the same procedure as for compound **39** (0.5 g, 70% yield).

^{1}H-NMR (400 MHz, DMSO-d_6): δ 12.51 (s, 1H, OH); 8.18 (t, J=1.8, 1H, 2-H); 8.01-7.95 (m, 2H, 4-H and 6-H); 7.66 (d, J=16.2, 1H, 1^{I}-H); 7.57 (t, J=7.7, 1H, 5-H); 6.61 (d, J=16.2, 1H, 2^{I}-H); 4.34 (q, J=7.1, 2H, $\underline{CH_2}CH_3$); 1.34 (t, J=7.1, 3H, $CH_2\underline{CH_3}$).

Synthesis of Ethyl-4-{2^{I}-[(tert-butoxycarbonyl)aminophen-2^{II}-yl]carbamoyl-vinyl}benzoate

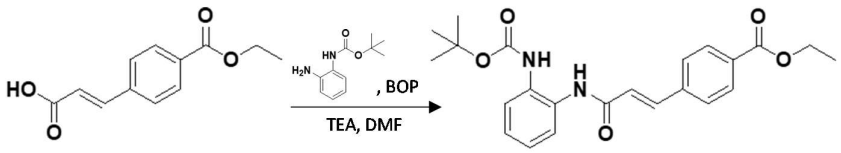

39 **41**

Compound **41** was obtained starting from 4-(ethoxycarbonyl)cinnamic acid (0.2 g, 0.7 mmol) and 2-(tert-butoxycarbonyl)aminoaniline (0.2 g, 0.8 mmol) with general method A (TLC: $CHCl_3$/MeOH 9/1), (0.2 g, 76% yield).

^{1}H-NMR (400 MHz, DMSO-d_6): δ 9.76 (s, 1H, NH); 8.49 (s, 1H, NH); 8.02 (d, J=8.4, 2H, 2-H and 6-H); 7.78 (d, J=8.4, 2H, 3-H and 5-H); 7.65 (d, J=16.0, 1H, 1^{I}-H); 7.62-7.43 (m, 2H, 3^{II}-H and 6^{II}-H); 7.19-7.09 (m, 2H, 4^{II}-H and 5^{II}-H); 7.05 (d, J=16.0, 1H, 2^{I}-H); 4.33 (q, J=7.2, 2H, $\underline{CH_2}CH_3$); 1.46 (s, 9H, 3 x CH_3), 1.34 (t, J=7.2, 3H, $CH_2\underline{CH_3}$).

Synthesis of Ethyl-3-{2^{I}-[(tert-butoxycarbonyl)aminophen-2^{II}-yl]carbamoyl-vinyl}benzoate

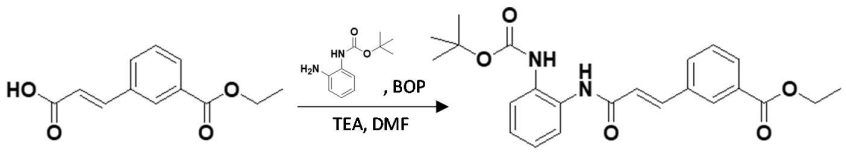

40 **42**

Compound **42** was obtained starting from 3-(ethoxycarbonyl)cinnamic acid (0.3 g, 1.5 mmol) and 2-(tert-butoxycarbonyl)aminoaniline (0.3 g, 1.6 mmol) with general method A (TLC: $CHCl_3$/MeOH 9/1), (0.6 g, 92% yield).

^{1}H-NMR (300 MHz, DMSO-d_6): δ 9.74 (broad s, 1H, NH); 8.51 (broad s, 1H, NH); 8.24 (s, 1H, 2-H); 7.98 (d, J=8.0, 1H, 6-H); 7.91 (d, J=8.0, 1H, 4-H); 7.71-7.54 (m, 4H, 5-H, 1^{I}-H, 3^{II}-H and 6^{II}-H); 7.20-7.08 (m, 2H, 4^{II}-H and 5^{II}-H); 7.05 (d, J=16.3, 1H, 2^{I}-H); 4.36 (q, J=7.0, 2H, $\underline{CH_2}CH_3$); 1.46 (s, 9H, 3 x CH_3); 1.35 (t, J=7.0, 3H, $CH_2\underline{CH_3}$).

Synthesis of Ethyl-4-{2^{I}-[O-(tetrahydro-pyran-2^{II}-yl)hydroxylamino]carbonyl-vinyl}benzoate

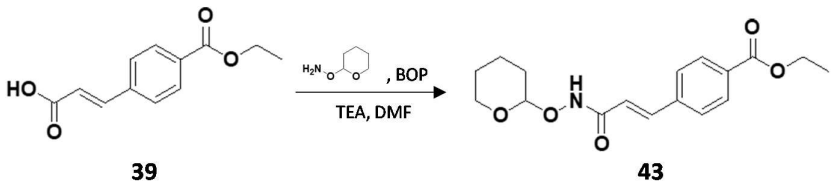

39 **43**

A mixture of 4-(ethoxycarbonyl)cinnamic acid (0.9 g, 4.1 mmol), *O*-(tetrahydro-2*H*-pyran-2-yl)hydroxylamine (0.5 g, 4.5 mmol), BOP (2.0 g, 4.5 mmol) and TEA (1.2 ml, 9.0 mmol) was stirred at room temperature for 24 hours (TLC: $CHCl_3$/MeOH 9/1 + vanillin). The mixture was diluted with a saturated water solution of NH_4Cl (50 mL) and extracted with EtOAc (3 x 20 ml). The organic phase was dried over sodium sulfate, filtered and the solvent evaporated under vacuum. The solid residue was purified by flash chromatography (eluted with CE/EtOAc 4/6) to give **Ethyl-4-{2^{I}-[O-(tetrahydro-pyran-2^{II}-yl)hydroxylamino]carbonyl-vinyl}benzoate** (0.8 g, yield 53%).

^{1}H-NMR (400 MHz, DMSO-d_6): δ 11.31 (broad s, 1H, NH); 7.98 (d, J=8.4, 2H, 2-H and 6-H); 7.72 (d. J=8.4, 2H, 3-H and 5-H); 7.54 (d, J=16.1, 1H, 1^{I}-H); 6.63 (d, J=16.1, 1H, 2^{I}-H); 4.92 (broad s, 1H, 2^{II}-H); 4.32 (q, J=7.1, 2H, $\underline{CH_2}CH_3$); 4.00-3.91 (m, 1H, tetrahydropyran CH_2); 3.58-3.50 (m, 1H, tetrahydropyran CH_2); 1.76-1.66 (m, 3H, tetrahydropyran CH_2); 1.61-1.48 (m, 3H, tetrahydropyran CH_2); 1.33 (t, J=7.1, 3H, $CH_2\underline{CH_3}$).

Synthesis of Ethyl-3-{2^{I}-[O-(tetrahydro-pyran-2^{II}-yl)hydroxylamino]carbonyl-vinyl}benzoate

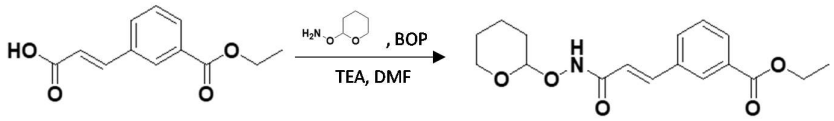

40 **44**

Compound **44** was obtained starting from 4-(ethoxycarbonyl)cinnamic acid (0.5 g, 2.1 mmol) and *O*-(tetrahydro-2*H*-pyran-2-yl)hydroxylamine (0.3 g, 2.3 mmol) with the same procedure as for compound **43** (0.5 g, yield 68%).

^{1}H-NMR (400 MHz, DMSO-d_6): δ 11.26 (s, 1H, NH); 8.14 (s, 1H, 2-H); 7.95 (d. J=7.7, 1H, 6-H); 7.85 (d, J=7.7, 1H, 4-H); 7.58 (t, J=7.7, 1H, 5-H); 7.56 (d, J=15.8, 1H); 6.62 (d, J=15.8, 1H, 2^{I}-H); 4.92 (broad s, 1H, 2^{II}-H); 4.34 (q, J=6.9, 2H, $\underline{CH_2}CH_3$); 4.00-3.91 (m, 1H, tetrahydropyran CH_2); 3.58-3.51 (m, 1H, tetrahydropyran CH_2); 1.76-1.64 (m, 3H, tetrahydropyran CH_2); 1.61-1.50 (m, 3H, tetrahydropyran CH_2); 1.34 (t, J=6.9, 3H, $CH_2\underline{CH_3}$).

Synthesis of 4-{2^{I}-[(tert-butoxycarbonyl)aminophen-2^{II}-yl]carbamoyl-vinyl}benzoic acid

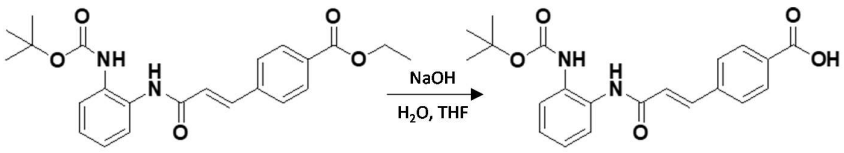

41 **29**

Compound **29** was obtained starting from Ethyl-4-{2^{I}-[(tert-butoxycarbonyl)aminophen-2^{II}-yl]carbamoyl-vinyl}benzoate (0.2 g, 0.4 mmol) in THF with general method B (TLC: $CHCl_3$/MeOH 9/1), (0.1 g, yield 77%).

^{1}H-NMR (400 MHz, DMSO-d_6): δ 9.78 (s, 1H, NH); 8.46 (s, 1H, NH); 8.15 (d, J=8.4, 2H, 2-H and 6-H); 7.95 (d, J=8.4, 2H, 3-H and 5-H); 7.68 (d, J=16.0, 1H, 1^{I}-H); 7.63-7.43 (m, 2H, 3^{II}-H and 6^{II}-H); 7.19-7.07 (m, 2H, 4^{II}-H and 5^{II}-H); 7.10 (d, J=16.0, 1H, 2^{I}-H); 1.43 (s, 9H, 3 x CH_3).

Synthesis of 3-{2^{I}-[(tert-butoxycarbonyl)aminophen-2^{II}-yl]carbamoyl-vinyl}benzoic acid

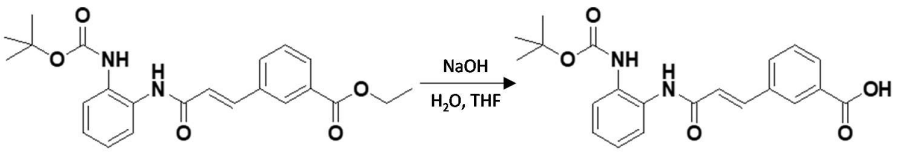

42 **30**

Compound **30** was obtained starting from Ethyl-3-{2^{I}-[(tert-butoxycarbonyl)aminophen-2^{II}-yl]carbamoyl-vinyl}benzoate (0.5 g, 1.3 mmol) in THF with general method B (TLC: $CHCl_3$/MeOH 9/1), (0.4 g, yield 81%).

^{1}H-NMR (300 MHz, DMSO-d_6): δ 9.72 (broad s, 1H, NH); 8.51 (broad s, 1H, NH); 8.24 (s, 1H, 2-H); 7.96 (d, J=7.7, 1H, 6-H); 7.86 (d, J=7.7, 1H, 4-H); 7.70-7.53 (m, 4H, 5-H, 1^{I}-H, 3^{II}-H and 6^{II}-H); 7.19-7.10 (m, 2H, 4^{II}-H and 5^{II}-H); 7.06 (d, J=15.5, 1H, 2^{I}-H); 1.46 (s, 9H, 3 x CH_3).

Synthesis of 4-{2^{I}-[O-(tetrahydro-pyran-2^{II}-yl)hydroxylamino]carbonyl-vinyl}benzoic acid

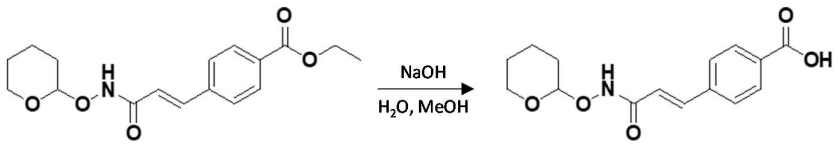

43 **31**

A solution of NaOH (0.1 g, 2 mmol) in H_2O (10 ml) was poured to a solution of Ethyl-4-{2^{I}-[*O*-(tetrahydro-pyran-2^{II}-yl)hydroxylamino]carbonyl-vinyl}benzoate (0.3 g, 0.9 mmol) in MeOH (10 ml). The mixture was heated at 70°C for 16 hours (TLC: $CHCl_3$/MeOH 9/1 + vanillin). After cooling, the organic solvent was evaporated and the aqueous mixture was acidified with HCl 0.1M (pH = 6). The mixture was extracted with Et_2O (3 x 5 ml), the organic phase was dried over sodium sulfate, filtered and the solvent evaporated under vacuum to afford **4-{2^{I}-[*O*-(tetrahydro-pyran-2^{II}-yl)hydroxylamino]carbonyl-vinyl}benzoic acid** (0.2 g, yield 78%).

^{1}H-NMR (300 MHz, DMSO-d_6): δ 11.34 (broad s, 1H, NH); 7.95 (d, J=8.5, 2H, 2-H and 6-H); 7.67 (d. J=8.5, 2H, 3-H and 5-H); 7.53 (d, J=15.9, 1H, 2^{I}-H); 6.63 (d, J=15.9, 1H, 1^{I}-H); 4.92 (broad s, 1H, 2^{II}-H); 4.001-3.90 (m, 1H, tetrahydropyran CH_2); 3.59-3.50 (m, 1H, tetrahydropyran CH_2); 1.77-1.62 (m, 3H, tetrahydropyran CH_2); 1.60-1.48 (m, 3H, tetrahydropyran CH_2).

Synthesis of 3-{2^{I}-[O-(tetrahydro-pyran-2^{II}-yl)hydroxylamino]carbonyl-vinyl}benzoic acid

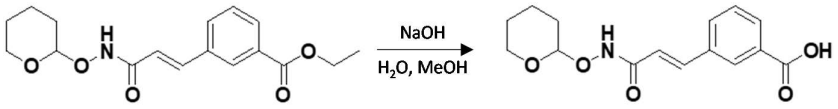

44 **32**

Compound **32** was obtained starting from Ethyl-3-{2^{I}-[O-(tetrahydro-pyran-2^{II}-yl)hydroxylamino]carbonyl-vinyl}benzoate (0.5 g, 1.4 mmol) with the same procedure as for compound **31** (0.2 g, yield 86%).

^{1}H-NMR (400 MHz, DMSO-d_6): δ 11.23 (s, 1H, NH); 8.13 (s, 1H, 2-H); 7.94 (d. J=7.7, 1H, 6-H); 7.82 (d, J=7.7, 1H, 4-H); 7.58-7.51 (m, 2H, 5-H and 1^{I}-H); 6.62 (d, J=16.0, 1H, 2^{I}-H); 4.92 (broad s, 1H, 2^{II}-H); 4.00-3.91 (m, 1H, tetrahydropyran CH_2); 3.58-3.51 (m, 1H, tetrahydropyran CH_2); 1.76-1.64 (m, 3H, tetrahydropyran CH_2); 1.61-1.50 (m, 3H, tetrahydropyran CH_2).

5.3.1.4 SYNTHESIS OF *m/p*-{2^{IV}-CARBAMOYL-VINYL}-*N*-{4^{I}-METHYL-3^{I}-[4^{II}-(PYRIDIN-3^{III}-YL)PYRIMIDIN-2^{II}-YL]AMINOPHENYL}BENZAMIDE DERIVATIVES

Synthesis of 4-{2^{IV}-[(tert-butoxycarbonyl)aminophen-2^{V}-yl]carbamoyl-vinyl}-N-{4^{I}-methyl-3^{I}-[4^{II}-(pyridin-3^{III}-yl)pyrimidin-2^{II}-yl]aminophenyl}benzamide

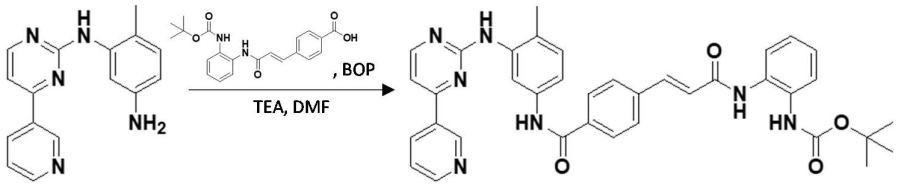

20 **45**

Compound **45** was obtained starting from 4-{2^{I}-[(tert-butoxycarbonyl)aminophen-2^{II}-yl]carbamoyl-vinyl}benzoic acid (0.1 g, 0.2 mmol) and *N*^{I}-(2-methyl-5-aminophenyl)-*N*-[4^{I}-(pyridin-3^{II}-yl)pyrimidin-2^{I}-yl]amine (0.1 g, 0.3 mmol) with general method A (TLC: $CHCl_3$/MeOH 9/1), (0.2 g, quantitative yield).

^{1}H-NMR (400 MHz, DMSO-*d*$_6$): δ 10.27 (broad s, 1H, NH); 9.75 (broad s, 1H, NH); 9.28 (dd, J=2.3, J=0.7, 1H, 2^{III}-H); 8.98 (s, 1H, NH); 8.69 (dd, J=4.9, J=1.7, 1H, 6^{III}-H); 8.52 (d, J=5.3, 1H, 6^{II}-H); 8.49 (broad s, 1H, NH); 8.47 (ddd, J=8.1, J=2.3, J=1.7, 1H, 4^{III}-H); 8.10 (d, J=2.1, 1H, 2^{I}-H); 8.03 (d, J=8.4, 2H, 2-H and 6-H); 7.79 (d, J=8.4, 2H, 3-H and 5-H); 7.67 (d, J=15.8, 1H, 1^{IV}-H); 7.62-7.56 (m, 2H, 3^{V}-H and 6^{V}-H); 7.52 (ddd, J=8.1, J=4.9, J=0.7, 1H, 5^{III}-H); 7.50 (dd, J=8.0, J=2.1, 1H, 6^{I}-H); 7.43 (d, J=5.3, 1H, 5^{II}-H); 7.22 (d, J=8.0, 1H, 5^{I}-H); 7.19-7.09 (m, 2H, 4^{V}-H and 5^{V}-H); 7.04 (d, J=15.8, 1H, 2^{IV}-H); 2.23 (s, 3H, CH_3); 1.46 (s, 9H, 3 x CH_3).

Synthesis of 3-{2^{IV}-[(tert-butoxycarbonyl)aminophen-2^{V}-yl]carbamoyl-vinyl}-N-{4^{I}-methyl-3^{I}-[4^{II}-(pyridin-3^{III}-yl)pyrimidin-2^{II}-yl]aminophenyl}benzamide

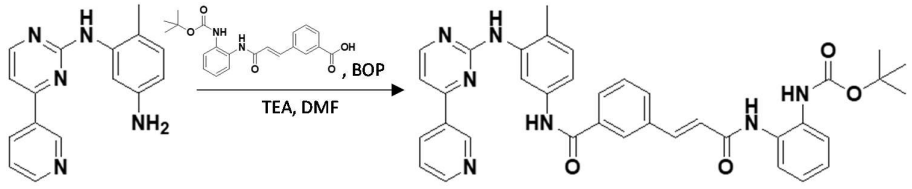

20 **46**

Compound **46** was obtained starting from 3-{2^{I}-[(tert-butoxycarbonyl)aminophen-2^{II}-yl]carbamoyl-vinyl}benzoic acid (0.2 g, 0.4 mmol) and *N^{I}*-(2-methyl-5-aminophenyl)-*N*-[4^{I}-(pyridin-3^{II}-yl)pyrimidin-2^{I}-yl]amine (0.1 g, 0.4 mmol) with general method A (TLC: $CHCl_3$/MeOH 9/1), (0.2 g, quantitative yield).

^{1}H-NMR (400 MHz, DMSO-*d$_6$*): δ 10.30 (broad s, 1H, NH); 9.73 (broad s, 1H, NH); 9.28 (d, J=2.1, 1H, 2^{III}-H); 8.97 (s, 1H, NH); 8.69 (dd, J=4.6, J=1.6, 1H, 6^{III}-H); 8.52 (d, J=5.1, 1H, 6^{II}-H); 8.50-8.44 (m, 2H, NH and 4^{III}-H); 8.23 (t, J=1.6, 1H, 2-H); 8.08 (d, J=2.1, 1H, 2^{I}-H); 7.97 (d, J=7.8, 1H, 6-H); 7.84 (d, J=7.8, 1H, 4-H); 7.74-7.65 (m, 2H, 1^{IV}-H and 5^{III}-H); 7.52-7.49 (m, 4H, 5-H, 6^{I}-H, 3^{V}-H and 6^{V}-H); 7.43 (d, J=5.1, 1H, 5^{II}-H); 7.23 (d, J=8.5, 1H, 5^{I}-H); 7.19-7.09 (m, 2H, 4^{V}-H and 5^{V}-H); 7.04 (d, J=16.1, 1H, 2^{IV}-H); 2.23 (s, 3H, CH_3); 1.46 (s, 9H, 3 x CH_3).

Synthesis of 4-{2^{IV}-[O-(tetrahydro-pyran-2^{V}-yl)hydroxylamino]carbonyl-vinyl}-N-{4^{I}-methyl-3^{I}-[4^{II}-(pyridin-3^{III}-yl)pyrimidin-2^{II}-yl]aminophenyl}benzamide

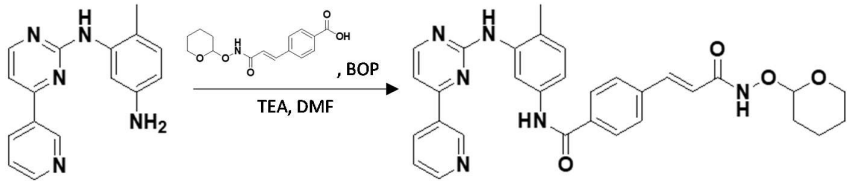

20 **47**

Compound **47** was obtained starting from 4-{2^{I}-[*O*-(tetrahydro-pyran-2^{II}-yl)hydroxylamino]carbonyl-vinyl}benzoic acid (0.2 g, 0.7 mmol) and *N*^{I}-(2-methyl-5-aminophenyl)-*N*-[4^{I}-(pyridin-3^{II}-yl)pyrimidin-2^{I}-yl]amine (0.2 g, 0.8 mmol) with general method A (TLC: $CHCl_3$/MeOH 9/1 + vanillin), (0.2 g, yield 52%).

^{1}H-NMR (400 MHz, DMSO-d_6): δ 11.30 (broad s, 1H, NH); 10.24 (s, 1H, NH); 9.28 (dd, J=2.2, J=0.6, 1H, 2^{III}-H); 8.96 (s, 1H, NH); 8.68 (dd, J=4.8, J=1.7, 1H, 6^{III}-H); 8.51 (d, J=5.1, 1H, 6^{II}-H);8.48 (ddd, J=8.0, J=2.2, J=1.7, 1H-4^{III}-H); 8.09 (d, J=2.0, 1H, 2^{I}-H); 7.99 (d, J=8.4, 2H,2-H and 6-H); 7.72 (d, J=8.4, 2H, 3-H and 5-H); 7.59-7.47 (m, 3H, 1^{IV}-H, 5^{III}-H and 6^{I}-H); 7.43 (d, J=5.1, 1H, 5^{II}-H); 7.21 (d, J=8.3, 1H, 5^{I}-H); 6.63 (d, J=16.0, 1H, 2^{IV}-H); 4.93 (broad s, 1H, 2^{V}-H); 4.01-3.92 (m, 1H, tetrahydropyran CH_2); 3.58-3.51 (m, 1H, tetrahydropyran CH_2); 2.23 (s, 3H, CH_3); 1.76-1.64 (m, 3H, tetrahydropyran CH_2); 1.62-1.49 (m, 3H, tetrahydropyran CH_2).

Synthesis of 3-{2^{IV}-[O-(tetrahydro-pyran-2^{V}-yl)hydroxylamino]carbonyl-vinyl}-N-{4^{I}-methyl-3^{I}-N-[4^{II}-(pyridin-3^{III}-yl)pyrimidin-2^{II}-yl]aminophenyl}benzamide

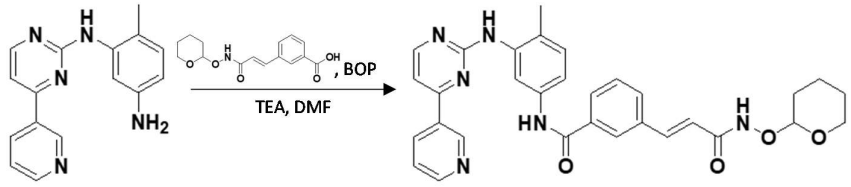

20 **48**

Compound **48** was obtained starting from 3-{2^{I}-[O-(tetrahydro-pyran-2^{II}-yl)hydroxylamino]carbonyl-vinyl}benzoic acid (0.2 g, 0.8 mmol) and *N^{I}*-(2-methyl-5-aminophenyl)-*N*-[4^{I}-(pyridin-3^{II}-yl)pyrimidin-2^{I}-yl]amine (0.3 g, 0.9 mmol) with general method A (TLC: $CHCl_3$/MeOH 9/1 + vanillin), (0.2 g, yield 40%).

^{1}H-NMR (400 MHz, DMSO-*d$_6$*): δ 11.27 (broad s, 1H, NH); 10.27 (s, 1H, NH); 9.28 (dd, J=2.2, J=0.7, 1H, 2^{III}-H); 8.97 (s, 1H, NH); 8.69 (dd, J=4.8, J=1.8, 1H, 6^{III}-H); 8.52 (d, J=5.3, 1H, 6^{II}-H);8.47 (ddd, J=8.0, J=2.2, J=1.8, 1H-4^{III}-H); 8.15 (t, J=1.4, 1H, 2-H); 8.09 (d, J=2.1, 1H, 2^{I}-H); 7.94 (dt, J=7.9, J=1.4, 1H, 6-H); 7.78 (dt, J=7.9, J=1.4, 1H, 4-H); 7.57 (t, J=7.9, 1H, 5-H); 7.56 (d, J=16.1, 1H, 1^{IV}-H); 7.52 (ddd, J=8.0, J=4.8, J=0.7, 1H, 5^{III}-H); 7.49 (dd, J=8.3, J=2.1, 1H, 6^{I}-H);7.43 (d, J=5.3, 1H, 5^{II}-H); 7.22 (d, J=8.3, 1H, 5^{I}-H); 6.63 (d, J=16.1, 1H, 2^{IV}-H); 4.93 (broad s, 1H, 2^{V}-H); 3.99-3.92 (m, 1H, tetrahydropyran CH_2); 3.57-3.50 (m, 1H, tetrahydropyran CH_2); 2.24 (s, 3H, CH_3); 1.73-1.66 (m, 3H, tetrahydropyran CH_2); 1.60-1.48 (m, 3H, tetrahydropyran CH_2).

Synthesis of 4-[2^{IV}-(aminophen-2^{V}-yl)carbamoyl-vinyl]-N-{4^{I}-methyl-3^{I}-[4^{II}-(pyridin-3^{III}-yl)pyrimidin-2^{II}-yl]aminophenyl}benzamide

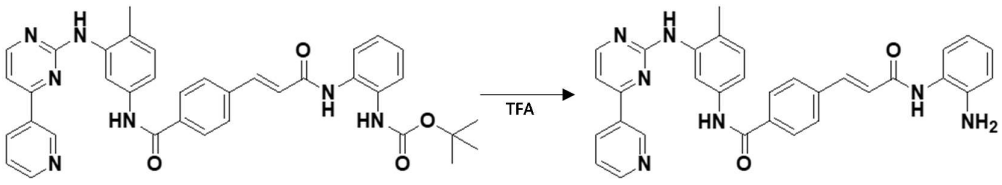

45 **1**

Compound **1** was obtained starting from 4-{2^{IV}-[(tert-butoxycarbonyl)aminophen-2^{V}-yl]carbamoyl-vinyl}-*N*-{4^{I}-methyl-3^{I}-[4^{II}-(pyridin-3^{III}-yl)pyrimidin-2^{II}-yl]aminophenyl}benzamide (0.2 g, 0.3 mmol) accordingly to the general method C (TLC: $CHCl_3$/MeOH 9/1), (0.1 g, yield 72%).

^{1}H-NMR (400 MHz, DMSO-d_6): δ 10.27 (s, 1H, NH); 9.75 (broad s, 1H, NH); 9.28 (dd, J=2.2, J=0.7, 1H, 2^{III}-H); 8.98 (s, 1H, NH); 8.69 (dd, J=4.7, J=1.7, 1H, 6^{III}-H); 8.52 (d, J=5.0, 1H, 6^{II}-H); 8.48 (ddd, J=8.0, J=2.2, J=1.7, 1H, 4^{III}-H); 8.10 (d, J=2.0, 1H, 2^{I}-H); 8.03 (d, J=8.5, 2H, 2-H and 6-H); 7.79 (d, J=8.5, 2H, 3-H and 5-H); 7.67 (d, J=15.6, 1H, 1^{IV}-H); 7.62-7.56 (m, 2H, 3^{V}-H and 6^{V}-H); 7.53 (ddd, J=8.0, J=4.7, J=0.7, 1H, 5^{III}-H); 7.50 (dd, J=8.1, J=2.0, 1H, 6^{I}-H); 7.43 (d, J=5.0, 1H, 5^{II}-H); 7.22 (d, J=8.1, 1H, 5^{I}-H); 7.17 (td, J=7.7, J=1.7, 1H, 4^{v}-H); 7.12 (td, J=7.7, J=1.7, 1H, 5^{V}-H); 7.04 (d, J=15.8, 1H, 2^{IV}-H); 2.23 (s, 3H, CH_3).

Synthesis of 3-[2^{IV}-(aminophen-2^{V}-yl)carbamoyl-vinyl]-N-{4^{I}-methyl-3^{I}-[4^{II}-(pyridin-3^{III}-yl)pyrimidin-2^{II}-yl]aminophenyl}benzamide

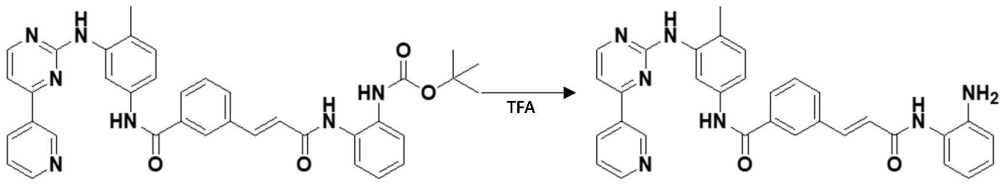

46 **2**

Compound **2** was obtained starting from 3-{2^{Iv}-[(tert-butoxycarbonyl)aminophen-2^{v}-yl]carbamoyl-vinyl}-*N*-{4^{I}-methyl-3^{I}-[4^{II}-(pyridin-3^{III}-yl)pyrimidin-2^{II}-yl]aminophenyl}benzamide (0.3 g, 0.4 mmol) accordingly to the general method C (TLC: $CHCl_3$/MeOH 9/1), (0.2 g, quantitative yield).

^{1}H-NMR (300 MHz, DMSO-d_6): δ 10.32 (s, 1H, NH); 9.45 (s, 1H, NH); 9.28 (d, J=1.5, 1H, 2^{III}-H); 9.00 (s, 1H, NH); 8.69 (dd, J=4.8, J=1.5, 1H, 6^{III}-H); 8.52 (d, J=5.3, 1H, 6^{II}-H); 8.48 (dt, J=7.9, J=1.5, 1H, 4^{III}-H); 8.20 (s, 1H, 2-H); 8.09 (d, J=1.5, 1H, 2^{I}-H); 7.96 (d, J=7.7, 1H, 6-H); 7.82 (d, J=7.7, 1H, 4-H); 7.64 (d, J=15.9, 1H, 1^{IV}-H); 7.62-7.48 (m, 3H, 5-H, 6^{I}-H and 5^{III}-H); 7.43 (d, J=5.3, 1H, 5^{II}-H); 7.36 (dd, J=7.9, J=1.4, 1H, 6^{V}-H); 7.23 (d, J=7.9, 1H, 5^{I}-H); 7.03 (d, J=15.9, 1H, 2^{IV}-H); 6.93 (td, J=7.9, J=1.4, 1H, 4^{V}-H); 6.75 (dd, J=7.9, J=1.4, 1H, 3^{V}-H); 6.59 (td, J=7.9, J=1.4, 1H, 5^{V}-H); 4.97 (broad s, 1H, NH); 2.23 (s, 3H, CH_3).

Synthesis of 4-[2^{IV}-(hydroxylamino)carbonyl-vinyl]-N-{4^{I}-methyl-3^{I}-[4^{II}-(pyridin-3^{III}-yl)pyrimidin-2^{II}-yl]aminophenyl}benzamide

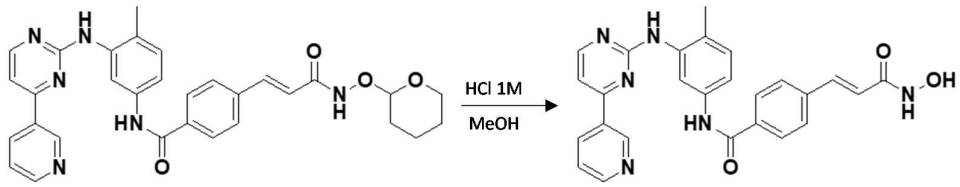

47 **3**

Compound **3** was obtained starting from 4-{2^{Iv}-[*O*-(tetrahydro-pyran-2^{v}-yl)hydroxylamino]carbonyl-vinyl}-*N*-{4^{I}-methyl-3^{I}-[4^{II}-(pyridin-3^{III}-yl)pyrimidin-2^{II}-yl]aminophenyl}benzamide (0.2 g, 0.4 mmol) accordingly to the general method D (TLC: $CHCl_3$/MeOH 9/1 + vanillin), (55 mg, yield 33%).

^{1}H-NMR (400 MHz, DMSO-*d*$_6$): δ 10.26 (s, 1H, NH); 9.38 (d, J=1.7, 1H, 2^{III}-H); 9.08 (s, 1H, NH); 8.82 (dd, J=5.2, J=1.7, 1H, 6^{III}-H); 8.79 (dt, J=8.0, J=1.7, 1H, 4^{III}-H);8.58 (d, J=5.0, , 1H-6^{II}-H); 8.13 (d, J=1.9, 1H, 2^{I}-H); 8.00 (d, J=8.2, 2H,2-H and 6-H); 7.79 (dd, J=8.0, J=5.2, 1H, 5^{III}-H); 7.70 (d, J=8.2, 2H, 3-H and 5-H); 7.55-7.49 (m, H, 1^{IV}-H and 5^{II}-H); 7.47 (dd, J=8.2, J=1.9, 1H, 6^{I}-H); 7.22 (d, J=8.2, 1H, 5^{I}-H); 6.59 (d, J=15.9, 1H, 2^{IV}-H); 2.23 (s, 3H, CH_3).

Synthesis of 3-[(2^{IV}-hydroxylamino)carbonyl-vinyl]-N-{4^{I}-methyl-3^{I}-N-[4^{II}-(pyridin-3^{III}-yl)pyrimidin-2^{II}-yl]aminophenyl}benzamide

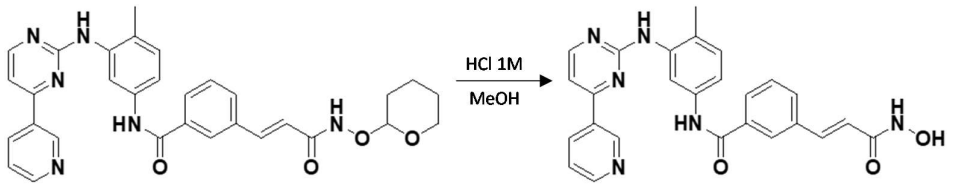

48 **4**

Compound **4** was obtained starting from 3-{2^{Iv}-[*O*-(tetrahydro-pyran-2^{v}-yl)hydroxylamino]carbonyl-vinyl}-*N*-{4^{I}-methyl-3^{I}-[4^{II}-(pyridin-3^{III}-yl)pyrimidin-2^{II}-yl]aminophenyl}benzamide (0.2 g, 0.3 mmol) accordingly to the general method D (TLC: $CHCl_3$/MeOH 9/1 + vanillin), (0.1 g, yield 55%).

^{1}H-NMR (500 MHz, DMSO-*d*$_6$): δ 10.37 (s, 1H, NH); 9.52 (d, J=1.4, 1H, 2^{III}-H); 9.26 (s, 1H, NH); 9.12 (dt, J= 8.0, J=1.4, 1H, 4^{III}-H); 8.98 (d, J=5.0, 1H, 6^{III}-H); 8.64 (d, J=5.2, 1H, 6^{II}-H); 8.17 (d, J=2.2, 1H, 2^{I}-H); 8.15 (t, J=1.6, 1H, 2-H); 8.07 (dd, J=8.0, J=5.0, 1H, 5^{III}-H); 7.96 (dt, J=8.2, J=1.6, 1H, 6-H); 7.76 (dt, J=8.2, J=1.6, 1H, 4-H); 7.61 (d, J=5.2, 1H, 5^{II}-H); 7.56 (t, J=8.2, 1H, 5-H); 7.53 (d, J=16.0, 1H, 1^{IV}-H); 7.46 (dd, J=8.3, J=2.2, 1H, 6^{I}-H); 7.23 (d, J=8.3, 1H, 5^{I}-H); 6.62 (d, J=16.0, 1H, 2^{IV}-H); 2.24 (s, 3H, CH_3).

^{13}C-NMR (500 MHz, DMSO-*d*$_6$): δ 165.12; 162.43; 160.75; 159.81; 159.31; 145.05; 142.38; 141.45; 137.52; 137.34; 137.12; 135.70; 135.01; 134.85; 130.43; 130.24; 129.08; 128.64; 127.65; 126.62; 126.52; 120.31; 117.21; 117.03; 107.97; 17.64.

IR ν_{max}/cm^{-1}: 3423 (hydroxamic acid N-H); 3233 (hydroxamic acid O-H); 1654 (benzamide C=O); 1581 (hydroxamic acid C=O); 1552 (hydroxamic acid C-N).

Elemental analysis for $C_{26}H_{22}N_6O_3$:

Calcd: C 66.94%; H 4.75%; N 18.02%. Found: C 65.80%; H 4.05%; N 16.98%.

5.3.1.5 SYNTHESIS OF PHTHALAMIC ACID MOIETIES

Synthesis of Methyl-N-[2^{I}-(tert-butoxycarbonyl)aminophenyl]terephthalamate

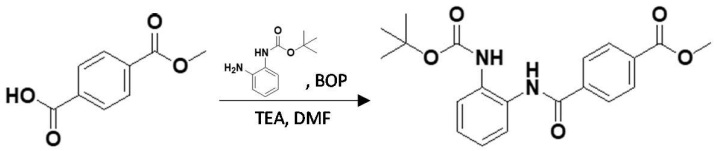

53 **55**

Compound **55** was obtained starting from mono-methyl terephthalate (0.3 g, 1.5 mmol) and 2-(tert-butoxycarbonyl)aminoaniline (0.3 g, 1.6 mmol) with general method A (TLC: $CHCl_3$/MeOH 9/1), (0.6 g, quantitative yield), m.p. 145°C.

^{1}H-NMR (400 MHz, DMSO-d_6): δ 9.97 (broad s, 1H, NH); 8.69 (broad s, 1H, NH); 8.13-8.06 (m, 4H, 2-H, 3-H, 5-H and 6-H); 7.58-7.51 (m, 2H, 3^{I}-H and 6^{I}-H); 7.24-7.12 (m, 2H, 4^{I}-H and 5^{I}H); 3.90 (s, 3H, CH_3); 1.44 (s, 9H, 3 x CH_3).

Synthesis of Methyl-N-[2^{I}-(tert-butoxycarbonyl)aminophenyl]isophthalamate

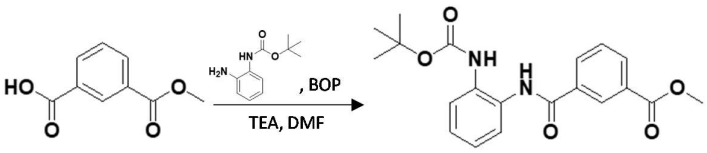

54 **56**

Compound **56** was obtained starting from mono-methyl isophthalate (0.2 g, 1.0 mmol) and 2-(tert-butoxycarbonyl)aminoaniline (0.2 g, 1.1 mmol) with general method A (TLC: $CHCl_3$/MeOH 9/1), (0.3 g, yield 80%), m.p.130°C.

^{1}H-NMR (400 MHz, DMSO-d_6): δ 10.02 (broad s, 1H, NH); 8.70 (broad s, 1H, NH); 8.54 (t, J=1.6, 1H, 2-H); 8.23 (dt, J=7.7, J=1.6, 1H, 6-H); 8.18 (dt, J=7.7, J=1.6, 1H, 4-H); 7.71 (t, J=7.7, 1H, 5-H)); 7.59-7.49 (m, 2H, 3^{I}-H and 6^{I}-H); 7.25-7.12 (m, 2H, 4^{I}-H and 5^{I}H); 3.91 (s, 3H, CH_3); 1.43 (s, 9H, 3 x CH_3).

Synthesis of Methyl-N-[O-(tetrahydro-pyran-2^{l}-yl)hydroxy]terephthalamate

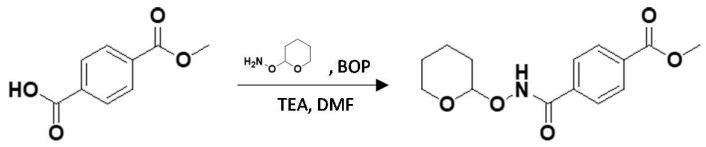

53 **57**

Compound **57** was obtained starting from mono-methyl terephthalate (0.1 g, 0.7 mmol) and *O*-(tetrahydro-2*H*-pyran-2-yl)hydroxylamine (0.1 g, 0.8 mmol) with general method A (TLC: $CHCl_3$/MeOH 9/1), (0.2 g, yield 86%), m.p. 79°C.

^{1}H-NMR (400 MHz, DMSO-d_6): δ 8.04 (d, J=8.3, 2H,2-H and 6-H); 7.88 (d, J=8.3, 2H, 3-H and 5-H); 5.02 (broad s, 1H, 2^{l}-H); 4.10-4.00 (m, 1H, tetrahydropyran CH_2); 3.88 (s, 3H, CH_3); 3.57-3.49 (m, 1H, tetrahydropyran CH_2); 1.77-1.66 (m, 3H, tetrahydropyran CH_2); 1.62-1.50 (m, 3H, tetrahydropyran CH_2).

Synthesis of N-[2^{I}-(tert-butoxycarbonyl)aminophenyl]terephthalamic acid

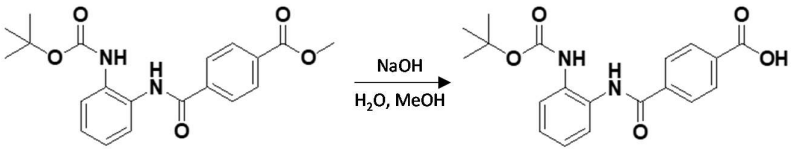

55 **50**

Compound **50** was obtained starting from Methyl-*N*-[2^{I}-(tert-butoxycarbonyl)aminophenyl]terephthalamate (0.6 g, 1.5 mmol) in MeOH with general method B (TLC: $CHCl_3$/MeOH 9/1), (0.3 g, yield 58%), m.p. 190°C.

^{1}H-NMR (400 MHz, DMSO-d_6): δ 9.93 (broad s, 1H, NH); 8.69 (broad s, 1H, NH); 8.09-8.00 (m, 4H, 2-H, 3-H, 5-H and 6-H); 7.57-7.52 (m, 2H, 3^{I}-H and 6^{I}-H); 7.24-7.13 (m, 2H, 4^{I}-H and 5^{I}H); 1.44 (s, 9H, 3 x CH_3).

Synthesis of N-[2^{I}-(tert-butoxycarbonyl)aminophenyl]isophthalamic acid

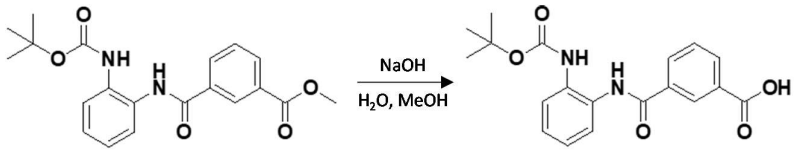

56 **51**

Compound **51** was obtained starting from Methyl-*N*-[2^{I}-(tert-butoxycarbonyl)aminophenyl]isophthalamate (0.3 g, 0.8 mmol) in MeOH with general method B (TLC: $CHCl_3$/MeOH 9/1), (0.2 g, yield 76%).

^{1}H-NMR (400 MHz, *Acetone-d$_6$*): δ 9.85 (broad s, 1H, NH); 8.68 (t, J=1.7, 1H, 2-H); 8.29-8.23 (m, 2H, 4-H and 6-H); 7.79-7.67 (m, 2H, 5-H and 3^{I}-H or 6^{I}-H); 7.62 (dd, J=7.7, J=1.7, 1H, 3^{I}-H or 6^{I}-H); 7.26-7.17 (m, 2H, 4^{I}-H and 5^{I}-H); 1.47 (s, 9H, 3 x CH_3).

Synthesis of N-[O-(tetrahydro-pyran-2^{l}-yl)hydroxy]terephthalamic acid

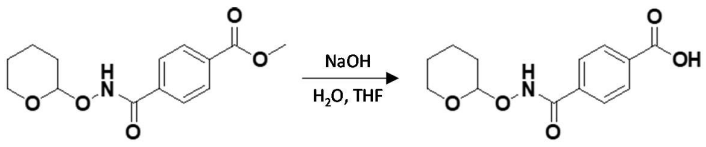

57 **52**

Compound **52** was obtained starting from Methyl-4-{[*O*-(tetrahydro-pyran-2^{l}-yl)hydroxylamino]carbonyl}benzoate (0.2 g, 0.6 mmol) in THF with general method B (TLC: $CHCl_3$/MeOH 9/1), (0.1 g, yield 74%), m.p. 180°C.

^{1}H-NMR (400 MHz, DMSO-d_6): δ 11.79 (s, 1H, NH); 8.01 (d, J=8.4, 2H,2-H and 6-H); 7.85 (d, J=8.4, 2H, 3-H and 5-H); 5.01 (broad s, 1H, 2^{l}-H); 4.10-4.00 (m, 1H, tetrahydropyran CH_2); 3.57-3.49 (m, 1H, tetrahydropyran CH_2); 1.77-1.66 (m, 3H, tetrahydropyran CH_2); 1.62-1.50 (m, 3H, tetrahydropyran CH_2).

5.3.1.6 SYNTHESIS OF *N*-{4^{I}-METHYL-3^{I}-[4^{II}-(PYRIDIN-3^{III}-YL)PYRIMIDIN-2^{II}-YL]AMINOPHENYL}PHTHALAMIDE DERIVATIVES

Synthesis of N^{I}-[(tert-butoxycarbonyl)aminophen-2^{IV}-yl]-N-{4^{I}-methyl-3^{I}-[4^{II}-(pyridin-3^{III}-yl)pyrimidin-2^{II}-yl]aminophenyl}terephthalamide

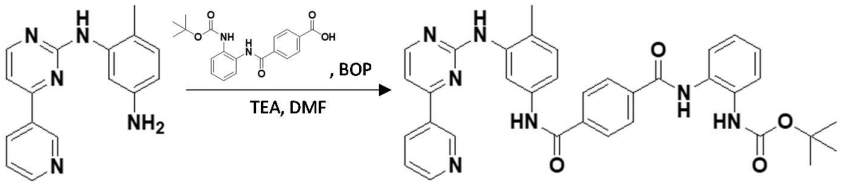

20 **58**

Compound **58** was obtained starting from *N*-[2^{I}-(tert-butoxycarbonyl)aminophenyl]terephthalamic acid (0.1 g, 0.2 mmol) and *N*^{I}-(2-methyl-5-aminophenyl)-*N*-[4^{I}-(pyridin-3^{II}-yl)pyrimidin-2^{I}-yl]amine (0.1 g, 0.3 mmol) with general method A (TLC: $CHCl_3$/MeOH 9/1), (0.2 g, quantitative yield).

^{1}H-NMR (400 MHz, DMSO-*d*$_6$): δ 10.35 (broad s, 1H, NH); 9.95 (broad s, 1H, NH); 9.28 (dd, J=2.2, J=0.8, 1H, 2^{III}-H); 8.97 (broad s, 1H, NH); 8.70 (broad s, 1H, NH); 8.69 (dd, J=4.9, J=1.7, 1H, 6^{III}-H); 8.52 (d, J=5.1, 1H, 6^{II}-H); 8.48 (ddd, J=8.0, J=2.2, J=1.7, 1H, 4^{III}-H); 8.13-8.06 (m, 5H, 5 x Ar-H); 7.56 (dd, J=8.1, J=1.5, 1H, 6^{I}-H); 7.54-7.49 (m, 3H, 3 x Ar-H); 7.44 (d, J=5.1, 1H, 5^{II}-H); 7.26-7.14 (m, 3H, 3 x Ar-H); 2.24 (s, 3H, CH_3); 1.45 (s, 9H, 3 x CH_3).

Synthesis of N^{I}-[(tert-butoxycarbonyl)aminophen-2^{IV}-yl]-N-{4^{I}-methyl-3^{I}-[4^{II}-(pyridin-3^{III}-yl)pyrimidin-2^{II}-yl]aminophenyl}isophthalamide

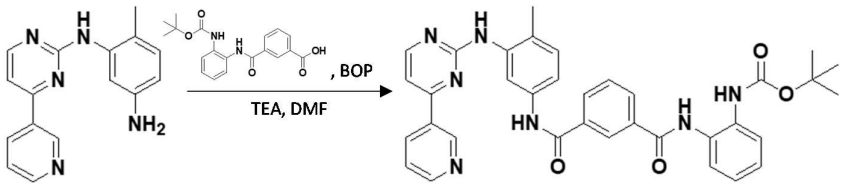

20 **59**

Compound **59** was obtained starting from *N*-[2^{I}-(tert-butoxycarbonyl)aminophenyl]isophthalamic acid (0.2 g, 0.4 mmol) and N^{I}-(2-methyl-5-aminophenyl)-*N*-[4^{I}-(pyridin-3^{II}-yl)pyrimidin-2^{I}-yl]amine (0.1 g, 0.4 mmol) with general method A (TLC: $CHCl_3$/MeOH 9/1), (0.2 g, yield 95%).

^{1}H-NMR (400 MHz, *Acetone-d_6*): δ 9.89 (broad s, 1H, NH); 9.86 (broad s, 1H, NH); 9.33 (dd, J=2.0, J=0.9, 1H, 2^{III}-H); 8.68-5.56 (m, 4H, NH and 3 x Ar-H); 8.53 (dd, J=5.1, J=1.7, 1H, 6^{II}-H); 8.25-8.17 (m, 2H, 4-H and 6-H); 8.01 (broad s, 1H, NH); 7.74-7.67 (m, 2H, 5-H and 3^{IV}-H or 6^{IV}-H); 7.65 (dd, J=8.0, J=1.5, 1H, 6^{I}-H); 7.60 (d, J=8.2,1H, 3^{IV}-H or 6^{IV}-H); 7.49 (dd, J=8.1, J=5.1, 1H, 5^{III}-H); 7.42 (d, J=5.1, 1H, 5^{II}-H);7.27-7.23 (m, 2H, 4^{IV}-H and 5^{IV}-H); 7.22 (m, 2H, 2 x Ar-H); 2.37 (s, 3H, CH_3); 1.45 (s, 9H, 3 x CH_3).

Synthesis of N^{I}-[O-(tetrahydro-pyran-2^{IV}-yl)hydroxy]-N-{4^{I}-methyl-3^{I}-[4^{II}-(pyridin-3^{III}-yl)pyrimidin-2^{II}-yl]aminophenyl}therephthalamide

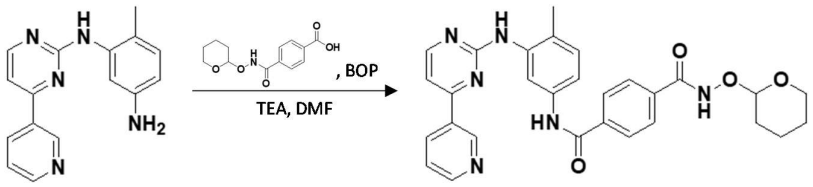

20 **60**

Compound **60** was obtained starting from *N*-[*O*-(tetrahydro-pyran-2^{Iv}-yl)hydroxy]terephthalamic acid (0.1 g, 0.4 mmol) and N^{I}-(2-methyl-5-aminophenyl)-*N*-[4^{I}-(pyridin-3^{II}-yl)pyrimidin-2^{I}-yl]amine (0.1 g, 0.5 mmol) with general method A (TLC: $CHCl_3$/MeOH 9/1 + vanillin), (0.2 g, quantitative yield).

^{1}H-NMR (400 MHz, DMSO-d_6): δ 11.79 (s, 1H, NH); 10.31 (broad s, 1H, NH); 9.28 (dd, J=2.0, J=0.6, 1H, 2^{III}-H); 8.96 (broad s, 1H, NH); 8.68 (dd, J=4.7, J=2.0, 1H, 6^{III}-H); 8.52 (d, J=5.2, 1H, 6^{II}-H);8.48 (dt, J=7.9, J=2.0, 1H, 4^{III}-H); 8.10 (d, J=1.9, 1H, 2^{I}-H); 8.04 (d, J=8.3, 2H, 2-H and 6-H); 7.89 (d, J=8.4, 2H, 3-H and 5-H); 7.52 (ddd, J=7.9, J=4.7, J=0.6, 1H, 5^{III}-H); 7.49 (dd, J=8.3, J=1.9, 1H, 6^{I}-H); 7.43 (d, J=5.2, 1H, 5^{II}-H); 7.22 (d, J=8.3, 1H, 5^{I}-H); 5.03 (s, 1H, 2^{IV}-H); 4.12-4.03 (m, 1H, tetrahydropyran CH_2); 3.59-3.50 (m, 1H, tetrahydropyran CH_2); 2.23 (s, 3H, CH_3); 1.79-1.67 (m, 3H, tetrahydropyran CH_2); 1.63-1.49 (m, 3H, tetrahydropyran CH_2).

Synthesis of N^{I}-(aminophen-2^{IV}-yl)-N-{4^{I}-methyl-3^{I}-[4^{II}-(pyridin-3^{III}-yl)pyrimidin-2^{II}-yl]aminophenyl}terephthalamide

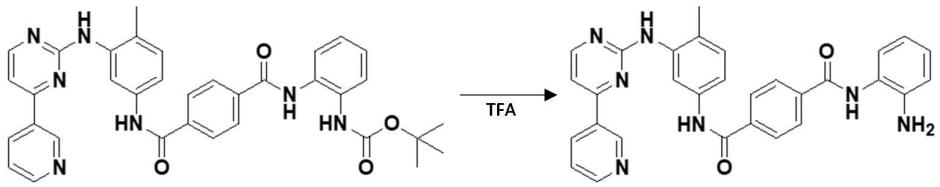

58 **5**

Compound **5** was obtained starting from N^{I}-[(tert-butoxycarbonyl)aminophen-2^{IV}-yl]-*N*-{4^{I}-methyl-3^{I}-[4^{II}-(pyridin-3^{III}-yl)pyrimidin-2^{II}-yl]aminophenyl}terephthalamide (0.3 g, 0.5 mmol) with general method C (TLC: $CHCl_3$/MeOH 9/1), (0.2 g, yield 72%).

^{1}H-NMR (400 MHz, DMSO-d_6): δ 10.33 (broad s, 1H, NH); 9.79 (broad s, 1H, NH); 9.28 (dd, J=2.0, 1H, 2^{III}-H); 8.97 (broad s, 1H, NH); 8.69 (dd, J=5.0, J=1.5, 1H, 6^{III}-H); 8.52 (d, J=5.1, 1H, 6^{II}-H); 8.48 (dd, J=8.0, J=2.0, 1H, 4^{III}-H); 8.15-8.06 (m, 5H, 5 x Ar-H); 7.55-7.49 (m, 2H, 2 x Ar); 7.44 (d, J=5.1, 1H, 5^{II}-H); 7.23 (d, J=8.3, 1H, 5^{I}-H); 7.19 (dd, J=7.5, J=1.5, 1H, 6^{IV}-H); 6.99 (td, J=7.5, J=1.5, 1H, 4^{IV}-H); 6.79 (d, J=7.5, J=1.5, 1H, 3^{IV}-H); 6.61 (d, J=7.5, J=1.5, 1H, 5^{IV}-H); 4.94 (s, 2H, NH_2); 2.24 (s, 3H, CH_3).

Synthesis of N^{I}-(aminophen-2^{IV}-yl)-N-{4^{I}-methyl-3^{I}-[4^{II}-(pyridin-3^{III}-yl)pyrimidin-2^{II}-yl]aminophenyl}isophthalamide

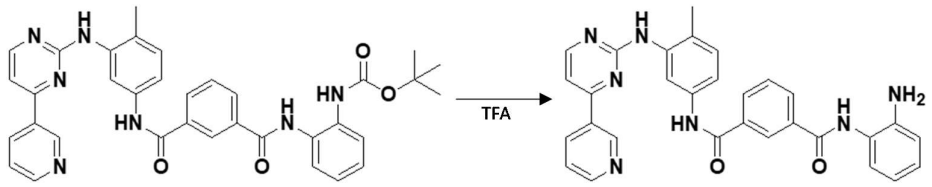

59 **6**

Compound **6** was obtained starting from *N^{I}*-[(tert-butoxycarbonyl)aminophen-2^{IV}-yl]-*N*-{4^{I}-methyl-3^{I}-[4^{II}-(pyridin-3^{III}-yl)pyrimidin-2^{II}-yl]aminophenyl}isophthalamide (0.4 g, 0.6 mmol) with general method C (TLC: $CHCl_3$/MeOH 9/1), (0.4 g, quantitative yield).

^{1}H-NMR (400 MHz, *Acetone-d_6*): δ 9.78 (broad s, 1H, NH); 9.33 (dd, J=2.0, 1H, 2^{III}-H); 8.66 (dd, J=4.8, J=2.0, 1H, 6^{III}-H); 8.63-8.56 (m, 2H, 2^{I}-H and 4^{III}-H); 8.53 (d, J=5.1, 1H, 6^{II}-H); 8.48 (t, J=1.5, 1H, 2-H); 8.22 (dt, J=7.8, J=1.4, 1H, 4-H or 6-H); 8.08 (dt, J=7.8, J=1.4, 1H, 4-H or 6-H); 7.69 (t, J=7.8, 1H, 5-H); 7.56 (dt, J=8.3, J=2.1, 1H, 6^{I}-H); 7.50 (dd, J=8.0, J=4.8, 1H, 5^{III}-H); 7.43 (d, J=5.1, 1H, 5^{II}-H); 7.26 (d, J=8.1, 1H, 5^{I}-H);7.17-7.08 (m, 2H, 4^{IV}-H and 5^{IV}-H); 6.81-6.77 (m, 2H, 3^{IV}-H and 6^{IV}-H);2.37 (s, 3H, CH_3).

Synthesis of N^{I}-hydroxy-N-{4^{I}-methyl-3^{I}-[4^{II}-(pyridin-3^{III}-yl)pyrimidin-2^{II}-yl]aminophenyl}therephthalamide

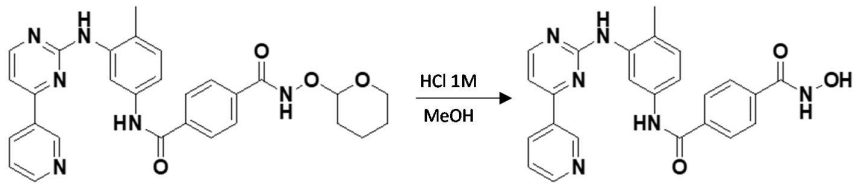

60 **7**

Compound **7** was obtained starting from N^{I}-[*O*-(tetrahydro-pyran-2^{IV}-yl)hydroxy]-*N*-{4^{I}-methyl-3^{I}-[4^{II}-(pyridin-3^{III}-yl)pyrimidin-2^{II}-yl]aminophenyl}therephthalamide (0.2 g, 0.4 mmol) with general method D (TLC: $CHCl_3$/MeOH 9/1), (40 mg, 20% yield).

^{1}H-NMR (400 MHz, DMSO-d_6): δ 11.37 (broad s, 1H, NH); 10.31 (s, 1H, NH); 9.36 (d, J=1.5, 1H, 2^{III}-H); 9.06 (broad s, 1H, NH); 8.79 (dd, J=5.0, J=1.5, 1H, 6^{III}-H); 8.72(dt, J=8.3, J=1.5, 1H, 4^{III}-H); 8.56 (d, J=5.2, 1H, 6^{II}-H); 8.13 (d, J=1.9, 1H, 2^{I}-H); 8.02 (d, J=8.3, 2H, 2-H and 6-H); 7.88 (d, J=8.4, 2H, 3-H and 5-H); 7.73 (dd, J=8.3, J=5.0, 1H, 5^{III}-H); 7.49 (d, J=5.2, 1H, 5^{II}-H); 7.47 (d, J=8.0, J=1.9, 1H, 6^{I}-H); 7.22 (d, J=8.0, 1H, 5^{I}-H); 2.23 (s, 3H, CH_3).

5.3.1.7 SYNTHESIS OF 3-{2^{IV}-CARBAMOYL-VINYL}-5-TRIFLUOROMETHYL-*N*-{4^{I}-METHYL-3^{I}-[4^{II}-(PYRIDIN-3^{III}-YL)PYRIMIDIN-2^{II}-YL]AMINOPHENYL} BENZAMIDE DERIVATIVES

Synthesis of 3-Bromo-5-trifluoromethylbenzoic acid

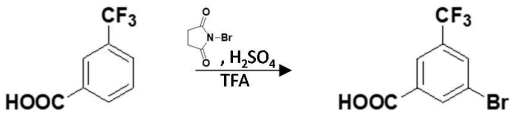

61 **62**

N-Bromosuccinimide (1.3 g, 7.5 mmol) and sulphuric acid 18M (0.7 ml) were added to a solution of 3-trifluoromethylbenzoic acid (1.0 g, 5.0 mmol) in trifluoroacetic acid (2.5 ml). The mixture was stirred 5 hours at 60°C (TLC: $CHCl_3$/MeOH 9/1). After cooling the mixture was poured into water and ice (30 ml) and the obtained precipitate was collected by filtration to give **3-Bromo-5-trifluoromethylbenzoic acid** (1.2 g, 91% yield), mp: 134°C.

^{1}H-NMR (400 MHz, $CDCl_3$-*d*): δ 8.38 (t, J=1.6, 1H, 2-H); 8.23 (t, J=1.6, 1H, 6-H); 8.09 (t, J=1.6, 1H, 4-H).

Synthesis of 3-(2^{I}-ethoxycarbonyl-vinyl)-5-trifluoromethylbenzoic acid

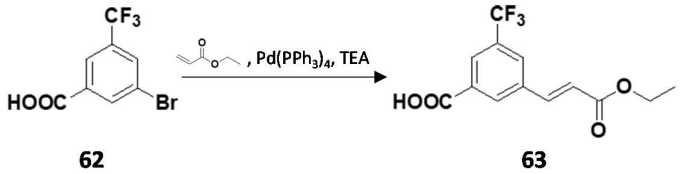

62 **63**

A mixture of 3-bromo-5-trifluoromethylbenzoic acid (1.1 g, 4.0 mmol), ethyl acrylate (0.5 ml, 5.0 mmol), tetrakis(triphenilphosphine)palladium(0) (9 mg, 0.04 mmol) and TEA (0.7 ml, 5.0 mmol) was sealed into a vial. The mixture was heated at 100°C for 16 hours ((TLC: CE/EtOAc 2/8). After cooling the mixture was added to HCl 0.1M (40 ml) and the precipitate collected by filtration and washed with n-hexane to give the **3-(2^{I}-ethoxycarbonyl-vinyl)-5-trifluoromethylbenzoic acid** (0.7 g, 62% yield).

^{1}H-NMR (400 MHz, MeOD-*d*$_4$): δ 8.46 (broad s, 1H, 2-H); 8.27 (broad s, 1H, 6-H); 8.13 (broad s, 1H, 4-H); 7.79(d, J=16.1, 1H, 1^{I}-H); 6.71 (d, J=16.1, 1H, 2^{I}-H); 4.27 (q, J=7.3, 2H, $\underline{CH_2}CH_3$); 1.34 (t, J=7.3, 3H, $CH_2\underline{CH_3}$).

Synthesis of 3-(2^{IV}-ethoxycarbonyl-vinyl)-5-trifluoromethyl-N-{4^{I}-methyl-3^{I}-[4^{II}-(pyridin-3^{III}-yl)pyrimidin-2^{II}-yl]aminophenyl}benzamide

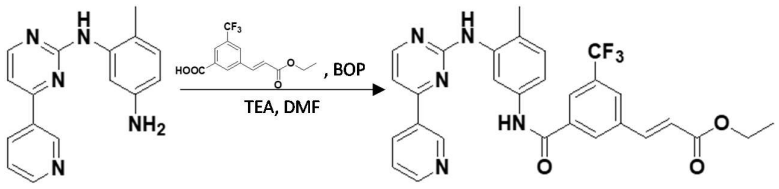

20 **64**

Compound **64** was obtained starting from 3-(2^{I}-ethoxycarbonyl-vinyl)-5-trifluoromethylbenzoic acid (0.6 g, 2.0 mmol) and *N^{I}*-(2-methyl-5-aminophenyl)-*N*-[4^{I}-(pyridin-3^{II}-yl)pyrimidin-2^{I}-yl]amine (0.6 g, 2.2 mmol) with condensation method A (TLC: $CHCl_3$/MeOH 9/1), (1.2 g, quantitative yield).

^{1}H-NMR (300 MHz, DMSO-*d_6*): δ 10.45 (s, 1H, NH); 9.30 (dd, J=2.2, J=0.8, 1H, 2^{III}-H); 9.0 (s, 1H, NH); 8.69 (dd, J=4.8, J=1.7, 1H, 6^{III}-H);8.60 (broad s, 1H, 2-H); 8.52 (d, J=5.1, 1H, 6^{II}-H); 8.48 (ddd, J=8.0, J=2.2, J=1.7, 1H-4^{III}-H); 8.35 (broad s, 1H, 6-H); 8.26 (broad s, 1H, 4-H); 8.11 (d, J=1.9, 1H, 2^{I}-H); 7.84 (d, J=16.1, 1H, 1^{IV}-H); 7.53 (ddd, J=8.0, J=4.8, J=0.8, 1H, 5^{III}-H); 7.49 (dd, J=8.2, J=1.9, 1H, 6^{I}-H); 7.45 (d, J=5.1, 1H, 5^{II}-H); 7.25 (d, J=8.2, 1H, 5^{I}-H); 6.97 (d, J=16.1, 1H, 2^{IV}-H); 4.22 (q, J=7.2, 2H, $\underline{CH_2}CH_3$); 2.24 (s, 3H, CH_3); 1.27 (t, J=7.2, 3H, $CH_2\underline{CH_3}$).

Synthesis of 3-(2^{IV}-hydroxycarbonyl-vinyl)-5-trifluoromethyl-N-{4^{I}-methyl-3^{I}-[4^{II}-(pyridin-3^{III}-yl)pyrimidin-2^{II}-yl]aminophenyl}benzamide

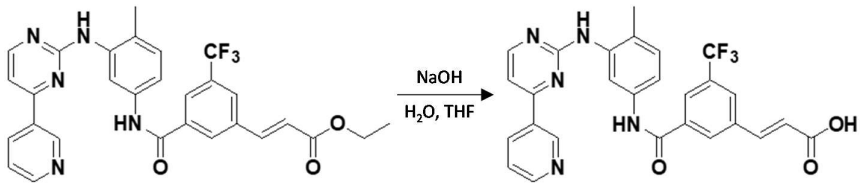

64 **65**

Compound **65** was obtained starting from 3-(2^{IV}-ethoxycarbonyl-vinyl)-5-trifluoromethyl-*N*-{4^{I}-methyl-3^{I}-[4^{II}-(pyridin-3^{III}-yl)pyrimidin-2^{II}-yl]aminophenyl}benzamide (1.1 g, 2.0 mmol) in THF with general method B (TLC: $CHCl_3$/MeOH 9/1), (1.0 g, 92% yield).

^{1}H-NMR (300 MHz, DMSO-d_6): δ 12.65 (broad s, 1H, OH); 10.46 (s, 1H, NH); 9.31 (dd, J=2.2, J=0.7, 1H, 2^{III}-H); 9.02 (s, 1H, NH); 8.71 (dd, J=4.8, J=1.6, 1H, 6^{III}-H); 8.58 (t, J=1.7, 1H, 2-H); 8.53 (d, J=5.2, 1H, 6^{II}-H); 8.52 (ddd, J=8.0, J=2.2, J=1.6, 1H, 4^{III}-H); 8.30 (t, J=1.7, 1H, 6-H); 8.25 (t, J=1.7, 1H, 4-H); 8.11 (d, J=2.1, 1H, 2^{I}-H); 7.77 (d, J=16.0, 1H, 1^{IV}-H); 7.56 (ddd, J=8.0, J=4.8, J=0.7, 1H, 5^{III}-H); 7.49 (dd, J=8.2, J=2.1, 1H, 6^{I}-H); 7.46 (d, J=5.2, 1H, 5^{II}-H); 7.25 (d, J=8.2, 1H, 5^{I}-H); 6.85 (d, J=16.1, 1H, 2^{IV}-H); 2.24 (s, 3H, CH_3).

Synthesis of 3-{2^{IV}-[2^{V}-(tert-butoxycarbonyl)aminophenyl]carbamoyl-vinyl}-5-trifluoromethyl-N-{4^{I}-methyl-3^{I}-N-[4^{II}-(pyridin-3^{III}-yl)pyrimidin-2^{II}-yl]aminophenyl}benzamide

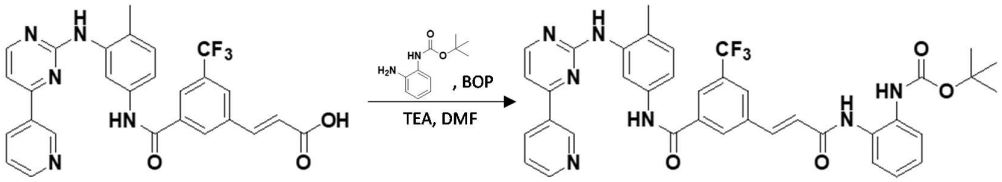

65 **66**

Compound **66** was obtained starting from 3-(2^{IV}-hydroxycarbonyl-vinyl)-5-trifluoromethyl-*N*-{4^{I}-methyl-3^{I}-[4^{II}-(pyridin-3^{III}-yl)pyrimidin-2^{II}-yl]aminophenyl}benzamide (0.3 g, 0.5 mmol) and 2-(tert-butoxycarbonyl)aminoaniline (0.1 g, 0.6 mmol) accordingly to the general method B (TLC: $CHCl_3$/MeOH 9/1), (0.4 g, quantitative yield).

^{1}H-NMR (300 MHz, Acetone-*d*$_6$): δ 9.88 (s broad, 1H, NH); 9.42 (s broad, 1H, NH); 9.37 (d, J=1.6, 1H, 2^{III}-H); 8.70 (dd, J=5.1, J=1.6, 1H, 6^{III}-H); 8.61-8.52 (m, 4H, 2^{I}-H, 6^{II}-H, 4^{III}-H and NH); 8.33 (s, 1H, 2-H); 8.18 (s, 1H, 6-H); 8.03 (s, 1H, 4-H); 7.87 (d, J=16.0, 1H, 1^{IV}-H); 7.71 (d, J=8.1, 1H, 6^{V}-H); 7.63-7.54 (m, 2H, 6^{I}-H and 3^{V}-H); 7.52 (dd, J=8.0, J=5.1, 1H, 5^{III}-H); 7.44 (d, J=5.1, 1H, 5^{II}-H); 7.30-7.23 (m, 4H, 5^{I}-H, 2^{IV}-H, 4^{V}-H and 5^{V}-H); 2.38 (s, 3H, CH_3); 1.47 (s, 9H, 3 x CH_3).

Synthesis of 3-{2^{IV}-[O-(tetrahydro-pyran-2^{V}-yl)hydroxylamino]carbonyl-vinyl}-5-trifluoromethyl-N-{4^{I}-methyl-3^{I}-N-[4^{II}-(pyridin-3^{III}-yl)pyrimidin-2^{II}-yl]aminophenyl}benzamide

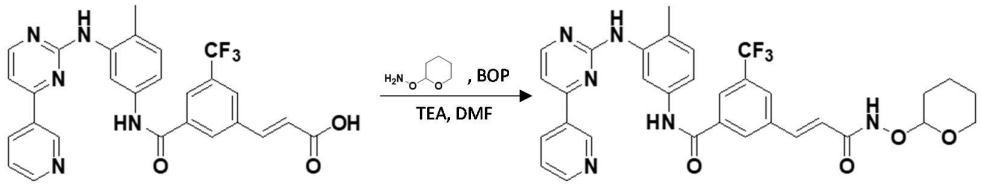

65 **67**

Compound **67** was obtained starting from 3-(2^{IV}-hydroxycarbonyl-vinyl)-5-trifluoromethyl-*N*-{4^{I}-methyl-3^{I}-[4^{II}-(pyridin-3^{III}-yl)pyrimidin-2^{II}-yl]aminophenyl}benzamide (0.3 g, 0.5 mmol) and *O*-(tetrahydro-2*H*-pyran-2-yl)hydroxylamine (64 mg, 0.6 mmol) with general method A (TLC: $CHCl_3$/MeOH 9/1 + vanillin), (0.3 g, quantitative yield).

^{1}H-NMR (300 MHz, DMSO-d_6): δ 11.34 (s broad, 1H, NH); 10.49 (s, 1H, NH); 9.29 (d, J=1.6, 1H, 2^{III}-H); 9.01 (s, 1H, NH); 8.69 (dd, J= 4.7, J=1.4, 1H, 6^{III}-H); 8.52 (d, J=5.4, 1H, 6^{II}-H); 8.50-8.42 (m, 2H, 2^{I}-H and 4^{III}-H); 8.26 (s, 1H, 2-H); 8.17 (s, 1H, 6-H); 8.08 (s, 1H, 4-H); 7.67 (d, J=16.1, 1H,1^{IV}-H); 7.52 (dd, J=7.5, J=4.7, 1H, 5^{III}-H); 7.49 (dd, J=8.5, J=2.3, 1H, 6^{I}-H); 7.44 (d, J=5.4, 1H, 5^{II}-H); 7.25 (d, J=8.5, 1H, 5^{I}-H); 6.77 (d, J=16.1, 1H, 2^{IV}-H); 4.93 (broad s, 1H, 2^{V}-H); 4.01-3.89 (m, 2H, tetrahydropyran CH_2); 2.24 (s, 3H, CH_3); 1.76-1.67 (m, 3H, tetrahydropyran CH_2); 1.58-1.50 (m, 3H, tetrahydropyran CH_2).

Synthesis of 3-[2^{IV}-(aminophen-2^{V}-yl)carbamoyl-vinyl]-5-trifluoromethyl-N-{4^{I}-methyl-3^{I}-N-[4^{II}-(pyridin-3^{III}-yl)pyrimidin-2^{II}-yl]aminophenyl}benzamide

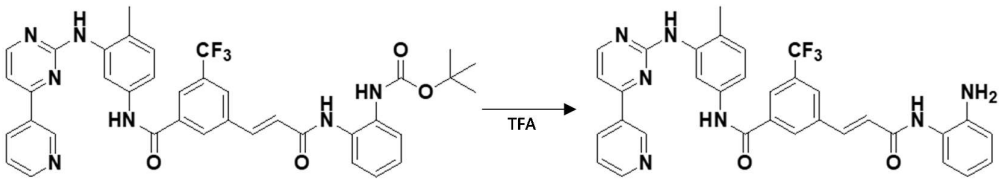

66 **8**

Compound **8** was obtained starting from 3-{2^{IV}-[2^{V}-(tert-butoxycarbonyl)aminophenyl]carbamoyl-vinyl}-5-trifluoromethyl-*N*-{4^{I}-methyl-3^{I}-*N*-[4^{II}-(pyridin-3^{III}-yl)pyrimidin-2^{II}-yl]aminophenyl}benzamide (0.4 g, 0.5 mmol) with general method C (TLC: $CHCl_3$/MeOH 9/1), (0.3 g, 88% yield).

^{1}H-NMR (400 MHz, DMSO-*d*$_6$): δ 10.51 (s broad, 1H, NH); 9.42 (s broad, 1H, NH); 9.29 (d, J=1.7, 1H, 2^{III}-H); 9.01 (s broad, 1H, NH); 8.69 (dd, J=4.7, J=1.7, 1H, 6^{III}-H); 8.52 (d, J=5.2, 1H, 6^{II}-H); 8.50-8.46 (m, 2H, 2^{I}-H and 4^{III}-H); 8.29 (s, 1H, 2-H); 8.20 (s, 1H, 6-H); 8.09 (s, 1H, 4-H); 7.73 (d, J=15.8, 1H, 1^{IV}-H); 7.55 (m, 2H, 6^{I}-H and 5^{III}-H); 7.44 (d, J=5.2, 1H, 5^{II}-H); 7.40 (dd, J=8.2, J=1.2, 1H, 3^{V}-H); 7.25 (d, J=8.4, 1H, 5^{I}-H); 7.16 (d, J=15.8, 1H, 2^{IV}-H); 6.93 (td, J=8.2, J=1.2, 1H, 5^{V}-H); 6.76 (dd, J=8.2, 1.2, 1H, 6^{V}-H); 6.58 (td, J=8.2, J=1.2, 1H, 4^{V}-H); 2.24 (s, 3H, CH_3).

Synthesis of 3-[(2^{IV}-hydroxylamino)carbonyl-vinyl]-5-trifluoromethyl-N-{4^{I}-methyl-3^{I}-N-[4^{II}-(pyridin-3^{III}-yl)pyrimidin-2^{II}-yl]aminophenyl}benzamide

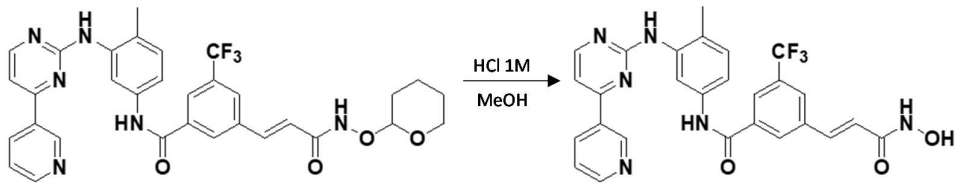

67 **9**

Compound **9** was obtained starting From 3-{2^{IV}-[*O*-(tetrahydro-pyran-2^{V}-yl)hydroxylamino]carbonyl-vinyl}-5-trifluoromethyl-*N*-{4^{I}-methyl-3^{I}-*N*-[4^{II}-(pyridin-3^{III}-yl)pyrimidin-2^{II}-yl]aminophenyl}benzamide with general method D (TLC: $CHCl_3$/MeOH 9/1 + vanillin), (0.2 g, 75% yield).

^{1}H-NMR (500 MHz, DMSO-*d*$_6$): δ 10.57 (s, 1H, NH); 9.49 (d, J=1.7, 1H, 2^{III}-H); 9.22 (s, 1H, NH); 9.02 (dt, J= 8.1, J=1.7, 1H, 4^{III}-H); 8.95 (d, J=5.5, 1H, 6^{III}-H); 8.63 (d, J=5.2, 1H, 6^{II}-H); 8.46 (t, J=1.5, 1H, 2-H); 8.26 (t, J=1.5, 1H, 6-H); 8.17-8.13 (m, 2H, 4-H and 2^{I}-H); 8.0 (dd, J=8.1, J=5.5, 1H, 5^{III}-H); 7.63 (d, J=16.2, 1H, 1^{IV}-H); 7.59 (d, J=5.2, 1H, 5^{II}-H); 7.47 (dd, J=8.4, J=2.0, 1H, 6^{I}-H); 7.26 (d, J=8.4, 1H, 5^{I}-H); 6.75 (d, J=16.2, 1H, 2^{IV}-H); 2.24 (s, 3H, CH_3).

^{13}C-NMR (500 MHz, DMSO-*d*$_6$): δ 163.54; 161.64; 161.16; 159.49; 151.41; 148.21; 148.23; 146.25; 137.93; 136.69; 136.61; 136.54; 135.95; 134.41; 132.18; 130.18; 129.86; 128.06; 126.95; 124.66; 123.78; 122.41; 117.27; 116.80; 107.62; 90.36; 17.66.

IR ν_{max}/cm^{-1}: 3428 (hydroxamic acid N-H); 3240 (hydroxamic acid O-H); 1663 (benzamide C=O); 1583 (hydroxamic acid C=O); 1552 (hydroxamic acid C-N).

Elemental analysis for $C_{27}H_{21}F_3N_6O_3$:

Calcd: C 60.67%; H 3.96%; N 15.72%. Found: C 61.47%; H 3.93%; N 15.39%.

5.3.1.8 SYNTHESIS OF 3-{4^{IV}-[(2^{V}-HYDROXYLAMINO)CARBONYL-VINYL]IMIDAZOL-1^{IV}-YL}-5-TRIFLUOROMETHYLBENZAMIDE DERIVATIVES

Synthesis of Ethyl urocanate

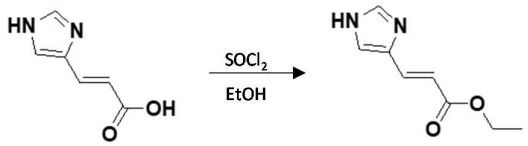

70 **71**

A mixture of $SOCl_2$ (1.1 ml, 15.0 mmol) and urocanic acid (1.4 g, 10.0 mmol) suspended in EtOH (50 ml) was heated to reflux for 3 hours (TLC: $CHCl_3$/MeOH 9/1 + 1% Formic acid). After cooling the solvent was evaporated under vacuum and then the mixture was diluted with H_2O (50 ml) and was neutralized with $NaHCO_3$. The water solution was extracted with EtOAc (3 x 25 ml); the organic phase was dried over anhydrous sodium sulfate and evaporated to give **ethyl urocanate** (1.7 g, quantitative yield).

^{1}H-NMR (300 MHz, DMSO-*d*$_6$): δ 12.46 (broad s, 1H, NH); 7.77 (s, 1H, 2-H); 7.54 (s, 1H, 5-H); 7.52 (d, J=16.0, 1H, 1^{I}-H); 6.32 (d, J=16.0, 1H, 2^{I}-H); 4.14 (q, J=7.2, 2H, $\underline{CH_2}CH_3$); 1.23 (t, J=7.2, 3H, $CH_2\underline{CH_3}$).

Synthesis of 3-Fluoro-5-trifluoromethyl-N-{4^{I}-methyl-3^{I}-[4^{II}-(pyridin-3^{III}-yl)pyrimidin-2^{II}-yl]aminophenyl}benzamide)

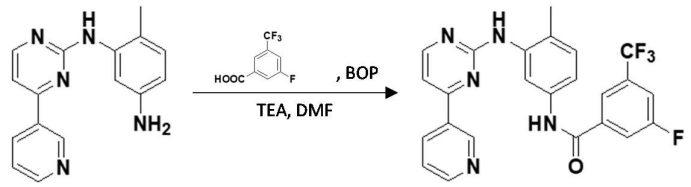

20 **73**

Compound **73** was obtained starting from 3-Fluoro-5-trifluoromethylbenzoic acid (0.1 g, 0.5 mmol) and *N^{I}*-(2-methyl-5-aminophenyl)-*N*-[4^{I}-(pyridin-3^{II}-yl)pyrimidin-2^{I}-yl]amine (0.2 g, 0.6 mmol) with the general method A (TLC: $CHCl_3$/MeOH 9/1), (0.2 g, quantitative yield).

^{1}H-NMR (400 MHz, *Acetone-d$_6$*): δ 9.83 (s, 1H, NH); 9.34 (dd, J=2.2, J=0.9, 1H, 2^{III}-H); 8.68 (dd, J=4.9, J=1.9, 1H; 6^{III}-H); 8.58 (ddd, J=7.7, J=4.9, J=1.6, 1H, 4^{III}-H); 8.54 (d, J=5.1, 1H, 6^{II}-H); 8.53 (s, 1H, NH); 8.20 (s, 1H, 2^{I}-H); 8.10 (dt, J=8.5, J=1.5, 1H, 2-H); 8.02 (s, 1H, 6-H); 7.76 (dt, J=8.5, J=1.5, 1H, 4-H); 7.53-7.47 (m, 2H, 6^{I}-H and 5^{III}-H); 7.43 (d, J=5.1, 1H, 5^{II}-H); 7.26 (d, J=8.2, 1H, 5^{I}-H); 2.37 (s, 3H, CH_3).

Synthesis of 3-[4^{IV}-(2^{V}-ethoxycarbonyl-vinyl)imidazol-1^{IV}-yl]-5-trifluoromethyl-N-{4^{I}-methyl-3^{I}-[4^{II}-(pyridin-3^{III}-yl)pyrimidin-2^{II}-yl]aminophenyl}benzamide

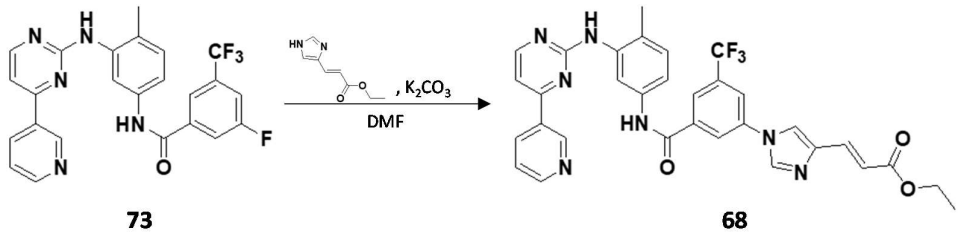

73 **68**

A mixture of 3-Fluoro-5-trifluoromethyl-*N*-{4^{I}-methyl-3^{I}-[4^{II}-(pyridin-3^{III}-yl)pyrimidin-2^{II}-yl]aminophenyl}benzamide (0.3 g, 0.6 mmol), ethyl urocanate (0.5 g, 3.0 mmol) and K_2CO_3 (0.8 g, 6.0 mmol) in DMF (6 ml) was sealed in a tube under nitrogen atmosphere. The mixture was heated to 120°C for 10 hours (TLC: $CHCl_3$/MeOH 9/1). After cooling, the mixture was diluted with a saturated solution of NH_4Cl in H_2O (60 ml), the solid precipitate was collected by filtration and washed with abundant water to give **3-[4^{IV}-(2^{V}-ethoxycarbonyl-vinyl)imidazol-1^{IV}-yl]-5-trifluoromethyl-*N*-{4^{I}-methyl-3^{I}-[4^{II}-(pyridin-3^{III}-yl)pyrimidin-2^{II}-yl]aminophenyl}benzamide** (0.3 g, 86 % yield).

^{1}H-NMR (300 MHz, DMSO-d_6): δ 10.55 (s, 1H, NH); 9.29 (d, J=2.1, 1H, 2^{III}-H); 9.02 (s, 1H, NH); 8.68 (dd, J=5.0, J=1.5, 1H, 6^{III}-H); 8.64 (s, 1H, 2^{IV}-H); 8.56-8.43 (m, 4H, 6-H, 6^{II}-H, 4^{III}-H and 5^{IV}-H); 8.32 (s, 1H, 2-H); 8.25 (s, 1H, 4-H); 8.10 (d, J=1.4, 1H, 2^{I}-H); 7.59-7.49 (m, 3H, 6^{I}-H, 5^{III}-H and 1^{V}-H); 7.45 (d, J=5.1, 1H, 5^{II}-H); 7.26 (d, J=8.0, 1H, 5^{I}-H); 6.48 (d, J=15.5, 1H, 2^{V}-H); 4.17 (q, J=7.0, 2H, $\underline{CH_2}CH_3$); 2.25 (s, 3H, CH_3); 1.25 (t, J=7.0, 3H, $CH_2\underline{CH_3}$).

Synthesis of 3-bromo-5-trifluoromethylnitrobenzene

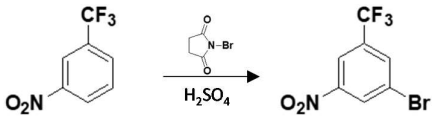

74 **75**

A solution of 3-nitrobenzotrifluoride (1.9 g, 10.0 mmol) in H_2SO_4 conc. (10 ml) was warmed to 60°C and then *N*-Br-succinimide (2.1 g, 12.0 mmol) was added to the mixture. The mixture was stirred at 60°C for 2 hours (TLC: $CHCl_3$/CE 1/1). After cooling the mixture was poured into H_2O (200 ml) and extracted with CH_2Cl_2 (3 x 70 ml), the organic phase was subsequently dried over anhydrous sodium sulfate and evaporated to give **3-bromo-5-trifluoromethylnitrobenzene** (2.3 g, 87% yield).

^{1}H-NMR (300 MHz, $CDCl_3$-*d*): δ 8.57 (t, J=1.7, 1H, 2-H); 8.44 (t, J=1.7, 1H, 6-H); 8.10 (t, J=1.7, 1H, 4-H).

Synthesis of 3-[4^{I}-(2^{II}-ethoxycarbonyl-vinyl)imidazol-1^{I}-yl]-5-trifluoromethyl-nitrobenzene

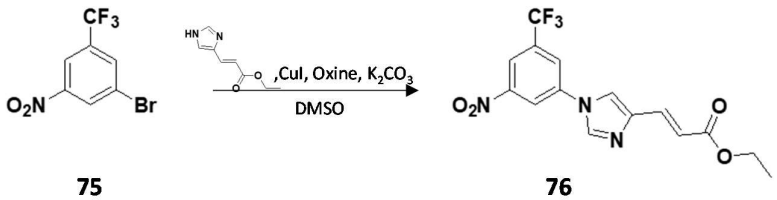

75 **76**

A mixture of 3-bromo-5-trifluoromethylnitrobenzene (1.6 g, 6.0 mmol), CuI (0.2 g, 1.2 mmol), 8-hydroxyquinoline (0.2 g, 1.2 mmol), ethyl urocanate (2.0 g, 12.0 mmol) and K_2CO_3 (1.7 g, 12.0 mmol) in DMSO (30 ml) was sealed in a tube under nitrogen atm. The mixture was heated to 100°C for 24 hours (TLC: $CHCl_3$/MeOH 9/1). After cooling, the mixture was poured into a saturated water solution of NH_4Cl (500 ml) and was extracted with EtOAc (3 x 150 ml). The organic phase was dried over anhydrous sodium sulfate and evaporated to give **3-[4^{I}-(2^{II}-ethoxycarbonyl-vinyl)imidazol-1^{I}-yl]-5-trifluoromethyl-nitrobenzene** (0.7 g, 35% yield).

^{1}H-NMR (400 MHz, DMSO-d_6): δ 8.84 (t, J=1.8, 1H, 2-H); 8.72 (d, J=0.8, 1H, 2^{I}-H); 8.60 (t, J=1.8, 1H, 6-H); 8.54 (d, J=0.8, 1H, 5^{I}-H); 8.47 (t, J=1.8, 1H, 4-H); 7.53 (d, J=15.7, 1H, 1^{II}-H); 6.49 (d, J=15.7, 1H, 2^{II}-H); 4.18 (q, J=7.0, 2H, $\underline{CH_2}CH_3$); 1.26 (t, J=7.0, 3H, $CH_2\underline{CH_3}$).

Synthesis of 3-{4^{I}-(2^{II}-ethoxycarbonyl-vinyl)imidazol-1^{I}-yl}-5-trifluoromethylaniline

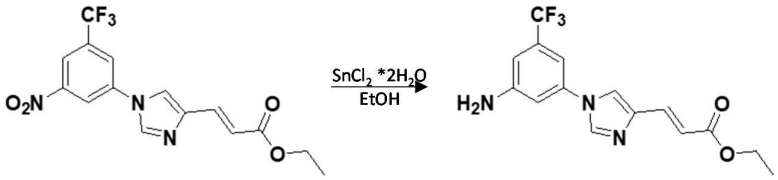

76 **77**

A mixture of 3-[4^{I}-(2^{II}-ethoxycarbonyl-vinyl)imidazol-1^{I}-yl]-5-trifluoromethyl-nitrobenzene (0.4 g, 1.0 mmol) and $SnCl_2$*$2H_2O$ (1.3 g, 6.0 mmol) in EtOH (10 ml) was heated at 60°C for 1 hour (TLC: $CHCl_3$/MeOH 9/1). After cooling, the solvent was evaporated under vacuum and an aqueous solution of saturated $NaHCO_3$ (100 ml) was added to the solid residue. The mixture was extracted with Et_2O (3 x 40 ml), the organic phase was dried over anhydrous sodium sulphate and evaporated to give **3-{4^{I}-(2^{II}-ethoxycarbonyl-vinyl)imidazol-1^{I}-yl}-5-trifluoromethylaniline** (0.3 g, 97% yield).

^{1}H-NMR (400 MHz, DMSO-*d*$_6$): δ 8.31 (d, J=0.8, 1H, 2^{I}-H); 8.14 (d, J=0.8, 1H, 5^{I}-H); 7.54 (d, J=15.5, 1H, 1^{II}-H); 7.04 (t, J=1.9, 1H, 4-H); 6.97 (t, J=1.9, 1H, 2-H); 6.88 (t, J=1.9, 1H, 6-H); 6.44 (d, J=15.5, 1H, 2^{II}-H); 4.17 (q, J=7.2, 2H, $\underline{CH_2}CH_3$); 1.25 (t, J=7.2, 3H, $CH_2\underline{CH_3}$).

Synthesis of 4-methyl-N-{3^{III}-[4^{IV}-(2^{V}-ethoxycarbonyl-vinyl)imidazol-1^{IV}-yl]-5^{III}-trifluoromethyl-phenyl}-3-{[4^{I}-(pyridin-3^{II}-yl)pyrimidin-2^{I}-yl]amino}benzamide

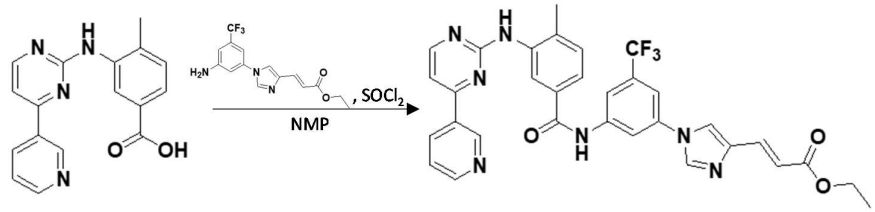

21 **69**

A solution of 4-methyl-3-{[4^{I}-(pyridin-3^{II}-yl)pyrimidin-2^{I}-yl]amino}benzoic acid (0.1 g, 0.3 mmol), 3-{4^{I}-(2^{II}-ethoxycarbonyl-vinyl)imidazol-1^{I}-yl}-5-trifluoromethylaniline (0.1 g, 0.3 mmol) and $SOCl_2$ (0.1 ml, 1.2 mmol) in NMP (0.5 ml) was heated at 90°C for 16 hours (TLC: $CHCl_3$/MeOH 9/1). After cooling, the mixture was poured into a saturated solution of $NaHCO_3$ in H_2O (20 ml). The solid precipitate was collected by filtration. The residue was purified by flash chromatography (EtOAc/n-ex 95/5), to give **4-methyl-*N*-{3^{III}-[4^{IV}-(2^{V}-ethoxycarbonyl-vinyl)imidazol-1^{IV}-yl]-5^{III}-trifluoromethyl-phenyl}-3-{[4^{I}-(pyridin-3^{II}-yl)pyrimidin-2^{I}-yl]amino}benzamide** (0.1 g, 45% yield).

^{1}H-NMR (400 MHz, DMSO-*d*$_6$): δ 10.68 (s, 1H, NH); 9.28 (dd, J=2.1, J=0.7, 1H, 2^{II}-H); 9.15 (s, 1H, NH); 8.68 (dd, J=4.8, J=1.5, 1H, 6^{II}-H); 8.55 (d, J=5.0, 1H, 6^{I}-H); 8.44 (ddd, J=8.0, J=2.1, J=1.5, 1H, 4^{II}-H); 8.43 (d, J=1.0, 1H, 2^{IV}-H); 8.38 (t, J=1.8, 1H, 2^{III}-H); 8.33 (d, J=1.7, 1H, 2-H); 8.24 (d, J=1.0, 1H, 5^{IV}-H); 8.21 (t, J=1.8, 1H, 6^{III}-H); 7.80 (t, J=1.8, 1H, 4^{III}-H); 7.77 (dd, J=8.2, J=1.7, 1H, 6-H); 7.57 (d, J=15.8, 1H, 1^{V}-H); 7.51 (ddd, J=8.0, J=4.8, J=0.7, 1H, 5^{II}-H); 7.48 (d, J=5.0, 1H, 5^{I}-H); 7.46 (d, J=8.2, 1H, 5-H); 6.47 (d, J=15.8, 1H, 2^{V}-H); 4.18 (q, J=7.2, 2H, $\underline{CH_2}CH_3$); 2.33 (s, 3H, CH_3); 1.25 (t, J=7.2, 3H, $CH_2\underline{CH_3}$).

Synthesis of 3-[4^{IV}-(2^{V}-hydroxycarbonyl-vinyl)imidazol-1^{IV}-yl]-5-trifluoromethyl-N-{4^{I}-methyl-3^{I}-[4^{II}-(pyridin-3^{III}-yl)pyrimidin-2^{II}-yl]aminophenyl}benzamide

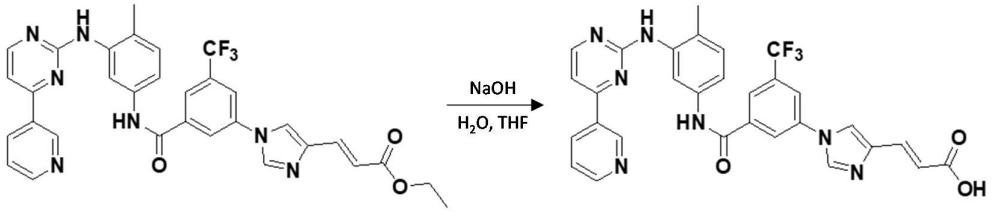

68 **78**

Compound **78** was obtained starting from 3-[4^{IV}-(2^{V}-ethoxycarbonyl-vinyl)imidazol-1^{IV}-yl]-5-trifluoromethyl-*N*-{4^{I}-methyl-3^{I}-[4^{II}-(pyridin-3^{III}-yl)pyrimidin-2^{II}-yl]aminophenyl}benzamide (0.3 g, 0.5 mmol) in THF with the general method B (TLC: $CHCl_3$/MeOH 9/1), (0.1 g, 47% yield).

^{1}H-NMR (400 MHz, DMSO-d_6): δ 10.52 (s, 1H, NH); 9.32 (d, J=2.1, 1H, 2^{III}-H); 9.02 (s, 1H, NH); 8.72 (dd, J=4.8, J=1.7, 1H, 6^{III}-H); 8.65 (s, 1H, 2^{IV}-H); 8.59-8.52 (m, 3H, 6-H, 6^{II}-H and 4^{III}-H); 8.42 (s, 1H, 5^{IV}-H); 8.33 (s, 1H, 2-H); 8.26 (s, 1H, 4-H); 8.11 (d, J=1.8, 1H, 2^{I}-H); 7.60 (dd, J=8.0, J=4.8, 1H, 5^{III}-H); 7.54-7.45 (m, 3H, 6^{I}-H, 5^{II}-H and 1^{V}-H); 7.27 (d, J=8.4, 1H, 5^{I}-H); 6.48 (d, J=16.0, 1H, 2^{V}-H); 2.25 (s, 3H, CH_3).

Synthesis of 4-methyl-N-{3^{III}-[4^{IV}-(2^{V}-hydroxycarbonyl-vinyl)imidazol-1^{IV}-yl]-5^{III}-trifluoromethyl-phenyl}-3-{[4^{I}-(pyridin-3^{II}-yl)pyrimidin-2^{I}-yl]amino}benzamide

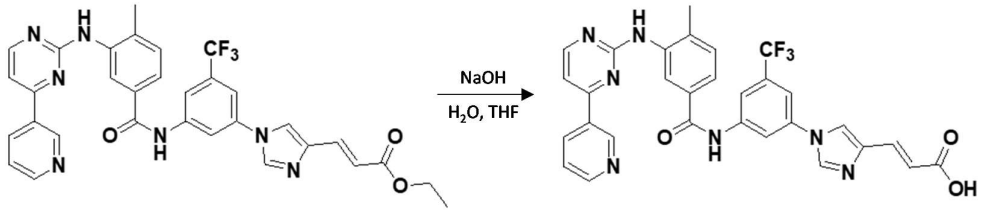

69 **79**

Compound **79** was obtained starting from 4-methyl-*N*-{3^{III}-[4^{Iv}-(2^{v}-ethoxycarbonyl-vinyl)imidazol-1^{Iv}-yl]-5^{III}-trifluoromethyl-phenyl}-3-{[4^{I}-(pyridin-3^{II}-yl)pyrimidin-2^{I}-yl]amino}benzamide (0.1 g, 0.1 mmol) in THF with the hydrolysis general method B (TLC: $CHCl_3$/MeOH 9/1), (42 mg, 55% yield).

^{1}H-NMR (400 MHz, DMSO-*d*$_6$): δ 12.22 (broad s, 1H, OH); 10.67 (s, 1H, NH); 9.28 (d, J=1.8, 1H, 2^{II}-H); 9.15 (s, 1H, NH); 8.68 (dd, J=4.7, J=1.8, 1H, 6^{II}-H); 8.55 (d, J=5.1, 1H, 6^{I}-H); 8.44 (dt, J=8.1, J=1.8, 1H, 4^{II}-H); 8.42 (s, 1H, 2^{Iv}-H); 8.37 (s, 1H, 2^{III}-H); 8.33 (d, J=1.6, 1H, 2-H); 8.23-8.19 (m, 2H, 6^{III}-H and 5^{Iv}-H); 7.81 (s, 1H, 4^{III}-H); 7.77 (dd, J=8.0, J=1.6, 1H, 6-H); 7.54-7.44 (m, 4H, 5-H, 5^{I}-H, 5^{II}-H and 1^{v}-H); 6.42 (d, J=15.5, 1H, 2^{v}-H); 2.36 (s, 3H, CH_3).

Synthesis of 3-(4^{IV}-{2^{V}-[O-(tetrahydro-pyran-2^{VI}-yl)hydroxylamino]carbonyl-vinyl}imidazol-1^{IV}-yl)-5-trifluoromethyl-N-{4^{I}-methyl-3^{I}-[4^{II}-(pyridin-3^{III}-yl)pyrimidin-2^{II}-yl]aminophenyl}benzamide

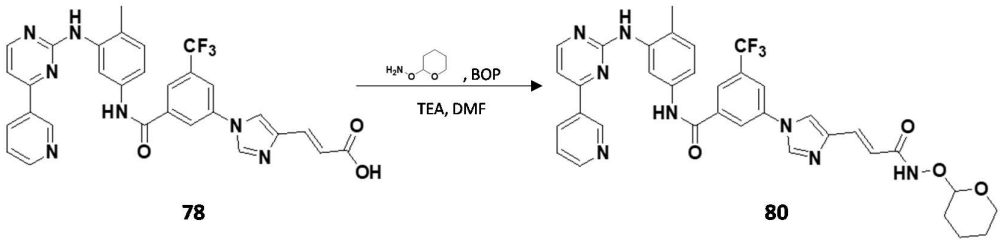

Compound **80** was obtained starting from 3-[4^{IV}-(2^{V}-hydroxycarbonyl-vinyl)imidazol-1^{IV}-yl]-5-trifluoromethyl-*N*-{4^{I}-methyl-3^{I}-[4^{II}-(pyridin-3^{III}-yl)pyrimidin-2^{II}-yl]aminophenyl}benzamide (0.1 g, 0.2 mmol) and *O*-(tetrahydro-2*H*-pyran-2-yl)hydroxylamine (31.0 mg, 0.3 mmol) with general method A (TLC: $CHCl_3$/MeOH 9/1 + vanillin), (0.1 g, 55% yield).

^{1}H-NMR (400 MHz, DMSO-*d*$_6$): δ 11.21 (broad s, 1H,NH); 10.49 (s, 1H, NH); 9.29 (dd, J=2.0, J=0.6, 1H, 2^{III}-H); 8.98 (s, 1H, NH); 8.68 (dd, J=4.6, J=2.0, 1H, 6^{III}-H); 8.59 (s, 1H, 2^{IV}-H);8.52 (d, J=5.2, 1H, 6^{II}-H); 8.51 (s, 1H, 6-H); 8.48 (dt, J=8.0, J=2.0, 1H, 4^{III}-H); 8.33-8.28 (m, 2H, 2-H and 5^{IV}-H); 8.23 (s, 1H, 4-H); 8.10 (d, J=2.0, 1H, 2^{I}-H); 7.55-7.49 (m, 2H, 6^{I}-H and 5^{III}-H); 7.44 (d, J=5.1, 1H, 5^{II}-H); 7.40 (d, J=15.6, 1H, 1^{V}-H); 7.27 (d, J=8.4, 1H, 5^{I}-H); 6.58 (d, J=15.6, 1H, 2^{V}-H); 4.91 (s, 1H, 2^{VI}-H); 4.00-3.92 (m, 1H, tetrahydropyran CH_2); 3.57-3.49 (m, 1H, tetrahydropyran CH_2); 2.25 (s, 3H, CH_3); 1.74-1.64 (m, 3H, tetrahydropyran CH_2); 1.60-1.47 (m, 3H, tetrahydropyran CH_2).

Synthesis of 4-methyl-N-[3^{III}-(4^{IV}-{2^{V}-[O-(tetrahydro-pyran-2^{VI}-yl)hydroxylamino]carbonyl-vinyl}imidazol-1^{IV}-yl)-5^{III}-trifluoromethyl-phenyl]-3-{[4^{I}-(pyridin-3^{II}-yl)pyrimidin-2^{I}-yl]amino}benzamide

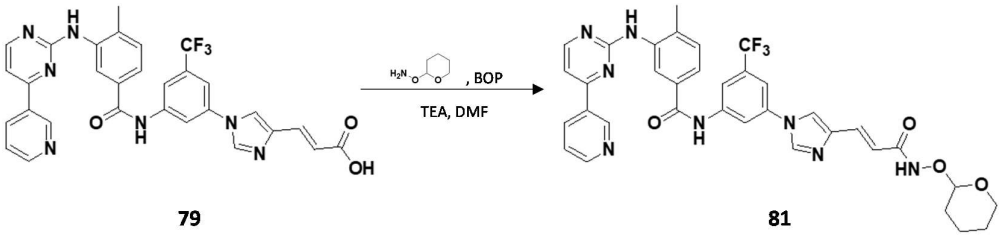

79 **81**

Compound **81** was obtained starting from 4-methyl-*N*-{3^{III}-[4^{IV}-(2^{V}-hydroxycarbonyl-vinyl)imidazol-1^{IV}-yl]-5^{III}-trifluoromethyl-phenyl}-3-{[4^{I}-(pyridin-3^{II}-yl)pyrimidin-2^{I}-yl]amino}benzamide (41 mg, 0.1 mmol) and *O*-(tetrahydro-2*H*-pyran-2-yl)hydroxylamine (10 mg, 0.1 mmol) with general method A (TLC: $CHCl_3$/MeOH 9/1 + vanillin), (34 mg, 55% yield).

^{1}H-NMR (400 MHz, DMSO-d_6): δ 11.21 (broad s, 1H, NH); 10.66 (s, 1H, NH); 9.28 (d, J=1.9, 1H, 2^{II}-H); 9.15 (s, 1H, NH); 8.68 (dd, J=4.8, J=1.9, 1H, 6^{II}-H); 8.55 (d, J=5.1, 1H, 6^{I}-H); 8.44 (dt, J=7.9, J=1.9, 1H, 4^{II}-H); 8.40 (s, 1H, 2^{IV}-H); 8.36 (s, 1H, 2^{III}-H); 8.33 (d, J=1.6, 1H, 2-H); 8.21 (s, 1H, 6^{III}-H); 8.09 (s, 1H, 5^{IV}-H); 7.80 (s, 1H, 4^{III}-H); 7.77 (dd, J=8.0, J=1.6, 1H, 6-H); 7.51 (dd, J=7.9, J=4.8, 1H, 5^{II}-H); 7.48 (d, J=5.1, 1H, 5^{I}-H); 7.46 (d, J=8.0, 1H, 5-H); 7.41 (d, J=15.5, 1H, 1^{V}-H); 6.57 (d, J=15.5, 1H, 2^{V}-H); 4.91 (s, 1H, 2^{VI}-H); 4.01-3.91 (m, 1H, tetrahydropyran CH_2); 3.58-3.49 (m, 1H, tetrahydropyran CH_2); 2.36 (s, 3H, CH_3); 1.76-1.64 (m, 3H, tetrahydropyran CH_2); 1.60-1.48 (m, 3H, tetrahydropyran CH_2).

Synthesis of 3-{4^{IV}-[(2^{V}-hydroxylamino)carbonyl-vinyl]imidazol-1^{IV}-yl}-5-trifluoromethyl-N-{4^{I}-methyl-3^{I}-[4^{II}-(pyridin-3^{III}-yl)pyrimidin-2^{II}-yl]aminophenyl}benzamide

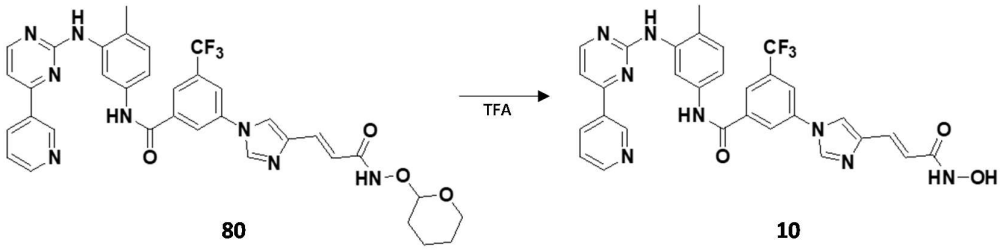

80 **10**

Compound **10** was obtained starting from 3-(4^{IV}-{2^{V}-[O-(tetrahydro-pyran-2^{VI}-yl)hydroxylamino]carbonyl-vinyl}imidazol-1^{IV}-yl)-5-trifluoromethyl-*N*-{4^{I}-methyl-3^{I}-[4^{II}-(pyridin-3^{III}-yl)pyrimidin-2^{II}-yl]aminophenyl}benzamide (0.1 g, 0.1 mmol) with general method D (TLC: $CHCl_3$/MeOH 9/1 + vanillin), (24 mg, 31% yield).

^{1}H-NMR (400 MHz, DMSO-d_6): δ 10.49 (s, 1H, NH); 9.30 (d, J=1.5, 1H, 2^{III}-H); 8.98 (s, 1H, NH); 8.69 (dd, J=4.7, J=1.5, 1H, 6^{III}-H); 8.57-8.50 (m, 3H, 6-H, 6^{II}-H and 2^{IV}-H); 8.48 (dt, J=7.8, J=1.5, 1H, 4^{III}-H); 8.30 (s, 1H, 2-H); 8.21 (s, 1H, 5^{IV}-H); 8.19 (s, 1H, 4-H); 8.10 (d, J=1.7, 1H, 2^{I}-H); 7.56-7.49 (m, 2H, 6^{I}-H and 5^{III}-H); 7.44 (d, J=5.4, 1H, 5^{II}-H); 7.26 (d, J=8.5, 1H, 5^{I}-H);7.20 (d, J=15.6, 1H, 1^{V}-H); 6.54 (d, J=15.6, 1H, 2^{V}-H); 2.25 (s, 3H, CH_3).

Synthesis of 4-methyl-N-(3^{III}-{4^{IV}-[(2^{V}-hydroxylamino)carbonyl-vinyl]imidazol-1^{IV}-yl)-5^{III}-trifluoromethyl-phenyl]-3-{[4^{I}-(pyridin-3^{II}-yl)pyrimidin-2^{I}-yl]amino}benzamide

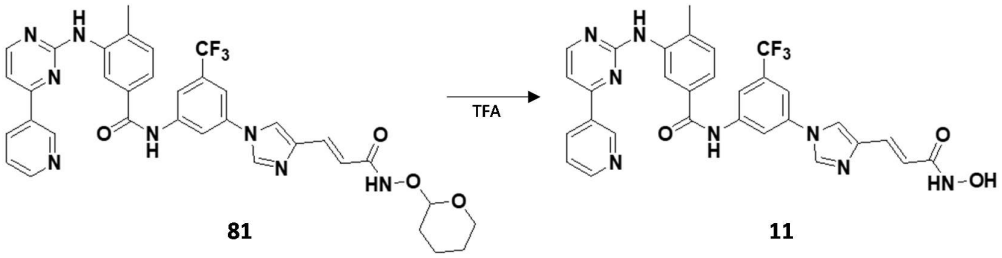

Compound **11** was obtained starting from 4-methyl-*N*-[3^{III}-(4^{IV}-{2^{V}-[O-(tetrahydro-pyran-2^{VI}-yl)hydroxylamino] carbonyl-vinyl}imidazol-1^{IV}-yl)-5^{III}-trifluoromethyl-phenyl]-3-{[4^{I}-(pyridin-3^{II}-yl) pyrimidin-2^{I}-yl]amino}benzamide (34 mg, 50 μm), with general method C (TLC: $CHCl_3$/MeOH 9/1 + vanillin), (8 mg, 30% yield).

^{1}H-NMR (400 MHz, DMSO-d_6): δ 10.67 (s, 1H, NH); 9.28 (dd, J=1.9, J=0.7, 1H, 2^{II}-H); 9.17 (s, 1H, NH); 8.68 (dd, J=4.9, J=1.9, 1H, 6^{II}-H); 8.55 (d, J=5.3, 1H, 6^{I}-H); 8.44 (dt, J=8.1, J=1.9, 1H, 4^{II}-H); 8.39 (s, 1H, 2^{Iv}-H); 8.35 (s, 1H, 2^{III}-H); 8.33 (d, J=1.8, 1H, 2-H); 8.21 (s, 1H, 6^{III}-H); 8.06 (s, 1H, 5^{Iv}-H); 7.80 (s, 1H, 4^{III}-H); 7.77 (dd, J=8.0, J=1.8, 1H, 6-H); 7.51 (ddd, J=8.1, J=4.9, J=0.7, 1H, 5^{II}-H); 7.48 (d, J=5.3, 1H, 5^{I}-H); 7.46 (d, J=8.0, 1H, 5-H); 7.41 (d, J=15.7, 1H, 1^{v}-H); 6.53 (d, J=15.7, 1H, 2^{v}-H); 2.36 (s, 3H, CH_3).

5.3.1.9 SYNTHESIS OF *N*^{I}-[5^{IV}-(IMIDAZOL-1^{V}-YL)-2^{IV}-AMINOPHENYL]-*N*-{4^{I}-METHYL-3^{I}-[4^{II}-(PYRIDIN-3^{III}-YL)PYRIMIDIN-2^{II}-YL]AMINOPHENYL}ISOPHTALAMIDE DERIVATIVES

Synthesis of 4-(imidazol-1^{I}-yl)-2-nitroaniline

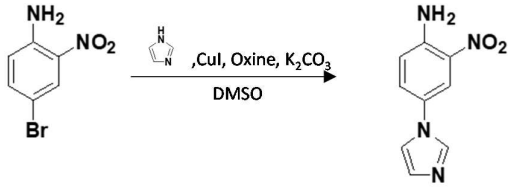

82 **83**

A mixture of 4-bromo-2-nitroaniline (0.5 g, 2.5 mmol), imidazole (0.7 g, 10.0 mmol), CuI (0.1 mg, 0.5 mmol), 8-hydroxyquinoline (0.1 g, 0.5 mmol) and K_2CO_3 (1.4 g, 10.0 mmol) in DMSO (13 ml) was sealed in a tube under nitrogen atm. The mixture was heated at 130°C for 16 hours (TLC: CH_2Cl_2/MeOH 95/5). After cooling, the mixture was diluted with a saturated solution of NH_4Cl in H_2O (500 ml) and extracted with EtOAc (3 x 150 ml). The organic phase was dried over anhydrous sodium sulphate and was concentrated under vacuum. The residue was purified by flash chromatography (CH_2Cl_2/MeOH 95:5) to afford **4-(imidazol-1^{I}-yl)-2-nitroaniline** (0.3 g, 31% yield).

^{1}H-NMR (400 MHz, DMSO-*d*$_6$): δ 8.15 (t, J=1.2, 1H, 2^{I}-H); 8.12 (d, J=3.0, 1H, 3-H); 7.72 (dd, J=9.0, J=3.0, 1H, 5-H); 7.67 (t, J=1.2, 1H, 5^{I}-H); 7.56 (broad s, 1H, NH_2); 7.16 (d, J=9.0, 1H, 6-H); 7.07 (t, J=1.2, 1H, 4^{I}-H).

Synthesis of 4-(4^{I}-methylimidazol-1^{I}-yl)-2-nitroaniline

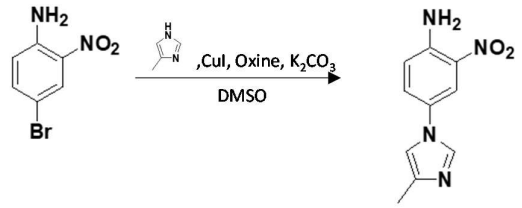

82 **84**

Compound **84** was obtained starting from 4-bromo-2-nitroaniline (0.5 g, 2.5 mmol) and 4-methylimidazole (0.3 g, 4.0 mmol) with the same procedure as for compound **83** (0.1 g, 66% yield).

^{1}H-NMR (300 MHz, DMSO-d_6): δ 8.05 (d, J=2.6, 1H, 3-H); 8.02 (d, J=1.0, 1H, 2^{I}-H); 7.68 (dd, J=9.2, J=2.6, 5-H); 7.56 (broad s, 2H, NH_2); 7.36 (d, J=1.0, 1H, 5^{I}-H); 7.13 (d, J=9.2, 1H, 6-H); 2.14 (s, 3H, CH_3).

Synthesis of 4-(imidazol-1^{I}-yl)-2-nitro-(tert-butoxycarbonyl)aniline

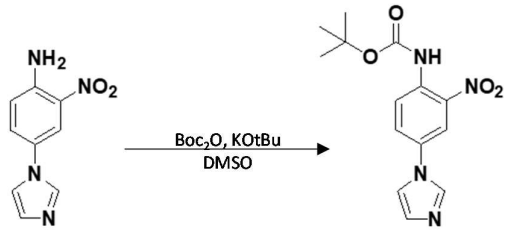

83 **85**

Potassium *tert*-butoxide (0.1 g, 1.2 mmol) was slowly added to solution of 4-(imidazol-1^{I}-yl)-2-nitroaniline (0.2 g, 1.0 mmol) in DMSO (3 ml) stirred at 5°C. The mixture was left over stirring for 30 minutes at 5°C. A solution of Boc_2O (0.3 g, 1.2 mmol) in DMSO (1 ml) was poured into the mixture. The mixture was stirred at room temperature for 2 hours (TLC: CH_2Cl_2/MeOH 95/5); it was subsequently diluted with a saturated solution of NH_4Cl in H_2O (50 ml) and extracted with EtOAc (3 x 20 ml). The organic phase was dried over anhydrous sodium sulfate and concentrated under vacuum to give **4-(imidazol-1^{I}-yl)-2-nitro-(*tert*-butoxycarbonyl)aniline** (0.2 g, 73% yield).

^{1}H-NMR (400 MHz, DMSO-d_6): δ 9.67 (s, 1H, NH); 8.34 (t, J=1.2, 1H, 2^{I}-H); 8.23 (d, J=2.6, 1H, 3-H); 7.97 (dd, J=9.1, J=2.6, 1H, 5-H); 7.83 (t, J=1.2, 1H, 5^{I}-H); 7.71 (d, J=9.1, 1H, 6-H); 7.13 (t, J=1.2, 1H, 4^{I}-H); 1.45 (s, 9H, 3 x CH_3).

Synthesis of 4-(4^{I}-methylimidazol-1^{I}-yl)-2-nitro-(tert-butoxycarbonyl)aniline

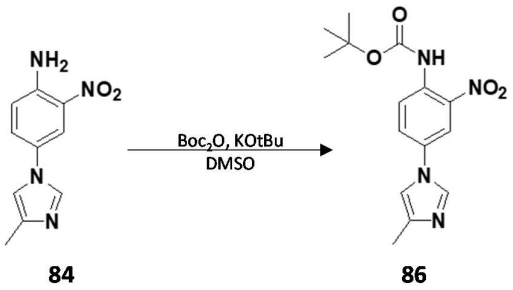

84 **86**

Compound **86** was obtained starting from 4-(4^{I}-methylimidazol-1^{I}-yl)-2-nitroaniline (0.2 g, 1.0 mmol) with the same procedure as for compound **85** (0.1 g, 45% yield).

^{1}H-NMR (400 MHz, DMSO-d_6): δ 8.21 (d, J=1.2, 1H, 2^{I}-H); 8.17 (d, J=2.6, 1H, 3-H); 7.92 (dd, J=8.9, J=2.6, 5-H); 7.68 (d, J=8.9, 1H, 6-H); 7.52 (d, J=1.2, 1H, 5^{I}-H); 2.16 (s, 3H, CH_3); 1.43 (s, 9H, 3 x CH_3).

Synthesis of 4-(imidazol-1^{I}-yl)-2-amino-(tert-butoxycarbonyl)aniline

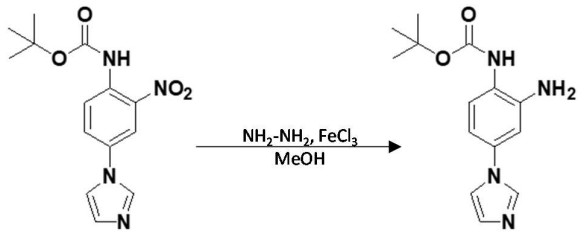

85 **87**

Hydrazine monohydrate (2.0 g, 40.0 mmol) and $FeCl_3$ (6 mg, 40 µmol) were added to a solution of 4-(imidazol-1^{I}-yl)-2-nitro-(tert-butoxycarbonyl)aniline (0.2 g, 0.8 mmol) in MeOH (4 ml). The mixture was heated at reflux for 2 hours (TLC: $CHCl_3$/MeOH 9/1). After cooling, the mixture was diluted with MeOH (50 ml), was filtered on celite and was concentrated under vacuum to obtain a residue. A saturated solution of NH_4Cl in H_2O (50 ml) was added to the residue and stirred at room temperature for 1 hour, the precipitate was collected by filtration to afford **4-(imidazol-1^{I}-yl)-2-amino-(tert-butoxycarbonyl)aniline** (0.1 g, 50% yield).

^{1}H-NMR (400 MHz, DMSO-d_6): δ 8.37 (broad s, 1H, NH); 8.01 (s, 1H, 2^{I}-H); 7.51 (s, 1H, 5^{I}-H); 7.31 (d, J=9.0, 1H, 6-H); 7.06 (s, 1H, 4^{I}-H); 6.86 (d, J=2.3, 1H, 3-H); 6.74 (dd, J=9.0, J=2.3, 1H, 5-H); 5.14 (s, 2H, NH_2); 1.45 (s, 9H, 3 x CH_3).

Synthesis of 4-(4^{I}-methylimidazol-1^{I}-yl)-2-amino-(tert-butoxycarbonyl)aniline

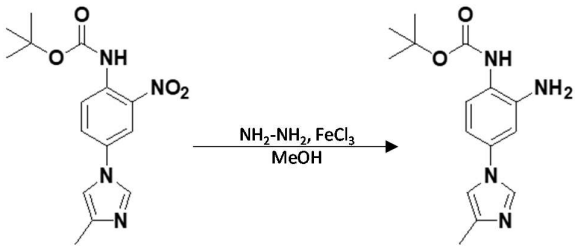

86 **88**

Compound **88** was obtained starting from 4-(4^{I}-methylimidazol-1^{I}-yl)-2-nitro-(tert-butoxycarbonyl)aniline (0.2 g, 0.5 mmol) with the same procedure as for compound **87** (0.1 g, 70% yield).

^{1}H-NMR (400 MHz, DMSO-d_6): δ 8.37 (broad s, 1H, NH); 7.88 (d, J=1.2, 1H, 2^{I}-H); 7.27 (d, J=8.5, 1H, 6-H); 7.21 (d, J=1.2, 5^{I}-H); 6.81 (d, J=2.5, 1H, 3-H); 6.68 (dd, J=8.5, J=2.5, 1H, 5-H); 5.12 (s, 2H, NH_2); 2.14 (s, 3H, CH_3); 1.46 (s, 9H, 3 x CH_3).

Synthesis of 3-ethoxycarbonyl-[5^{I}-(imidazol-1^{II}-yl)-2^{I}-(tert-butoxycarbonyl)aminophenyl]benzamide

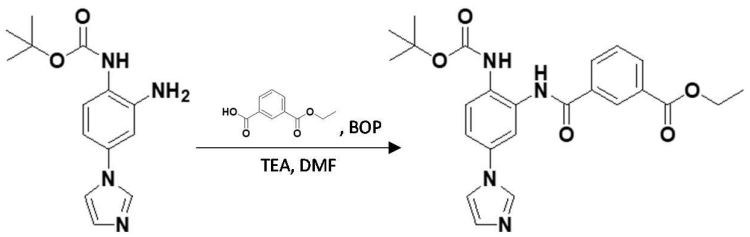

87 **89**

Compound **89** was obtained starting from mono-ethyl isophtalate (62 mg, 0.3 mmol) and 4-(imidazol-1^{I}-yl)-2-amino-(tert-butoxycarbonyl)aniline (0.1 g, 0.4 mmol) with the general condensation method A (TLC: $CHCl_3$/MeOH 9/1), (0.1 g, 75% yield).

^{1}H-NMR (400 MHz, DMSO-d_6): δ 10.15 (s, 1H, NH); 8.91 (s, 1H, NH); 8.56 (s, 1H, 2^{II}-H); 7.49 (s, 1H, 2-H); 8.25 (d, J=7.8, 1H, 4-H); 8.19 (d, J=8.4, 1H, 3^{I}-H); 7.84 (d, J=2.5, 1H, 6^{I}-H); 7.83-7.64 (m, 3H, 5-H, 6-H, 5^{II}-H); 7.54 (dd, J=8.4, J=2.5, 1H, 4^{I}-H); 7.27 (s, 1H, 4^{II}-H); 4.38 (q, J=7.0, 2H, $\underline{CH_2}CH_3$); 1.45 (s, 9H, 3 x CH_3), 1.36 (t, 3H, J=7.0, $CH_2\underline{CH_3}$).

Synthesis of 3-ethoxycarbonyl-[5^{I}-(4^{II}-methylimidazol-1^{II}-yl)-2^{I}-(tert-butoxycarbonyl)aminophenyl]benzamide

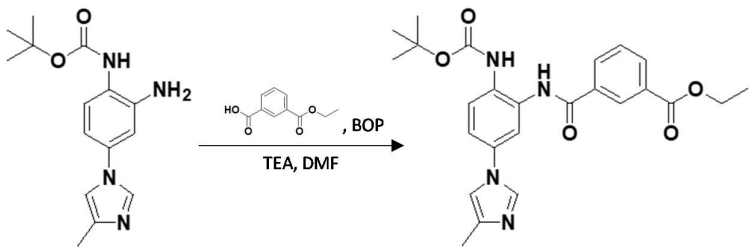

88 **90**

Compound **90** was obtained starting from mono-ethyl isophtalate (74 mg, 0.4 mmol) and 4-(4^{I}-methylimidazol-1^{I}-yl)-2-amino-(tert-butoxycarbonyl)aniline (0.1 g, 0.4 mmol) with the general condensation method A (TLC: $CHCl_3$/MeOH 9/1), (0.1 g, 50% yield).

^{1}H-NMR (300 MHz, DMSO-d_6): δ 10.12 (s, 1H, NH); 8.84 (s, 1H, NH); 8.55 (t, J=1.7, 1H, 2-H); 8.24 (dt, J=7.8, J=1.7, 1H, 4-H); 8.18 (dt, J=7.8, J=1.7, 1H, 6-H); 8.07 (d, J=1.2, 1H, 2^{II}-H); 7.76 (d, J=2.6, 1H, 6^{I}-H); 7.72 (t, J=8.0, 1H, 5-H); 7.68 (d, J=8.9, 1H, 3^{I}-H); 7.46 (dd, J=8.9, J=2.6, 1H, 4^{I}-H); 7.39 (d, J=1.2, 1H, 5^{II}-H); 4.38 (q, J=7.3, 2H, $\underline{CH_2}CH_3$); 2.16 (s, 3H, CH_3); 1.45 (s, 9H, 3 x CH_3); 1.36 (t, J=7.3, 3H, $CH_2\underline{CH_3}$).

Synthesis of 3-hydroxycarbonyl-[5^{I}-(imidazol-1^{II}-yl)-2^{I}-(tert-butoxycarbonyl)aminophenyl]benzamide

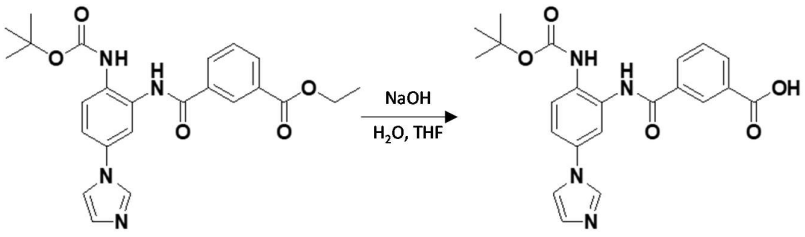

89 **91**

Compound **91** was obtained starting from 3-ethoxycarbonyl-[5^{I}-(imidazol-1^{II}-yl)-2^{I}-(tert-butoxycarbonyl)aminophenyl]benzamide (0.1 g, 0.3 mmol) in THF accordingly to the general method B (TLC: $CHCl_3$/MeOH 9/1), (34 mg, 31% yield).

^{1}H-NMR (400 MHz, DMSO-*d*$_6$): δ 10.06 (s, 1H, NH); 8.82 (s, 1H, NH); 8.55 (s, 1H, 2-H); 8.19 (t, J=1.1, 1H, 2^{II}-H); 8.11 (d, J=7.9, 1H, 4-H); 7.94 (d, J=7.9, 1H, 6-H); 7.82 (d, J=2.6, 1H, 6^{I}-H); 7.73-7.68 (m, 2H, 3^{I}-H and 5^{II}-H); 7.51-7.46 (m, 2H, 5-H and 4^{I}-H); 7.10 (t, J=1.1, 1H, 4^{II}-H); 1.45 (s, 9H, 3 x CH_3).

Synthesis of 3-hydroxycarbonyl-[5^{I}-(4^{II}-methylimidazol-1^{II}-yl)-2^{I}-(tert-butoxycarbonyl)aminophenyl]benzamide

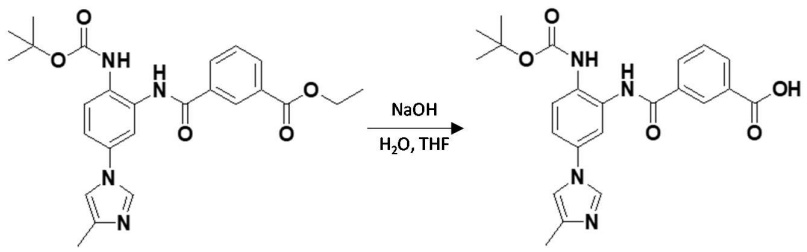

90 **92**

Compound **92** was obtained starting from 3-ethoxycarbonyl-[5^{I}-(4^{II}-methylimidazol-1^{II}-yl)-2^{I}-(tert-butoxycarbonyl)aminophenyl]benzamide (80 mg, 0.2 mmol) in THF accordingly to the general method B (TLC: $CHCl_3$/MeOH 9/1), (18 mg, 22% yield).

^{1}H-NMR (300 MHz, DMSO-d_6): δ 10.09 (s, 1H, NH); 8.82 (s, 1H, NH); 8.56 (t, J=1.6, 1H, 2-H); 8.21-8.14 (m, 2H, 4-H and 6-H); 8.07 (d, J=1.5, 1H, 2^{II}-H); 7.76 (d, J=2.5, 1H, 6^{I}-H); 7.71-7.74 (m, 2H, 5-H and 3^{I}-H); 7.45 (dd, J=8.8, J=2.7, 1H, 4^{I}-H); 7.39 (d, J=1.5, 1H, 5^{II}-H); 2.16 (s, 3H, CH_3); 1.45 (s, 9H, 3 x CH_3).

Synthesis of N^{I}-[5^{IV}-(imidazol-1^{V}-yl)-2^{IV}-(tert-butoxycarbonyl)aminophenyl]-N-{4^{I}-methyl-3^{I}-[4^{II}-(pyridin-3^{III}-yl)pyrimidin-2^{II}-yl]aminophenyl}isophtalamide

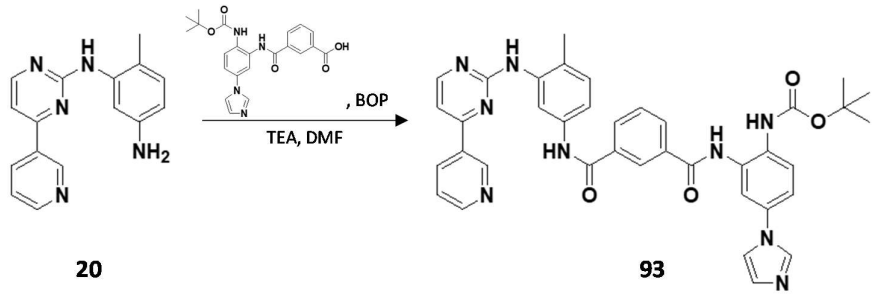

20 **93**

Compound **93** was obtained starting from 3-hydroxycarbonyl-[5^{I}-(imidazol-1^{II}-yl)-2^{I}-(tert-butoxycarbonyl)aminophenyl]benzamide (35 mg, 80 µmol) and N^{I}-(2-methyl-5-aminophenyl)-*N*-[4^{I}-(pyridin-3^{II}-yl)pyrimidin-2^{I}-yl]amine (24 mg, 88 µmol) with general method A (TLC: $CHCl_3$/MeOH 9/1), (31 mg, 56% yield).

^{1}H-NMR (400 MHz, DMSO-d_6): δ 10.40 (s, 1H, NH); 10.08 (s, 1H, NH); 9.27 (dd, J=2.2, J=0.7, 1H, 2^{III}-H); 8.98 (s, 1H, NH); 8.84 (broad s, 1H, NH); 8.67 (dd, J=4.7, J=1.6, 1H, 6^{III}-H); 8.55 (t, J=1.7, 1H, 2-H); 8.51 (d, J=5.4, 1H, 6^{II}-H); 8.47 (ddd, J=8.0, J=2.2, J=1.6, 1H, 4^{III}-H); 8.21-8.14 (m, 3H, 4-H, 6-H and 2^{V}-H); 8.09 (d, J=2.0, 1H, 2^{I}-H); 7.84 (d, J=2.7, 1H, 6^{IV}-H); 7.75-7.68 (m, 3H, 5-H, 3^{IV}-H and 5^{V}-H); 7.54-7.49 (m, 3H, 6^{I}-H, 5^{III}-H and 4^{IV}-H); 7.43 (d, J=5.4, 1H, 5^{II}-H); 7.23 (d, J=8.2, 1H, 5^{I}-H); 7.11 (t, J=1.0, 1H, 4^{V}-H) 2.24 (s, 3H, CH_3); 1.43 (s, 9H, 3 x CH_3).

Synthesis of N^{I}-[5^{IV}-(4^{V}-methylimidazol-1^{V}-yl)-2^{IV}-(tert-butoxycarbonyl)aminophenyl]-N-{4^{I}-methyl-3^{I}-[4^{II}-(pyridin-3^{III}-yl)pyrimidin-2^{II}-yl]aminophenyl}isophtalamide

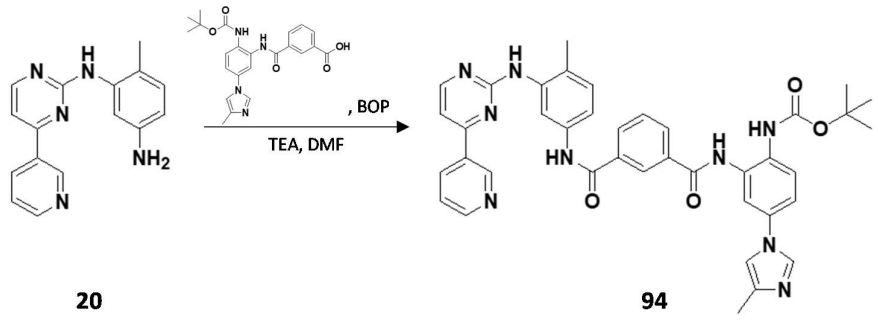

20 **94**

Compound **94** was obtained starting from 3-hydroxycarbonyl-[5^{I}-(4^{II}-methylimidazol-1^{II}-yl)-2^{I}-(tert-butoxycarbonyl)aminophenyl]benzamide (34 mg, 80 µmol) and *N*^{I}-(2-methyl-5-aminophenyl)-*N*-[4^{I}-(pyridin-3^{II}-yl)pyrimidin-2^{I}-yl]amine (24 mg, 88 µmol) with general method A (TLC: $CHCl_3$/MeOH 9/1), (36 mg, 65% yield).

^{1}H-NMR (300 MHz, DMSO-d_6): δ 10.41 (s, 1H, NH); 10.09 (s, 1H, NH); 9.27 (d, J=2.3, 1H, 2^{III}-H); 9.00 (s, 1H, NH); 8.86 (s, 1H, NH); 8.67 (dd, J=4.8, J=2.3, 1H, 6^{III}-H); 8.55 (t, J=1.7, 1H, 2-H); 8.51 (d, J=5.0, 1H, 6^{II}-H); 8.48 (dt, J=8.0, J=2.3, 1H, 4^{III}-H); 8.21-8.13 (m, 2H, 4-H and 6-H); 8.09 (d, J=1.9, 1H, 2^{I}-H); 7.81 (d, J=2.6, 1H, 6^{IV}-H); 7.72 (t, J=7.8, 1H, 5-H); 7.70 (d, J=9.0, 1H, 3^{IV}-H); 7.57-7.47 (m, 5H, 5 x Ar-H); 7.23 (d, J=8.5, 1H, 5^{I}-H); 2.23 (s, 3H, CH_3); 2.18 (s, 3H, CH_3); 1.43 (s, 9H, 3 x CH_3).

Synthesis of N^{I}-[5^{IV}-(imidazol-1^{V}-yl)-2^{IV}-aminophenyl]-N-{4^{I}-methyl-3^{I}-[4^{II}-(pyridin-3^{III}-yl)pyrimidin-2^{II}-yl]aminophenyl}isophtalamide

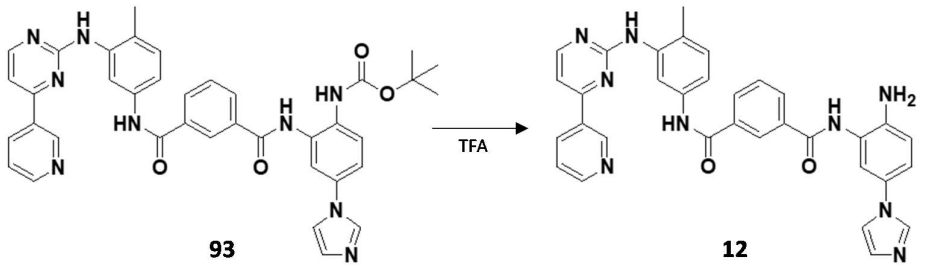

Compound **12** was obtained starting from N^{I}-[5^{Iv}-(imidazol-1^{v}-yl)-2^{Iv}-(tert-butoxycarbonyl)aminophenyl]-*N*-{4^{I}-methyl-3^{I}-[4^{II}-(pyridin-3^{III}-yl)pyrimidin-2^{II}-yl]aminophenyl}isophtalamide (31 mg, 45 µmol) accordingly to the deprotection method C (TLC: $CHCl_3$/MeOH 9/1), (26 mg, 94% yield).

^{1}H-NMR (400 MHz, DMSO-d_6): δ 10.37 (s, 1H, NH); 10.92 (s, 1H, NH); 9.27 (dd, J=2.1, 1H, 2^{III}-H); 8.97 (s, 1H, NH); 8.67 (dd, J=4.8, J=1.5, 1H, 6^{III}-H); 8.58 (t, J=1.7, 1H, 2-H); 8.51 (d, J=5.2, 1H, 6^{II}-H); 8.48 (ddd, J=7.8, J=2.1, J=1.5, 1H, 4^{III}-H); 8.20-8.13 (m, 2H, 4-H and 6-H); 8.10 (d, J=2.1, 1H, 2^{I}-H); 7.69 (t, J=7.7, 1H, 5-H); 7.59-7.47 (m, 4H, 6^{I}-H, 5^{III}-H, 2^{v}-H and 5^{v}-H); 7.43 (d, J=5.2, 1H, 5^{II}-H); 7.27-7.20 (m, 2H, 5^{I}-H and 4^{Iv}-H); 7.09 (broad s, 1H, 4^{v}-H); 7.97 (broad s, 1H, 6^{Iv}-H); 6.90 (d, J=8.7, 1H, 3^{Iv}-H); 5.22 (broad s, 2H, NH_2); 2.23 (s, 3H, CH_3);

Synthesis of N^{I}-[5^{IV}-(4^{V}-methylimidazol-1^{V}-yl)-2^{IV}-aminophenyl]-N-{4^{I}-methyl-3^{I}-N-[4^{II}-(pyridin-3^{III}-yl)pyrimidin-2^{II}-yl]aminophenyl}isophtalamide

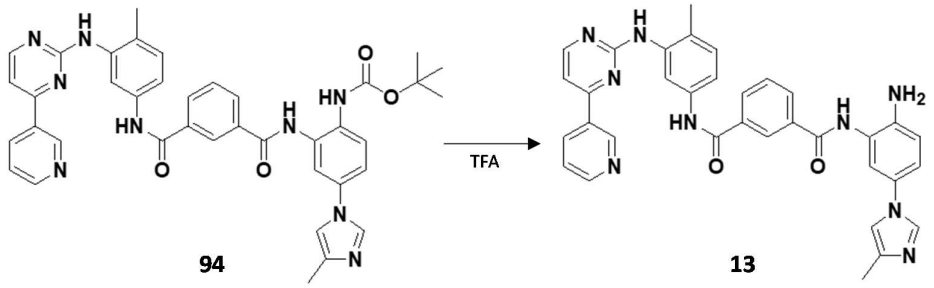

Compound **13** was obtained starting from N^{I}-[5^{IV}-(4^{V}-methylimidazol-1^{V}-yl)-2^{IV}-(tert-butoxycarbonyl)aminophenyl]-*N*-{4^{I}-methyl-3^{I}-[4^{II}-(pyridin-3^{III}-yl)pyrimidin-2^{II}-yl]aminophenyl}isophtalamide (36 mg, 52 µmol) with the general method C (TLC: $CHCl_3$/MeOH 9/1), (19 mg, 63% yield).

^{1}H-NMR (400 MHz, DMSO-d_6): δ 10.36 (s, 1H, NH); 9.89 (s, 1H, NH); 9.27 (d, J=2.2, 1H, 2^{III}-H); 8.97 (s, 1H, NH); 8.67 (dd, J=4.8, J=2.2, 1H, 6^{III}-H); 8.56 (t, J=1.6, 1H, 2-H); 8.51 (d, J=5.1, 1H, 6^{II}-H); 8.48 (dt, J=7.9, J=2.2, 1H, 4^{III}-H); 8.19-8.13 (m, 2H, 4-H and 6-H); 8.10 (d, J=2.0, 1H, 2^{I}-H); 7.86 (d, J=2.6, 1H, 6^{IV}-H); 7.69 (t, J=7.9, 1H, 5-H); 7.54-7.49 (m, 2H, 6^{I}-H and 5^{III}-H); 7.45-7.42 (m, 2H, 5^{II}-H and 2^{V}-H); 7.25-7.21 (m, 2H, 5^{I}-H and 5^{V}-H); 7.19 (dd, J=8.5, J=2.6, 1H, 4^{IV}-H); 6.87 (d, J=8.5, 1H, 3^{IV}-H); 5.16 (broad s, 2H, NH_2); 2.24 (s, 3H, CH_3); 2.14 (s, 3H, CH_3).

5.3.2 SYNTHESIS OF DUAL TYROSINE KINASES-HDAC INHIBITORS FUNCTIONALIZED WITH METALS

5.3.2.1 GENERAL METHOD

General method for the metal coordination

A solution of metal salt in MeOH (4 ml) was added to a solution of hydroxamic derivative, **4** or **9** (0.1 mmol) in MeOH (30 ml) neutralized to pH = 7 with aqueous KOH 10%. The mixture was stirred overnight at room temperature (TLC: $CHCl_3$/MeOH 9/1 + vanillin), the solvent was partially evaporated under vacuum and water (20 ml) was added to the residue. The solid precipitate was collected by filtration to afford the functionalized product.

Synthesis of 3-[(2^{IV}-hydroxylamino)carbonyl-vinyl]-N-{4^{I}-methyl-3^{I}-N-[4^{II}-(pyridin-3^{III}-yl)pyrimidin-2^{II}-yl]aminophenyl}benzamide zinc complex

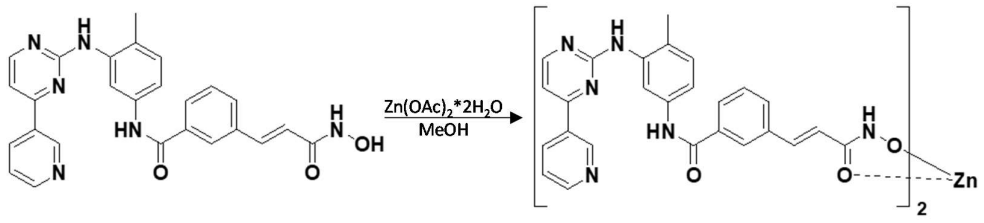

4 **14**

Starting from compound **4** and Zinc(II)acetate dehydrate (11 mg, 50 µmol) with the coordination general method was obtained compound **14** (36 mg, 72% yield).

^{1}H-NMR (500 MHz, DMSO-*d*$_6$): δ 10.29 (s, 1H, NH); 9.28 (dd, J=2.0, J=0.7, 1H, 2^{III}-H); 8.97 (s, 1H, NH); 8.70 (dd, J= 4.8, J=1.6, 1H, 6^{III}-H); 8.51 (d, J=5.2, 1H, 6^{II}-H); 8.47 (ddd, J=8.0, J=2.0, J=1.6, 1H, 4^{III}-H); 8.11 (broad s, 1H, 2-H); 8.09 (d, J=1.8, 1H, 2^{I}-H); 7.90 (d, J=7.8, 1H, 4-H); 7.74 (d, J=7.8, 1H, 6-H); 7.56 (t, J=7.8, 1H, 5-H); 7.52 (ddd, J=8.0, J=4.8, J=0.7, 1H, 5^{III}-H); 7.50 (dd, J=8.3, J=1.8, 1H, 6^{I}-H); 7.45 (d, J=16.0, 1H, 1^{IV}-H); 7.43 (d, J=5.2, 1H, 5^{II}-H); 7.22 (d, J=8.3, 1H, 5^{I}-H); 6.60 (d, J=16.0, 1H, 2^{IV}-H); 2.23 (s, 3H, CH_3).

^{13}C-NMR (500 MHz, DMSO-*d*$_6$): δ 165.17; 161.20; 159.35; 151.22; 148.10; 137.82; 137.49; 137.03; 136.46; 135.78; 134.42; 132.41; 132.19; 130.10; 129.93; 128.56; 127.48; 126.25; 123.79; 123.10; 122.70; 117.10; 116.66; 116.38; 107.63; 17.63.

IR ν_{max}/cm^{-1}: 3414 (hydroxamate N-H); 1649 (benzamide C=O); 1581 (hydroxamate C=O); 1552 (hydroxamate C-N).

Elemental analysis for $C_{52}H_{42}N_{12}O_6Zn$:
Calcd: C 62.68%; H 4.25%; N 16.87%. Found: C 63.00%; H 4.87%; N 17.50%.

Synthesis of 3-[(2^{IV}-hydroxylamino)carbonyl-vinyl]-5-trifluoromethyl-N-{4^{I}-methyl-3^{I}-N-[4^{II}-(pyridin-3^{III}-yl)pyrimidin-2^{II}-yl]aminophenyl}benzamide zinc complex

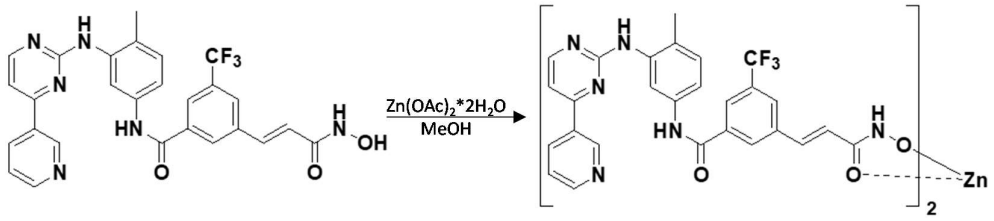

9 **15**

Starting from compound **9** and Zinc(II)acetate dehydrate (11 mg, 50 µmol) with the coordination general method was obtained compound **15** (50 mg, 88% yield).

^{1}H-NMR (500 MHz, DMSO-*d*$_6$): δ 10.50 (s, 1H, NH); 9.29 (d, J=1.7, 1H, 2^{III}-H); 9.00 (s, 1H, NH); 8.70 (dd, J=5.0, J=1.3, 1H, 6^{III}-H); 8.52 (d, J=5.2, 1H, 6^{II}-H); 8.48 (dt, J=8.1, J=1.7, 1H, 4^{III}-H); 8.41 (broad s, 1H, 2-H); 8.22 (broad s, 1H, 6-H); 8.13 (broad s, 1H, 4-H); 8.08 (d, J=1.5, 1H, 2^{I}-H); 7.59 (d, J=16.0, 1H, 2^{IV}-H); 7.52 (dd, J=8.1, J=5.0, 1H, 5^{III}-H); 7.50 (dd, J=8.3, J=1.5, 1H, 6^{I}-H); 7.44 (d, J=5.2, 1H, 5^{II}-H); 7.25 (d, J=8.3, 1H, 5^{I}-H); 6.73 (d, J=16.0, 1H, 1^{IV}-H); 2.24 (s, 3H, CH_3).

^{13}C-NMR (500 MHz, DMSO-*d*$_6$): δ 163.59; 161.67; 161.16; 159.58; 151.46; 151.20; 148.31; 148.23; 146.25; 137.95; 136.87; 135.95; 134.37; 132.26; 130.22; 129.97; 129.57; 128.12; 126.83; 123.86; 123.79; 122.41; 117.84; 116.64; 107.69; 90.36; 17.50.

IR ν_{max}/cm^{-1}: 3436 (hydroxamate N-H); 1662 (benzamide C=O); 1582 (hydroxamate C=O); 1555 (hydroxamate C-N).

Elemental analysis for $C_{54}H_{40}F_6N_{12}O_6Zn$:
Calcd: C 57.28%; H 3.56%; N 14.84%.Found: C 58.31%; H 4.35%; N 14.87%.

Synthesis of 3-[(2^{IV}-hydroxylamino)carbonyl-vinyl]-N-{4^{I}-methyl-3^{I}-N-[4^{II}-(pyridin-3^{III}-yl)pyrimidin-2^{II}-yl]aminophenyl}benzamide copper complex

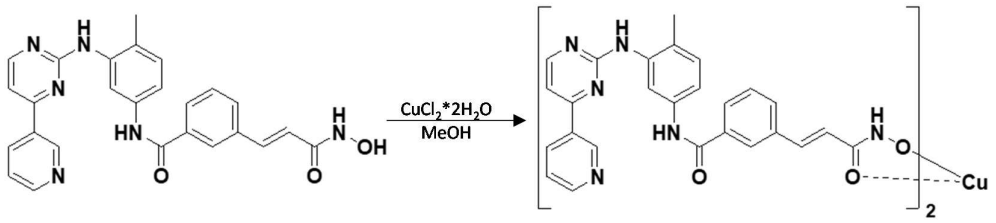

4 **16**

Starting from compound **4** and copper(II) chloride dihydrate (8 mg, 50 µmol) with the coordination general method was obtained compound **16** (37 mg, 74% yield).

IR ν_{max}/cm^{-1}: 3416 (hydroxamate N-H); 1655 (benzamide C=O); 1581 (hydroxamate C=O); 1552 (hydroxamate C-N).

Elemental analysis for $C_{54}H_{42}CuN_{12}O_6$:

Calcd: C 62.80%; H 4.26%; N 16.90%. Found: C 61.90%; H 4.35%; N 16.30%.

Synthesis of 3-[(2^{IV}-hydroxylamino)carbonyl-vinyl]-5-trifluoromethyl-N-{4^{I}-methyl-3^{I}-N-[4^{II}-(pyridin-3^{III}-yl)pyrimidin-2^{II}-yl]aminophenyl}benzamide copper complex

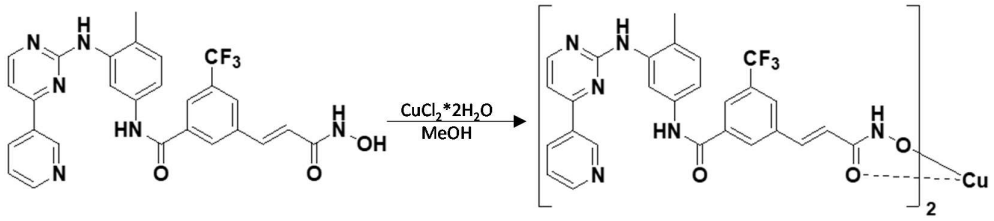

9 **17**

Starting from compound **9** and copper(II) chloride dihydrate (8 mg, 50 µmol) with the coordination general method was obtained compound **17** (55 mg, 97% yield).

IR ν_{max}/cm^{-1}: 3438 (hydroxamate N-H); 1650 (benzamide C=O); 1581 (hydroxamate C=O); 1552 (hydroxamate C-N).

Elemental analysis for $C_{54}H_{40}CuF_6N_{12}O_6$:

Calcd: C 57.37%; H 3.57%; N 14.87%. Found: C 57.15%; H 3.89%; N 14.76%.

Synthesis of 3-[(2^{IV}-hydroxylamino)carbonyl-vinyl]-N-{4^{I}-methyl-3^{I}-N-[4^{II}-(pyridin-3^{III}-yl)pyrimidin-2^{II}-yl]aminophenyl}benzamide iron complex

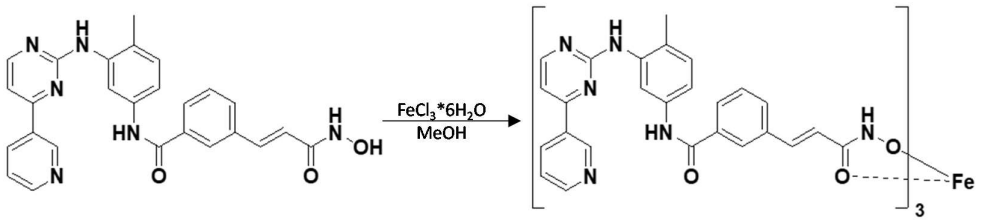

4 **18**

Starting from compound **4** and iron(III) chloride hexahydrate (9 mg, 35 µmol) with the coordination general method was obtained compound **18** (44 mg, 86% yield).

IR ν_{max}/cm^{-1}: 3422 (hydroxamate N-H); 1648 (benzamide C=O); 1581 (hydroxamate C=O); 1555 (hydroxamate C-N).

Elemental analysis for $C_{78}H_{63}FeN_{18}O_9$:

Calcd: C 64.51%; H 4.37%; N 17.36%. Found: C 63.89%; H 3.93%; N 16.18%.

Synthesis of 3-[(2^{IV}-hydroxylamino)carbonyl-vinyl]-5-trifluoromethyl-N-{4^{I}-methyl-3^{I}-N-[4^{II}-(pyridin-3^{III}-yl)pyrimidin-2^{II}-yl]aminophenyl}benzamide iron complex

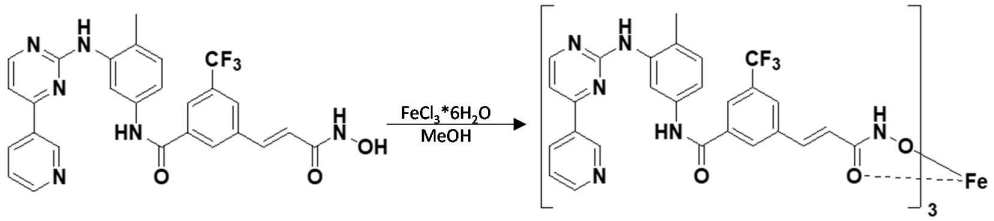

9 **19**

Starting from compound **9** and iron(III) chloride hexahydrate (9 mg, 35 μmol) with the coordination general method was obtained compound **19** (51 mg, 90% yield).

IR ν_{max}/cm^{-1}: 3435 (hydroxamate N-H); 1664 (benzamide C=O); 1581 (hydroxamate C=O); 1550 (hydroxamate C-N).

Elemental analysis for $C_{81}H_{60}F_9FeN_{18}O_9$:

Calcd: C 58.74%; H 3.65%; N 15.22%. Found: C 59.78%; H 4.49%; N 15.24%.

6. CONCLUSIONS

Starting from previously identified hit compounds (4-anilinoquinazolines EGFR inhibitors; *N*-[2-(dimethylamino)-ethyl]acridine-4-carboxamide topoisomerases I and II inhibitor; 4-anilinopyrimidines as multi kinases inhibitors; *N*-phenyl-*N*'-[4-(pyrimidin-4-ylami-no)phenyl]urea derivatives as class III TKs inhibitors; pyrido-pyrimidines as Abl inhibitors), we synthesized and tested several novel analogues with the aim of identifying novel promising multi-target inhibitors. Together, our data indicated:

- Quinazolinone derivatives as novel promising anti-fibrotic compounds with multiple kinases inhibitory properties. The synthesis of novel compounds and more exhaustive biological investigation on this novel class of multi-kinase inhibitors is in progress.
- Benzoquinoline moiety decorated with protonatable side chains could be a promising scaffold for the development of intercalating antitopoisomerase I and II agents.
- *N*-phenyl-*N*'-[4-(6-phenylpyrimidin-4-ylamino)phenyl]urea derivatives constitute a promising class of subfamily selective inhibitors of class III RTKs. To further develop these class of compounds novel analogues will be synthesized and biologically evaluated.
- *N*-(2-fluoro-5-trifluoromethylphenyl)-*N*'-{4'-[(2''-benzamido)pyridin-4''-ylamino] phenyl}urea will be soon *in vivo* tested to evaluate its efficacy and toxicity.
- 3-[(2^{IV}-hydroxylamino)carbonyl-vinyl]-*N*-{4^{I}-methyl-3^{I}-*N*-[4^{II}-(pyridin-3^{III}-yl)pyrimidin-2^{II}-yl]aminophenyl}benzamide (Compound **4**) and 3-[(2^{IV}-hydroxylamino)carbonyl-vinyl]-5-trifluoromethyl-*N*-{4^{I}-methyl-3^{I}-*N*-[4^{II}-(pyridin-3^{III}-yl)pyrimidin-2^{II}-yl]aminophenyl}benzamide (Compound **9**) will be soon *in vivo* tested to better investigate their pharmacokinetic, toxicity and efficacy.

- The metal complexes (**14-19**) will be submitted to *in vitro* tests as soon as possible. In particular, besides determining the ability of compounds to impair the redox homeostasis, we will evaluate the effect of the metal in the modulation of the pharmacokinetic properties. Indeed whether compounds **14**-**19** will possess anti-proliferative activity this will be due to the influence of the metal in the cell uptake. In fact the original ligand (**4** not bearing the CF_3 function) showed very low activity in MTT test due to poor cell permeation.

7. REFERENCES

1. Sawyers, C., Targeted cancer therapy. Nature **2004**, *432* (7015), 294-7.

2. Medina-Franco, J. L.; Giulianotti, M. A.; Welmaker, G. S.; Houghten, R. A., Shifting from the single to the multitarget paradigm in drug discovery. *Drug Discov Today* **2013**, *18* (9-10), 495-501.

3. Petrelli, A.; Giordano, S., From single- to multi-target drugs in cancer therapy: when aspecificity becomes an advantage. *Curr Med Chem* **2008**, *15* (5), 422-32.

4. Bayat Mokhtari, R.; Homayouni, T. S.; Baluch, N.; Morgatskaya, E.; Kumar, S.; Das, B.; Yeger, H., Combination therapy in combating cancer. *Oncotarget* **2017**, *8* (23), 38022-38043.

5. Nguyen, T.; Dai, Y.; Attkisson, E.; Kramer, L.; Jordan, N.; Nguyen, N.; Kolluri, N.; Muschen, M.; Grant, S., HDAC inhibitors potentiate the activity of the BCR/ABL kinase inhibitor KW-2449 in imatinib-sensitive or -resistant BCR/ABL+ leukemia cells in vitro and in vivo. *Clin Cancer Res* **2011**, *17* (10), 3219-32.

6. Okabe, S.; Tauchi, T.; Kimura, S.; Maekawa, T.; Kitahara, T.; Tanaka, Y.; Ohyashiki, K., Combining the ABL1 kinase inhibitor ponatinib and the histone deacetylase inhibitor vorinostat: a potential treatment for BCR-ABL-positive leukemia. *PLoS One* **2014**, *9* (2), e89080.

7. Anighoro, A.; Bajorath, J.; Rastelli, G., Polypharmacology: challenges and opportunities in drug discovery. *J Med Chem* **2014**, *57* (19), 7874-87.

8. Garuti, L.; Roberti, M.; Bottegoni, G., Multi-kinase inhibitors. *Curr Med Chem* **2015**, *22* (6), 695-712.

9. Covell, L. L.; Ganti, A. K., Treatment of advanced thyroid cancer: role of molecularly targeted therapies. *Target Oncol* **2015**, *10* (3), 311-24.

10. Mologni, L.; Dalla Via, M.; Chilin, A.; Palumbo, M.; Marzaro, G., Discovery of (wt) RET and (V804M) RET Inhibitors: From Hit to Lead. *ChemMedChem* **2017**, *12* (16), 1390-1398.

11. Gandin, V.; Ferrarese, A.; Dalla Via, M.; Marzano, C.; Chilin, A.; Marzaro, G., Targeting kinases with anilinopyrimidines: discovery of N-phenyl-N'-[4-(pyrimidin-4-ylamino)phenyl]urea derivatives as selective inhibitors of class III receptor tyrosine kinase subfamily. *Sci Rep* **2015**, *5*, 16750.

12. Matsui, A.; Ihara, T.; Suda, H.; Mikami, H.; Semba, K., Gene amplification: mechanisms and involvement in cancer. Biomol Concepts **2013**, *4* (6), 567-82.

13. Roskoski, R., A historical overview of protein kinases and their targeted small molecule inhibitors. *Pharmacol Res* **2015**, *100*, 1-23.

14. Liao, J. J., Molecular recognition of protein kinase binding pockets for design of potent and selective kinase inhibitors. *J Med Chem* **2007**, *50* (3), 409-24.

15. Roskoski, R., Classification of small molecule protein kinase inhibitors based upon the structures of their drug-enzyme complexes. *Pharmacol Res* **2016**, *103*, 26-48.

16. Regad, T., Targeting RTK Signaling Pathways in Cancer. *Cancers (Basel)* **2015**, *7* (3), 1758-84.

17. Spangle, J. M.; Roberts, T. M., Epigenetic regulation of RTK signaling. *J Mol Med (Berl)* **2017**, *95* (8), 791-798.

18. Hubbard, S. R.; Till, J. H., Protein tyrosine kinase structure and function. *Annu Rev Biochem* **2000**, *69*, 373-98.

19. Croce, C. M., Oncogenes and cancer. *N Engl J Med* **2008**, *358* (5), 502-11.

20. Pytel, D.; Sliwinski, T.; Poplawski, T.; Ferriola, D.; Majsterek, I., Tyrosine kinase blockers: new hope for successful cancer therapy. *Anticancer Agents Med Chem* **2009**, *9* (1), 66-76.

21. Panjarian, S.; Iacob, R. E.; Chen, S.; Engen, J. R.; Smithgall, T. E., Structure and dynamic regulation of Abl kinases. *J Biol Chem* **2013**, *288* (8), 5443-50.

22. Comert, M.; Baran, Y.; Saydam, G., Changes in molecular biology of chronic myeloid leukemia in tyrosine kinase inhibitor era. *Am J Blood Res* **2013**, *3* (3), 191-200.

23. Capdeville, R.; Buchdunger, E.; Zimmermann, J.; Matter, A., Glivec (STI571, imatinib), a rationally developed, targeted anticancer drug. *Nat Rev Drug Discov* **2002**, *1* (7), 493-502.

24. Cowan-Jacob, S. W.; Fendrich, G.; Floersheimer, A.; Furet, P.; Liebetanz, J.; Rummel, G.; Rheinberger, P.; Centeleghe, M.; Fabbro, D.; Manley, P. W., Structural biology contributions to the discovery of drugs to treat chronic myelogenous leukaemia. *Acta Crystallogr D Biol Crystallogr* **2007**, *63* (Pt 1), 80-93.

25. Ren, R., Mechanisms of BCR-ABL in the pathogenesis of chronic myelogenous leukaemia. *Nat Rev Cancer* **2005**, *5* (3), 172-83.

26. Saglio, G.; Kim, D. W.; Issaragrisil, S.; le Coutre, P.; Etienne, G.; Lobo, C.; Pasquini, R.; Clark, R. E.; Hochhaus, A.; Hughes, T. P.; Gallagher, N.; Hoenekopp, A.; Dong, M.; Haque, A.; Larson, R. A.; Kantarjian, H. M., Nilotinib versus imatinib for newly diagnosed chronic myeloid leukemia. *N Engl J Med* **2010**, *362* (24), 2251-9.

27. Olins, A. L.; Olins, D. E., Spheroid chromatin units (v bodies). *Science (New York)* **1974**, *183* (4122), 330-2.

28. Jenuwein, T.; Allis, C. D., Translating the histone code. *Science (New York)* **2001**, *293* (5532), 1074-80.

29. Miller, T. A.; Witter, D. J.; Belvedere, S., Histone deacetylase inhibitors. *J Med Chem* **2003**, *46* (24), 5097-116.

30. Wu, R.; Wang, S.; Zhou, N.; Cao, Z.; Zhang, Y., A proton-shuttle reaction mechanism for histone deacetylase 8 and the catalytic role of metal ions. *J Am Chem Soc* **2010**, *132* (27), 9471-9.

31. Zhou, J.; Wu, R.; Luo, H. B., Inhibition mechanism of SAHA in HDAC: a revisit. *Phys Chem Chem Phys* **2015**, *17* (44), 29483-8.

32. Qian, C.; Cai, X.; Gould, S.; Zhai, H. Quinazoline based EGFR inhibitors containing a zinc binding moiety. **2008**. WO2008033749.

33. Ndagi, U.; Mhlongo, N.; Soliman, M. E., Metal complexes in cancer therapy - an update from drug design perspective. *Drug Des Devel Ther* **2017**, *11*, 599-616.

34. Montagner, D.; Gandin, V.; Marzano, C.; Erxleben, A., DNA damage and induction of apoptosis in pancreatic cancer cells by a new dinuclear bis(triazacyclonane) copper complex. *J Inorg Biochem* **2015**, *145*, 101-7.

35. Walencik, P. K.; Stokowa-Sołtys, K.; Wieczorek, R.; Komarnicka, U. K.; Kyzioł, A.; Jeżowska-Bojczuk, M., Impact of the Cu(II) ions on the chemical and biological properties of goserelin - coordination pattern, DNA degradation, oxidative reactivity and in vitro cytotoxicity. *J Inorg Biochem* **2017**, *175*, 167-178.

36. Deo, K. M.; Pages, B. J.; Ang, D. L.; Gordon, C. P.; Aldrich-Wright, J. R., Transition Metal Intercalators as Anticancer Agents-Recent Advances. *Int J Mol Sci* **2016**, *17* (11).

37. Sambiagio, C.; Marsden, S. P.; Blacker, A. J.; McGowan, P. C., Copper catalysed Ullmann type chemistry: from mechanistic aspects to modern development. *Chem Soc Rev* **2014**, *43* (10), 3525-50.

38. Hassan, J.; Sévignon, M.; Gozzi, C.; Schulz, E.; Lemaire, M., Aryl-aryl bond formation one century after the discovery of the Ullmann reaction. *Chem Rev* **2002**, *102* (5), 1359-470.

8. PUBLISHED PAPERS

P04 Mologni L., Dalla Via M., Chilin A., Palumbo M., Marzaro G., Discovery of novel wtRET and V804MRET inhibitors: from hit to lead, *ChemMedChem*, 12, 1390-1398, **2017**

P03 Marzaro G., Dalla Via L., García-Argáez A.N., Dalla Via M., Chilin A., Novel benzoquinoline derivatives via unpredicted condensation of ethyl propiolate and naphthylamines: Synthesis and topoisomerase inhibition activity, *Bioorganic and Medicinal Chemistry Letters*, 26, 4875-4878, **2016**

P02 Marzaro G., Castagliuolo I., Schirato G., Palu' G., Dalla Via M., Chilin A., Brun P., Substituted quinazolinones as kinase inhibitors endowed with anti-fibrotic properties, *European Journal of Medicinal Chemistry*, 115, 416-425, **2016**

P01 Gandin V., Ferrarese A., Dalla Via M., Marzano C., Chilin A., Marzaro G., Targeting kinases with anilinopyrimidines: Discovery of N-phenyl-N'-[4-(pyrimidin-4-ylamino)phenyl]urea derivatives as selective inhibitors of class III receptor tyrosine kinase subfamily, *Scientific Reports*, 5, 16750, **2015**

Published in: ChemMedChem, 12, 1390-1398, 2017

Discovery of ^{wt}RET and ^{V804M}RET Inhibitors: From Hit to Lead

Luca Mologni[+],[a] Martina Dalla Via[+],[b] Adriana Chilin,[b] Manlio Palumbo,[b] and Giovanni Marzaro*[b]

Oncogenic activation of RET kinase has been found in several neoplastic diseases, like medullary thyroid carcinoma, multiple endocrine neoplasia, papillary thyroid carcinoma, and non-small-cell lung cancer. Currently approved RET inhibitors were not originally designed to be RET inhibitors, and their potency against RET kinase has not been optimized. Hence, novel compounds able to inhibit both wild-type RET (^{wt}RET) and its mutants (e.g., ^{V804M}RET) are needed. Herein we present the development and the preliminary evaluation of a new sub-micromolar ^{wt}RET/^{V804M}RET inhibitor, *N*-(2-fluoro-5-trifluoromethylphenyl)-*N*′-{4′-[(2′′-benzamido)pyridin-4′′-ylamino]phenyl}urea (**69**), endowed with a 4-anilinopyridine structure, starting from our previously identified 4-anilinopyrimidine hit compound. Profiling against a panel of kinases indicated **69** as a multi cKIT/^{wt}RET/^{V804M}RET inhibitor.

Introduction

Protein kinases (PKs) are among the most investigated targets for cancer therapy.[1] This class of enzymes regulates almost all cellular events by transferring a phosphate group from ATP to the target protein substrate.[2,3] The human kinome comprises 518 members, grouped in families, subfamilies, and classes, according to structural and functional similarities.[3] Of particular interest is the family of tyrosine kinases (TKs); their deregulation, through mutation or overexpression of TKs, is often related to cancer onset and progression,[4] and in the last two decades, a number of ATP-mimic TK inhibitors (TKIs) have been developed.[5] TKIs share some common pharmacophore features, like a nitrogen-containing heterocycle (for interaction with the kinase hinge region), a lipophilic moiety (for interaction with a hydrophobic region not exploited by ATP) and a bridge connecting the two.[1,6] According to the bound kinase conformation, TKIs are classified as type I, I$^1/_2$, II, III, and IV inhibitors. In particular, type II inhibitors bind the inactive kinase conformation, which bears a larger lipophilic cleft than the active conformation. Accordingly, type II inhibitors have a larger lipophilic moiety than type I inhibitors.[7]

As part of our kinase inhibitors discovery project,[8,9] we recently reported that some *N*-phenyl-*N*′-[4-(pyrimidin-4-ylamino)phenyl]urea derivatives behave as subfamily-selective class III multitarget kinase inhibitors.[9] To further investigate the usefulness of these compounds in developing novel TKIs, we tested compound **1** (selected as a hit compound in our previous study) against some kinases phylogenetically related

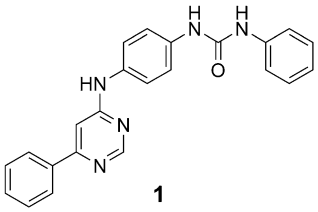

1

to the class III receptor TKs, that is, the FGFR family and the kinase RET. From this very preliminary screening, we found that **1** possessed a low but not negligible inhibitory activity against RET ($IC_{50} = 11.9$ μM).

The RET proto-oncogene has been recognized as an important therapeutic target in thyroid neoplasia and in a small subset of non-small-cell lung cancer (NSCLC) patients.[10,11] Oncogenic activation of RET occurs through one of two mechanisms: point mutations in the extracellular or the kinase domain of RET are frequently found in medullary thyroid carcinoma (MTC) and in multiple endocrine neoplasia, while chromosomal rearrangements involving the catalytic domain of RET are predominant in papillary thyroid carcinoma (PTC) and in NSCLC.[10] In both cases, aberrant RET-driven signaling ensues, leading to increased cell proliferation and survival. Thus, actual inhibition of RET kinase is paramount for effective treatment of these diseases. Four drugs (vandetanib, cabozan-

[a] *Dr. L. Mologni[+]*
School of Medicine and Surgery, University of Milano-Bicocca, via Cadore 48, 20900 Monza (Italy)

[b] *Dr. M. Dalla Via,[+] Prof. A. Chilin, Prof. M. Palumbo, Dr. G. Marzaro*
Department of Pharmaceutical and Pharmacological Sciences, University of Padova, via Marzolo 5, 35131 Padova (Italy)
E-mail: giovanni.marzaro@unipd.it

[+] *These authors contributed equally to this work.*

Supporting information and the ORCID identification number(s) for the author(s) of this article can be found under https://doi.org/10.1002/cmdc.201700243.

This article is part of a Special Issue on the XXIV National Meeting in Medicinal Chemistry (NMMC 2016, Perugia, Italy). To view the complete issue, visit: http://onlinelibrary.wiley.com/doi/10.1002/cmdc.v12.16/issuetoc.

tinib, sorafenib, and lenvatinib) have been recently approved for the treatment of thyroid cancer.[12] However, these compounds were not originally designed as RET inhibitors. A few more compounds are under investigation,[12] including a potent inhibitor of the V804M mutant.[13] Different strategies have been pursued for the identification of novel RET inhibitors, such as drug repurposing,[14] kinase profiling,[15] and use of multicomponent reaction libraries.[16] In this work, we report our efforts in the development of novel analogues of compound **1** endowed with sub-micromolar RET inhibitory potency. According to our previous results,[9] we hypothesized that **1** would bind the inactive kinase conformation. As no crystallographic structure has been deposited in the Protein Data Bank (PDB) to date for the inactive RET conformation, we decided to use a classical medicinal chemistry approach rather than a structure-based approach. However, to suggest a plausible binding mode supported by experimental evidence, a molecular docking study based on homology modeling is also presented.

Results and Discussion

Optimization of urea moiety

The first optimization step for hit compound **1** regarded the evaluation of different substituents on both phenyl rings on the urea functionality (Table 1). The diphenyl urea motif is present in several known type II kinase inhibitors and commonly interacts with the lipophilic cleft typical of TKs.[6] Hence, we decided to functionalize the terminal phenyl ring with lipophilic substituents, differing from the steric and electronic features. In particular, we focused our attention on substituents already evaluated for the development of kinase inhibitors, such as 2-fluoro-5-methyl,[17] 2-fluoro-5-trifluoromethyl,[18] 4-chloro-3-trifluoromethyl,[19] or 2,5-difluoro[20] substituents. The central aniline ring was functionalized with bulky moieties to obtain indirect information about the size of the hydrophobic cleft in the inactive RET conformation. Inhibitory potency against recombinant wild-type RET (^{wt}RET kinase), expressed as IC_{50} values (μM), allowed the derivation of useful SARs. Functionalization of the terminal ring was mandatory for enhancing activity. In particular, the presence of a methyl or trifluoromethyl functionality at the 5(3) position led to the most potent compounds in the series (**2**, **3**, and **5**). A 2-fluoro functionality was useful in the absence of any other substituent (compare **4** with **1**), or when a 5-trifluoromethyl functionality was also present (compare **5** with **3**). Conversely, when a 5-methyl functionality was present, the 2-fluoro substituent did not improve the activity (compare **7** with **3**). Bulky substituents were not well tolerated (**8**). The presence of a 4-chloro-3-trifluoromethyl functionality led to a completely inactive compound, and functionalization of the central aniline ring was detrimental for activity (see **10**–**12**). On the basis of inhibitory data and synthetic accessibility, compound **5** (bearing the 2-fluoro-5-trifluoromethyl pattern on the terminal phenyl group) was chosen as a model for further improvement. The compounds listed in Table 1 were synthesized according to Scheme 1.

Table 1. Structure and IC_{50} values (isolated ^{wt}RET) of compounds **1**–**12**.

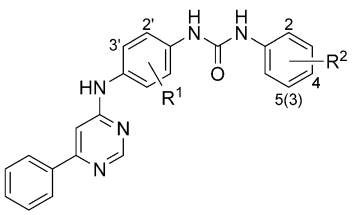

ID	R^1	R^2	IC_{50} [μM][a]
1	H	H	11.9 ± 0.7
2	H	3-Me	3.3 ± 0.5
3	H	3-CF_3	4.8 ± 0.2
4	H	2-F	6.1 ± 0.7
5	H	2-F,5-CF_3	4.1 ± 0.1
6	H	2,5-diF	6.2 ± 0.5
7	H	2-F,5-Me	7.1 ± 0.7
8	H	3-OMe	19.8 ± 0.8
9	H	4-Cl,3-CF_3	> 100
10	2′-OMe	2-F,5-CF_3	10.7 ± 0.7
11	2′-Br	2-F,5-CF_3	42.3 ± 5.5
12	3′-OMe	2-F,5-CF_3	> 100

[a] Values are the mean ± SEM of three determinations.

Briefly, 4,6-dichloropyrimidine was first condensed with phenylboronic acid and then with a slight excess of the appropriately substituted aniline. Compounds **16** and **17** were submitted to alkaline hydrolysis, whereas compound **20** was reduced with elemental iron in an aqueous ethanol solution, slightly acidified with acetic acid. All amino derivatives were finally condensed with the appropriate isocyanate derivatives in dichloromethane at room temperature, affording the desired ureas in moderate to good yields.

Optimization of nitrogen heterocycle

The second optimization step regarded the evaluation of different substituents at the 6′′ position of the pyrimidine ring (Table 2). At this position, we mainly chose to replace the phenyl ring with simple heterocycles (i.e., furan and thiophene, to verify the effect of electron density in this part of the moiety) or to insert a spacer (to potentially establish hydrogen bonds) between the aryl and the pyrimidine moiety. Substitution of the 6′′-phenyl ring with heteroaryls resulted in similar potencies (compare **22** and **23** with **5**). Conversely to what was previously observed for inhibition of class III receptor TK members,[9] the introduction of a polar functionality at the 6′′-phenyl ring decreased compound potency (see **24**). The greatest effect was observed when a spacer was introduced between the pyrimidine and the aryl; the NH functionality led to a totally inactive compound (**25**), whereas a carboxamido functionality (**26**) furnished the most active compound overall.

The compounds listed in Table 2 were synthesized according to Scheme 2. Compounds **22** and **23** were synthesized according to the same synthetic strategy as **5** (see Scheme 1), with the only difference being the nature of arylboronic acid used in the first step. Compounds **24** and **25** were synthesized following our previously reported strategy.[9] For the synthesis of

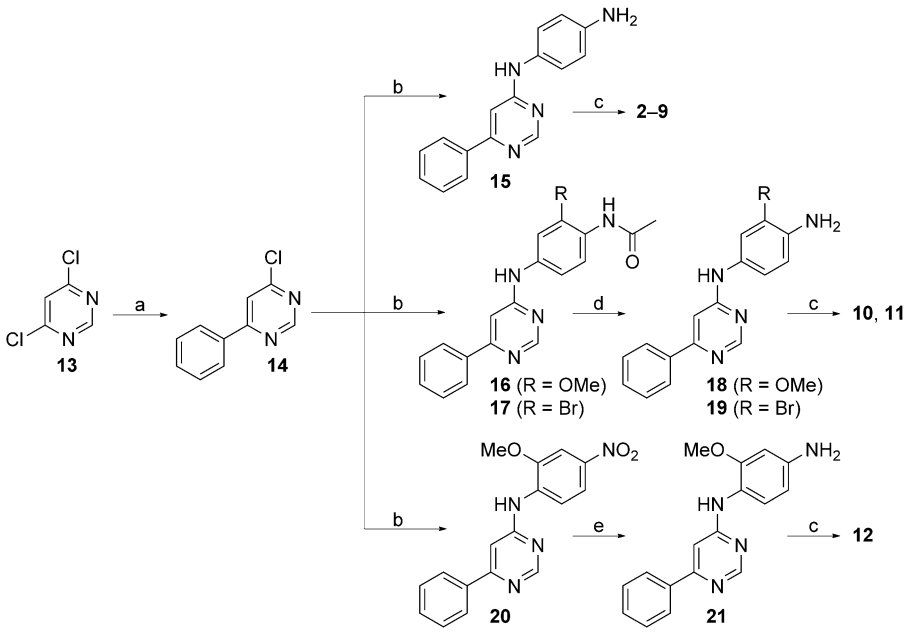

Scheme 1. Synthesis of compounds **2**–**12**. Reagents and conditions: a) phenylboronic acid, $Pd(PPh_3)_4$, Na_2CO_3, H_2O, DME, reflux, 16 h; b) aniline derivative, *i*PrOH, MW 80 °C, 3×20 min; c) phenylisocyanate derivative, CH_2Cl_2, RT, 16 h; d) NaOH, H_2O, RT, 16 h; e) Fe^0, acetic acid, EtOH, H_2O, reflux, 2 h.

Table 2. Structure and IC_{50} values (isolated ^{wt}RET) of compounds **22**–**26**.

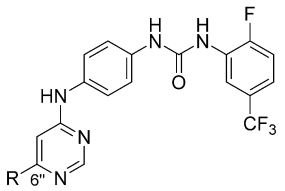

ID	R	IC_{50} [μM][a]
5		4.1 ± 0.1
22		3.8 ± 0.2
23		5.2 ± 0.1
24	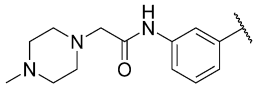	36.0 ± 2.4
25	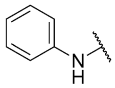	> 100
26	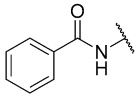	1.2 ± 0.3

[a] Values are the mean ± SEM of three determinations.

compound **26**, the starting dichloropyrimidine was first converted into the 6-amino-4-chloropyrimdine. Intermediate **38** was then condensed with benzoyl chloride in presence of DMAP, taking advantage of a microwave-assisted organic synthesis technique. Compound **39** was then submitted to the usual synthetic steps to obtain the desired urea derivative.

In parallel to the evaluation of different substituents at the 6′′ position of the pyrimidine ring, we also evaluated different pyrimidines, in terms of both the relative position of nitrogen atoms with respect to the phenyl ring and the presence of substituents (Table 3). As mentioned above, we decided to hinder the pyrimidine nucleus with different substituents (i.e., CN, Me, SMe) to explore the steric features of the ATP binding pocket of RET. In addition, we modified the number and relative position of the nitrogen atoms in the heterocycle to investigate the importance the of the hydrogen bond acceptor features of the scaffold. The addition of another substituent in

Table 3. Structure and IC_{50} values (isolated ^{wt}RET) of compounds **41**–**45**.

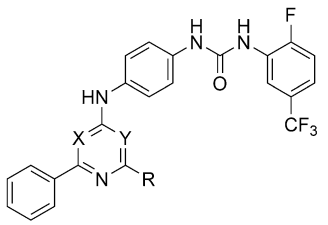

ID	X	Y	R	IC_{50} [μM][a]
5	CH	N	H	4.1 ± 0.1
41	C–CN	N	H	> 100
42	CH	N	Me	> 100
43	CH	N	S–Me	> 100
44	N	CH	H	1.5 ± 0.1
45	N	C–CN	H	> 100

[a] Values are the mean ± SEM of three determinations.

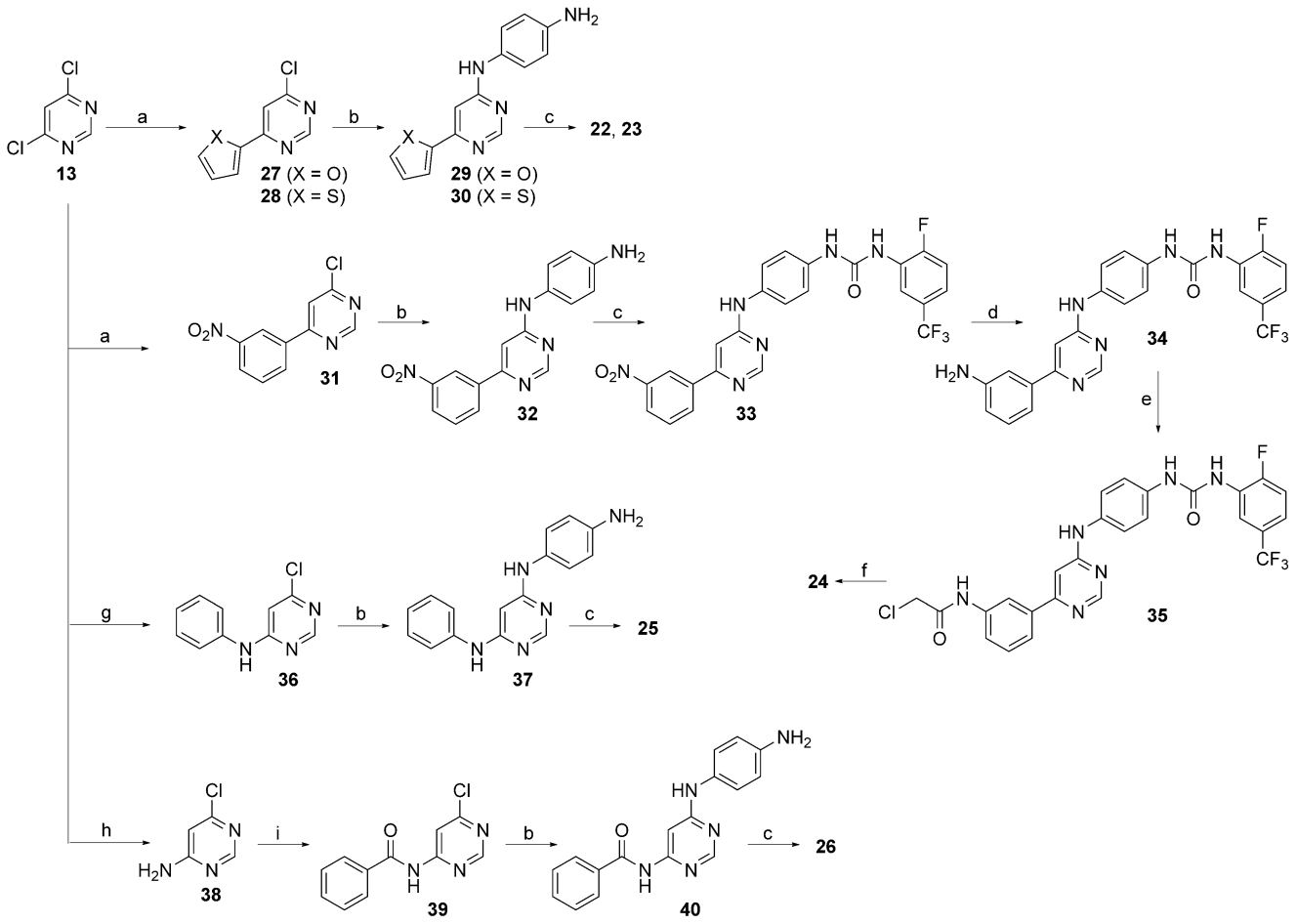

Scheme 2. Synthesis of compounds **22**–**26**. Reagents and conditions: a) arylboronic acid derivative, $Pd(PPh_3)_4$, Na_2CO_3, H_2O, DME, reflux, 16 h; b) *p*-phenylenediamine, *i*PrOH, MW, 80 °C, 3×20 min; c) 2-fluoro-5-trifluoromethylphenylisocyanate, CH_2Cl_2, RT, 16 h; d) Fe^0, AcOH, EtOH, H_2O, reflux, 2 h; e) chloroacetyl chloride, TEA, DME, RT, 16 h; f) *N*-methylpiperazine, KI, TEA, DMF, RT, 48 h; g) aniline, TEA, *i*PrOH, MW, 150 °C, 30 min; h) NH_4OH, *i*PrOH, 80 °C (sealed tube), 16 h; i) benzoyl chloride, DMAP, MW, 100 °C, 5 min.

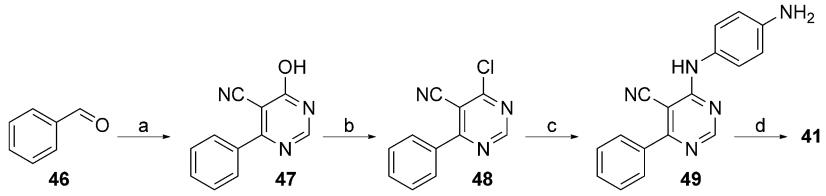

Scheme 3. Synthesis of compound **41**. Reagents and conditions: a) ethyl cyanoacetate, formamidine acetate, K_2CO_3, EtOH, reflux, 16 h; b) $POCl_3$, reflux, 2 h; c) *p*-phenylenediamine, *i*PrOH, 80 °C, 20 min; d) 2-fluoro-5-trifluoromethylphenylisocyanate, CH_2Cl_2, RT, 16 h.

the pyrimidine ring led to fully inactive compounds (**41**–**43** and **45**). Conversely, a change in the pyrimidine ring geometry from a 4-anilino-6-phenyl to a 4-anilino-2-phenyl led to an interesting improvement in activity (compare **44** with **5**). At this stage, a preliminary cytotoxicity test was run on RET+ thyroid carcinoma cells at a fixed compound concentration (10 μM), using the molecules that showed activity toward the recombinant enzyme. The analysis confirmed **22**, **26**, and **44** as the most active compounds, showing, on average, >75% cell growth inhibition (Figure S2, Supporting Information). Compounds listed in Table 3 were synthesized according to Schemes 3–5.

Compound **41** was synthesized starting from benzaldehyde, which was condensed in a single-pot reaction with ethyl cyanoacetate and formamidine to yield hydroxypyrimidine **47** (Scheme 3). Standard chlorination and condensation with *p*-phenylenediamine and the isocyanate furnished the desired final product. The 2-substituted pyrimidine derivatives were prepared in two different ways. Compound **42** (Scheme 4 A) was prepared starting from dichloropyrimidine **50**, which was

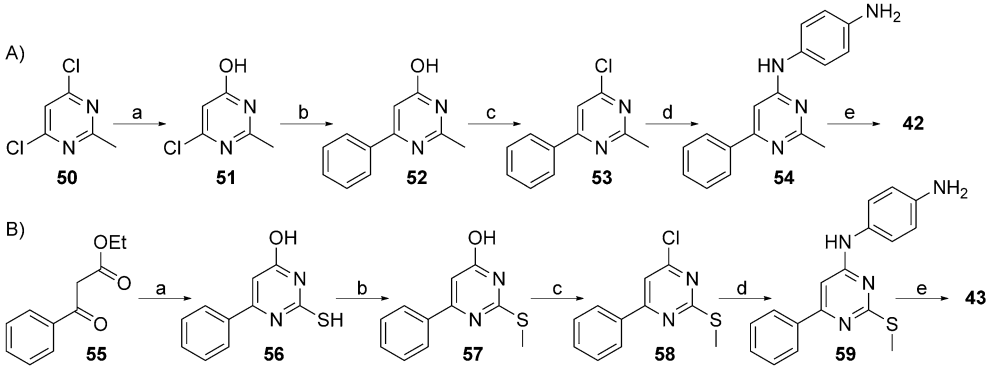

Scheme 4. Synthesis of compounds A) **42** and B) **43**. Reagents and conditions: (A) a) HCl 3 M, *n*BuOH, MW, 125 °C, 10 min; b) phenylboronic acid, $Pd(PPh_3)_4$, K_2CO_3, DME, H_2O, MW, 130 °C, 5 min; c) $POCl_3$, 80 °C, 4 h; d) *p*-phenylenediamine, *i*PrOH, MW, 150 °C, 20 min; e) 2-fluoro-5-trifluoromethylphenylisocyanate, CH_2Cl_2, RT, 16 h. (B) a) NaOEt 20% in EtOH, RT, 20 min, then thiourea, reflux, 24 h; b) MeI, NaOH, H_2O, RT, 16 h; c) $POCl_3$, 80 °C, 4 h; d) *p*-phenylenediamine, *i*PrOH, MW, 150 °C, 20 min; e) 2-fluoro-5-trifluoromethylphenylisocyanate, CH_2Cl_2, RT, 16 h.

selectively monohydrolyzed to compound **51** before being submitted to Suzuki reaction and subsequent chlorination. Unfortunately, all attempts to perform the Suzuki reaction on **50** to directly obtain compound **53** was unsuccessful. For compound **43** (Scheme 4B), the thiopyrimidine ring was obtained by treating ethyl benzoylacetate with thiourea. Compounds **44** and **45** were synthesized starting from benzamidine **60**, which was condensed with either ethyl propiolate or with 2-cyano-3-ethoxyacrylate (Scheme 5). In all the cases, the hydroxypyrimidine intermediates (i.e., **52**, **57**, **61**, and **64**) were chlorinated and submitted to condensation with *p*-phenylenediamine and then with the isocyanate.

Development of lead compound

The acquired biological data were then used to design three novel compounds bearing the features of the most active derivatives (Table 4). The optimization steps previously described suggested the importance of a benzamido substituent on the pyrimidine ring (**26**) and the nitrogen heterocycle geometry (**44**). Starting from these observations, two novel compounds were designed and synthesized that shared two common features: the presence of the benzamido functionality and the absence of a nitrogen atom at the Y position of the nitrogen heterocycle (see Table 4 for structure clarification). Compound **68** was a 4-anilino-2-substituted pyrimidine, whereas compound **69** was a 4-anilinopyridine. Surprisingly, compound **68** showed poor activity, despite bearing the structural features of the two most active compounds identified during our work. On the contrary, replacement of the pyrimidine ring with a pyridine furnished the first sub-micromolar RET inhibitor in our series (**69**). Compound **69** was profiled against a panel of kinases selected from the ScanEDGE subset of DiscoverX (http://www.discoverx.com/services/drug-discovery-development-services/kinase-profiling/kinomescan/scanedge). In particular, we tested our lead compound at a single concentration (1 μM) against the target kinases of starting hit compound **1** (i.e., FLT3, cKIT, and PDGFRβ) and against the most common targets of other RET inhibitors (i.e., Abl1, BRAF, ERK1, MET, Src, and VEGFR2) using the KinomeScan platform. The KinomeScan technology measures the ability of the tested compound to displace the target kinase from a high affinity ATP mimic probe. The result of the assay is expressed as a percent of control (POC) value that is statistically correlated with the dissociation constant. The lower the POC, the higher the affinity of the test compound for the target kinase. For a more exhaustive

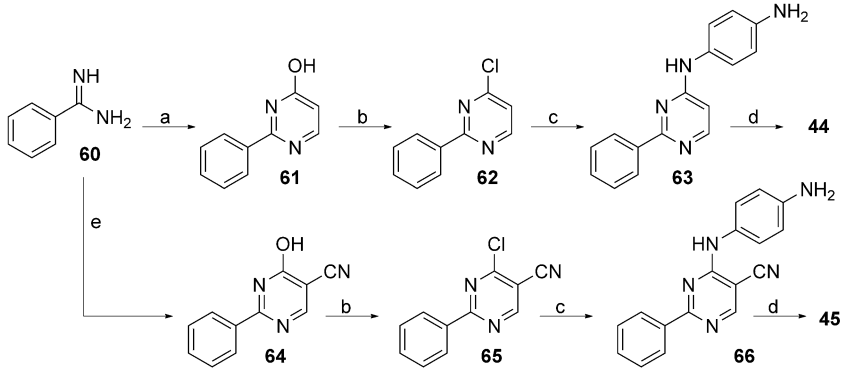

Scheme 5. Synthesis of compounds **44** and **45**. Reagents and conditions: a) ethyl propiolate, K_2CO_3, EtOH, reflux, 16 h; b) $POCl_3$, 80 °C, 4 h; c) *p*-phenylenediamine, *i*PrOH, MW, 80 °C, 40 min; d) 2-fluoro-5-trifluoromethylphenylisocyanate, CH_2Cl_2, RT, 16 h; e) ethyl (ethoxymethylene)cyanoacetate, DMF, reflux, 96 h.

Table 4. Structure and IC_{50} values (isolated ^{wt}RET) of compounds **67–69**.

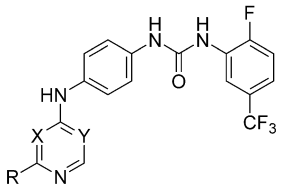

ID	X	Y	R	IC_{50} [μM][a]
5	CH	N		4.1 ± 0.1
26	CH	N	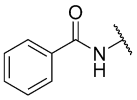	1.2 ± 0.3
44	N	CH		1.5 ± 0.1
68	N	CH	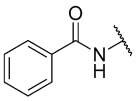	31.8 ± 1.3
69	CH	CH	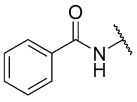	0.24 ± 0.01

[a] Values are the mean ± SEM of three determinations.

description of POC and of KinomeScan technology, see https://www.discoverx.com/tools-resources/leadhunter-study-reports-data-analysis. Results are listed in Table 5.

Table 5. Selectivity profile of compound **69**.

Kinase	POC [1 μM]
Abl1	12
BRAF	67
ERK1	100
FLT3	1.5
cKIT	< 0.5
MET	76
PDGFRβ	0.95
RET	< 0.5
Src	28
VEGFR2	8

Together, our results identified **69** as a multi cKIT/^{wt}RET/^{V804M}RET inhibitor. Notably, hit compound **1** was previously identified as a dual cKIT/PDGFRβ inhibitor (POC values < 0.5 against both kinases under the same experimental conditions).[9] Hence, our efforts to improve activity against RET kinases also led to a slightly lower potency against PDGFRβ. Compounds listed in Table 4 were synthesized according to Scheme 6, starting from the commercially available 2-amino-4-chloro-pyrimidine and -pyridine.

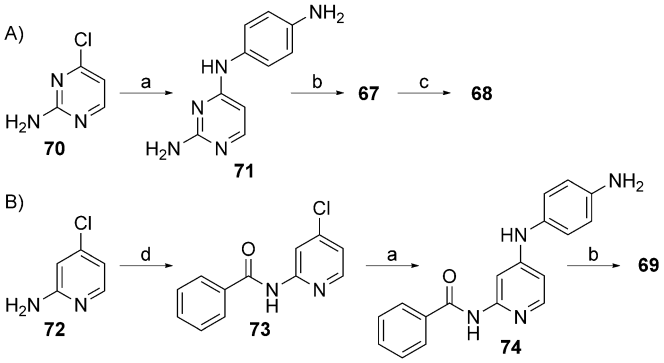

Scheme 6. Synthesis of compounds A) **67**–**68** and B) **69**. Reagents and conditions: a) *p*-phenylenediamine, *i*PrOH, MW, 80 °C, 40 min; b) 2-fluoro-5-trifluoromethylphenylisocyanate, CH_2Cl_2, RT, 16 h; c) benzoic acid, PyBOP, TEA, DMF, RT, 30 min; d) benzoyl chloride, DMAP, MeCN, MW, 100 °C, 5 min.

Compound **70** was condensed with *p*-phenylenediamine and with the substituted isocyanate. The last synthetic step was the PyBOP-mediated condensation of the free amino functionality with benzoic acid. For the synthesis of compound **69**, conversely, formation of the benzamido functionality was performed as the first synthetic step.

In vitro testing

The most active compounds (**22**, **26**, **44**, and **69**) were then tested against the recombinant ^{V804M}RET mutant and in cellular assays against selected RET+ and RET− cell lines (Table 6). Vandetanib, a kinase inhibitor clinically used to treat thyroid cancer, was used for comparison purposes. All compounds (with the only exception of **22**, which bears a 6′′-furyl substituent) were more potent against the mutant than the wild-type RET kinase. The novel RET inhibitors showed promising cytotoxic effects on RET+ cancer cell lines of both thyroid and lung origin. Interestingly, three of four tested compounds showed selective cytotoxicity in RET+ versus RET− thyroid carcinoma cells. In particular, the activity and selectivity of compound **69** were similar to that of vandetanib. We then analyzed RET autophosphorylation in the presence of **69** in TPC-1 cells harboring the CCDC6/RET fusion and in HEK293 ectopically expressing the V804M mutation.[13] Compound **69** was able to inhibit RET activation at low micromolar concentrations, in line with cell growth data (Figure 1). The inhibition of RET auto-

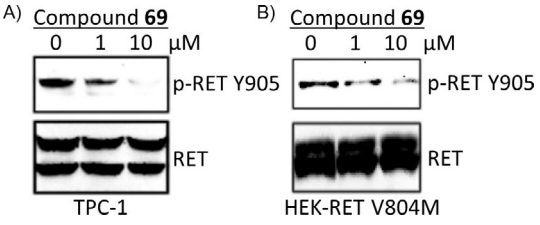

Figure 1. Western blot analysis of RET phosphorylation inhibition by compound **69** at the indicated micromolar concentrations in A) TPC-1 and B) HEK-RET^{V804M} cells. Total RET is shown for loading control.

Table 6. Biological evaluation of selected compounds.

ID	IC_{50} [μM][a]								SI[b]
	^{wt}RET	^{V804M}RET	TPC-1 [CCDC6/RET]	TT [^{C634W}RET]	MZ-CRC-1 [^{M918T}RET]	Lc2/ad [CCDC6/RET]	ARO [^{V600E}BRAF]	NPA [^{V600E}BRAF]	
22	3.8 ± 0.2	60.4	8.5 ± 0.8	6.3 ± 0.8	15.8 ± 1.4	2.6 ± 0.02	6.3 ± 0.4	7.8 ± 0.02	1
26	1.2 ± 0.3	0.65 ± 0.04	3.6 ± 0.3	0.46 ± 0.01	4.6 ± 0.5	0.62 ± 0.01	8.6 ± 2.8	7.9 ± 2.3	4
44	1.5 ± 0.1	0.74 ± 0.19	5.2 ± 0.03	3.7 ± 0.1	12.1 ± 0.2	4.1 ± 0.1	37.8 ± 13.7	20.5 ± 3.9	5
69	0.24 ± 0.01	0.11 ± 0.02	1.9 ± 0.3	0.26 ± 0.01	1.3 ± 0.06	0.16 ± 0.01	7.0 ± 0.6	7.2 ± 0.02	8
Van[c]	0.10 ± 0.01	> 10	0.41 ± 0.04	0.86 ± 0.03	1.2 ± 0.3	0.22 ± 0.02	2.6 ± 0.1	7.0 ± 0.9	7

[a] Values are the mean ± SEM of three determinations. [b] Selectivity index: IC_{50} value ratio of non-target (RET–, ARO, and NPA) to target cell. [c] Vandetanib.

phosphorylation was also determined in NIH3T3-PTC2 (see Figure S3).

Molecular docking

Preliminary molecular modeling studies were used to propose the binding mode for compound **69** in both wild-type and mutant RET. As mentioned above, no crystallographic structure has been deposited to date in the PDB for the inactive RET conformation. Hence, homology models for both ^{wt}RET and ^{V804M}RET kinases were computed using SwissModel.[21] The coordinates for VEGFR2 in complex with sorafenib (PDB ID: 3WZE)[22] were used as a template. The comparison between the active and inactive conformations for RET is reported in Figure S4.

AutoDock Vina was used to predict the binding modes for compound **69** with ^{wt}RET (Figure 2A–C) and ^{V804M}RET (Figure 2D–F). Compound **69** was predicted to establish two hydrogen bonds with the Ala807 in the hinge region. In particular, the hydrogen bond between the carboxamide NH of **69**

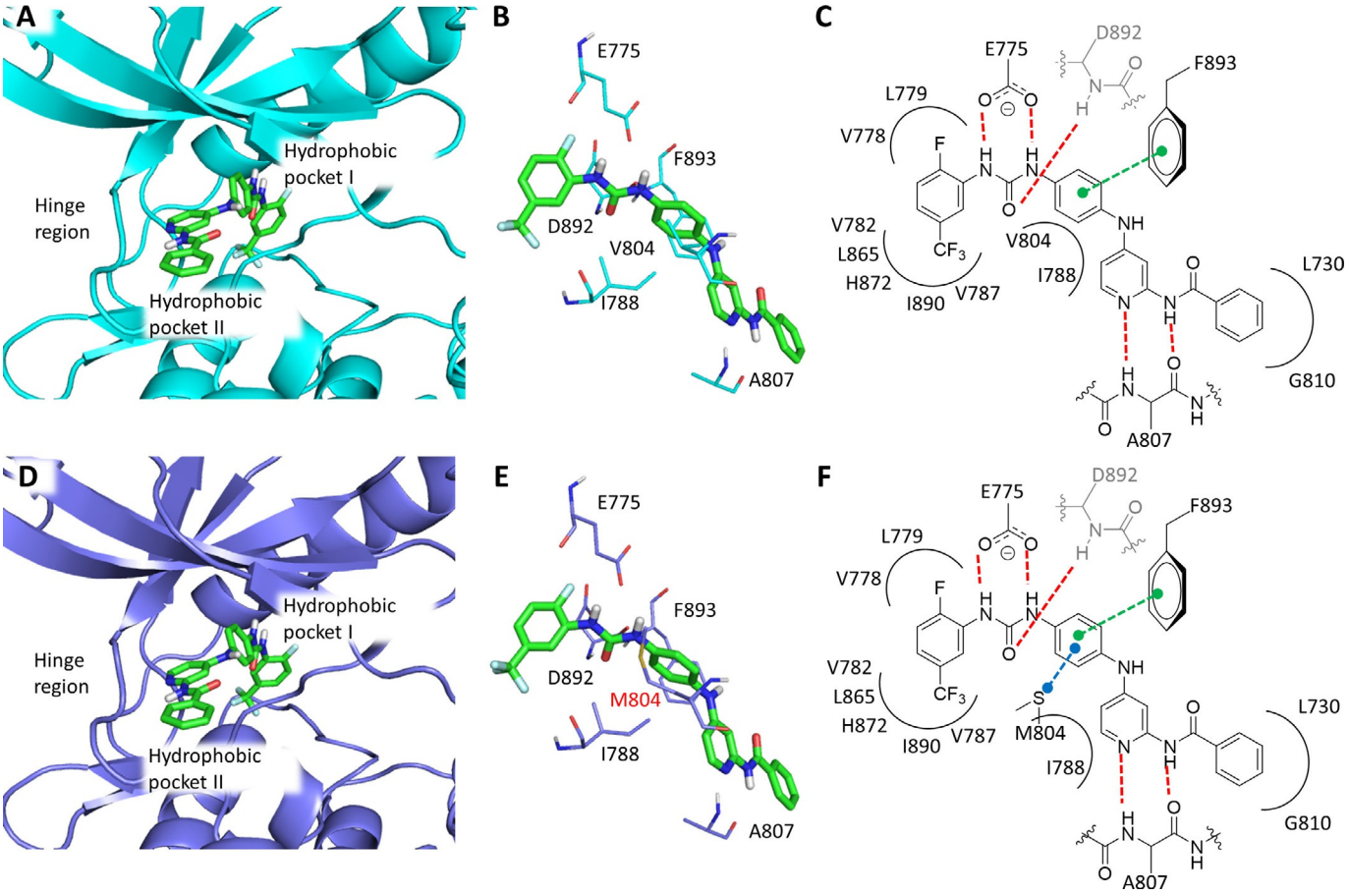

Figure 2. A) Predicted binding mode for **69** and ^{wt}RET. B) Details of the ^{wt}RET residues surrounding compound **69**. C) Schematic representation of the interactions between **69** and ^{wt}RET. Hydrogen bonds are shown as dashed red lines; the arene–arene interaction is shown as a dashed green line; hydrophobic interactions are represented by black solid curved lines. D) Predicted binding mode for **69** and ^{V804M}RET. E) Details of the ^{V804M}RET residues surrounding **69**. F) Schematic representation of the interactions between **69** and ^{V804M}RET. Hydrogen bonds are shown as dashed red lines; the arene–arene interaction is shown as a dashed green line; hydrophobic interactions are represented by black solid curved lines; the sulfur–arene interaction is shown as a dashed blue line.

with the carboxylic functionality of Ala 807 could justify the importance of an amide substituent. The urea moiety was hypothesized to interact with both the carboxylate of the conserved Glu 775 from the αC helix and with the backbone amide of Asp 892 (which belongs to the DFG motif). The terminally substituted ring fits well in the hydrophobic pocket, establishing lipophilic interactions with several amino acids. In the case of RET, the hinge region and the gatekeeper residue are highly hydrophobic. Hence, we concluded that **69** was more active than **26** due to the presence of a less hydrophilic moiety (pyridine in place of a pyrimidine). Finally, as hypothesized in our previous work with ponatinib, the observed activity of **69** against the V804M mutant may be due to the ability to induce the DFG-out conformation of the kinase; in this case, the compound would fit in the active site without clashing with the bulky mutant gatekeeper.[13] Moreover, the slightly improved activity of the compound against the V804M mutant relative to wild-type enzyme was possibly due to the ability of **69** to establish a sulfur–arene interaction with the mutated gatekeeper. With respect to the nitrogen heterocycle, molecular docking simulations failed in suggesting a reason for the higher activity of pyridine derivative **69** with respect to pyrimidine analogue **68**. Docking simulations of **68** in RET furnished results similar to those of **69**, in terms of either binding pose or Vina Score (data not shown). Hence, our findings constitute an example of how a classical medicinal chemistry approach can still offer new (and less predictable) insight into protein–ligand binding.

Conclusions

Starting from our previously identified hit compound **1** (dual cKIT/PDGFRβ inhibitor), we synthesized and tested several novel analogues with the aim of identifying novel promising RET inhibitors. Together, our data suggest that the 4-anilinopyridine scaffold rather than the 4-anilinopyrimidine scaffold can be used for the development of RET inhibitors. Molecular modeling simulations were not useful in justifying this observation, suggesting the importance of using a classical medicinal chemistry approach in hit-to-lead and lead optimization processes. The compounds reported herein showed a slight preference toward the ^{V804M}RET mutant, making them attractive lead compounds. In particular, compound **69** (multi cKIT/^{wt}RET/^{V804M}RET inhibitor) was considered the most promising lead in the series for further derivatization to obtain new potent inhibitors of RET tyrosine kinase for the specific treatment of RET+ cancer. Future work addressing the efficacy and toxicity of **69** in vivo is needed.

Experimental Section

See the Supporting Information for the synthesis and characterization of compounds.

Biochemical and cellular assays: The recombinant RET catalytic domain (WT and V804M mutant, aa 700–1020) was expressed as a His-tagged protein in baculovirus and purified by affinity chromatography as described.[23] Inhibitors were tested for activity using an ELISA-based kinase assay as described previously.[24] All cell lines were purchased from the American Type Culture Collection (ATCC) and maintained in DMEM medium (except Lc2/ad, which grow in Ham's F12 medium) supplemented with 10% fetal bovine serum, L-glutamine (2 mM), penicillin–streptomycin (100 U mL^{-1}), and gentamicin (100 U mL^{-1}). TT, TPC-1, and MZ-CRC-1 are thyroid carcinoma cell lines expressing oncogenic RET;[13] ARO and NPA thyroid cancer cells are not dependent on RET activity, rather they express the ^{V600E}BRAF oncogene;[25] Lc2/ad is an NSCLC cell line harboring the CCDC6/RET fusion.[26] Cell growth assays were performed using MTS assays (CellTiter 96 Aqueous One Solution Cell Proliferation Assay, Promega) after 72 h incubation of cells (10 000 per well) with increasing compounds concentrations in 96-well plates. Dose–response curves were generated by GraphPad Prism software by plotting log inhibitor concentration versus normalized kinase activity, and IC_{50} values were calculated as the concentrations causing half-maximal responses relative to control. Data were generated in triplicate and repeated in at least two independent experiments. Ponatinib and vandetanib were purchased from Selleck Chemicals, dissolved in DMSO, aliquoted, and stored at −20 °C.

Computational methods: Computational studies were carried out on a 4 CPU (Intel Core2 Quad CPU Q9550, 2.83 GHz) ACPI ×64 Linux workstation with Ubuntu 16.10 operating system. The tridimensional structure of the template for homology modeling was downloaded from the PDB (PDB ID: 3WZE). The sequences of the kinase domain of ^{wt}RET and of ^{V804M}RET were downloaded from PubMed Protein (https://www.ncbi.nlm.nih.gov/protein). The ^{wt}RET and ^{V804M}RET homology models were prepared with SwissModel Automatic Modelling Mode (swissmodel.expasy.org)[21] as previously reported.[16] The structure of compound **69** was prepared with MarvinSketch 5.5.0.1 software (www.chemaxon.com/products). The lowest-energy conformations and the degree of protonation at pH 7.4 were determined with OpenBabel software[27] using the MMFF94s force field. For all molecules, the appropriate.pdbqt files were prepared with the AutoDockTools graphical interface of AutoDock 4 software.[28] All docking studies were performed with AutoDock Vina[29] using a docking box of 22.5×16.5×20.25 Å dimensions and exhaustiveness = 20. Finally, the lowest energy conformation for both **69**/^{wt}RET and **69**/^{V804M}RET was analyzed.

Acknowledgements

The present work was carried out with financial support from the University of Padova (Progetto Giovani Studiosi 2012 to G.M.). M.D.V. thanks the Fondazione Cariparo for a PhD student grant.

Conflict of interest

The authors declare no conflict of interest.

Keywords: hit-to-lead · kinases · pyridines · pyrimidines · RET inhibitors

[1] J. Zhang, P. L. Yang, N. S. Gray, *Nat. Rev. Cancer* **2009**, *9*, 28–39.
[2] D. R. Robinson, Y. M. Wu, S. F. Lin, *Oncogene* **2000**, *19*, 5548–5557.
[3] G. Manning, D. B. Whyte, R. Martinez, T. Hunter, S. Sudarsanam, *Science* **2002**, *298*, 1912–1934.
[4] a) A. Arora, E. M. Scholar, *J. Pharmacol. Exp. Ther.* **2005**, *315*, 971–979; b) M. K. Paul, A. K. Mukhopadhyay, *Int. J. Med. Sci.* **2004**, *1*, 101–115.
[5] S. Gross, R. Rahal, N. Stransky, C. Lengauer, K. P. Hoeflich, *J. Clin. Invest.* **2015**, *125*, 1780–1789.

[6] Y. Liu, N. S. Gray, *Nat. Chem. Biol.* **2006**, *2*, 358 – 364.
[7] R. Roskoski, *Pharmacol. Res.* **2016**, *103*, 26 – 48.
[8] a) A. Chilin, M. T. Conconi, G. Marzaro, A. Guiotto, L. Urbani, F. Tonus, P. Parnigotto, *J. Med. Chem.* **2010**, *53*, 1862 – 1866; b) M. T. Conconi, G. Marzaro, L. Urbani, I. Zanusso, R. Di Liddo, I. Castagliuolo, P. Brun, F. Tonus, A. Ferrarese, A. Guiotto, A. Chilin, *Eur. J. Med. Chem.* **2013**, *67*, 373 – 383; c) G. Marzaro, I. Castagliuolo, G. Schirato, G. Palu', M. Dalla Via, A. Chilin, P. Brun, *Eur. J. Med. Chem.* **2016**, *115*, 416 – 425.
[9] V. Gandin, A. Ferrarese, M. Dalla Via, C. Marzano, A. Chilin, G. Marzaro, *Sci. Rep.* **2015**, *5*, 16750.
[10] I. Plaza-Menacho, L. Mologni, N. Q. McDonald, *Cell. Signalling* **2014**, *26*, 1743 – 1752.
[11] M. Song, *J. Med. Chem.* **2015**, *58*, 3672 – 3681.
[12] L. Mologni, C. Gambacorti-Passerini, P. Goekjian, L. Scapozza, *Expert Opin. Ther. Pat.* **2017**, *27*, 91 – 99.
[13] L. Mologni, S. Redaelli, A. Morandi, I. Plaza-Menacho, C. Gambacorti-Passerini, *Mol. Cell. Endocrinol.* **2013**, *377*, 1 – 6.
[14] a) L. M. Mulligan, *Expert Rev. Proteomics* **2016**, *13*, 631 – 633; b) D. Viola, L. Valerio, E. Molinaro, L. Agate, V. Bottici, A. Biagini, L. Lorusso, V. Cappagli, L. Pieruzzi, C. Giani, E. Sabini, P. Passannati, L. Puleo, A. Matrone, B. Pontillo-Contillo, V. Battaglia, S. Mazzeo, P. Vitti, R. Elisei, *Endocr.-Relat. Cancer* **2016**, *23*, R185 – R205.
[15] K. C. Duong-Ly, K. Devarajan, S. Liang, K. Y. Horiuchi, Y. Wang, H. Ma, J. R. Peterson, *Cell Rep.* **2016**, *14*, 772 – 781.
[16] B. Frett, M. Moccia, F. Carlomagno, M. Santoro, H. Y. Li, *Eur. J. Med. Chem.* **2014**, *86*, 714 – 723.
[17] Y. Dai, K. Hartandi, Z. Ji, A. A. Ahmed, D. H. Albert, J. L. Bauch, J. J. Bouska, P. F. Bousquet, G. A. Cunha, K. B. Glaser, C. M. Harris, D. Hickman, J. Guo, J. Li, P. A. Marcotte, K. C. Marsh, M. D. Moskey, R. L. Martin, A. M. Olson, D. J. Osterling, L. J. Pease, N. B. Soni, K. D. Stewart, V. S. Stoll, P. Tapang, D. R. Reuter, S. K. Davidsen, M. R. Michaelides, *J. Med. Chem.* **2007**, *50*, 1584 – 1597.
[18] M. Hasegawa, N. Nishigaki, Y. Washio, K. Kano, P. A. Harris, H. Sato, I. Mori, R. I. West, M. Shibahara, H. Toyoda, L. Wang, R. T. Nolte, J. M. Veal, M. Cheung, *J. Med. Chem.* **2007**, *50*, 4453 – 4470.
[19] S. Wilhelm, C. Carter, M. Lynch, T. Lowinger, J. Dumas, R. A. Smith, B. Schwartz, R. Simantov, S. Kelley, *Nat. Rev. Drug Discovery* **2006**, *5*, 835 – 844.
[20] K. Kubo, T. Shimizu, S. Ohyama, H. Murooka, A. Iwai, K. Nakamura, K. Hasegawa, Y. Kobayashi, N. Takahashi, K. Takahashi, S. Kato, T. Izawa, T. Isoe, *J. Med. Chem.* **2005**, *48*, 1359 – 1366.
[21] K. Arnold, L. Bordoli, J. Kopp, T. Schwede, *Bioinformatics* **2006**, *22*, 195 – 201.
[22] K. Okamoto, M. Ikemori-Kawada, A. Jestel, K. von König, Y. Funahashi, T. Matsushima, A. Tsuruoka, A. Inoue, J. Matsui, *ACS Med. Chem. Lett.* **2015**, *6*, 89 – 94.
[23] E. Sala, L. Mologni, S. Cazzaniga, E. Papinutto, C. Gambacorti-Passerini, *Int. J. Biol. Macromol.* **2006**, *39*, 60 – 65.
[24] L. Mologni, E. Sala, B. Riva, L. Cesaro, S. Cazzaniga, S. Redaelli, O. Marin, N. Pasquato, A. Donella-Deana, C. Gambacorti-Passerini, *Protein Expression Purif.* **2005**, *41*, 177 – 185.
[25] E. Sala, L. Mologni, S. Truffa, C. Gaetano, G. E. Bollag, C. Gambacorti-Passerini, *Mol. Cancer Res.* **2008**, *6*, 751 – 759.
[26] D. Matsubara, Y. Kanai, S. Ishikawa, S. Ohara, T. Yoshimoto, T. Sakatani, S. Oguni, T. Tamura, H. Kataoka, S. Endo, Y. Murakami, H. Aburatani, M. Fukayama, T. Niki, *J. Thorac. Oncol.* **2012**, *7*, 1872 – 1876.
[27] N. M. O'Boyle, M. Banck, C. A. James, C. Morley, T. Vandermeersch, G. R. Hutchison, *J. Cheminf.* **2011**, *3*, 33.
[28] G. M. Morris, R. Huey, W. Lindstrom, M. F. Sanner, R. K. Belew, D. S. Goodsell, A. J. Olson, *J. Comput. Chem.* **2009**, *30*, 2785 – 2791.
[29] O. Trott, A. J. Olson, *J. Comput. Chem.* **2010**, *31*, 455 – 461.

Published in: Bioorganic and Medicinal Chemistry Letters, 26, 4875-4878, 2016

Novel benzoquinoline derivatives via unpredicted condensation of ethyl propiolate and naphthylamines: Synthesis and topoisomerase inhibition activity

Giovanni Marzaro [a,†], Lisa Dalla Via [a,†], Aída Nelly García-Argáez [a,b], Martina Dalla Via [a], Adriana Chilin [a,*]

[a] Department of Pharmaceutical and Pharmacological Sciences, University of Padova, via Marzolo 5, 35131 Padova, Italy
[b] Fondazione per la Biologia e la Medicina della Rigenerazione T.E.S.—Tissue Engineering and Signalling Onlus, Via F. Marzolo 13, 35131 Padova, Italy

A B S T R A C T

An unpredicted condensation of naphthylamine with two molecules of ethyl propiolate yields directly carbethoxy benzoquinoline in high yield. Some benzoquinoline carboxamide derivatives with protonatable side chains were then synthesized and evaluated for antiproliferative activity on human tumor cell lines. The most active compound (**7a**) demonstrated to intercalate into DNA and to inhibit the relaxation activity mediated by topoisomerase II.

Keywords:
Benzoquinolines
Microwave chemistry
Synthesis
DNA
Topoisomerase II

Topoisomerases are still a major target in the field of anticancer agents. Topoisomerase inhibitors, as anthracyclines, mitoxantrone, amsacrine, camptothecin,[1,2] impair DNA replication and transcription by blocking the DNA relaxation process, thus exerting antiproliferative activity.[3]

Due to our interest in designing DNA-intercalating topoisomerase inhibitors,[4–6] we planned to synthesize and study novel nitrogen-containing polycyclic aromatic compounds decorated with cationic side chain, taking *N*-[2-(dimethylamino)-ethyl] acridine-4-carboxamide (DACA, **1**) and *N*-[2-(dimethyl-amino) ethyl]-2,6-dimethyl-1-oxo-1,2-dihydrobenzo[*b*]-1,6-naphthyridine-4-carboxamide (SN 28049, **2**) (Fig. 1) as model compounds.

DACA, in which the acridine moiety allows DNA intercalation and the carboxamide side chain provides GC-selectivity,[7] demonstrated so good antitopoisomerase activity to enter phase I and II clinical trials,[8,9] also proving to overcome multidrug resistance,[10] but low dose potency and an unusual form of toxicity prevented further development.[11] SN28049 was developed as DACA analogue,[12] with a benzonaphthyridine rather than an acridine chromophore,[13] and demonstrated 20-fold higher dose potency and lower toxicity.[11]

At the beginning, we planned to prepare benzo[*f*]quinolin-3-one derivatives (**3**) as angular isoster of **1** and **2**. Thus 2-naphthylamine (**4**) and ethyl propiolate (**5**) were condensed in dichloromethane at reflux in the presence of palladium acetate and trifluoroacetic acid (TFA), as described for oxygenated analogues (coumarin derivatives).[14] However in these conditions no reaction product was formed, probably due to the difference in reactivity between amino and hydroxyl group.

Since we had previously experienced that the Microwave Assisted Organic Synthesis (MAOS) can dramatically affect the reaction course,[15,16] we performed the planned synthesis under microwave irradiation in TFA. Surprisingly, we found that, doubling the stoichiometric quantity of propiolate in the absence of palladium acetate, a novel product was formed, identified by means of ^{1}H NMR and HRMS as ethyl benzo[*f*]quinoline-2-carboxylate (**6**), instead of the expected benzo[*f*]quinolin-3-one (**3**) (Scheme 1).

The reaction mechanism probably involves the initial formation of a 3-(naphthalene-2-ylamino)acrylate intermediate through the addition of arylamine to a protonated propiolate molecule, a reaction extensively described.[17,18] The β-enamino ester intermediate undergoes to a Stork-like enamine addition[19] to another protonated propiolate molecule, enabling the next acid catalyzed intramolecular cyclization. Finally, the elimination of an ethyl acetate molecule allows to obtain a fully aromatic system, yielding compound **6** (Scheme 2).

* Corresponding author. Tel.: +39 049 827 5349.
E-mail address: adriana.chilin@unipd.it (A. Chilin).
† First two authors contributed equally to this work and should be considered co-first authors.

http://dx.doi.org/10.1016/j.bmcl.2016.09.031

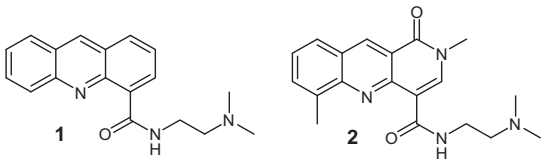

Figure 1. Structure of DACA (**1**) and SN 28049 (**2**).

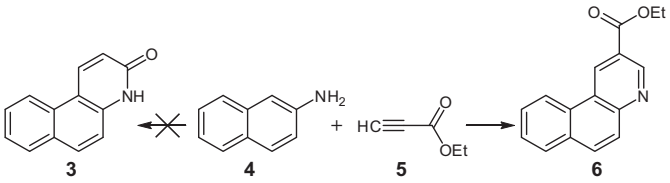

Scheme 1. Unpredicted synthesis of carbethoxy benzo[*f*]quinoline **6**.

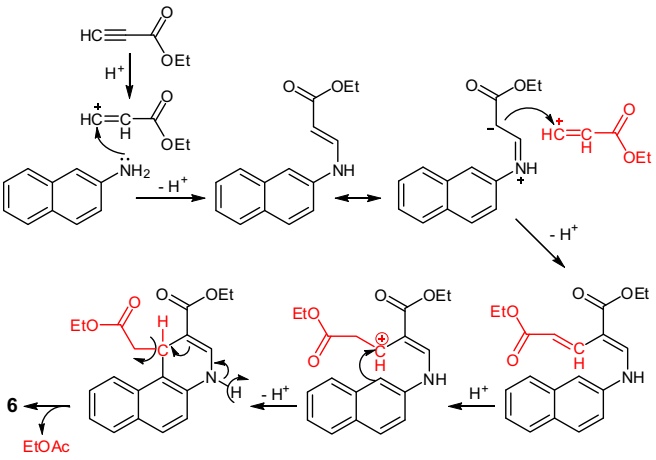

Scheme 2. Proposed mechanism for the formation of compound **6**.

The condensation of two molecules of β-enamino ester to 1,2-dihydroquinoline in acid medium (i.e. HI) has already been described,[20,21] but the final aromatization did not take place in that condition. In those reactions the arylamine:propiolate ratio was 1:1, affording at most 0.5 equivalents of quinoline (hence yield could be at most 50%). Conversely, in our method the stoichiometry is 1:2, affording up to 1 equivalent of quinoline (as confirmed by our reported yields higher than 50%).

The reaction of propiolate and arylamines to afford quinoline derivatives has also been reported, but besides these two reagents, a further reactant is needed for the completion of the nitrogen nucleus. A carbonyl compound (aldehyde or ketone)[22–25] or a carboxyl compound (formic acid)[26] is required, whose carbonyl will represent the carbon in 4 position of the final quinoline nucleus. In our reaction the carbon in 4 position is the omega carbon of the second propiolate molecule, thus the further carbonyl compound is no longer needed to obtain the quinoline nucleus.

Since the elimination of ethyl acetate is not a common event in organic reaction, our hypothesis was assessed by means of GC analysis of the reaction mixture. Indeed, the experiments confirmed the EtOAc elimination (see Supplementary Material for details).

Several reaction conditions were then tested (see Table 1S in Supplementary Material). The best experimental conditions involves the use of toluene as solvent, TFA as acid and microwave irradiation at 150 °C (50 W) for 7 min and furnished the title compound with the easiest work-up: by simply cooling the reaction mixture with vigorous stirring, the benzoquinoline slowly crystallized in high purity.

The reaction protocol was applied also to 1-naphthylamine, obtaining the corresponding benzo[*h*]quinoline in good yields (**9**; Scheme 3B). Compounds **6** and **9** are already known, even if synthesized by different synthetic pathway.[26–31] As the compounds bear the carboxylic function as DACA and SN28049, we took benzoquinolines **6** and **9** as starting nitrogen-containing polycyclic aromatic compounds and we synthesized some carboxamide derivatives with cationic side chain as potential DNA-intercalating topoisomerase inhibitors.

The carbethoxybenzoquinolines **6** and **9** were coupled with *N*,*N*-diethylethylenediamine, 2-morpholinoethylamine or 1-(2-aminoethyl)piperazine in DMSO and catalytic amount of copper iodide under microwave irradiation to provide compounds **7a–c** and **10a–c** (Scheme 3A and B).

To increase the hydrophilicity of carboxamide derivatives and to determine the role of another condensed ring on biological activity, the 8,9-ethylendioxybenzo[*h*]quinoline analogues **14a–c** were synthesized (Scheme 4).

Compound **11**[31] was reduced to **12** by catalytic hydrogenation over Pd/C, then condensed with ethyl propiolate as above described and functionalized with the cationic side chains to the desired carboxamide **14a–c** (Scheme 4).

The cytotoxic activity of benzoquinolines **6**, **7a–c**, **9**, **10a–c**, **13** and **14a–c** was assayed by means of an in vitro assay[32] on three

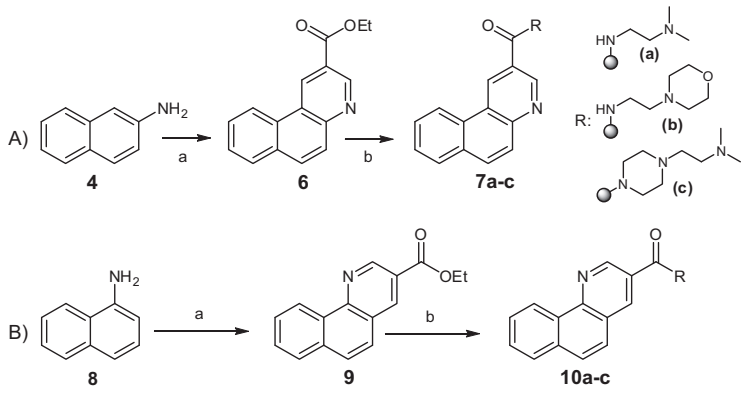

Scheme 3. Synthesis of compounds **7a–c** and **10a–c**. Reaction conditions: (a) **5**, TFA, MW, 50 W, 150 °C, 7 min, 68–70%; (b) amine, CuI, DMSO, MW, 100 W, 180 °C, 15 min, 9–45%.

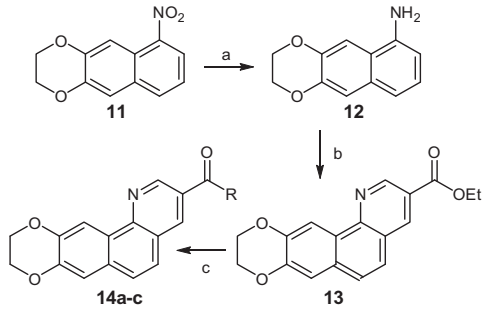

Scheme 4. Synthesis of compounds **14a–c**. Reaction conditions: (a) H_2, Pd/C 10%, abs. EtOH, 2 h, 92%; (b) **5**, TFA, MW, 50 W, 150 °C, 7 min, 59%; (c) amine, CuI, DMSO, MW, 100 W, 180 °C, 15 min, 10–60%.

Table 1
Cell growth inhibition in the presence of benzoquinolines **6**, **7a–c**, **9**, **10a–c**, **13** and **14a–c**

Compound	Cell line GI_{50} (μM)[a]		
	HL-60	Hep-G2	HeLa
6	⩾50	⩾50	>50
7a	24.1 ± 2.3	27.8 ± 1.4	>50
7b	>50	>50	>50
7c	>50	>50	>50
9	>50	⩾50	>50
10a	29.8 ± 3.3	32.2 ± 2.6	>50
10b	>50	>50	>50
10c	>50	>50	>50
13	>50	>50	>50
14a	30.0 ± 3.3	>50	>50
14b	32.5 ± 2.8	>50	>50
14c	33.8 ± 4.3	39.4 ± 2.5	>50
m-AMSA[b]	0.012 ± 0.002	0.0060 ± 0.0011	0.17 ± 0.02

[a] Values are the mean ± SD of at least three independent experiments.
[b] See Ref. 5.

human tumor cell lines: HL-60 (human acute promyelocytic leukemia cells), HepG2 (human hepatocellular carcinoma cells) and HeLa (human cervix adenocarcinoma cells). The results, expressed as GI_{50} values, that is the concentration of the test agent inducing 50% reduction in cell number compared with control cultures, are shown in Table 1.

The obtained values indicate for **7a** and **10a** the capacity to induce the most significant cytotoxic effect on both HL-60 and Hep-G2 cell lines, with GI_{50} values ranging from 24.1 to 32.2 μM. Otherwise, on HeLa cells they appear inactive at the concentrations taken into account. As regard the others benzoquinolines belonging to these series (**7b**, **7c**, **10b** and **10c**), they are ineffective on all cell lines taken into consideration, like the unsubstituted **6** and **9**. These results suggest an important role in the antiproliferative activity for the dimethylamino substituent and this assumption could be valid also for the dioxolane derivatives **13** and **14a–c**. Also in this latter series indeed, the lower GI_{50} value is shown by the dimethylamino derivative **14a**. Nevertheless, by considering **14a–c**, also the fourth dioxolane ring seems to participate in the cytotoxicity, because they are all active on HL-60 cells that appear as the most sensitive cell line.

Due to the presence of the planar benzoquinoline moiety, it was hypothesized that the antiproliferative activity of the most active **7a** could be related to the formation of a molecular complex with DNA following an intercalative mode of binding. To verify this hypothesis, flow linear dichroism (LD) experiments were performed as previously described[33] and the spectra of DNA solution alone and in the presence of **7a** at [drug]/[DNA] ratios = 0.08 are reported in Figure 2. The DNA spectrum (dotted line) shows the

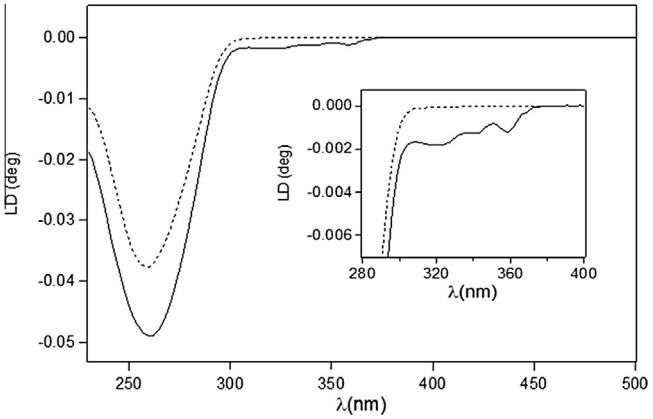

Figure 2. Linear flow dichroism spectra for compound **7a** at [drug]/[DNA] ratios: 0 (dotted line) and 0.08 (continuous line). [DNA] = 1.9×10^{-3} M.

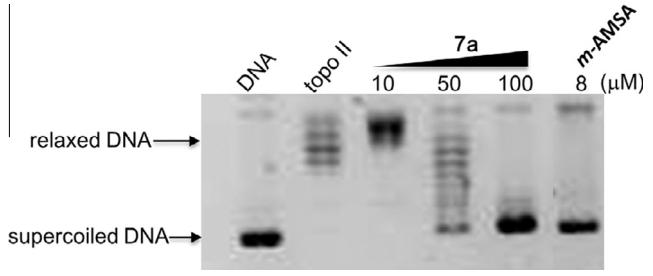

Figure 3. Effect of the benzoquinoline **7a** on the relaxation of supercoiled plasmid DNA mediated by human recombinant topoisomerase II. Supercoiled DNA (DNA) was incubated with topoisomerase II in the absence (topo II) and presence of test compound at indicated concentrations (μM). 8 μM *m*-AMSA was used as reference drug.

typical negative dichroic signal at 260 nm, due to the purine and pyrimidine chromophores. The addition of **7a** (continuous line) induces the appearance of a further negative signal at higher wavelengths (310–380 nm). The presence of a LD signal in this spectral region, where only the added benzoquinoline chromophore can absorb, indicates the occurrence of a complexation with the macromolecule. Moreover, the negative sign of this latter LD signal, as that due to the DNA bases, highlighted an intercalative mode of binding, i.e. an orientation of the molecular plane of the benzoquinoline chromophore parallel to the plane of the purine and pyrimidine bases.

The ability of **7a** to form a molecular intercalative complex with DNA suggested the possibility that the benzoquinoline derivative could interfere with the catalytic activity of nuclear enzymes, like topoisomerase II. Indeed, for a number of antiproliferative intercalative agents the ability to inhibit topoisomerase II was demonstrated.[34] In this connection, we investigated the effect of **7a** on the relaxation of supercoiled pBR322 plasmid DNA mediated by human recombinant topoisomerase II,[35] and the results are shown in Figure 3. The well-known antitopoisomerase II drug *m*-AMSA was taken as reference compound and used at 8 μM.

In the presence of topoisomerase II the supercoiled plasmid DNA (lane 'DNA') relaxes and indeed, the disappearance of the supercoiled form, along with the concurrent formation of a number of topoisomers can be observed (lane 'topo II'). The addition of increasing concentrations of **7a** induces a dose-dependent inhibition of the enzyme activity. Indeed, at 50 μM the appearance of the supercoiled form can already be detected, and at 100 μM the complete absence of topoisomers along with an amount of supercoiled form higher to that obtained with the reference drug, can be observed.

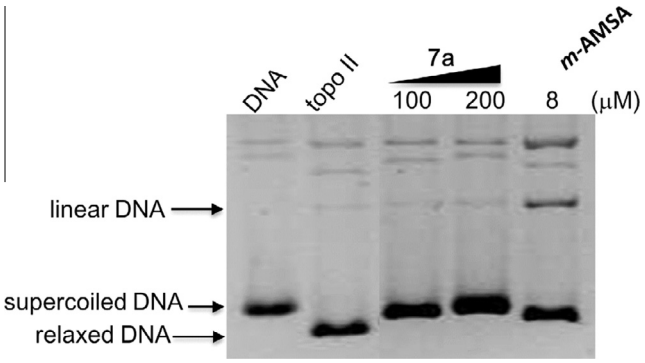

Figure 4. Effect of **7a** on the stabilization of covalent-DNA-topoisomerase II complex. Supercoiled DNA (DNA) was incubated with topoisomerase II in the absence (topo II) and presence of **7a** at indicated concentrations (μM). 8 μM *m*-AMSA was used as reference.

Many intercalative agents, such as adriamycin, *m*-AMSA and mitoxantrone, are able to inhibit topoisomerase II catalytic cycle by stabilizing an intermediate, known as cleavable complex, into a lethal condition for the cell. The drugs that exert this ability are named topoisomerase II poisons.[34,36,37] The poisoning effect can be experimentally demonstrated by a cleavable complex assay which allows the detection of the topoisomerase II-dependent formation of linear from supercoiled DNA.[38] Figure 4 shows the results obtained from the cleavage complex assay carried out in the presence of two concentrations of **7a**, i.e. 100 and 200 μM, and of *m*-AMSA at 8 μM, as reference.

The relaxation activity of topoisomerase II (lane 'topo II') provokes the relaxation of supercoiled pBR322 DNA and the reference drug induces, as expected, the formation of a detectable amount of linear DNA (lane '*m*-AMSA'). In the presence of **7a**, even at the highest concentration taken into consideration (200 μM), the formation of linear DNA does not occur, indicating the inability of the benzoquinoline derivative to act as topoisomerase II poison.

In conclusion we have developed a novel single step strategy to access to carbethoxy benzoquinoline starting from both 1- and 2-naphtyhlamines with good yields, short reaction times, very easy work-up procedures and absence of any metal catalyst.

The derivatives carrying a dimethylamino side chain induce an antiproliferative effect on leukemic cells and interestingly, the most active **7a** demonstrates the ability to form a molecular intercalative complex with DNA. Moreover, **7a** shows a significant inhibition of the relaxation activity mediated by the nuclear enzyme topoisomerase II.

Overall, these results suggest that benzoquinoline moiety decorated with protonatable side chains could be a promising scaffold for the development of intercalating antitopoisomerase II agents.

Author contributions

G.M. developed the new synthetic strategy to benzoquinolines. G.M., M.D.V. and A.C. synthesized the benzoquinoline derivatives. L.D.V. and A.N.G.-A. conducted the biological experiments. L.D.V and A.C. wrote the paper. All the authors revised the manuscript.

Acknowledgments

The present work has been carried out with the financial support of the University of Padova 'Progetto Giovani Studiosi 2012' to G.M. M.D.V. thanks the Fondazione Cariparo for a PhD student grant.

Supplementary data

Supplementary data (all experimental details including synthetic procedures, compound characterizations, ^{1}H NMR and ^{13}C NMR spectra and biological evaluations) associated with this article can be found, in the online version, at http://dx.doi.org/10.1016/j.bmcl.2016.09.031.

References and notes

1. Salerno, S.; Da Settimo, F.; Taliani, S.; Simorini, F.; La Motta, C.; Fornaciari, G.; Marini, A. M. *Curr. Med. Chem.* **2010**, *17*, 4270.
2. Dezhenkova, L. G.; Tsvetkov, V. B.; Shtil, A. A. *Russ. Chem. Rev.* **2014**, *83*, 82.
3. Wang, J. C. *Nat. Rev. Mol. Cell Biol.* **2002**, *3*, 430.
4. Chilin, A.; Marzaro, G.; Marzano, C.; Dalla Via, L.; Ferlin, M. G.; Pastorini, G.; Guiotto, A. *Bioorg. Med. Chem.* **2009**, *17*, 523.
5. Marzaro, G.; Dalla Via, L.; Toninello, A.; Guiotto, A.; Chilin, A. *Bioorg. Med. Chem.* **2011**, *19*, 1197.
6. Dalla Via, L.; Marzaro, G.; Ferrarese, A.; Gia, O.; Chilin, A. *Eur. J. Med. Chem.* **2014**, *77*, 103.
7. Finlay, G. J.; Riou, J. F.; Baguley, B. C. *Eur. J. Cancer* **1996**, *32A*, 708.
8. McCrystal, M. R.; Evans, B. D.; Harvey, V. J.; Thompson, P. I.; Porter, D. J.; Baguley, B. C. *Cancer Chemother. Pharmacol.* **1999**, *44*, 39.
9. Twelves, C.; Campone, M.; Coudert, B.; Van den, B. M.; de Jonge, M.; Dittrich, C.; Rampling, R.; Sorio, R.; Lacombe, D.; de Balincourt, C.; Fumoleau, P. *Ann. Oncol.* **2002**, *13*, 777.
10. Davey, R. A.; Su, G. M.; Hargrave, R. M.; Harvie, R. M.; Baguley, B. C.; Davey, M. W. *Cancer Chemother. Pharmacol.* **1997**, *39*, 424.
11. Baguley, B. C. In *Horizons in Cancer Research*; Watanabe, H. S., Ed.; Nova Publishers, 2012; Vol. 48, pp 47–65.
12. Deady, L. W.; Rodemann, T.; Zhuang, L.; Baguley, B. C.; Denny, W. A. *J. Med. Chem.* **2003**, *46*, 1049.
13. Bridewell, D. J.; Porter, A. C.; Finlay, G. J.; Baguley, B. C. *Cancer Chemother. Pharmacol.* **2008**, *62*, 753.
14. Jia, C. G.; Lu, W. J.; Oyamada, J.; Kitamura, T.; Matsuda, K.; Irie, M.; Fujiwara, Y. *J. Am. Chem. Soc.* **2000**, *122*, 7252.
15. Marzaro, G.; Guiotto, A.; Chilin, A. *Green Chem.* **2009**, *11*, 774.
16. Chilin, A.; Marzaro, G.; Zanatta, S.; Guiotto, A. *Tetrahedron Lett.* **2007**, *48*, 3229.
17. Huisgen, R.; Herbig, K.; Siegel, K.; Huber, H. *Chem. Ber.* **1966**, *99*, 2526.
18. Mohri, K.; Kanie, A.; Horiguchi, Y.; Isobe, K. *Heterocycles* **1999**, *51*, 2377.
19. Smith, M. B. In *March's Advanced Organic Chemistry: Reactions, Mechanisms, and Structure*, 6th ed.; Wiley-Interscience: Hoboken, NJ, 2007; pp 634–636.
20. Matsumoto, S.; Mori, T.; Akazome, M. *Synthesis* **2010**, 3615.
21. Zhuo, J. C. *Molecules* **1999**, *4*, M118.
22. Kozlov, N. G.; Gusak, K. N.; Kadutskii, A. P. *Chem. Heterocycl. Compd.* **2010**, *46*, 505 (and citation therein).
23. Sun, J.; Gao, H.; Wu, O.; Yan, C. G. *Beilstein J. Org. Chem.* **2012**, *8*, 1839.
24. Wang, X. S.; Zhou, J.; Zhang, M. M.; Wang, W.; Li, Y. L. *Monatsh. Chem.* **2012**, *143*, 935.
25. Karmakar, R.; Kayal, U.; Bhattacharya, B.; Maiti, G. *Tetrahedron Lett.* **2014**, *55*, 1370.
26. Gadakh, S. K.; Sudalai, A. Patent WO2015/198349 A1, 2015.
27. Beller, N. R.; Neckers, D. C.; Papadopoulos, E. P. *J. Org. Chem.* **1977**, *42*, 3514.
28. Tummatorn, J.; Thongsornkleeb, C.; Ruchirawat, S.; Gettongsong, T. *Org. Biomol. Chem.* **2013**, *11*, 1463.
29. Erickson, E. H.; Hainline, C. F.; Lenon, L. S.; Matson, C. J.; Rice, T. K.; Swingle, K. F.; Van Winkle, M. *J. Med. Chem.* **1979**, *22*, 816.
30. Gadakh, S. K.; Dey, S.; Sudalai, A. *Org. Biomol. Chem.* **2016**, *14*, 2969.
31. Heertjes, P. M.; Ter Horst, A. M.; Persijn, J. M. *Recl. Trav. Chim. Pay-Bas* **1954**, *73*, 513.
32. Dalla Via, L.; Mejia, M.; García-Argáez, A. N.; Braga, A.; Toninello, A.; Martínez-Vázquez, M. *Bioorg. Med. Chem.* **2015**, *23*, 5816.
33. Ferlin, M. G.; Gia, O.; Dalla Via, L. *ChemMedChem* **2011**, *6*, 1872.
34. Nitiss, J. L. *Nat. Rev. Cancer* **2009**, *9*, 338.
35. Christodoulou, M. S.; Fokialakis, N.; Passarella, D.; García-Argáez, A. N.; Gia, O.; Pongratz, I.; Dalla Via, L.; Haroutounian, S. A. *Bioorg. Med. Chem.* **2013**, *21*, 4120.
36. Chen, A. Y.; Liu, L. F. *Annu. Rev. Pharmacol. Toxicol.* **1994**, *34*, 191.
37. Pommier, Y.; Leo, E.; Zhang, H. L.; Marchand, C. *Chem. Biol.* **2010**, *17*, 421.
38. Christodoulou, M. S.; Calogero, F.; Baumann, M.; García-Argaez, A. N.; Pieraccini, S.; Sironi, M.; Dapiaggi, F.; Bucci, R.; Broggini, G.; Gazzola, S.; Liekens, S.; Silvani, A.; Lahtela-Kakkonen, M.; Martinet, N.; Nonell-Canals, A.; Santamaría-Navarro, E.; Baxendale, I. R.; Dalla Via, L.; Passarella, D. *Eur. J. Med. Chem.* **2015**, *92*, 766.

Published in: European Journal of Medicinal Chemistry, 115, 416-425, 2016

Substituted quinazolinones as kinase inhibitors endowed with anti-fibrotic properties

Giovanni Marzaro [a, *], Ignazio Castagliuolo [b], Giulia Schirato [b], Giorgio Palu' [b], Martina Dalla Via [a], Adriana Chilin [a], Paola Brun [b]

[a] Department of Pharmaceutical and Pharmacological Sciences, University of Padova, Via Marzolo 5, 35131 Padova, Italy
[b] Department of Molecular Medicine, University of Padova, Via Gabelli 63, 35121 Padova, Italy

A B S T R A C T

Some new 3-substituted quinazolinones were synthesized and evaluated as inhibitors of kinases involved in fibrogenic process. The compounds were tested against a panel of both tyrosine and serine −threonine kinases. The profile of selectivity of some representative compounds was investigated through molecular docking studies. The most interesting compounds were also evaluated *in vitro* as potential agents for the treatment of fibrotic diseases. Quinazolinone derivatives reduced proliferation and expression of genes involved in the fibrogenic process in hepatic stellate cells (HSCs) and intestinal subepithelial myofibroblasts (ISEMFs). Furthermore some compounds downregulated phosphorylation of p38MAPK. Our findings provide evidences that 3-substituted quinazolinones target multiple essential pathways of the fibrogenic process.

Keywords:
Quinazolinones
Tyrosine kinases
Multi kinase inhibitors
Fibrosis

1. Introduction

Protein kinases are ubiquitous enzymes devoted to the regulation of almost all cellular events. The kinases catalyze the transfer of a phosphate group from the ATP to specific substrate eventually leading to transduction and propagation of cellular signal [1]. Deregulated activity, mutation or over-expression of these enzymes have been correlated to cancer [2], chronic inflammatory disorders [3], diabetes [4], cardiovascular diseases [5] and hypertension [6]. According to the targeted amino acids, kinases are commonly grouped in two major families: the tyrosine kinases (TKs) and the serine−threonine kinases (STKs). Among the TKs, the epidermal growth factor receptor (EGFR), the type 2 vascular endothelial receptor (VEGFR2 or KDR), the type 1 fibroblast growth factor receptor (FGFR1), and the cytoplasmic enzymes Abl1 and Src play crucial roles in cell proliferation as well as in cancer onset and progression [7]. On the other hand, the phosphatidylinositol-3 kinase (PI3K) is mainly a lipid kinase that, along with the mammalian target of rapamycin (mTOR), is included in the STK family. Indeed, by phosphorylation of serine or threonine containing proteins the mTOR/AKT/PI3K pathway controls several cellular functions including inflammatory responses and cancer development [8].

Remarkably, TKs and STKs -induced intracellular signals are important modulators of fibrogenic process in lung, liver, pancreas, heart, and gut. Fibrosis can occur during tissue repair or inflammation as a result of persistent activation of fibrogenic cells, which leads to aberrant extracellular matrix (ECM) deposition and progressive substitution of the normal parenchyma by scar tissue [9]. For instance, persistent liver injury and unrestrained inflammatory cascade lead to EGFR-mediated proliferation and migration of hepatic stellate cells (HSCs), the cellular population involved in the deposition of ECM in the liver [10]. In addition, release of specific growth factors triggers the synergistic activation of a number of protein kinase pathways that serve different biological roles related to fibrogenesis [11]. Inhibition of KDR by neutralizing monoclonal antibody ameliorated carbon tetrachloride induced hepatic fibrosis in mice not only by suppressing the neovascularisation but also by reducing the α1(I)-procollagen mRNA expression in HSCs [12]. Likewise, preliminary randomized double-blind clinical trials

Abbreviations: CAN, cerium ammonium nitrate; CD, Crohn's Desease; COL1A1, prepro-alpha 1 collagen; DMF, dimethylformamide; ECM, extracellular matrix; EGFR, epidermal growth factor receptor; FGFR1, type 1 fibroblast growth factor receptor; FN1, fibronectin 1; HSC, hepatic stellate cells; ISEMF, intestinal subepithelial myofibroblasts; KDR, type 2 vascular endothelial receptor; mTOR, mammalian target of rapamycin; PDGFR, platelet-derived growth factor receptor; PI3K, phosphatidylinositol-3 kinase; STK, serine−threonine kinases; TFA, trifluoroacetic acid; TIMP1, tissue inhibitor of metalloproteinase 1; TK, tyrosine kinases; VEGFR2, type 2 vascular endothelial receptor.

* Corresponding author.
E-mail address: giovanni.marzaro@unipd.it (G. Marzaro).

http://dx.doi.org/10.1016/j.ejmech.2016.03.053

indicate that sirolimus and everolimus, two mTOR inhibitors, induce remission in refractory Crohn's Disease (CD) by decreasing the number of intestinal subepithelial myofibroblasts (ISEMFs) and the expression of pro-fibrotic cytokines [13–15]. Currently, the pharmacological care in patients with tissue fibrosis relies on corticosteroids and immunosuppressant drugs but fibrosis-related consequences remain a major causes of morbidity and mortality [16].

The pivotal role of kinases as targets for novel drugs is clearly demonstrated by the huge amount of ATP-mimic kinase inhibitors, mainly TK inhibitors, developed in the last two decades [17]. The ATP-mimic kinase inhibitors belong to different chemical classes of compounds. However they share a common pharmacophore [17] that is generally composed by: *i*) a scaffold (mainly a nitrogen containing heterocycle) able to interact through an H-bond with the kinase *hinge region*; *ii*) a lipophilic moiety (mainly an aromatic or an heteroaromatic system) that occupy a pocket opened by the so called *gatekeeper* residue; *iii*) a spacer between the heterocycle and the hydrophobic moiety; *iv*) solvent exposed residues. As part of our novel bioactive compounds discovery projects [18–20] and due to our experience in quinazoline compounds [18,19,21], we decided to investigate whether it was possible to develop novel quinazolinone-based kinase inhibitors able to restrain the activation of fibrogenic cells. Quinazolinone compounds are endowed with a number of biological activities comprising antiviral [22], antitubercular [23], antimicrobial [24], antitubulin [25], antifolate [26], anticonvulsivant [27], anti-inflammatory [28], antifibrotic [29] and anticancer [30–32] properties. Their kinase inhibitory activity however has not been extensively explored.

Herein we report the synthesis and the preliminary evaluation of several 3-substituted quinazolinones against a panel of kinases mainly involved in the fibrogenic process. The binding mode of several compounds with the target kinases was investigated by means of molecular docking studies. The anti-fibrotic activity of the compounds was assessed *in vitro*.

2. Results and discussion

2.1. Chemistry

The general structure of the novel compounds is reported in Fig. 1A.

The 3-substituted quinazoline compounds are structurally related to another well known class of kinases inhibitors, the 4-anilinoquinazolines [34,35] (Fig. 1B), as demonstrated by the superimposition with erlotinib in its binding conformation with EGFR (Fig. 1C and D). According to our previous studies [19], the 6 and 7 positions of the quinazolinone scaffold were functionalized with dimethoxy functions or with fused dialkoxy rings, namely a dioxane and a dioxolane ring. The 3 position of the quinazolinone was substituted with several lipophilic moieties (2-bromopyridine, biphenyl, halophenyl) linked to the quinazolinone nitrogen with a bridge of variable sizes and chemical properties (methylene, 2-hydroxyethylene, 2-oxoethylene). According to the type of substitution at the positions 6 and 7, the newly synthesized compounds were grouped in three classes (Table 1). All the compounds have been synthesized starting from the appropriate aniline derivatives through quinazoline intermediates, taking advantage of an already reported synthetic strategy [36] (Scheme 1).

Briefly, anilines **16a-c** were protected as carbamates, submitted to condensation with hexametylenetetramine in TFA under microwave irradiation and then to aromatization with potassium ferricyanide in hydroalcoholic KOH at reflux. The obtained quinazoline **18a-c** were oxidized with CAN in acetic acid to quinazolinones **19a-c** [18], which were finally condensed with the suitable halobenzyl derivatives, aryloxyrane or haloacetophenones and NaH in DMF under microwave irradiation give the final products **1**–**15**.

2.2. Kinase screening

To outline the profile of activity/selectivity, all the synthesized compounds were preliminarily screened for their ability to counteract the kinase activity of a selected panel of kinases (both TKs and STKs) involved in fibrosis [37–43]. Thus, in this study the synthesized compounds have been tested at 1 μM against a panel of six tyrosine kinases and two serine–threonine kinases. Vatalanib (PTK787/ZK-22258, a poly-tyrosine kinase inhibitor endowed with anti-fibrotic and anti-neoplastic activities) [44,45] has been used as positive control. The results of the screening are summarized in Table 2.

Many compounds inhibited the activity of KDR or EGFR, though to a lower extent than vatalanib. The majority of these compounds (**6**, **10**, **11**, and **14**) were dual KDR and EGFR inhibitors, whereas compound **1** was a dual EGFR/PDGFRβ (Platelet-Derived Growth Factor Receptor β-isoform) inhibitor. Moreover compounds **7** and **11** were also active against one of the tested STKs. All the compounds were inactive against the cytoplasmic kinases Abl1 and Src and the receptor kinase FGFR1.

2.3. Molecular docking

To rationalize the activity profile of some representative compounds, molecular modelling studies were performed. In particular we focused on compounds **1** (active against EGFR; inactive against KDR), **11** (active against KDR, EGFR and PI3K; inactive against mTOR) and **7** (active against mTOR; moderately active against PI3K).

As depicted in Fig. 2A, compound **1** was expected to interact through the N^1-quinazoline nitrogen and the pyridine nitrogen with the hinge region residue M793 and with the gatekeeper T790

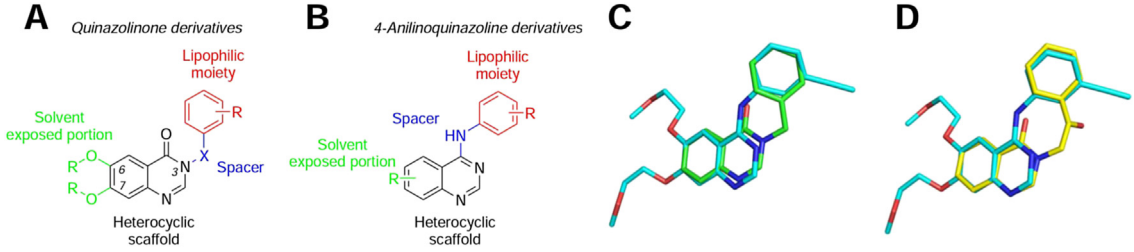

Fig. 1. (A) General structure of quinazolinone derivatives. (B) General structure of 4-anilinoquinazoline kinase inhibitors. (C) Superimposition of the 3-benzylquinazolin-4-one scaffold (green carbon sticks) and erlotinib (cyan carbon sticks). (D) Superimposition of the 3-(benzoylmethyl)quinazolin-4-one scaffold (yellow carbon sticks) and erlotinib (cyan carbon sticks). The tridimensional structure of erlotinib was extracted by the crystallographic complex with EGFR (PDB ID: 1M17) [33]. (For interpretation of the references to colour in this figure legend, the reader is referred to the web version of this article.)

Table 1
Structures of the synthesized compounds.

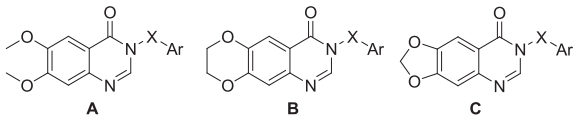

Compd	Series	X	Ar
1	A	-CH_2-	
2	A	-CH_2-	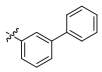
3	A	-CH_2-	
4	A	-CH_2-	
5	A	-CH_2CO-	
6	A	-$CH_2CH(OH)$-	
7	B	-CH_2-	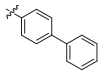
8	B	-CH_2-	
9	B	-CH_2-	
10	B	-CH_2CO-	
11	B	-CH_2CO-	
12	B	-$CH_2CH(OH)$-	
13	C	-CH_2-	
14	C	-CH_2-	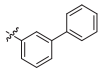
15	C	-CH_2-	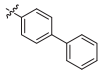

of EGFR respectively. No consistent binding mode for compound **1** in KDR was obtained. Probably, the presence of the V916 as gatekeeper in KDR was detrimental for the activity: when the pose obtained for compound **1** in EGFR was inserted in KDR a clash between the valine and the lipophilic moiety was observed (Fig. 2B).

The presence of a longer bridge with H-bond acceptor feature in compound **11** was probably the key to achieve dual EGFR/KDR inhibition (Fig. 3). Again, the N^1-quinazoline nitrogen was expected to form an H-bond with the hinge residues (M790 in EGFR, Fig. 3A; C918 in KDR, Fig. 3B). In the case of EGFR, an additional H-bond between the alcoholic function of T790 and the carbonyl of **11** was suggested by molecular docking, whereas in KDR the bromophenyl function probably established lipophilic interaction with the gatekeeper (V916).

Notably, a similar behaviour was found also for compound **5** and **10**, bearing the same $CH_2C{=}O$ bridge (data not shown).

Besides being a dual EGFR/KDR inhibitor, compound **11** was also able to inhibit PI3K while it was inactive against the other tested STK, mTOR. On the contrary, the shorter bridge in compounds **7** and **8** led to compounds endowed with moderate dual mTOR/PI3K inhibitory activity. As depicted in Fig. 4, **7** (Fig. 4A) and **11** (Fig. 4B) showed comparable binding modes in PI3K. Docking studies suggested that the dioxane oxygens could establish H-bonds with the hinge residue V848, the N^1-quinazoline nitrogen atoms could interact with the K799 and the lipophilic moieties may be involved in T-shaped arene–arene interactions with the W781 aromatic side chains.

Conversely, in mTOR kinase, compound **7** was expected to interact with the hinge residue V2240 through an H-bond, with the W2239 through a T-shaped arene–arene interaction and with the DFG-motif (Fig. 5A). A similar pose was not obtained for compound **11**. Indeed, the alignment of compound **11** on the pose obtained for compound **7** in mTOR revealed two clashes between the carbonyl in the bridge and the W2239 and between the bromine atom and the I2163 side chain (Fig. 5B).

Finally, we used molecular docking studies also to investigate the differences in potencies of compounds **1**, **3** and **4** against EGFR. Indeed, very small variation in structures (compounds mainly differed for the relative position of the bromine atom and for the presence of a pyrimidine in place of a phenyl function at position 3) caused quite high differences. As shown in Fig. 6A, there were probably no differences in binding modes for compounds **1** and **3**. Hence, the lower activity of **3** could be ascribed to the lack of interaction with the T790 (due to the absence of the nitrogen atom in the benzyl portion) rather than to the bromine atom position. On

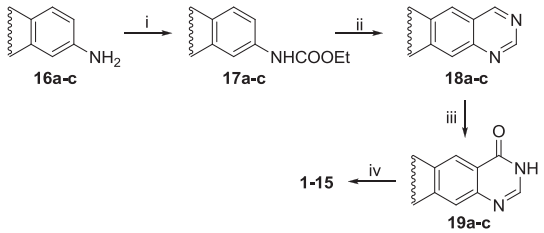

[a]Reagents and conditions: (i) ClCOOEt, TEA, THF, rt, 30 min; (ii) 1. HMTA, TFA, MW, 110 °C, 10 min. 2. $K_3Fe(CN)_6$, KOH 10%, EtOH/H_2O 1/1, reflux, 4 h; (iii) CAN, AcOH, H_2O, rt, 5 min; (iv) 2-bromo-3-bromethylpyridine (**1**) or 3-phenyl-benzylbromide (**2**, **14**) or 3-bromobenzylbromide (**3**, **8**) or 4-bromobenzylbromide (**4**, **9**, **13**) or 4-phenylbenzylchloride (**7**, **15**) or 2,4'-dibromoaceto-phenone (**5**, **10**) or 2,3'-dibromo-acetophenone (**11**), or 2-(4-bromophenyl)oxirane (**6**) or 2-(3-chlorophenyl)oxirane (**12**), NaH, anhydrous DMF, MW, 120 °C, 5 min.

Scheme 1. General strategy for the synthesis of quinazolinone derivatives as kinase inhibitors[a].

Table 2
Kinase inhibition profile.

Compd	% inhibition ([I] = 1 μM) against isolated kinases[a]							
	KDR	EGFR	FGFR1	Abl1	Src	PDGFRβ	mTOR	PI3K
1	24	49	13	0	3	37	30	25
2	33	16	13	0	0	4	34	21
3	31	35	11	0	0	22	18	15
4	25	23	14	0	0	0	25	0
5	53	33	7	0	4	1	17	0
6	44	53	8	0	0	0	33	5
7	45	29	10	0	5	13	37	25
8	12	23	7	0	0	0	28	28
9	12	31	1	0	0	1	13	0
10	35	43	18	0	0	1	23	17
11	36	47	18	0	0	4	2	35
12	26	38	5	1	0	0	1	0
13	27	0	1	0	0	45	17	7
14	35	41	8	0	0	0	0	0
15	25	0	6	4	0	4	10	0
Vat	58	67	31	25	16	72	49	18

[a]The results are expressed as mean of three independent experiments. See Supplementary Data for all the measured values. Strong inhibition (≥50%) is highlighted by black boxes; good inhibition (≥35%) is highlighted by grey boxes; weak inhibition (<35%) is not highlighted. Vat: vatalanib.

the contrary, docking studies suggested a worse complementarity with the ATP pocket for compound **4** (Fig. 6B), probably caused by the hindrance of the *para*-bromine atom.

2.4. In vitro anti-fibrotic activity

As many substituted quinazolinones are endowed with good/strong inhibition activity towards kinases involved in the fibrogenic process (Table 2), we decided to assess the biological effect of the active compounds in modulating the activation of fibrogenic cells, namely HSCs and ISEMFs. Primary cells were isolated from human liver or gut specimens and cultured in plastic support to induce *in vitro* fibrogenic activation. As reported in Fig. 7, at 1 μM compounds **6**, **7**, **10**, **11**, and **14** were the most effective in reducing the mRNA levels specific for COL1A1 in HSCs and ISEMFs. The mRNA transcript levels specific for FN1 and TIMP1 were decreased also by compounds **1** and **5**. Noteworthy, compounds **6**, **7**, **10**, **11**, and **14** showed a unique profile of activity in the series since they were able to inhibit KDR with strong/good potency and at least another kinase (Table 2). Compounds **1** and **5** effectively reduced the mRNA expression levels of TIMP1 and FN1 in pathological samples (*i.e.* ISEMFs cultured from patients suffering from Crohn's disease) with poor effect on myofibroblasts obtained from healthy subjects in which the fibrogenic activation is probably less important. For all the tested genes, the reduction in the mRNA expression was comparable to one reported for vatalanib. Finally, compounds endowed

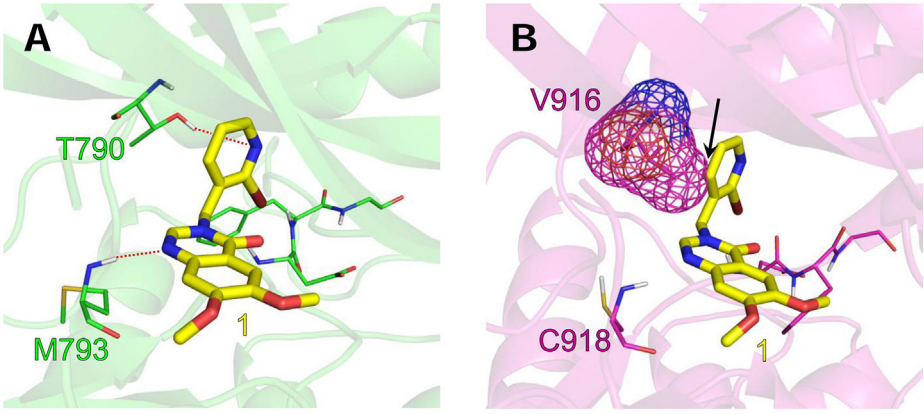

Fig. 2. (A) Binding mode proposed for **1** in EGFR. (B) Clash (black arrow) between **1** and V916 in KDR (V916 is represented as mesh surface). In both cases, the kinase hinge region is on the left side of the pictures, while the kinase solvent accessible region is on the right side.

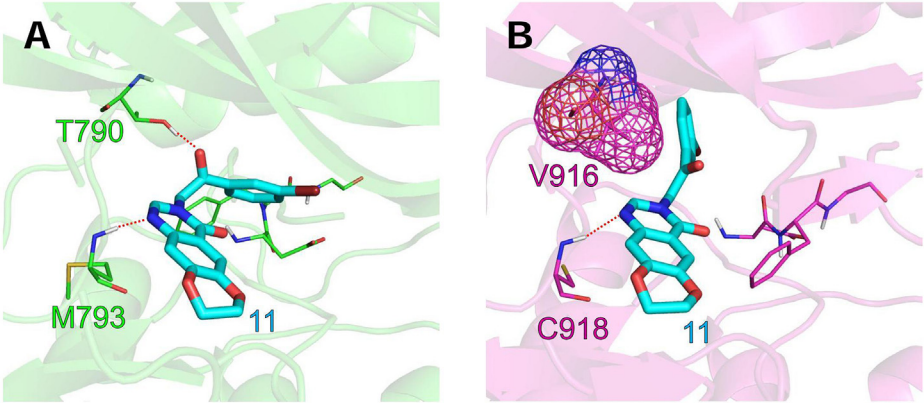

Fig. 3. (A) Binding mode proposed for **11** in EGFR. (B)Binding mode proposed for **11** in KDR (V916 is represented as mesh surface). In both cases, the kinase hinge region is on the left side of the pictures, while the kinase solvent accessible region is on the right side.

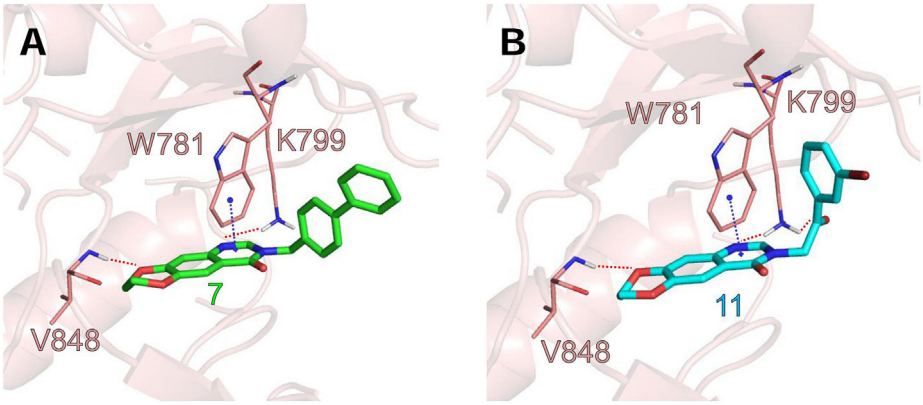

Fig. 4. (A) Binding modes proposed for **7** in PI3K. (B) Binding mode proposed for **11** in PI3K. In both cases, the kinase hinge region is on the left side of the pictures, while the kinase solvent accessible region is on the right side.

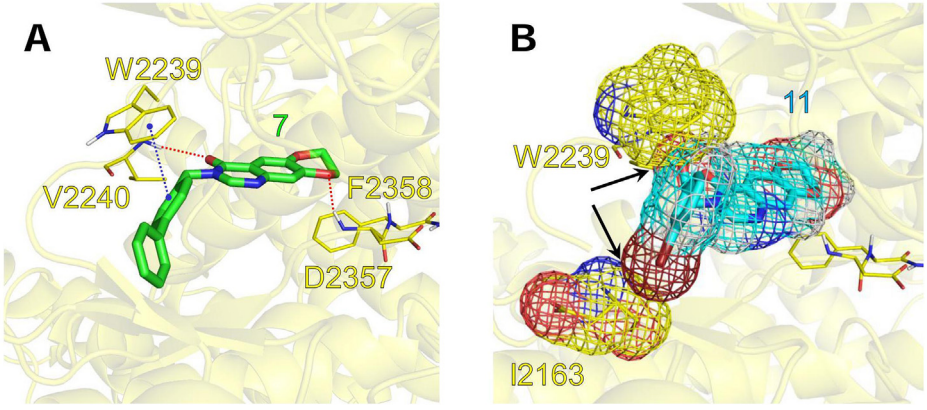

Fig. 5. (A) Binding proposed for **7** in mTOR. (B) Clashes (black arrows) between **11** and W2239 and I2163 in mTOR (**11**, W2239 and I2163 are depicted as mesh surfaces). In both cases, the kinase hinge region is on the left side of the pictures, while the kinase solvent accessible region is on the right side.

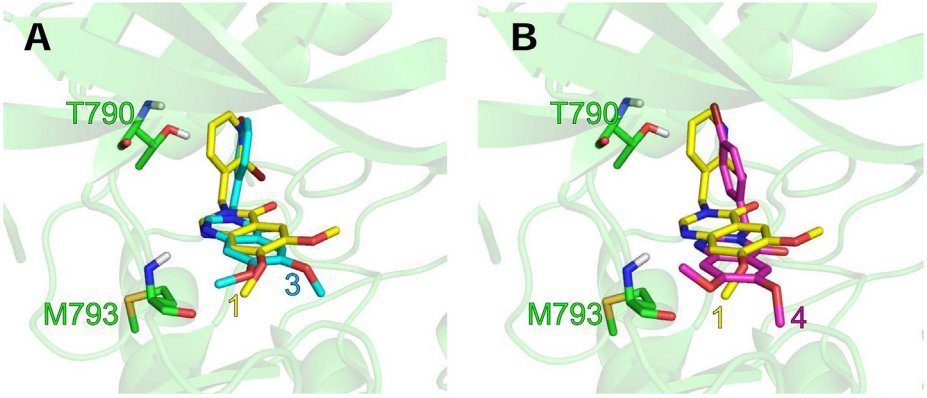

Fig. 6. (A) Comparison between the binding modes suggested by docking studies for **1** (yellow carbon sticks) and **3** (cyan carbon sticks) in EGFR. (B) Comparison between binding modes of **1** (yellow carbon sticks) and **4** (pink carbon sticks) in EGFR. In both cases, the kinase hinge region is on the left side of the pictures, while the kinase solvent accessible region is on the right side. (For interpretation of the references to colour in this figure legend, the reader is referred to the web version of this article.)

with weak inhibitor activity (**3**, **12**, **13**) did not significantly reduce the expression of genes involved in the fibrogenic process.

Compounds **1**, **6**, and **13** also inhibited proliferation in HSCs and ISEMFs. Consistent with previous reports, VEGF induces proliferation in HSCs [46]. As reported in Fig. 8, treatment of cells with 1 μM for 72 h significantly decreased VEGF-induced proliferation. The effect was more evident in cells treated with compounds **1** and **13**, the only quinazolinone derivatives endowed with good inhibition of PDGFR.

Most important, the treatment for 72 h with compounds at 1 μM did not compromise cell viability (Fig. 9). On the contrary, under the same conditions vatalanib reduced cell viability, as previously reported [47].

The anti-fibrogenic and anti-proliferative effects of compounds

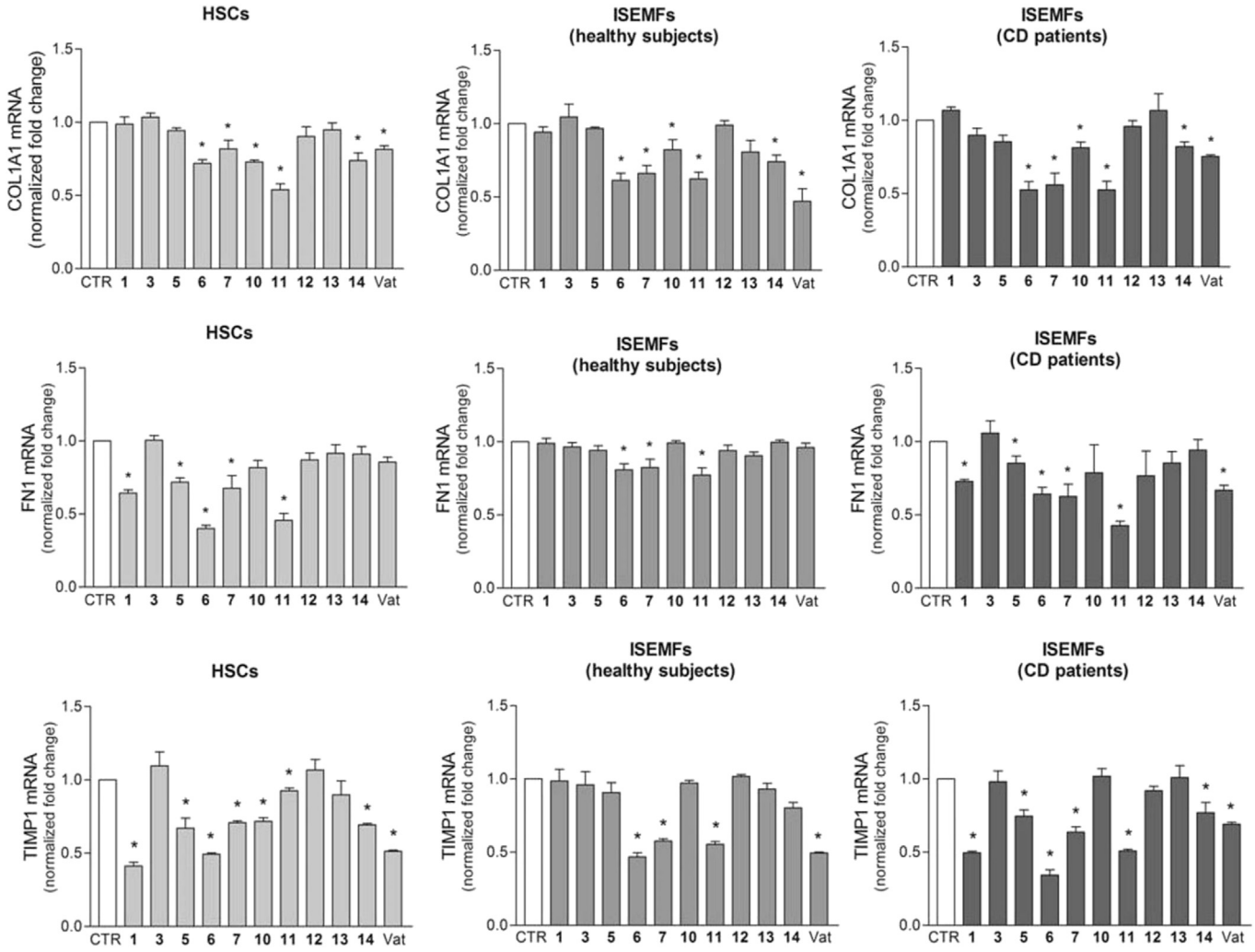

Fig. 7. Expression levels of mRNA transcripts specific for prepro-alpha 1 collagen (COL1A1), fibronectin (FN1), and tissue inhibitor of metalloproteinase 1 (TIMP1) assessed by quantitative RT-PCR on hepatic stellate cells (HSCs) and intestinal subepithelial myofibroblasts (ISEMFs) cultured from specimens obtained by healthy subjects and patients suffering from Crohn's disease (CD). Data are reported as mean ± SE. * denotes $P < 0.05$ *vs* untreated, control cells (CTR). Vat: vatalanib.

1, **6**, and **11** were associated with reduced phosphorylation of p38 MAPK. Thus, phosphorylation of p38MAPK is augmented in activated HSCs mediating the upregulation of COL1A1 mRNA levels [48]. Indeed, phospho-p38MAPK levels mainly decreased in HSCs treated for 4 h with compounds **1**, **6** and **11** at 1 μM as compare to untreated cells (Fig. 10). Similar results were obtained in ISEMFs cultured from patients suffering from Crohn's disease (data not shown).

3. Conclusions

The evaluation of kinase inhibitors bearing the quinazolinone core has not yet been extensively studied, although this scaffold is present in a number of biologically active compounds. In this work the synthesis and the preliminary biological evaluation of quinazolinone derivatives as kinase inhibitors have been described. The synthesized compounds have been tested towards a panel of six tyrosine kinases and two serine−threonine kinases. The profile of selectivity of some representative compounds has been rationalized through molecular docking studies, furnishing useful suggestions for further development of this class of compounds.

The kinase inhibition profile evaluated by *in vitro* assay (Table 2) prompted us to investigate the anti-fibrotic properties of quinazolinone derivatives. Our data revealed that the synergistic inhibition of EGFR and KDR efficaciously reduced the levels of mRNA transcripts involved in the fibrogenic activation of both HSCs and ISEMFs, the cell populations mainly involved in the fibrosis of liver and gut, respectively. Indeed, compounds **6**, **10**, **11** and **14**, showing the dual EGFR/KDR inhibitory activity, significantly reduced COL1A1 mRNA expression as compare to non-treated *in vitro* activated cells to an extent comparable to or even greater than vatalanib. Previous studies reported the involvement of EGFR and KDR in the regulation of HSCs [10,12] but to our knowledge this is the first time that dual inhibitors of TKs efficaciously control expression of fibrogenic genes. The simultaneous inhibition of KDR and EGFR however is not mandatory for the anti-fibrotic effect. Indeed, compounds **1**, **5**, and **7** revealed different gene-related and cellular specific effects. In particular, compound **7** endowed with dual KDR/mTOR inhibitory activity, significantly downregulated the expression of pro-fibrogenic genes. Thus, several soluble factors and signalling pathways are central to the fibrotic process. Besides EGFR and KDR, PDGFR has been reported as the most potent proliferative factor toward HSCs and myofibroblasts [49]. Because of their combined role in fibrosis, inhibition of both proliferation and fibrogenesis is an attractive target for antifibrotic therapy. Among our synthetized quinazolinone derivatives only compound **1**

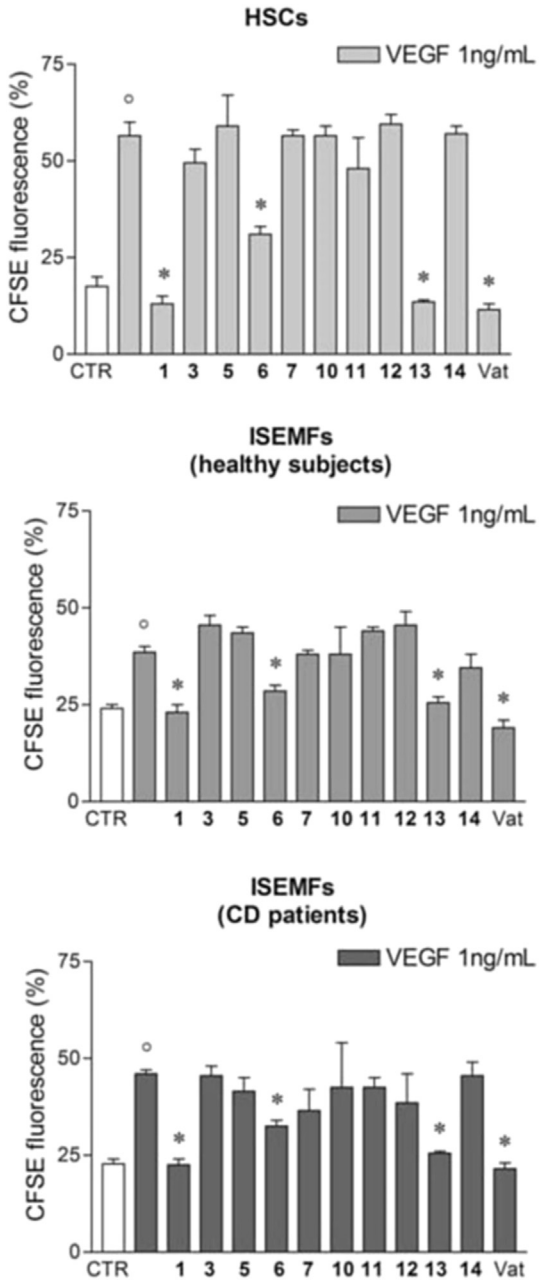

Fig. 8. Cell proliferation assessed as carboxyfluorescein diacetate succinimidyl ester (CFSE) positive cells (percentage). HSCs and ISEMFs were treated with 1 ng/ml VEGF and compounds for 72 h. Fluorescence was then evaluated by FACS analysis. Data are reported as mean ± SE. ° denotes $P < 0.05$ *vs* untreated, control cells (CTR). * denotes $P < 0.05$ *vs* VEGF-treated cells. Vat: vatalanib.

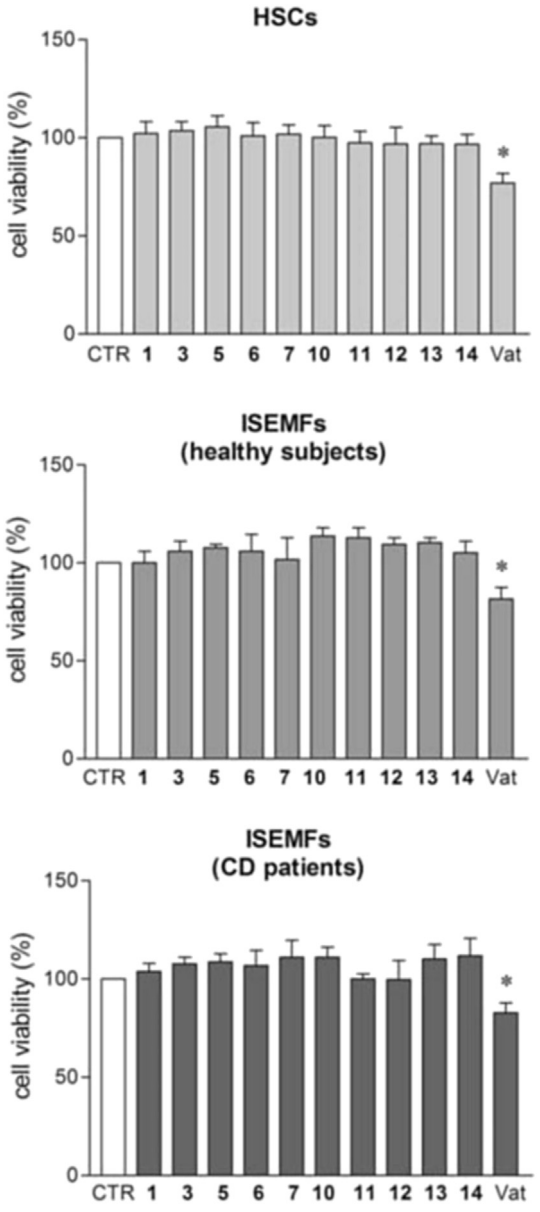

Fig. 9. Percentage of vital HSCs and ISEMFs following treatment with compounds for 72 h. Data are reported as mean ± SE. * denotes $P < 0.05$ *vs* untreated, control cells (CTR). Vat: vatalanib.

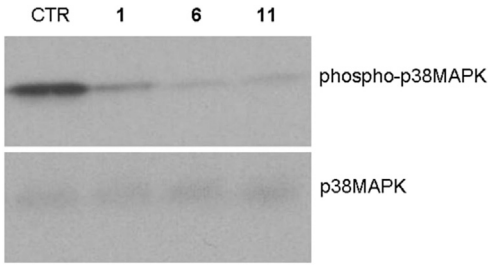

Fig. 10. Inhibition of p38MAPK phosphorylation assessed by western blot analysis in HSCs untreated (CTR) or treated for 4 h with compounds 1 μM.

inhibits both PDGFR and EGFR (Table 2). Consistently, compound **1** reported good anti-fibrotic activity, reducing FN1 and TIMP1 mRNA transcript levels and also inhibited VEGF-induced cell proliferation. However, even if at lower extent compound **6** reported anti-proliferative activity, too, proving that quinazolinone derivatives inhibit activated fibrogenic cells by complex mechanisms. Indeed, compounds **1**, **6**, and **11** exert their anti-fibrotic and anti-proliferative effects on p38MAPK pathway although we can not exclude other intracellular signaling cascades.

On the basis of the acquired data and of the docking studies, novel compounds with improved inhibitory activity against STKs will be synthesized, with the aim to strengthen the anti-fibrotic properties of quinazolinone derivatives. Fully exhaustive relationship between kinases inhibition profile and biological activity is however not derivable mainly because *i*) the expression of the

different ECM proteins is driven by several intracellular pathways and *ii*) different kinases are specifically elicited in distinct cell populations (*i.e.* HSCs and ISEMFs) as well as at different step of the fibrogenic process (compare effects on ISEMFs from healthy subjects and patients suffering for Crohn's disease). Indeed, a complex network of extracellular factors (*e.g.* endocrine system, metabolism, growth factor and metalloproteinase secretion) characterizes fibroblast activation and ECM deposition in every tissue-related fibrogenic process [50,51]. The acquired data indicate compounds **1**, **6**, and **11** as novel promising anti-fibrotic compounds endowed with multiple kinases inhibitory properties. The synthesis of novel compounds as well as a more exhaustive biological investigation on this novel class of multi-kinase inhibitors is in progress. Overall, our data suggest that the quinazolinone is an attractive scaffold for the development of novel inhibitors of kinases involved in the fibrogenic process.

4. Experimental

4.1. Chemistry

See Supplementary Data for general synthetic methods, for the synthesis of 2-bromo-3-bromethylpyridine and for the analytical details (mp, NMR, HRMS, elemental analyses) of all compounds. Purity of all tested compounds was determined by elemental analyses and was found equal or more than 95%. Compounds **19a** [21] and **19b-c** [18] were synthesized as previously reported.

General procedure for quinazolinones 1–15. A mixture of quinazolinone **19a** [21] or **19b-c** [18] (1.0 mmol) and NaH in DMF was maintained under N_2 for 5 min. The appropriate haloderivative or aryloxirane was added (1.0 mmol) and the mixture was microwave irradiated at 120 °C (power 250 W; hold time 5 min). After cooling, the mixture was poured in sat. NH_4Cl solution (30 mL) and the obtained precipitate were collected by filtration. The solid was purified by crystallization to give the title compounds (yields 10–52%).

4.2. Computational methodologies

The computational experiments were performed on a 4 CPUs (Intel Core2 Quad CPU Q9550 @ 2.83 GHz) ACPI ×64 Linux workstation (operating system: Ubuntu ver. 12.04). Protein structures were handled with Chimera 1.5.3 software [52]. The structures of the quinazolinone compounds were prepared using MarvinSketch 5.5.0.1 software [53] and OpenBabel 2.2.3 softwares [54]. The docking studies were conducted with AutoDock 4.2 software [55] as previously reported [19]. Further details are given in Supplementary Data.

4.3. Biology

4.3.1. In vitro kinase assays

Synthesized compounds were tested *in vitro* for inhibition of a panel of TKs and STKs, as previously reported [19]. See Supplementary Data for a detailed description.

4.3.2. Cell isolation and culture

Human hepatic stellate cells (HSCs) were freshly isolated from non-pathological fragments of liver tissue collected during surgical procedures. Samples were processed separately and HSCs were cultured as previously described [56]. Briefly, following digestion with collagenase and pronase, HSCs were isolated by centrifugation over a gradient of Percoll (Amersham Biosciences, Sweden) and cultured in DMEM containing 10% vol/vol fetal bovine serum, 2 mM L-glutamine, 100 U/ml penicillin and 100 μg/ml streptomycin, (all provided by Gibco, Milan, Italy). Purity of cultured HSCs was assessed by immunocytochemistry using anti-αSMA antibody (Sigma).

Human intestinal subepithelial myofibroblasts (ISEMFs) were isolated from non-pathological colonic biopsies collected during colonoscopy for cancer screening and from patients with Crohn's disease collected during routine follow-up endoscopy program. Tissue samples were processed separately. Biopsies were diced and digested for 30 min at 37 °C in collagenase (0.25 mg/ml, Sigma). Recovered cells were suspended in DMEM with 20% vol/vol FBS, 2 mM L-glutamine, 1 mM sodium pyruvate, 0.1 mM nonessential amino acids, 100 U/ml penicillin, 100 μg/ml streptomycin and 2 ng/mL fungizone (Gibco). Purity of cultured ISEMFs was ascertained by fluorescence-activated cell sorting (FACS) analysis using anti-CD90 antibody (ImmunoTools, Germany). HSCs and ISEMFs were cultured at 37 °C in a 5% CO_2 humidified incubator. At confluence, cells were detached using 0.05% Trypsin-EDTA (Gibco). The study protocol followed the principles expressed in the Declaration of Helsinki and was approved by the Ethical Committee of the University Hospital of Padova. Each patient was provided with detailed information about the study aims and protocols, and gave their written, informed consent.

4.3.3. RNA isolation and quantitative polymerase chain reaction

HSCs and ISEMFs were cultured in 6 well plates and treated for 24 h with 1 μM of test compounds or vatalanib. Total RNA was extracted using the SV total RNA isolation system (Promega, Italy) according to the manufacturer's instructions. Contaminating DNA was removed by DNase I treatment (Promega). cDNA was synthesized using 2 μg RNA as template, random hexamer primers and MuLV Reverse Transcriptase (Applied Biosystems, Milan, Italy). Gene expression was evaluated by quantitative polymerase chain reactions (qPCR) using ABI Prism 7700 Sequence Detection System (Applied Biosystems), TaqMan qPCR Master Mix (Applied Biosystems), and specific oligonucleotides and probes (Universal Probe Library system, UPL, Roche Applied Science, Monza, Italy) for prepro-alpha 1 collagen (COL1A1), fibronectin 1 (FN1), and tissue inhibitor of metalloproteinase 1 (TIMP1). The expression of the target gene was normalized to the level of the housekeeping gene 18S ribosomal RNA (18SrRNA). Experiments were performed in triplicate for each isolated cell batch. The relative changes in gene expression were analyzed using the ΔΔCT method. Oligonucleotides and probes are reported in Supplementary Data.

4.3.4. Proliferation assay

HSCs and ISEMFs were incubated at 37 °C for 10 min in prewarmed PBS containing 0.1% vol/vol BSA (Sigma) and 25 mM carboxyfluorescein diacetate succinimidyl ester (CFSE, Molecular Probe, Invitrogen). Staining was quenched by adding 5 volumes of ice-cold culture media. Sixteen hrs later the cells were washed and treated with 1 μM compounds or vatalanib for 72 h. Cell proliferation was evaluated by the partitioning of fluorescent dye between daughter cells using BD FACS-Calibur flow cytometer. Experiments were performed in duplicate for each isolated cell batch. Results were analyzed using the WinMDI 2.9 (Windows Multiple Document Interface for Flow Cytometry) program.

4.3.5. Cell viability assay

To evaluate cell viability, HSCs and ISEMFs were seeded into 96-well plates at 2×10^3 cells/well. Cells were then exposed for 72 h to 1 μM tested compounds or vatalanib and finally added with 3-(4,5-dimethylthiazol-2-yl)-2,5-dimethyltetrazolium bromide (MTT, 0.50 mg/ml, Sigma) for 4 h. Formazan crystals were dissolved in 10% w/vol SDS containing 0.01 M HCl. Optical densities were measured at 450 nm using a microplate reader (Sunrise, Tecan; Switzerland).

Experiments were performed in triplicate for each isolated cell batch and cell viability was expressed as a percentage relative to respective untreated cells.

4.3.6. Western blotting

HSCs and ISEMFS isolated from gut specimens of patients suffering from Crohn's disease were treated for 4 h with compounds at 1 μM. For Western blot analysis total proteins from cultured cells were extracted in RIPA buffer (150 mM NaCl, 50 mM Tris−HCl, 0.25% wt/vol sodium deoxycholate, 0.1% Nonidet P-40, 100 μM NaVO4, 1 mM NaF, 1 mM phenylmethylsulfonyl fluoride, 10 μg/ml aprotinin, 10 μg/ml leupeptin). Particulate material was removed by centrifugation. Proteins were separated with 10% SDS PAGE and then transferred to nitrocellulose membranes (BioRad, Italy). Membranes were probed with phospho-p38 MAP Kinase antibody (Cell Signaling) and then incubated with anti-rabbit HRP-conjugated secondary antibodies. Immune complexes were visualized using enhanced chemiluminescence (Millipore). Membranes were then re-probed with p-38 MAP Kinase antibody as loading control. Experiments were performed in duplicate. Images were captured using Hyper Film MP (GE Healthcare).

4.3.7. Statistical analysis

Statistical analysis was performed using GraphPad Prism 3.03 software (San Diego, California, USA). One-way analysis of variance followed by the Bonferroni post-hoc test was used to compare multiple experimental groups. P values < 0.05 were considered statistically significant.

Acknowledgment

The present work has been carried out with the financial support of the University of Padova “Progetto di Ricerca di Ateneo 2008” CPDA084954/08 to A.C. and “Progetto Giovani Studiosi 2012” to G.M.. M.D.V. thanks the Fondazione Cariparo for a PhD student grant.

Appendix A. Supplementary data

Supplementary data related to this article can be found at http://dx.doi.org/10.1016/j.ejmech.2016.03.053.

Author contributions

The manuscript was written through contributions of all authors. All authors have given approval to the final version of the manuscript.

References

[1] G. Manning, D.B. Whyte, R. Martinez, T. Hunter, S. Sudarsanam, The protein kinase complement of the human genome, Science 298 (2002) 1912−1934.
[2] C. Tsatsanis, D.A. Spandidos, The role of oncogenic kinases in human cancer (Review), Int. J. Mol. Med. 5 (2000) 583−590.
[3] M. Gaestel, A. Mengel, U. Bothe, K. Asadullah, Protein kinases as small molecule inhibitor targets in inflammation, Curr. Med. Chem. 14 (2007) 2214−2234.
[4] D. Koya, G.L. King, Protein kinase C activation and the development of diabetic complications, Diabetes 47 (1998) 859−866.
[5] K.P. Nunes, C.S. Rigsby, R.C. Webb, RhoA/Rho-kinase and vascular diseases: what is the link? Cell. Mol. Life Sci. 67 (2010) 3823−3836.
[6] A. Wirth, Rho kinase and hypertension, Biochim. Biophys. Acta 1802 (2010) 1276−1284.
[7] M.K. Paul, A.K. Mukhopadhyay, Tyrosine kinase - role and significance in Cancer, Int. J. Med. Sci. 1 (2004) 101−115.
[8] D. Morgensztern, H.L. McLeod, PI3K/Akt/mTOR pathway as a target for cancer therapy, Anticancer Drugs 16 (2005) 797−803.
[9] G.C. Gurtner, S. Werner, Y. Barrandon, M.T. Longaker, Wound repair and regeneration, Nature 453 (2008) 314−321.
[10] C.Q. Yang, M. Zeisberg, B. Mosterman, A. Sudhakar, U. Yerramalla, K. Holthaus, L.M. Xu, F. Eng, N. Afdhal, R. Kalluri, Liver fibrosis: insights into migration of hepatic stellate cells in response to extracellular matrix and growth factors, Gastroenterology 124 (2003) 147−159.
[11] M. Presta, P. Dell'Era, S. Mitola, E. Moroni, R. Ronca, M. Rusnati, Fibroblast growth factor/fibroblast growth factor receptor system in angiogenesis, Cytokine Growth Factor Rev. 16 (2005) 159−178.
[12] H. Yoshiji, S. Kuriyama, J. Yoshii, Y. Ikenaka, R. Noguchi, D.J. Hicklin, Y. Wu, K. Yanase, T. Namisaki, M. Yamazaki, H. Tsujinoue, H. Imazu, T. Masaki, H. Fukui, Vascular endothelial growth factor and receptor interaction is a prerequisite for murine hepatic fibrogenesis, Gut 52 (2003) 1347−1354.
[13] B. Osman, S. Akool el, A. Doller, R. Muller, J. Pfeilschifter, W. Eberhardt, Differential modulation of the cytokine-induced MMP-9/TIMP-1 protease-antiprotease system by the mTOR inhibitor rapamycin, Biochem. Pharmacol. 81 (2011) 134−143.
[14] J. Dumortier, M.G. Lapalus, O. Guillaud, G. Poncet, M.C. Gagnieu, C. Partensky, J.Y. Scoazec, Everolimus for refractory Crohn's disease: a case report, Inflamm. Bowel. Dis. 14 (2008) 874−877.
[15] D.C.O. Massey, F. Bredin, M. Parkes, Use of sirolimus (rapamycin) to treat refractory Crohn's disease, Gut 57 (2008) 1294−1296.
[16] J.P. Iredale, Cirrhosis: new research provides a basis for rational and targeted treatments, Bmj 327 (2003) 143−147.
[17] J. Zhang, P.L. Yang, N.S. Gray, Targeting cancer with small molecule kinase inhibitors, Nat. Rev. Cancer 9 (2009) 28−39.
[18] A. Chilin, M.T. Conconi, G. Marzaro, A. Guiotto, L. Urbani, F. Tonus, P. Parnigotto, Exploring epidermal growth factor receptor (EGFR) inhibitor features: the role of fused dioxygenated rings on the quinazoline scaffold, J. Med. Chem. 53 (2010) 1862−1866.
[19] M.T. Conconi, G. Marzaro, L. Urbani, I. Zanusso, R. Di Liddo, I. Castagliuolo, P. Brun, F. Tonus, A. Ferrarese, A. Guiotto, A. Chilin, Quinazoline-based multi-tyrosine kinase inhibitors: synthesis, modeling, antitumor and antiangiogenic properties, Eur. J. Med. Chem. 67 (2013) 373−383.
[20] V. Gandin, A. Ferrarese, M. Dalla Via, C. Marzano, A. Chilin, G. Marzaro, Targeting kinases with anilinopyrimidines: discovery of N-phenyl-N'-[4-(pyrimidin-4-ylamino)phenyl]urea derivatives as selective inhibitors of class III receptor tyrosine kinase subfamily, Sci. Rep. 5 (2015) 16750.
[21] G. Marzaro, A. Guiotto, G. Pastorini, A. Chilin, A novel approach to quinazolin-4(3H)-one via quinazoline oxidation: an improved synthesis of 4-anilinoquinazolines, Tetrahedron 66 (2010) 962−968.
[22] Z. Wang, M. Wang, X. Yao, Y. Li, J. Tan, L. Wang, W. Qiao, Y. Geng, Y. Liu, Q. Wang, Design, synthesis and antiviral activity of novel quinazolinones, Eur. J. Med. Chem. 53 (2012) 275−282.
[23] J. Kunes, J. Bazant, M. Pour, K. Waisser, M. Slosarek, J. Janota, Quinazoline derivatives with antitubercular activity, Farmaco 55 (2000) 725−729.
[24] M.A. Khalil, N.S. Habib, Synthesis of thiadiazol derivatives of 4(3H)-quinazolinone as potential antimicrobial agents, Farm. Sci. 42 (1987) 973−978.
[25] M.J. Hour, K.T. Lee, Y.C. Wu, C.Y. Wu, B.J. You, T.L. Chen, H.Z. Lee, A novel antitubulin agent, DPQZ, induces cell apoptosis in human oral cancer cells through Ras/Raf inhibition and MAP kinases activation, Arch. Toxicol. 87 (2013) 835−846.
[26] S.T. Al-Rashood, G.S. Hassan, S.M. El-Messery, M.N. Nagi, S.E. Habib el, F.A. Al-Omary, H.I. El-Subbagh, Synthesis, biological evaluation and molecular modeling study of 2-(1,3,4-thiadiazolyl-thio and 4-methyl-thiazolyl-thio)-quinazolin-4-ones as a new class of DHFR inhibitors, Bioorg. Med. Chem. Lett. 24 (2014) 4557−4567.
[27] N. Das, D. Garabadu, A. Banerjee, S. Krishnamurthy, S. Shrivastava, Synthesis and pharmacological evaluation of some N3-aryl/heteroaryl-substituted 2-(2-chlorostyryl)-6,7-dimethoxy-quinazolin-4(3H)-ones as potential anticonvulsant agents, Med. Chem. Res. 23 (2014) 4167−4176.
[28] D.S. Brown, J.G. Cumming, P. Bethel, J. Finlayson, S. Gerhardt, I. Nash, R.A. Pauptit, K.G. Pike, A. Reid, W. Snelson, S. Swallow, C. Thompson, The discovery of N-cyclopropyl-4-methyl-3-[6-(4-methylpiperazin-1-yl)-4-oxoquinazolin-3(4H)-yl]benzamide (AZD6703), a clinical p38alpha MAP kinase inhibitor for the treatment of inflammatory diseases, Bioorg. Med. Chem. Lett. 22 (2012) 3879−3883.
[29] N.P. McLaughlin, P. Evans, M. Pines, The chemistry and biology of febrifugine and halofuginone, Bioorg. Med. Chem. 22 (2014) 1993−2004.
[30] A.M. Alafeefy, A.E. Ashour, O. Prasad, L. Sinha, S. Pathak, F.A. Alasmari, A.K. Rishi, H.A. Abdel-Aziz, Development of certain novel N-(2-(2-(2-oxoindolin-3-ylidene)hydrazinecarbonyl)phenyl)-benzamides and 3-(2-oxoindolin-3-ylideneamino)-2-substituted quinazolin-4(3H)-ones as CFM-1 analogs: design, synthesis, QSAR analysis and anticancer activity, Eur. J. Med. Chem. 92 (2015) 191−201.
[31] M. Mahdavi, K. Pedrood, M. Safavi, M. Saeedi, M. Pordeli, S.K. Ardestani, S. Emami, M. Adib, A. Foroumadi, A. Shafiee, Synthesis and anticancer activity of N-substituted 2-arylquinazolinones bearing trans-stilbene scaffold, Eur. J. Med. Chem. 95 (2015) 492−499.
[32] S. Yin, L. Zhou, J. Lin, L. Xue, C. Zhang, Design, synthesis and biological activities of novel oxazolo[4,5-g]quinazolin-2(1H)-one derivatives as EGFR inhibitors, Eur. J. Med. Chem. 101 (2015) 462−475.
[33] J. Stamos, M.X. Sliwkowski, C. Eigenbrot, Structure of the epidermal growth factor receptor kinase domain alone and in complex with a 4-anilinoquinazoline inhibitor, J. Biol. Chem. 277 (2002) 46265−46272.
[34] G. Marzaro, A. Guiotto, A. Chilin, Quinazoline derivatives as potential anticancer agents: a patent review (2007-2010), Expert. Opin. Ther. Pat. 22 (2012)

223–252.
[35] S. Ravez, O. Castillo-Aguilera, P. Depreux, L. Goossens, Quinazoline derivatives as anticancer drugs: a patent review (2011-present), Expert. Opin. Ther. Pat. 25 (2015) 789–804.
[36] A. Chilin, G. Marzaro, S. Zanatta, A. Guiotto, A microwave improvement in the synthesis of the quinazoline scaffold, Tetrahedron Lett. 48 (2007) 3229–3231.
[37] X.M. Ou, W.C. Li, D.S. Liu, Y.P. Li, F.Q. Wen, Y.L. Feng, S.F. Zhang, X.Y. Huang, T. Wang, K. Wang, X. Wang, L. Chen, VEGFR-2 antagonist SU5416 attenuates bleomycin-induced pulmonary fibrosis in mice, Int. Immunopharmacol. 9 (2009) 70–79.
[38] B.C. Fuchs, Y. Hoshida, T. Fujii, L. Wei, S. Yamada, G.Y. Lauwers, C.M. McGinn, D.K. DePeralta, X. Chen, T. Kuroda, M. Lanuti, A.D. Schmitt, S. Gupta, A. Crenshaw, R. Onofrio, B. Taylor, W. Winckler, N. Bardeesy, P. Caravan, T.R. Golub, K.K. Tanabe, Epidermal growth factor receptor inhibition attenuates liver fibrosis and development of hepatocellular carcinoma, Hepatology 59 (2014) 1577–1590.
[39] N. Lin, S. Chen, W. Pan, L. Xu, K. Hu, R. Xu, NP603, a novel and potent inhibitor of FGFR1 tyrosine kinase, inhibits hepatic stellate cell proliferation and ameliorates hepatic fibrosis in rats, Am. J. Physiol. Cell Physiol. 301 (2011) C469–C477.
[40] E. Karimizadeh, N. Motamed, M. Mahmoudi, S. Jafarinejad-Farsangi, A. Jamshidi, H. Faridani, F. Gharibdoost, Attenuation of fibrosis with selective inhibition of c-Abl by siRNA in systemic sclerosis dermal fibroblasts, Arch. Dermatol. Res. 307 (2014) 135–142.
[41] J.H. Distler, O. Distler, Intracellular tyrosine kinases as novel targets for antifibrotic therapy in systemic sclerosis, Rheumatol. Oxf. 47 (Suppl. 5) (2008) v10–11.
[42] G. Son, I.N. Hines, J. Lindquist, L.W. Schrum, R.A. Rippe, Inhibition of phosphatidylinositol 3-kinase signaling in hepatic stellate cells blocks the progression of hepatic fibrosis, Hepatology 50 (2009) 1512–1523.
[43] D. Shegogue, M. Trojanowska, Mammalian target of rapamycin positively regulates collagen type I production via a phosphatidylinositol 3-kinase-independent pathway, J. Biol. Chem. 279 (2004) 23166–23175.
[44] Y. Liu, X.M. Wen, E.L. Lui, S.L. Friedman, W. Cui, N.P. Ho, L. Li, T. Ye, S.T. Fan, H. Zhang, Therapeutic targeting of the PDGF and TGF-beta-signaling pathways in hepatic stellate cells by PTK787/ZK22258, Lab. Invest. 89 (2009) 1152–1160.
[45] J.R. Hecht, T. Trarbach, J.D. Hainsworth, P. Major, E. Jager, R.A. Wolff, K. Lloyd-Salvant, G. Bodoky, K. Pendergrass, W. Berg, B.L. Chen, T. Jalava, G. Meinhardt, D. Laurent, D. Lebwohl, D. Kerr, Randomized, placebo-controlled, phase III study of first-line oxaliplatin-based chemotherapy plus PTK787/ZK 222584, an oral vascular endothelial growth factor receptor inhibitor, in patients with metastatic colorectal adenocarcinoma, J. Clin. Oncol. 29 (2011) 1997–2003.
[46] V. Ankoma-Sey, M. Matli, K.B. Chang, A. Lalazar, D.B. Donner, L. Wong, R.S. Warren, S.L. Friedman, Coordinated induction of VEGF receptors in mesenchymal cell types during rat hepatic wound healing, Oncogene 17 (1998) 115–121.
[47] Y. Liu, E.L. Lui, S.L. Friedman, L. Li, T. Ye, Y. Chen, R.T. Poon, J. Wo, T.W. Kok, S.T. Fan, PTK787/ZK22258 attenuates stellate cell activation and hepatic fibrosis in vivo by inhibiting VEGF signaling, Lab. Invest. 89 (2009) 209–221.
[48] M. Varela-Rey, C. Montiel-Duarte, J.A. Oses-Prieto, M.J. Lopez-Zabalza, J.P. Jaffrezou, M. Rojkind, M.J. Iraburu, p38 MAPK mediates the regulation of alpha1(I) procollagen mRNA levels by TNF-alpha and TGF-beta in a cell line of rat hepatic stellate cells(1), FEBS Lett. 528 (2002) 133–138.
[49] C. Yin, K.J. Evason, K. Asahina, D.Y. Stainier, Hepatic stellate cells in liver development, regeneration, and cancer, J. Clin. Invest. 123 (2013) 1902–1910.
[50] S.P. Yun, S.J. Lee, Y.H. Jung, H.J. Han, Galectin-1 stimulates motility of human umbilical cord blood-derived mesenchymal stem cells by downregulation of smad2/3-dependent collagen 3/5 and upregulation of NF-kappa B-dependent fibronectin/laminin 5 expression, Cell Death Dis. 5 (2014).
[51] S. Al Saleh, L.H. Sharaf, Y.A. Luqmani, Signalling pathways involved in endocrine resistance in breast cancer and associations with epithelial to mesenchymal transition (Review), Int. J. Oncol. 38 (2011) 1197–1217.
[52] E.F. Pettersen, T.D. Goddard, C.C. Huang, G.S. Couch, D.M. Greenblatt, E.C. Meng, T.E. Ferrin, UCSF, Chimera–a visualization system for exploratory research and analysis, J. Comput. Chem. 25 (2004) 1605–1612.
[53] Marvin, Version 5.5.0.1, Program B; ChemAxon: Budapest, Hungary; www.chemaxon.com/products (accessed 05/01/2015).
[54] N.M. O'Boyle, M. Banck, C.A. James, C. Morley, T. Vandermeersch, G.R. Hutchison, Open Babel: an open chemical toolbox, J. Cheminform 3 (2011) 33.
[55] G.M. Morris, R. Huey, W. Lindstrom, M.F. Sanner, R.K. Belew, D.S. Goodsell, A.J. Olson, AutoDock4 and AutoDockTools4: automated docking with selective receptor flexibility, J. Comput. Chem. 30 (2009) 2785–2791.
[56] P. Brun, I. Castagliuolo, M. Pinzani, G. Palu, D. Martines, Exposure to bacterial cell wall products triggers an inflammatory phenotype in hepatic stellate cells, Am. J. Physiol. Gastrointest. Liver Physiol. 289 (2005) G571–G578.

SCIENTIFIC REPORTS

OPEN

Received: 03 July 2015
Accepted: 19 October 2015
Published: 16 November 2015

Targeting kinases with anilinopyrimidines: discovery of *N*-phenyl-*N*′-[4-(pyrimidin-4-ylamino)phenyl]urea derivatives as selective inhibitors of class III receptor tyrosine kinase subfamily

Valentina Gandin, Alessandro Ferrarese, Martina Dalla Via, Cristina Marzano, Adriana Chilin & Giovanni Marzaro

Kinase inhibitors are attractive drugs/drug candidates for the treatment of cancer. The most recent literature has highlighted the importance of multi target kinase inhibitors, although a correct balance between specificity and non-specificity is required. In this view, the discovery of multi-tyrosine kinase inhibitors with subfamily selectivity is a challenging goal. Herein we present the synthesis and the preliminary kinase profiling of a set of novel 4-anilinopyrimidines. Among the synthesized compounds, the *N*-phenyl-*N*′-[4-(pyrimidin-4-ylamino)phenyl]urea derivatives selectively targeted some members of class III receptor tyrosine kinase family. Starting from the structure of *hit compound* 19 we synthesized a further compound with an improved affinity toward the class III receptor tyrosine kinase members and endowed with a promising antitumor activity both *in vitro* and *in vivo* in a murine solid tumor model. Molecular modeling simulations were used in order to rationalize the behavior of the title compounds.

Protein kinases (PKs) are key enzymes that regulate almost all cell processes. PKs transfer a phosphate group from ATP (or GTP) to specific residues (mainly tyrosine, threonine or serine) located in the target proteins, thus promoting specific pathways[1,2]. The human kinome contains 518 different protein kinases grouped into eight major families on the basis of structural similarity[2,3]. The overexpression or deregulation of kinases (in particular tyrosine kinases, TKs) are often linked to cancer onset and progression[4]. Hence, TKs are among the major classes of biological targets for modern cancer therapy[5]. The TK family contains both receptor (RTK) and cytoplasmic enzymes[3]. Among the RTKs, of particular interest are the ErbB family[6] (or class I RKT, comprising the four receptors ErbB1-4) and the platelet-derived growth factor family[7] (PDGF; or class III RTK). Activating mutations of ErbB1 (also known as epidermal growth factor receptor, EGFR) are correlated with onset and progression of different solid cancers[8] and in particular with lung cancer[9]. Mutations in class III RTK members (*i.e.* Fms-like TK-3, FLT3; colony stimulating factor-1 receptor, CSF1R; KIT; PDGFRα; PDGFRβ) are associated with hyper-proliferative pathologies as hematologic neoplasms[10,11], lung cancer[12] and pancreatic cancer[13,14].

The high number of FDA approved drugs in the last 15 years reveals the growing interest in TK inhibitors (TKIs)[15,16]. In most cases, TKIs act as ATP-mimic compounds, although several allosteric inhibitors

Department of Pharmaceutical and Pharmacological Sciences, University of Padova, via Marzolo, I-35131, Padova (Italy). Correspondence and requests for materials should be addressed to G.M. (email: giovanni.marzaro@unipd.it)

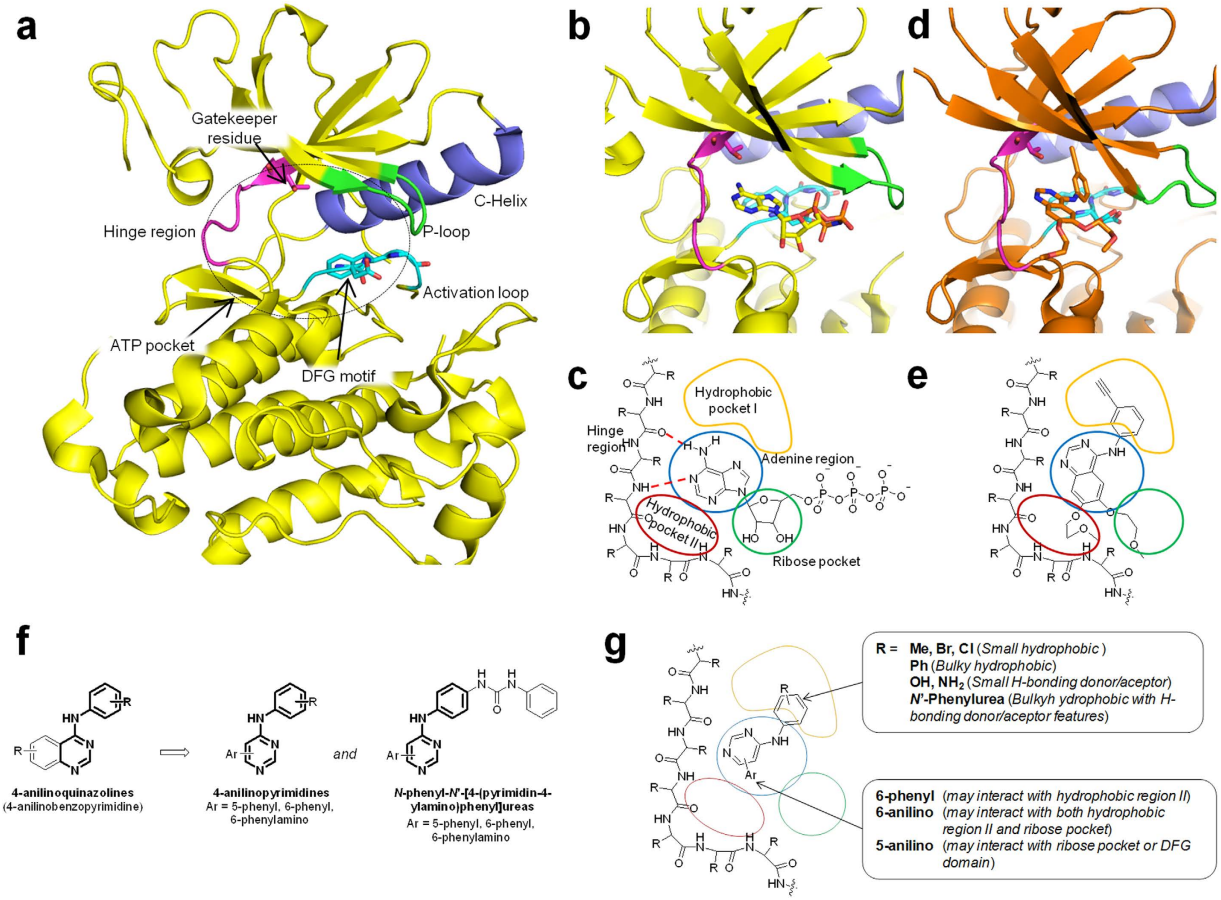

Figure 1. Structure of kinases and of designed compounds. (**a**) Main element in kinase structure. (**b**) Binding of AMP-ANP (PDB ID: 2GS7). (**c**) Schematic representation of binding of ATP and features of the ATP binding pocket. (**d**) Detail of binding of a kinase inhibitor (erlotinib; PDB ID: 1M17). (**e**) Schematic representation of binding of inhibitor (erlotinib) with respect to the features of the ATP binding pocket. Image partially readapted from ref. 22. (**f**) General structures of designed compounds and their structural relationship with 4-anilinoquinazolines. (**g**) Supposed binding mode of designed compounds in the ATP binding pocket.

are under investigations[17]. Cancer is a multi factorial disease and recent findings have highlighted the importance of multi targeting compounds, *i.e.* compounds able to inhibit, with comparable potencies, more than one TK[18]. However, both selective (*e.g.* erlotinib and gefitinib) and unselective (*e.g.* sunitinib and dasatinib) kinase inhibitors are useful anticancer drugs. Hence, whether multi-kinase inhibitors have significant advantages than single kinase inhibitors is still debated[19]. Only some specific kinases should be targeted by multi-inhibitors to guarantee high efficacy while maintaining an acceptable safety: in 2010 Morphy used the term "selectively nonselective" TKIs to describe compounds with an ideal profile of kinase inhibition[20].

Currently, a number of multi kinase inhibitors have been discovered, both by chance and by design[19]. The rational design of "selectively nonselective" TKIs is a challenging and fascinating goal: the ATP binding pocket is quite conserved in the entire kinome, and it is particularly conserved inside each PKs subfamily. In this view, an achievable and promising aim could be the design/development of subfamily selective kinase inhibitors. However, as recently reported, the inhibition of all the members of a single subfamily can lead to substantial toxicity[21].

The ATP pocket is delimited by the hinge region (containing also the gatekeeper residue), the P-loop, the C-helix and the activation loop (containing the highly conserved DFG motif; Fig. 1a). The ATP binding pocket is constituted by the adenine pocket, the hydrophilic ribose pocket and two hydrophobic regions (Fig. 1b,c). Accordingly, TKIs are commonly constituted by *i*) a nitrogen containing heterocycle able to form an H-bond with the hinge region; *ii*) an hydrophobic moiety interacting with the hydrophobic region I of the kinase; *iii*) a spacer between the heterocycle and the hydrophobic moiety (Fig. 1d,e)[15,22].

A recurring motif in kinase inhibitors is the pyrimidine nucleus. Some symmetric 4,6-dianilinopyrimidines were reported as selective EGFR inhibitors[23]. However, the selectivity profile was reported only for few compounds[23]. Similar compounds were also patented by Avila therapeutics (WO2009/051822), but few kinases were considered as targets. A number of 4-anilino-6-phenylpyrimidines were patented as cyclin-dependent kinase (CDK) inhibitors (see for example WO2008/129080 and WO2011/077171). Phosphorous containing pyrimidines as CDK inhibitors were recently published[24]. Examples of FDA approved pyrimidine based TKIs are imatinib[25] (Abl/KIT/PDGFRβ inhibitor) and dasatinib[26] (dual Abl/Src inhibitor). Examples of compounds involved in clinical trials are BAY1000394[27] and the fused pyrimidine PHA-848125[28] (pan CDK inhibitors). Nevertheless, in most cases the pyrimidine nucleus is not the main "nitrogen containing heterocycle", since it does not interact with the hinge region, as shown by X-ray crystallography[29].

Another interesting class of TKIs is constituted by the 4-anilinoquinazolines[30]. These compounds are mainly known as high selective EGFR[31], dual EGFR/ErbB2[32] or dual EGFR/VEGFR2[33] (vascular endothelial growth factor receptor-2). We have recently reported that the *m*-biphenylamine as aniline moiety led to multi kinase inhibitors targeting EGFR, fibroblast growth factor receptor-1 (FGFR1), VEGFR2, PDGFRβ, Src and Abl at nanomolar concentrations[34,35]. Indeed, 4-anilinoquinazolines could be considered as fused pyrimidine (*i.e.* 4-anilinobenzopyrimidine).

On these basis, we planned the synthesis of novel potential TKIs bearing the 4-anilinopyrimidine core as the nitrogen containing heterocycle (Fig. 1f). The compounds were further characterized by 5-phenyl, 6-phenyl or 6-phenylamino moieties designed to interact with the hydrophobic region II of the ATP pocket, the ribose pocket or the DFG motif (Fig. 1g). The 4-anilino portion of the compounds was supposed to interact with the hydrophobic pocket I (HP-I) of the kinase, in analogy to 4-anilinoquinazolines. The interactions with HP-I have often been used to obtain selectivity in kinase inhibitions[36–38]. For example, very small differences in position or nature of 4-anilinosubstituent in quinazoline compounds led to selective EGFR[39], VEGFR2[40] or janus kinase (JAK)[41] inhibitors. Hence, we functionalized the 4-anilino moiety with substituent differing in the hydrophobicity/hydrophilicity, in the ability to act as H-bond donor or acceptor, in the position and in the size. Since our purpose was to determine how the functionalization of the pyrimidine nucleus at 4 and 5 or at 4 and 6 positions could modulate the kinase selectivity profile, at this stage, we considered only simple commercially available or easily accessible anilines. Several papers and patents describing very similar compounds as kinase inhibitors are present in literature (a selection of representative bibliography is reported in Table S2). The novelty of our work relies in the evaluation of a library of simple 4-anilinopyrimidines against a wide panel of kinases and human cancer cell lines to discover novel "selective unselective" hit compounds. Indeed, through this approach we identified the 6-phenyl-4-anilinopyrimidine derivative **19** as a selective dual KIT/PDGFRβ inhibitor. Compound **19** was further improved, leading to a novel and more potent KIT/PDGFRα/PDGFRβ inhibitor (**27**) endowed with a promising anticancer potential. Molecular modeling studies were used to clarify the structure activity relationships emerged by K_d determination. Since both **19** and **27** targeted only few specific members of a TK family, they can be considered as novel "selectively nonselective" TKIs.

Results

Compounds synthesis. The structures of synthesized compounds are reported in Fig. 2 (see also Table S1).

Compounds **1–7** and **8–12** were obtained starting from 4,6-dichloropyrimidine **28** (Fig. 3a). In case of unsymmetrical compounds (**1–7**), compound **28** was first condensed with a slight excess of aniline in *i*-PrOH in the presence of triethylamine (TEA) and then with the appropriate aniline derivatives in *i*-PrOH, in both cases taking advantage from the Microwave Assisted Organic Synthesis (MAOS). Diarylurea derivative **7** was obtained by the reaction of aminoderivative **6** with phenyl isocyanate in dichloromethane.

In case of symmetrical compounds (**8–12**), compound **28** was reacted with a double amount of the appropriate aniline derivatives, but in this case, the nucleophilic aromatic substitutions were performed in *i*-PrOH at reflux without the presence of TEA.

Compounds **13–19** were synthesized starting from ethyl benzoylacetate (**30**; Fig. 3b) which was reacted with thiourea in anhydrous alkaline medium obtaining the corresponding thiopyrimidinol **31**. The thiol function was removed through Ni-Raney reduction. Compound **32** was then activated toward nucleophilic substitution by reaction with $POCl_3$/TEA. Finally, the chloropyrimidine **33** was condensed with the appropriate aniline derivatives in *i*-PrOH, under microwave irradiation. Compound **19** was obtained from aminoderivative **18** as above described for compound **7**.

Compounds **20–26** were synthesized adapting a previously reported synthetic strategy[42] (Fig. 3c). Thiourea **34** was firstly condensed with *N,N*-dimethylformamide dimethyl acetal and then treated with iodomethane in order to elicit the nucleophilic properties of the sulfur atom. Intermediate **36** was then reacted with phenylacetyl chloride in the presence of TEA. In this case we did not remove the sulfur function at this stage. In fact, the process worked better first activating compound **37** toward the nucleophilic aromatic substitution, then reacting compound **38** with the appropriate anilines and finally removing the sulfur function with the Ni-Raney system. Compound **26** was obtained from aminoderivative **25** as above described for compound **7**.

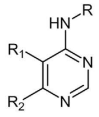

Compound	R	R_1	R_2	Compound	R	R_1	R_2
1	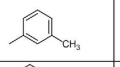	H		14	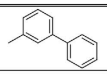	H	
2	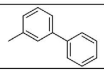	H		15		H	
3		H		16		H	
4		H		17		H	
5		H		18		H	
6		H		19	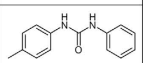	H	
7	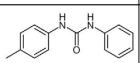	H		20			H
8		H	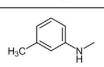	21	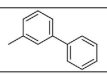		H
9		H	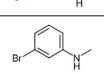	22			H
10	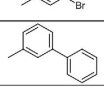	H	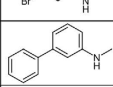	23			H
11		H		24			H
12		H		25			H
13		H		26			H

Figure 2. Structures of synthesized compounds.

Among all the synthesized compounds, only two were previously reported: compound **5** was cited as synthetic intermediate[43], whereas **8** was patented by Zeneca (US5880130). However, the two compounds were not previously screened against a panel of kinases. Compound **19** was commercially available in the Ambinter screening library. However, as reported in the Ambinter web site, it might be available only under re-synthesis with an extended delay, thus we synthesized it by ourselves. Besides, the compound was not present in academic accessible databases (*e.g.* PubChem, Reaxys).

Tyrosine kinases screening. Synthesized compounds were screened against a panel of 48 kinases selected within the ScanEDGE subset of DiscoverX (http://www.discoverx.com/services/drug-discovery-development-services/kinase-profiling/kinomescan/scanedge). The ScanEDGE includes 97 kinases and is an economical approach to assess compounds selectivity throughout the human kinome. All the wt-TKs along with some relevant mutants of Abl1 (T315I) and of EGFR (L858R and L858R/T790M) were chosen. The remaining 18 targets (3 Tyrosine Kinases-Like, TKLs; 15 Serine-Threonine Kinases, STKs) were selected among the remaining kinases in the ScanEDGE subset on the basis of their well established role in cancer (see Fig. S2 for a graphical representation of the selected kinases with reference to the kinome tree. Some references highlighting the role of each kinase in cancer are also reported in Table S3).

The compounds were evaluated using the KinomeScan™ platform (http://www.discoverx.com/services/drug-discovery-development-services/kinase-profiling/kinomescan), that measures the ability of the test compound to disrupt the complex between a high affinity ATP-mimic probe immobilized on a solid support and the kinase of interest. The KinomeScan is a very helpful technology for the fast and reliable screening of a number of compounds against a wide and customizable panel of kinases. Besides, it is not based on the use of hazardous radioactive ^{32}P-ATP and has a very low rate of false positive ($<1\%$)[44]. The screening platform outputs a "Percent of Control" (POC) value, statistically correlated to the dissociation constant (K_d) value (http://www.discoverx.com/tools-resources/leadhunter-study-reports-data-analysis), for each pair of kinase/ligand. The POC is calculated as reported in equation (1):

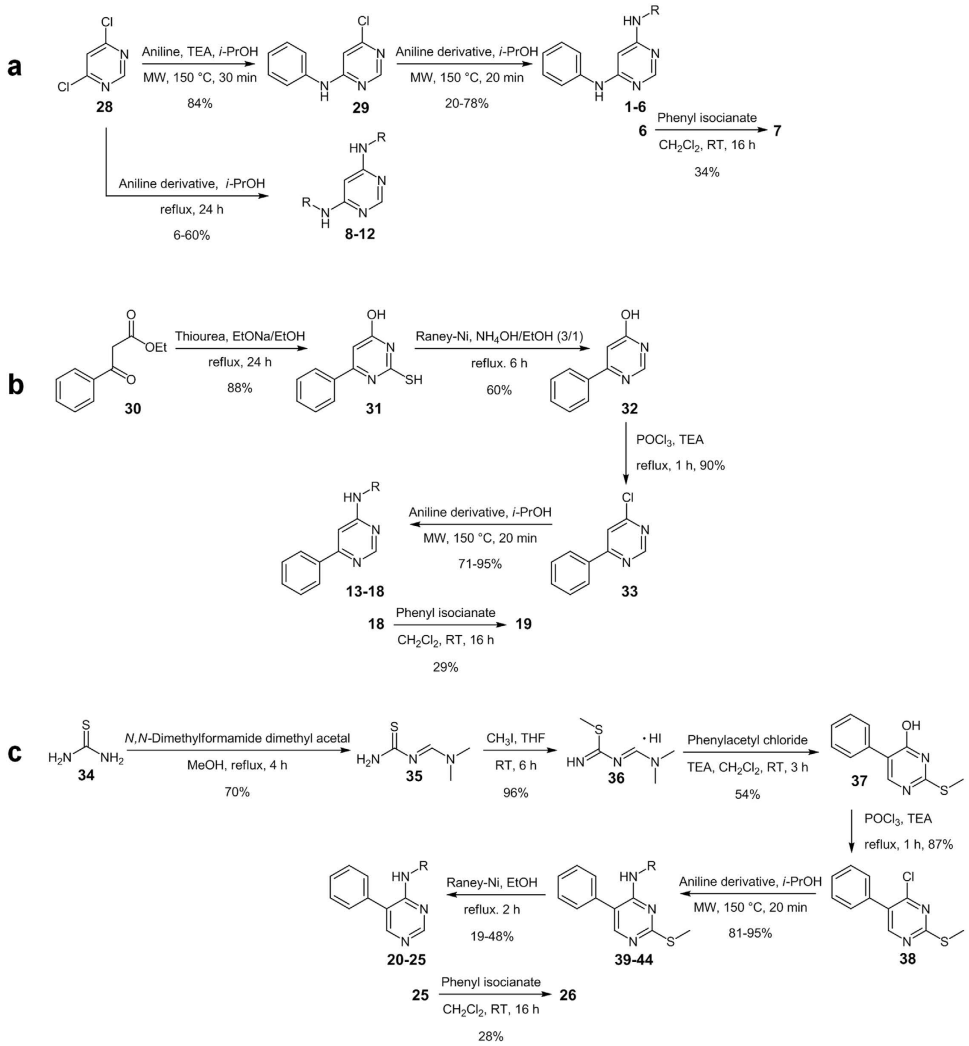

Figure 3. Synthesis of compounds 1–26. See Fig. 2 for R specification.

$$POC = \frac{test\ compound\ signal - positive\ control\ signal}{negative\ control\ signal - positive\ control\ signal} \times 100 \quad (1)$$

Where: test compound signal = amount of kinase still binding the probe after treatment with test compound; negative control signal = amount of kinase still binding the probe after treatment with DMSO (100% control); positive control signal = amount of kinase still binding the probe after treatment with control compound (0% control). Hence, low POC values indicate high affinity.

The compounds were tested at high concentration (10 μM), in order to highlight not only the main target but also the off-targets. The results of the preliminary screening are reported as heat map (Fig. 4; see also Table S4 for all the measured values), in which the compounds are grouped on the basis of the 6 or 5 substituent at the pyrimidine ring.

All the tested compounds were almost inactive against both TKL and STK members. The 6-phenylamino compounds targeted the ErbB family (comprising the wt-EGFR, ErbB2 and the two EGFR mutants L858R and L858R/T790M). Similarly to what previously reported[23], these derivatives were mainly active against wt-EGFR, although with different potencies. Some 6-phenylamino compounds and the three phenylurea derivatives (**7**, **19** and **26**) were active against the members of the class III RTKs family.

Structure activity relationship. Overall, 4-anilinopyrimidines targeted mainly the ErbB and the class III RTKs subfamilies.

With respect of targeting EGFR, the presence of a 5-phenyl or a 6-phenyl ring was detrimental (compare **1** with **13** and **20**; Fig. 5a). Hence, only 6-phenylamino-4-anilinopyrimidines were active against

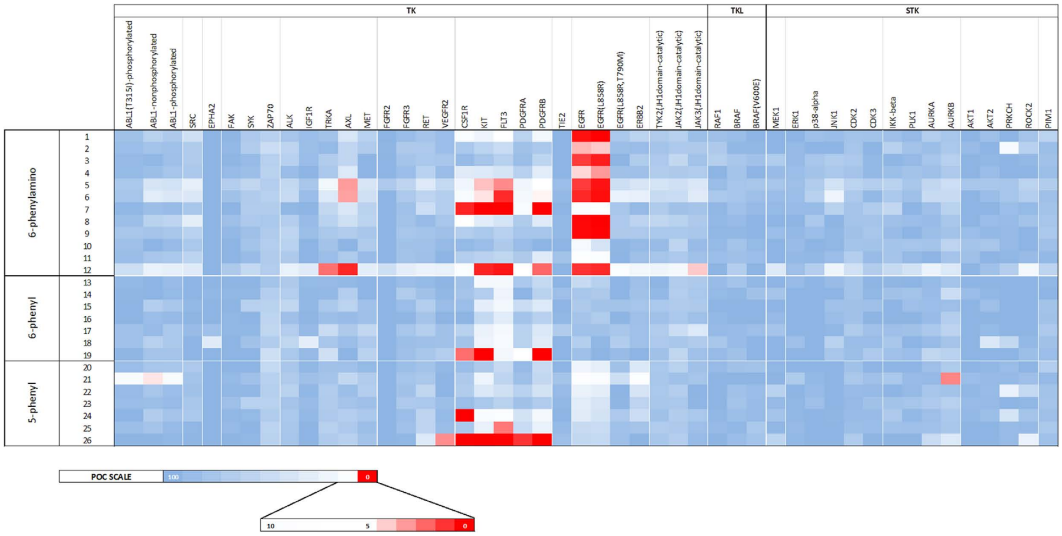

Figure 4. Results of primary screening of compounds against kinases. The heat map displays the results of the primary screening in terms of POC values for each pair of kinase/ligand. The lower the POC (white to red boxes), the tighter the binding. Compounds are listed according to Fig. 2.

EGFR. For these compounds, the substitution of the 4-aniline moiety with small *meta* lipophilic substituents was preferred (*e.g.* potencies: $\mathbf{1}_{m-Me} > \mathbf{4}_{p-Me}$; $\mathbf{8}_{m-Me} = \mathbf{1}_{m-Me} = \mathbf{9}_{m-Br} > \mathbf{11}_{p-Cl}$). Conversely to what previously reported for 4-anilinoquinazolines[34], a biphenylamino moiety was detrimental (see **2** and **10**). The L858R mutation (that causes an enhancement of the kinase activity without directly modifying the ATP site[45]) did not affect the ligand binding, whereas the T790M gatekeeper mutation dramatically impaired the interaction. Despite the high degree of similarity between wt-EGFR and ErbB2, compounds were not active against the latter kinase. The presence of small *meta* hydrophilic function (*i.e.* $\mathbf{3}_{m-OH}$) was well tolerated, still leading to selective EGFR inhibitors. Interestingly, small *para* hydrophilic substituents (OH, NH_2) led to less selective compounds: derivatives **5** and **6** targeted EGFR, some members of the class III RTKs and AXL. The lowest selectivity was obtained when the pyrimidine core was functionalized at both 4 and 6 position with *para*-hydroxyaniline moieties: indeed compound **12** targeted a number of kinases, comprising also the T790M mutant of EGFR. We are planning further investigation on this compound. When the 4-anilino was functionalized with bulky hydrophilic function (*i.e.* a phenylurea, see compound **7**), very poor activity against EGFR was observed.

With respect of targeting class III RTKs, as above mentioned, the presence of a *para* H-bonding substituent in the 4-aniline moiety was required (see compounds **5** and **6**). When the 4-aniline moiety was functionalized with a *para*-phenylurea substituent, selective class III RTK members inhibition was obtained. Indeed, in the case of phenylurea compounds (**7**, **19** and **26**), the functionalization at 5 or 6 position of the pyrimidine nucleus played a key role in determining the degree of selectivity within the subfamily. The inhibition of KIT and PDGFRβ was not affected by pyrimidine substitution at 5 or 6 position (potencies: $\mathbf{7}_{6-Phenylamino} = \mathbf{19}_{6-Phenyl} = \mathbf{26}_{5-Phenyl}$). Conversely, the inhibition of PDGFRα strongly depended on both the nature and the position of the pyrimidine substituent (potencies: $\mathbf{26}_{5-Phenyl} > \mathbf{19}_{6-Phenyl} > \mathbf{7}_{6-Phenylamino}$). The absence of a substituent at the 6 position led to the inhibition of all the members of the subfamily (see $\mathbf{26}_{5-Phenyl}$). On the other end, the presence of the 6-phenyl gave the highest selectivity (potencies for $\mathbf{19}_{6-Phenyl}$: KIT = PDGFRβ > PDGFRα > CSF1R > FLT3). Finally, the introduction of a linker between the phenyl and the pyrimidine nuclei gave an intermediate selectivity degree (potencies for $\mathbf{7}_{6-Phenylamino}$: KIT = PDGFRβ = FLT3 > CSF1R > PDGFRα).

The main structure activity relationships are resumed in Fig. 5b.

Cytotoxicity. Compounds active against at least one kinase among EGFR and class III RTKs were evaluated for their cytotoxic properties against two different human cancer cell lines, namely non small cells A549 lung cancer cells (sensitive to EGFR inhibitors)[46] and pancreatic BxPC3 adenocarcinoma (sensitive to both PDGFRβ and EGFR inhibitors)[47,48] cells. For comparison purposes, sunitinib (SU), a multi-kinase inhibitor[49], was evaluated under the same experimental conditions. The results, expressed as IC_{50} values (μM) calculated from the dose-survival curves obtained after 72 h of drug treatment from the MTT test, are reported in Table 1.

The newly synthesized compounds (excluding **8**, **9** and **12**) showed a cytotoxic potency in the micromolar range against both cancer cell lines. In particular, the two phenylurea derivatives **7** and **19** (see Fig. 5a for structures) were up to about 6 times more effective than the reference TKI against both A549 and BxPC3 cells (see potency relative to SU, calculated as the ratio between IC_{50} of sunitinib and

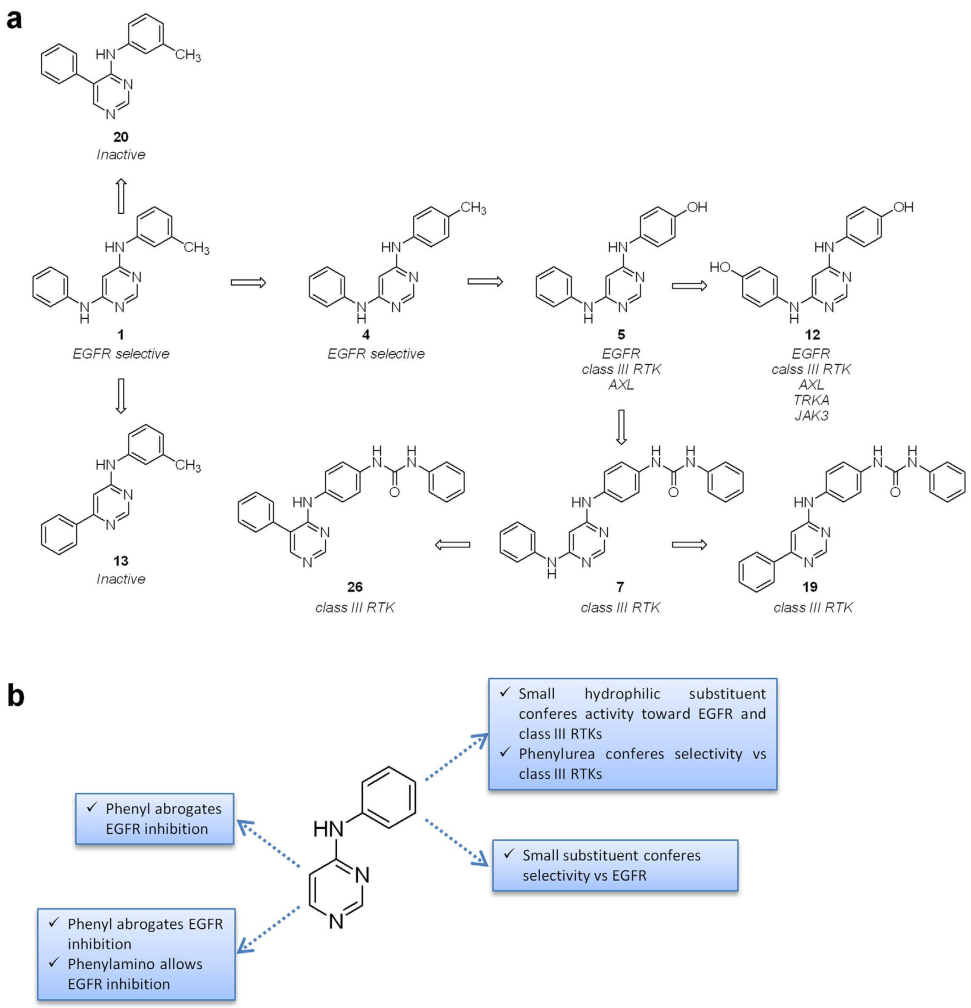

Figure 5. Structure activity relationships for 4-anilino compounds. (**a**) Selectivity profile of some selected compounds highlights the features required for selective EGFR, dual EGFR/class III RTKs or selective class III RTKs inhibition. (**b**) Schematic representation of main structure activity relationships with respect to 4-anilinopyrimidine core.

IC_{50} of tested compounds in Table 1). Tested against non-tumor cells in rapid proliferation, the human embryonic kidney HEK293 cells, **19** elicited selectivity index values (SI = quotient of the IC_{50} toward non cancerous cells divided by the average IC_{50} for the malignant cells) approximately 1.5-folds higher than that calculated with SU, thus attesting a preferential cytotoxicity versus neoplastic cells. On the contrary, compound **7** was more cytotoxic against non transformed cells ($SI < 1$).

Improvement of pharmacodynamic properties of *hit compound* 19. Based on the kinases screening results and on the IC_{50} and the SI values, we selected derivative **19** as our "*hit compound*". As mentioned above, the 6-phenyl ring was designed to occupy the hydrophobic pocket II (Fig. 1g), which is next to the hydrophilic ribose binding region of the kinases (Fig. 1c). Hence, we tried to improve the ability of the hit compound to interact with class III RTK members through the insertion of a small hydrophilic moiety, intended to occupy the sugar pocket of the kinases, thus obtaining compound **27** (Fig. 6; see also Supplementary Information for details on synthetic procedures).

The ability of compounds **19** and **27** to bind the class III RTK members was measured (Table 2; see also Figs S3 and S4 for dose/response curves).

As supposed, the further functionalization of the 6-phenyl ring with a polar moiety able to interact with the sugar pocket improved the binding affinity toward all the tested kinases. Nevertheless, for both compounds the main target remained KIT. The highest affinity improvement was observed for PDGFRα (nearly an order of magnitude), whereas the interaction with PDGFRβ was not substantially modified. Compound **19** was confirmed as a dual KIT/PDGFRβ inhibitor, while compound **27** should be considered as a KIT/PDGFRα/PDGFRβ inhibitor.

The cytotoxic profile of **19** and **27** was assessed on a wider panel of human tumor cell lines including also examples of breast (MCF-7), cervical (A431), colorectal (HCT-15), and ovarian (2008) cancers as

ID	A549 IC_{50} (μM) ± SD	Potency relative to SU	BxPC3 IC_{50} (μM) ± SD	Potency relative to SU	HEK293 IC_{50} (μM) ± SD	Selectivity Index
1	8.94 ± 2.18	0.70	6.43 ± 1.78	0.79	–	–
2	26.52 ± 3.85	0.23	17.90 ± 2.46	0.28	–	–
3	28.25 ± 5.46	0.22	8.19 ± 2.18	0.62	–	–
4	14.17 ± 2.75	0.44	23.25 ± 4.29	0.22	–	–
5	16.32 ± 4.24	0.38	6.51 ± 1.07	0.78	–	–
6	33.98 ± 4.98	0.18	16.13 ± 4.85	0.31	–	–
7	5.13 ± 0.94	1.21	4.60 ± 0.85	1.10	3.14 ± 0.57	0.64
8	>50	<0.12	>50	<0.10	–	–
9	>50	<0.12	>50	<0.10	–	–
12	>50	<0.12	>50	<0.10	–	–
19	3.16 ± 1.12	1.97	0.77 ± 0.21	6.56	7.33 ± 1.75	3.84
24	12.08 ± 1.99	0.51	16.43 ± 4.22	0.31	–	–
25	26.12 ± 4.55	0.24	27.85 ± 5.28	0.18	–	–
26	28.95 ± 5.86	0.21	30.85 ± 4.18	0.16	–	–
SU	6.22 ± 1.84	1.00	5.05 ± 1.34	1.00	12.19 ± 2.83	2.14

Table 1. Cytotoxicity of selected compounds against A549, BxPC3 and HEK293 cell lines.

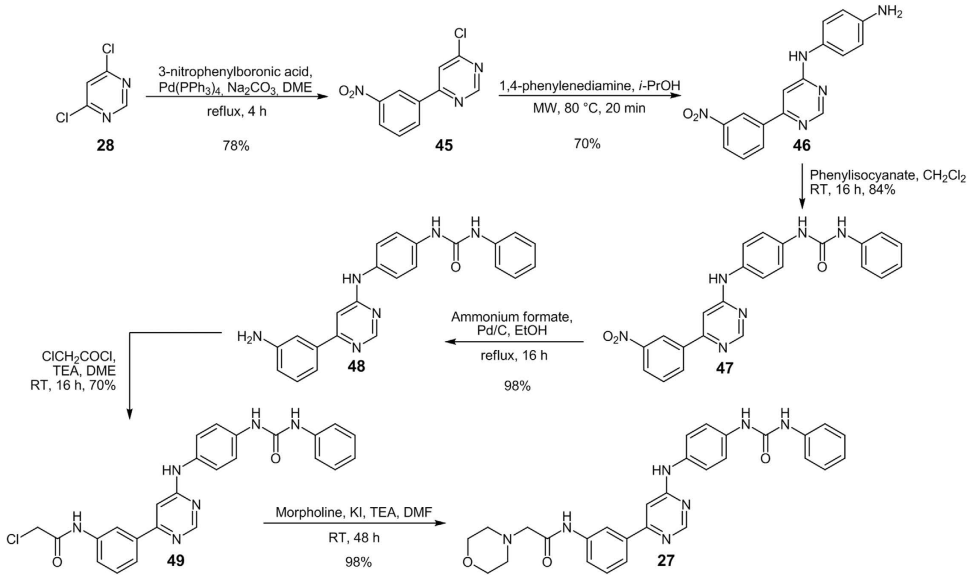

Figure 6. Synthesis of compound 27.

well as melanoma (A375), besides lung (A549) and pancreatic (BxPC3) cancer cells. IC_{50} values, calculated from the dose-survival curves obtained after 72 h of drug treatment from the MTT test, are reported in Table 2. Anilinopyrimidines **19** and **27** showed a quite similar pattern of cytotoxicity over the cancer cell lines panel. Both compounds were endowed with a cytotoxic potency higher than that of SU, eliciting IC_{50} values in the low micromolar range. Notably, IC_{50} values measured on pancreatic adenocarcinoma BxPC3 cells were in the sub-micromolar range, exceeding by a factor of 6 those detected with the reference TKI. When tested against non-cancer HEK293 cells, derivative **27** showed an antiproliferative activity even lower than that of the parental compound **19**, eliciting an average IC_{50} value of 10 μM, thus suggesting a preferential activity towards cancerous cells.

Preliminary *in vivo* evaluation of lead compound 27. Basing on *in vitro* screening, derivative **27** emerged as the most interesting compound since it was more effective than **19** against target kinases. Besides, it was as cytotoxic as **19** towards cancer cells while showing a more favorable selectivity index. On these basis, compound **27** was chosen for *in vivo* experiments against a syngeneic murine solid

Kinase profiling					
	19		27		Potency improvement
Kinase	K_d (nM)	K_{dRTK}/K_{dKIT}	K_d (nM)	K_{dRTK}/K_{dKIT}	K_d19/K_d27
CSF1R	2900	132	1100	110	2.6
KIT	22	1	10	1	2.2
FLT3	4600	209	1300	130	3.5
PDGFRα	960	44	110	11	8.7
PDGFRβ	80	4	70	7	1.1
Cytotoxicity					
	19		27		Sunitinib
	IC_{50} (μM) ± SD		IC_{50} (μM) ± SD		IC_{50} (μM) ± SD
A549	3.16 ± 1.12		3.11 ± 1.09		12.19 ± 2.83
BxPC3	0.77 ± 0.21		0.81 ± 0.32		5.05 ± 1.34
2008	1.98 ± 0.75		1.82 ± 0.73		3.52 ± 1.22
MCF-7	1.23 ± 0.89		1.55 ± 0.75		2.58 ± 0.85
A431	2.85 ± 1.03		1.96 ± 0.92		3.89 ± 1.15
LoVo	7.45 ± 1.53		7.76 ± 1.28		8.18 ± 2.67
A375	6.41 ± 2.02		5.56 ± 1.39		8.25 ± 2.88

Table 2. Activities of compounds 19 and 27 on isolated kinases and on cell viability.

tumor model, the murine Lewis Lung Carcinoma (LLC). The tumor growth inhibition induced by **27** was compared with that promoted by cisplatin (CDDP), the most common chemotherapeutic drug used in the treatment of lung cancers. Nine days after tumor inoculation, tumor-bearing mice were randomized into vehicle control and treatment groups (8 mice per group). Control mice received the vehicle ($0.2\%_{v/v}$ EtOH and $99.8\%_{v/v}$ of a saline solution), whereas treated groups received daily doses of **27** ($7.5\,mg\cdot kg^{-1}$ in the vehicle solution composed of $0.2\%_{v/v}$ EtOH and $99.8\%_{v/v}$ of saline solution) or CDDP ($1.5\,mg\cdot kg^{-1}$ in saline solution). Tumor growth was estimated at day 20 (Fig. 7a). As an indication of the adverse side effects, changes in the body weights of tumor-bearing mice were monitored at day 1 and daily from day 9. The intraperitoneal administration of **27** reduced by 84.7% the tumor mass compared to that of the control group (Fig. 7b, Table S5), promoting an *in vivo* antitumor activity even better than that exerted by CDDP which reduced the tumor mass of 71.6%.

Remarkably, even though **27** was administered at higher doses than CDDP, the time course of body weight changes indicated a more safety profile for our compound. Indeed, treatment with **27** resulted in a moderate body weight loss (<10%) whereas, as well documented, CDDP provoked elevated body weight loss (Fig. 7c).

The molecular basis for class III RTKs subfamily selectivity. To rationalize the selectivity profile showed by compounds **19** and **27**, we firstly analyzed some key residues of the ATP-pocket usually involved in the binding of TKIs (Fig. 8a).

The class III RTK members mainly differ in:

- the gatekeeper residue (threonine for CSF1R, KIT, PDGFRα and PDGFRβ; phenylalanine for FLT3). Threonine and phenylalanine don't have similar steric requirements (blocks substitution matrix, BLOSUM[50], $score_{F-T} = -2$);
- one amino acid in the DFG region sequence (cysteine for KIT, FLT3, PDGFRα and PDGFRβ; glycine for CSF1R). Cysteine and glycine don't have similar steric requirements (BLOSUM $score_{C-G} = -3$);
- the composition of the deeper part of hydrophobic pocket I, accessible only in the inactive kinase conformation (usually targeted by type II inhibitors), that was reported to account for the selectivity of certain type II kinase inhibitors[51]. Considering only the amino acids placing the side chains inside the binding pocket, the hydrophobic pockets differed only for one amino acid (leucine in KIT; methionine in the other kinases). However, leucine and methionine have similar steric requirements (BLOSUM $score_{M-L} = +2$). Remarkably, the sequences *xExxxLxxL* or *xExxxMxxL* are quite conserved in the TK family (see for example Src, Syk, ZAP70, TRKA, TIE2 and TYK2), thus the composition of the deeper part of hydrophobic pocket I could not mainly account for the overall observed selectivity of the compounds.

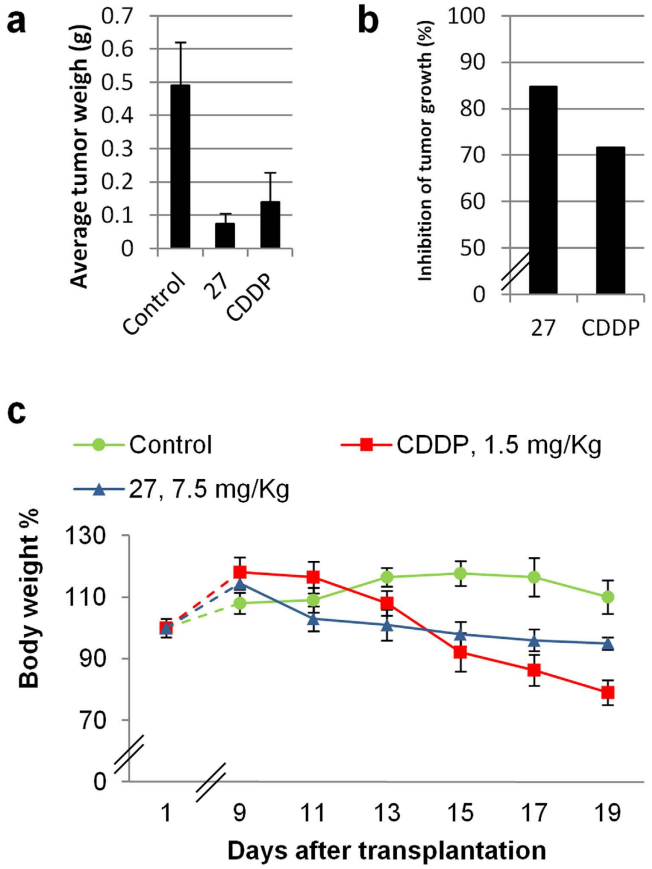

Figure 7. ***In vivo*** **testing of compound 27.** Lewis lung carcinoma (LLC) was implanted i.m. ($2 \cdot 10^6$ cells inoculum) into the right hind leg of 8-week old imbred C57BL mice. Nine days after tumor inoculation (palpable tumor), tumor-bearing mice were randomized into vehicle control and treatment groups (8 mice per group). Compound **27** was dosed daily at 7.5 mg/kg ip and CDDP was dosed daily at 1.5 mg/kg ip. At day 20, animals were sacrificed (*i.e.*, before tumor can cause the animal discomfort), the legs were amputated at the proximal end of the femur, and the inhibition of tumor growth was determined according to the difference in weight of the tumor-bearing leg and the healthy leg of the animals expressed as % referred to the control animals. Control was constituted by vehicle ($0.2\%_{v/v}$ EtOH and $99.8\%_{v/v}$ of saline solution). CDDP was used as positive reference. Both **27** and CDDP were administered at the highest not toxic doses (7.5 and 1.5 mg/kg, respectively), as determined by MTD studies. (**a**) Average tumor weight (**g**) after 20 days of treatment with control or compounds. (**b**) Percentage of reduction in tumor growth after 20 days of treatment with respect to control mice. (**c**) Body weight changes. The body weight changes of LLC bearing C57BL mice treated with vehicle or tested compounds. Each drug was administered daily after 9 days from the tumor cell inoculum. Weights were measured at day 1 and daily from day 9. Error bars indicate the standard deviation.

Since both **19** and **27** targeted preferentially KIT, PDGFRα and PDGFRβ, we supposed that the simultaneous presence of the threonine as gatekeeper and of the cysteine just before the DFG motif was fundamental. Notably, no other TKs (among the tested ones) presented these two features. Hence, we concluded that the selectivity observed for some members of the class III RTK was mainly due to the presence of the two residues.

Molecular modeling studies were then conducted on both **19** and **27** in order to propose a plausible binding mode with the class III RTK members. From among the available crystal structures, we selected 1T46 for KIT[52], 1RJB for FLT3[53] and 4HW7 for CSF1R[54]. These structures were chosen on the basis of the similarity with 4ASD (VEGFR2 kinase domain in complex with sorafenib[55]) because of the high degree of similarity of sorafenib with our compounds. Remarkably, no structure for PDGFRα and β were available in the Protein Data Bank, thus these kinases were no further considered in computational simulations. The docking experiments were conducted using the AutoDock software[56]. The importance of the gatekeeper residue suggested the presence of a water molecule mediated H-bond between the N3 of the pyrimidine and the threonine, as previously reported for the binding of quinazoline derivatives and EGFR (see for example the 1M17 PDB structure[57]). Remarkably, the supposed water molecule was not present in the 1T46 and 4HW7 protein structures. As recently reported, AutoDock software was

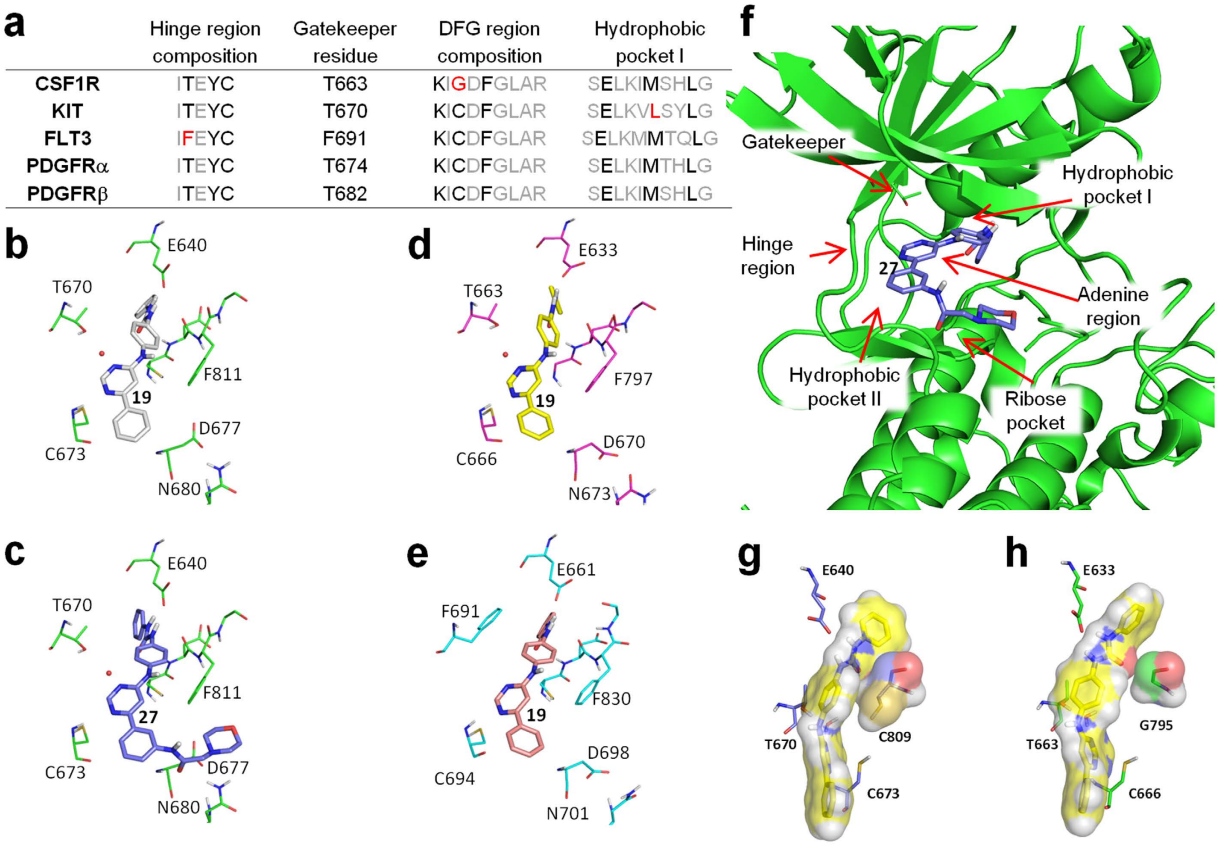

Figure 8. Binding mode study on compounds 19 and 27. (**a**) Sequences of hinge, DGF and hydrophobic pocket I regions of the ATP binding pocket for class III RTKs. Black (or red) characters indicate amino acids that place the side chain inside the ATP-pocket; grey characters indicate the amino acids that place the side chain outside the ATP-pocket. Amino acids that place the side chain inside the ATP-pocket and that differ between the five kinases are highlighted in red. The gatekeeper residue number is also reported. (**b**–**f**) Results of docking simulations: (**b**) Potential binding mode of **19** (gray stick) with KIT (green sticks); (**c**) Potential binding mode of **27** (blue stick) with KIT (green sticks); (**d**) Potential binding mode of **19** (yellow sticks) with CSF1R (pink sticks); (**e**) Potential binding mode of **19** (light pink sticks) with FLT3 (cyan sticks); (**f**) Potential binding mode of **27** (blue sticks) with KIT (green sticks and green cartoons), in context with the ATP binding site features. The 6-phenyl moiety of compound **27** is placed in the hydrophobic pocket II, whereas the hydrophilic function (*i.e.* the morpholine ring) is placed in the ribose pocket. (**g**,**h**) Details of docking simulations for compound **19** (yellow sticks) in KIT (blue sticks, panel (**g**)) and CSF1R (green sticks, panel (**h**)). Compound **19**, KIT_{C809} and $CSF1R_{G795}$ are depicted as transparent surfaces. The gatekeeper residues (KIT_{T670} and $CSF1R_{T663}$) as well as other protein residues are depicted as sticks in order to allow a better comprehension of the compound binding modes.

implemented with a specific force field with discrete displaceable waters in order to dock hydrated ligands[58]. Following this approach, water molecules were added to compounds **19** and **27** and then docked in the protein structures (Fig. 8b–e; the full details of the binding mode for **19** and **27** are reported in Figures from S5 to S8).

As supposed, a water molecule classified as "strong" by the scoring protocol[58] mediated the binding of both **19** and **27** with the threonine gatekeeper in KIT and CSF1R kinases, whereas it was displaced in FLT3. The lack of the water mediated H-bond in FLT3 was partially replaced by an edge-to-face arene-arene interaction between the aniline moiety and the F691, justifying the lower but not negligible binding. Beside the H-bonds, an additional edge-to-face arene-arene interaction was observed for the 4-anilino moiety of both **19** and **27** and the F811 of the DFG domain of KIT (centroids distance: 5.5 Å in both cases). The binding mode predicted for **27** in KIT was consistent with the initial hypothesis since the hydrophilic moiety interacted with the residues in the ribose pocket (Fig. 8f).

We also investigated the role of cysteine of the DFG domain. The KIT_{C809} (Fig. 8g) showed higher surface complementarity than the $CSF1R_{G795}$ (Fig. 8h) with the urea moiety of the ligand. Moreover, the distances between the sulfur atom of C809 and the aniline moiety suggested the formation of a

sulfur-arene interaction[59]. Furthermore, the higher steric hindrance of C809 constrained the urea moiety in a very favorable position to interact with the KIT_{E640} carboxylic function.

Discussion

Tyrosine kinases inhibitors are among the most attractive and promising anti-cancer compounds. Both selective and unselective kinase inhibitors have been approved for cancer treatment. For multi-kinase inhibitors a correct balance between specificity and non-specificity is required[20]. In this view, the discovery of compounds with subfamily selectivity is a challenging goal. The development of high-throughput screening technology to screen compounds against a number of kinases is having a high impact in the discovery of novel hit with interesting selectivity profile[60]. Due to our interest in discovering novel TKIs, we decided to explore the feasibility of obtaining novel multi-target TKIs bearing 4-anilinopyrimidine structure. Firstly we synthesized a small focused library of 26 different 4-anilinopyrimidine derivatives: the main scaffold was functionalized with different substituent at the 4-anilino moiety and at the 5 and 6 positions of the pyrimidine nucleus to determine the molecular features required for kinases inhibition. Then, the library was screened against a panel of 48 different kinases (comprising TKs, TKLs and STKs). All the compounds were inactive against STKs and TK-like enzymes. Among TKs, the compounds were able to target mainly EGFR and/or the member of the class III RTKs family (CSF1R, FLT3, KIT, PDGFRα and PDGFRβ). The substitution of the pyrimidine nucleus at 5 or 6 positions was fundamental: compounds bearing a 5-phenyl or a 6-phenyl moiety resulted totally inactive against EGFR. Conversely, almost all the 6-phenylamino compounds bound both wt-EGFR and L858R-EGFR mutant.

In the case of 6-phenylamino compounds, the 4-anilino moiety could be functionalized with small lipophilic substituents (methyl, bromo, chloro) at *meta* or *para* positions, with a slight preference for the *meta* position. The functionalization with a small *para* hydrophilic function (**5**$_{p-OH}$, **6**$_{p-NH2}$) extended the inhibitory spectrum, leading to EGFR/class III RTK/AXL inhibitors. The introduction of hydroxylic functions at both 4-anilino and 6-anilino moieties led to the wider spectrum of activity: compound **12** was able to target also TRKA and JAK3. Besides, compound **12** retained a low but not negligible activity also against the T790M mutant of EGFR. When the 4-aniline was functionalized with a *para*-phenylurea moiety, we obtained a selective class III RTKs inhibitor (**7**). Compound **7** probably was a type II inhibitor, thus requiring an inactive kinase conformation. However, EGFR is known to adopt a Src-like inactive conformation[61], which substantially differs from the KIT inactive conformation[52]: the DFG domain of inactive EGFR still remains close to the ATP binding pocket, thus limiting the dimension of the hydrophobic pocket I and impairing the binding with compound **7**. Conversely, inactive KIT adopt a true DFG-out conformation with a larger hydrophobic pocket I.

Remarkably, all the compounds bearing the *para*-phenylurea moiety (**7**, **19** and **26**) were selectively active against the class III RTK members. In this case, the substitution at 5 or 6 positions of the pyrimidine ring conferred selectivity inside the family: 5-phenyl compound (**26**) inhibited all the class III RTK members with comparable potencies; 6-phenyl compound (**19**) was a selective dual KIT/PDGFRβ inhibitor; 6-phenylamino compound (**7**) showed an intermediate selectivity degree between **19** and **26**.

Compounds active against at least one of the main target kinases (EGFR and/or class III RTKs) were screened for their cytotoxic potential against lung and pancreatic cancer cell lines. Many of the studied compounds showed a marked *in vitro* antitumor activity, with IC_{50} values in the micromolar range. However, only **7** and **19** showed lower average IC_{50} values than the reference multi TKI, sunitinib. In addition, when tested against non-tumor cells in rapid proliferation, only compound **19** showed a preferential antiproliferative activity toward neoplastic cells.

Dissociation constant determinations confirmed that compound **19** was a selective dual KIT/PDGFRβ inhibitor with nanomolar affinity. The structure of this *hit compound* was further modified in order to improve the pharmacodynamic properties. Hence, compound **27** (designed to interact also with the sugar pocket of the target kinases) showed overall lower Kd values against class III RTK members than **19**, resulting a multi KIT/PDGFRα/PDGFRβ inhibitor with nanomolar affinity (Kd against CSF1R and FLT3 were higher than 1 μM).

Tested against a wide panel of cancer cell lines, including examples of breast, ovarian cancers along with melanoma, compounds **19** and **27** showed a comparable activity profile and were more effective than sunitinib in inhibiting cancer cell proliferation. Remarkably, compound **27** was more selective against cancer cells than the hit compound **19**. Very preliminary *in vivo* studies were also conducted on compound **27**. On LLC murine model of solid tumor, compound **27** promoted a reduction of tumor mass higher than CDDP, the most widely used drug in the management of lung neoplasms, coupling with a reduced host weight loss. Based on these promising results, we are now planning pharmacokinetic studies on compound **27** in order to determine its effective anti-cancer.

Molecular modeling studies were conducted on compounds **19** and **27** to investigate the molecular basis for the class III RTKs subfamily selectivity. The threonine as gatekeeper and the presence of a cysteine residue in the DFG domain played a key role in determining the selectivity profile. On the contrary, the hydrophobic pocket I composition was not fundamental for the selectivity profile. These findings suggest that in the design of "selectively unselective" TKIs the gatekeeper and the DFG domain compositions must be strongly considered. In particular, the presence of sulfur-arene interactions (for CDFG containing kinases) and the role of water mediated hydrogen bonds (for threonine gatekeeper containing kinases) may play critical roles. Furthermore, as supposed, docking studies suggested that

the 6-phenyl moiety of compound **27** interacted with both the hydrophobic pocket II and with the sugar pocket of the kinases.

Overall, our data suggested that the *N*-phenyl-*N'*-[4-(6-phenylpyrimidin-4-ylamino)phenyl]urea derivatives constitute a promising class of subfamily selective inhibitors of class III RTKs deserving further development.

Methods

Computational Methodologies. All the computational studies were carried out on a 4 CPU (Intel Core2 Quad CPU Q9550, 2.83 GHz) ACPI ×64 Linux workstation with Ubuntu 12.04 operating system. The tridimensional structure of the kinases were downloaded from Protein Data Bank (PDB ID: 4HW7 for CSF1R in complex with PLX647-OME; 1T46 for KIT in complex with imatinib; 1RJB for FLT3). The structures were superimposed using the UCSF Chimera software[62] and the ligands, the ions and the water molecules were removed. The structure of compounds **19** and **27** were prepared with MarvinSketch 5.5.0.1 software (www.chemaxon.com/products). The lowest energy conformations and the degree of protonation at pH 7.4 were determined with OpenBabel software[63] using the MMFF94s force field. For all the molecules, the appropriate ".pdbqt" files were prepared with the AutoDockTools graphical interface of AutoDock 4 software[56]. Before docking simulations, the ".pdbqt" file of compounds **19** and **27** were solvated using the appropriate python script[33] (more details are reported in Supplementary Information). All the docking studies have been performed with AutoDock4 using a docking box of $52 \times 70 \times 40$ Å dimensions (centered on PLX647-OME coordinates) and 0.375 grid spacing. Each docking run consisted of 50 independent searches with a maximum of 2,500,000 energy evaluations based on Lamarkian Genetic Algorithm searching engine. For each pair kinase/ligand the lowest energy pose was retained.

Experiments with Cultured Human Cells. All compounds, except derivative **27**, were dissolved in DMSO just before the experiment, and a calculated amount of drug solution was added to the cell growth medium to a final solvent concentration of 0.5%, which had no discernible effect on cell killing. Compound **27** was dissolved in a 0.9% NaCl solution just before the experiment.

Sunitinib malate and MTT (3-(4,5-dimethylthiazol-2-yl)-2,5-diphenyltetrazolium bromide) were obtained from Sigma Chemical Co, St.Louis, USA. Antibody for β-actin and ubiquitin were from Santa Cruz Biotechnology (Santa Cruz Biotechnology Inc., Santa Cruz, CA, USA).

Cell cultures. Human lung (A549), breast (MCF-7), pancreas (BxPC3), and colon (LoVo) carcinoma cell lines along with melanoma (A375) were obtained from American Type Culture Collection (ATCC, Rockville, MD). Human non-tumor embryonic kidney HEK293 cells were obtained from European Collection of Cell Cultures (ECACC, Salisbury, UK). Human cervical carcinoma A431cells were kindly provided by Prof. F. Zunino (Division of Experimental Oncology B, Istituto Nazionale dei Tumori, Milan, Italy). Human ovarian cancer 2008 cells were kindly provided by Prof. G. Marverti (Dept. of Biomedical Science of Modena University, Italy). Cell lines were maintained in the logarithmic phase at 37 °C in a 5% carbon dioxide atmosphere using the following culture media containing 10% fetal calf serum (Euroclone, Milan, Italy), antibiotics (50 units $\cdot$ mL^{-1} penicillin and 50 μg $\cdot$ mL^{-1} streptomycin) and 2 mM l-glutamine: i) RPMI-1640 medium (Euroclone) for MCF-7, A431, BxPC3 and 2008 cells; ii) F-12 HAM'S (Sigma Chemical Co.) for A549 and LoVo cells; iii) D-MEM medium (Euroclone) for HEK293 cells.

Cytotoxicity MTT assay. The growth inhibitory effect towards human cell lines was evaluated by means of MTT (tetrazolium salt reduction) assay. Briefly, $3–8 \cdot 10^3$ cells/well, dependent upon the growth characteristics of the cell line, were seeded in 96-well microplates in growth medium (100 μL) and then incubated at 37 °C in a 5% carbon dioxide atmosphere. After 24 h, the medium was removed and replaced with a fresh one containing the test compound at the appropriate concentration. Triplicate cultures were established for each treatment. After 72 h, each well was treated with 10 μL of a 5 mg $\cdot$ mL-1 MTT (3-(4,5-dimethylthiazol-2-yl)-2,5-diphenyltetrazolium bromide) saline solution, and after 5 h additional incubation, 100 μL of a sodium dodecylsulfate (SDS) solution in HCl 0.01 M were added. After overnight incubation, the inhibition of cell growth induced by the tested complexes was detected by measuring the absorbance of each well at 570 nm using a Bio-Rad 680 microplate reader (Bio-Rad, Hercules, CA). Mean absorbance for each drug dose was expressed as a percentage of the control untreated well absorbance and plotted *vs* drug concentration. IC_{50} values represent the drug concentrations that reduced the mean absorbance at 570 nm to 50% of those in the untreated control wells.

***In vivo* anticancer activity toward Lewis Lung Carcinoma (LLC).** All studies involving animal testing were carried out in accordance with the ethical guidelines for animal research adopted by the University of Padua, acknowledging the Italian regulation (D.L.G.S. 116/92) and European Directive 86/609/EEC as to the animal welfare and protection and the related codes of practice. The experimental protocol was approved by the Italian Health Department according to the art. 7 of above mentioned D.L.G.S. 116/92. The mice were purchased from Charles River, Italy, housed in steel cages under controlled environmental conditions (constant temperature, humidity, and 12 h dark/light cycle), and alimented with commercial standard feed and tap water ad libitum. The LLC cell line was purchased from ECACC, United Kingdom. The LLC cell line was maintained in DMEM (Euroclone) supplemented with

10% heat inactivated fetal bovine serum (Euroclone), 10 mM L-glutamine, 100 U mL^{-1} penicillin, and 100 $\mu g \cdot mL^{-1}$ streptomycin in a 5% CO_2 air incubator at 37 °C. The LLC was implanted intramuscularly (i.m.) as a 2×10^6 cell inoculum into the right hind leg of 8 week old male and female C57BL mice (24 ± 3 g body weight). After 9 days from tumor implantation (palpable tumor), mice were randomly divided into 3 groups (8 animals per group) and subjected to daily i.p. administration of **27** ($7.5\ mg \cdot kg^{-1}$ dissolved in a vehicle solution composed of 0.2%$_{v/v}$ EtOH and 99.8%$_{v/v}$ of saline solution), cisplatin ($1.5\ mg \cdot kg^{-1}$ in saline solution), or the vehicle solution (0.2%$_{v/v}$ EtOH and 99.8%$_{v/v}$ of saline solution). At day 20, animals were sacrificed, the legs were amputated at the proximal end of the femur, and the inhibition of tumor growth was determined according to the difference in weight of the tumor-bearing leg and the healthy leg of the animals expressed as a percentage referring to the control animals. Body weight was daily measured and was taken as a parameter for systemic toxicity. All reported values are the means ± SD of no less than three measurements. Multiple comparisons were made by the Tukey−Kramer test (**$p < 0.01$; *or °$p < 0.05$).

Statistical analysis. All the values are the means ± S.D. of not less than three measurements. Multiple comparisons were made by ANOVA followed by Tukey–Kramer multiple comparison test, using GraphPad Software.

References

1. Robinson, D. R., Wu, Y. M. & Lin, S. F. The protein tyrosine kinase family of the human genome. *Oncogene* **19,** 5548–5557 (2000).
2. Manning, G., Whyte, D. B., Martinez, R., Hunter, T. & Sudarsanam, S. The protein kinase complement of the human genome. *Science* **298,** 1912–1934 (2002).
3. Duong-Ly, K. C. & Peterson, J. R. The Human Kinome and Kinase Inhibition in *Current Protocols in Pharmacology*. (John Wiley & Sons, Inc., 2001).
4. Paul, M. K. & Mukhopadhyay, A. K. Tyrosine kinase - Role and significance in Cancer. *Int J Med Sci* **1,** 101–115 (2004).
5. Cohen, P. Protein kinases–the major drug targets of the twenty-first century? *Nat Rev Drug Discov* **1,** 309–315 (2002).
6. Bublil, E. M. & Yarden, Y. The EGF receptor family: spearheading a merger of signaling and therapeutics. *Curr Opin Cell Biol* **19,** 124–134 (2007).
7. Williams, L. T. Signal transduction by the platelet-derived growth factor receptor. *Science* **243,** 1564–1570 (1989).
8. Normanno, N. *et al.* Epidermal growth factor receptor (EGFR) signaling in cancer. *Gene* **366,** 2–16 (2006).
9. da Cunha Santos, G., Shepherd, F. A. & Tsao, M. S. EGFR mutations and lung cancer. *Annu Rev Pathol* **6,** 49–69 (2011).
10. Stirewalt, D. L. & Radich, J. P. The role of FLT3 in haematopoietic malignancies. *Nat Rev Cancer* **3,** 650–665 (2003).
11. Kampa-Schittenhelm, K. M. *et al.* Quizartinib (AC220) is a potent second generation class III tyrosine kinase inhibitor that displays a distinct inhibition profile against mutant-FLT3, -PDGFRA and -KIT isoforms. *Mol Cancer* **12,** 19 (2013).
12. Micke, P. *et al.* Characterization of c-kit expression in small cell lung cancer: prognostic and therapeutic implications. *Clin Cancer Res* **9,** 188–194 (2003).
13. Esposito, I. *et al.* The stem cell factor-c-kit system and mast cells in human pancreatic cancer. *Lab Invest* **82,** 1481–1492 (2002).
14. Kimura, W. *et al.* Analysis of c-kit protein expression in pancreatic neoplasms and its implication for prognosis. *Hepatogastroenterology* **54,** 2203–2208 (2007).
15. Zhang, J., Yang, P. L. & Gray, N. S. Targeting cancer with small molecule kinase inhibitors. *Nat Rev Cancer* **9,** 28–39 (2009).
16. Hojjat-Farsangi, M. Small-molecule inhibitors of the receptor tyrosine kinases: promising tools for targeted cancer therapies. *Int J Mol Sci* **15,** 13768–13801 (2014).
17. Lamba, V. & Ghosh, I. New directions in targeting protein kinases: focusing upon true allosteric and bivalent inhibitors. *Curr Pharm Des* **18,** 2936–2945 (2012).
18. Petrelli, A. & Giordano, S. From single- to multi-target drugs in cancer therapy: when aspecificity becomes an advantage. *Curr Med Chem* **15,** 422–432 (2008).
19. Broekman, F., Giovannetti, E. & Peters, G. J. Tyrosine kinase inhibitors: Multi-targeted or single-targeted? *World J Clin Oncol* **2,** 80–93 (2011).
20. Morphy, R. Selectively nonselective kinase inhibition: striking the right balance. *J Med Chem* **53,** 1413–1437 (2010).
21. Wang kentin, A. A. *et al.* Overcoming myelosuppression due to synthetic lethal toxicity for FLT3-targeted acute myeloid leukemia therapy. *Elife* **3** (2014), doi: 10.7554/eLife.03445.
22. Liu, Y. & Gray, N. S. Rational design of inhibitors that bind to inactive kinase conformations. *Nat Chem Biol* **2,** 358–364 (2006).
23. Zhang, Q. *et al.* Discovery of EGFR selective 4,6-disubstituted pyrimidines from a combinatorial kinase-directed heterocycle library. *J Am Chem Soc* **128,** 2182–2183 (2006).
24. Nemeth, G. *et al.* Synthesis and evaluation of phosphorus containing, specific CDK9/CycT1 inhibitors. *J Med Chem* **57,** 3939–3965 (2014).
25. Capdeville, R., Buchdunger, E., Zimmermann, J. & Matter, A. Glivec (STI571, imatinib), a rationally developed, targeted anticancer drug. *Nat Rev Drug Discov* **1,** 493–502 (2002).
26. Kantarjian, H., Jabbour, E., Grimley, J. & Kirkpatrick, P. Dasatinib. *Nat Rev Drug Discov* **5,** 717–718 (2006).
27. Siemeister, G. *et al.* BAY 1000394, a novel cyclin-dependent kinase inhibitor, with potent antitumor activity in mono- and in combination treatment upon oral application. *Mol Cancer Ther* **11,** 2265–2273 (2012).
28. Caporali, S. *et al.* The cyclin-dependent kinase inhibitor PHA-848125 suppresses the *in vitro* growth of human melanomas sensitive or resistant to temozolomide, and shows synergistic effects in combination with this triazene compound. *Pharmacol Res* **61,** 437–448 (2010).
29. Getlik, M. *et al.* Hybrid compound design to overcome the gatekeeper T338M mutation in cSrc. *J Med Chem* **52,** 3915–3926 (2009).
30. Marzaro, G., Guiotto, A. & Chilin, A. Quinazoline derivatives as potential anticancer agents: a patent review (2007-2010). *Expert Opin Ther Pat* **22,** 223–252 (2012).
31. Li, J. *et al.* Gefitinib ('Iressa', ZD1839), a selective epidermal growth factor receptor tyrosine kinase inhibitor, inhibits pancreatic cancer cell growth, invasion, and colony formation. *Int J Oncol* **25,** 203–210 (2004).
32. Medina, P. J. & Goodin, S. Lapatinib: a dual inhibitor of human epidermal growth factor receptor tyrosine kinases. *Clin Ther* **30,** 1426–1447 (2008).
33. Yoshikawa, D. *et al.* Vandetanib (ZD6474), an inhibitor of VEGFR and EGFR signalling, as a novel molecular-targeted therapy against cholangiocarcinoma. *Br J Cancer* **100,** 1257–1266 (2009).

34. Conconi, M. T. *et al.* Quinazoline-based multi-tyrosine kinase inhibitors: synthesis, modeling, antitumor and antiangiogenic properties. *Eur J Med Chem* **67,** 373–383 (2013).
35. Marzaro, G. *et al.* Discovery of biarylaminoquinazolines as novel tubulin polymerization inhibitors. *J Med Chem* **57,** 4598–4605 (2014).
36. Wang, Z. *et al.* Structural basis of inhibitor selectivity in MAP kinases. *Structure* **6,** 1117–1128 (1998).
37. Schindler, T. *et al.* Crystal structure of Hck in complex with a Src family-selective tyrosine kinase inhibitor. *Mol Cell* **3,** 639–648 (1999).
38. Liao, J. J. Molecular recognition of protein kinase binding pockets for design of potent and selective kinase inhibitors. *J Med Chem* **50,** 409–424 (2007).
39. Fry, D. W. *et al.* A specific inhibitor of the epidermal growth factor receptor tyrosine kinase. *Science* **265,** 1093–1095 (1994).
40. Hennequin, L. F. *et al.* Design and structure-activity relationship of a new class of potent VEGF receptor tyrosine kinase inhibitors. *J Med Chem* **42,** 5369–5389 (1999).
41. Sudbeck, E. A. *et al.* Structure-based design of specific inhibitors of Janus kinase 3 as apoptosis-inducing antileukemic agents. *Clin Cancer Res* **5,** 1569–1582 (1999).
42. Grosjean, S., Triki, S., Meslin, J.-C., Julienne, K. & Deniaud, D. Synthesis of nitrogen bicyclic scaffolds: pyrimido[1,2-a] pyrimidine-2,6-diones. *Tetrahedron* **66,** 9912–9924 (2010).
43. Beattie, J. F. *et al.* Cyclin-dependent kinase 4 inhibitors as a treatment for cancer. Part 1: identification and optimisation of substituted 4,6-Bis anilino pyrimidines. *Bioorganic & Medicinal Chemistry Letters* **13,** 2955–2960 (2003).
44. Karaman, M. W. *et al.* A quantitative analysis of kinase inhibitor selectivity. *Nat Biotechnol* **26,** 127–132 (2008).
45. Sutto, L. & Gervasio, F. L. Effects of oncogenic mutations on the conformational free-energy landscape of EGFR kinase. *Proceedings of the National Academy of Sciences of the United States of America* **110,** 10616–10621 (2013).
46. Diaz, R. *et al.* Antitumor and antiangiogenic effect of the dual EGFR and HER-2 tyrosine kinase inhibitor lapatinib in a lung cancer model. *BMC Cancer* **10,** 188 (2010).
47. Chung, H. W. *et al.* Radiosensitization effect of STI-571 on pancreatic cancer cells *in vitro*. *Int J Radiat Oncol Biol Phys* **75,** 862–869 (2009).
48. Ali, S., El-Rayes, B. F., Sarkar, F. H. & Philip, P. A. Simultaneous targeting of the epidermal growth factor receptor and cyclooxygenase-2 pathways for pancreatic cancer therapy. *Mol Cancer Ther* **4,** 1943–1951 (2005).
49. Goodman, V. L. *et al.* Approval summary: sunitinib for the treatment of imatinib refractory or intolerant gastrointestinal stromal tumors and advanced renal cell carcinoma. *Clin Cancer Res* **13,** 1367–1373 (2007).
50. Henikoff, S. & Henikoff, J. G. Amino acid substitution matrices from protein blocks. *Proc Natl Acad Sci USA* **89,** 10915–10919 (1992).
51. Zhao, Z. *et al.* Exploration of type II binding mode: A privileged approach for kinase inhibitor focused drug discovery? *ACS Chem Biol* **9,** 1230–1241 (2014).
52. Mol, C. D. *et al.* Structural basis for the autoinhibition and STI-571 inhibition of c-Kit tyrosine kinase. *J Biol Chem* **279,** 31655–31663 (2004).
53. Griffith, J. *et al.* The structural basis for autoinhibition of FLT3 by the juxtamembrane domain. *Mol Cell* **13,** 169–178 (2004).
54. Zhang, C. *et al.* Design and pharmacology of a highly specific dual FMS and KIT kinase inhibitor. *Proc Natl Acad Sci USA* **110,** 5689–5694 (2013).
55. McTigue, M. *et al.* Molecular conformations, interactions, and properties associated with drug efficiency and clinical performance among VEGFR TK inhibitors. *Proc Natl Acad Sci USA* **109,** 18281–18289 (2012).
56. Morris, G. M. *et al.* AutoDock4 and AutoDockTools4: Automated docking with selective receptor flexibility. *J Comput Chem* **30,** 2785–2791 (2009).
57. Stamos, J., Sliwkowski, M. X. & Eigenbrot, C. Structure of the epidermal growth factor receptor kinase domain alone and in complex with a 4-anilinoquinazoline inhibitor. *J Biol Chem* **277,** 46265–46272 (2002).
58. Forli, S. & Olson, A. J. A force field with discrete displaceable waters and desolvation entropy for hydrated ligand docking. *J Med Chem* **55,** 623–638 (2012).
59. Cordomi, A., Gomez-Tamayo, J. C., Gigoux, V. & Fourmy, D. Sulfur-containing amino acids in 7TMRs: molecular gears for pharmacology and function. *Trends Pharmacol Sci* **34,** 320–331 (2013).
60. Ma, H., Deacon, S. & Horiuchi, K. The challenge of selecting protein kinase assays for lead discovery optimization. *Expert Opin Drug Discov* **3,** 607–621 (2008).
61. Zhang, X., Gureasko, J., Shen, K., Cole, P. A. & Kuriyan, J. An allosteric mechanism for activation of the kinase domain of epidermal growth factor receptor. *Cell* **125,** 1137–1149 (2006).
62. Pettersen, E. F. *et al.* UCSF Chimera--a visualization system for exploratory research and analysis. *J Comput Chem* **25,** 1605–1612 (2004).
63. O'Boyle, N. M. *et al.* Open Babel: An open chemical toolbox. *J Cheminform* **3,** 33 (2011).

Acknowledgements

The present work has been carried out with the financial support of the University of Padova 'Progetto Giovani Studiosi 2012' to G.M. A.F. thanks financial supports from the University of Padova for a PhD student grant. M.D.V. thanks the Fondazione Cariparo for a PhD student grant.

Author Contributions

V.G. and G.M. designed the study. V.G., A.C. and G.M. wrote the paper. V.G. and C.M. conducted the *in vitro* experiments. V.G. conducted the *in vivo* experiments. A.F., M.D.V., A.C. and G.M. synthesized the compounds. G.M. performed the computational studies. All the authors revised the manuscript.

Additional Information

Supplementary information accompanies this paper at http://www.nature.com/srep

Competing financial interests: The authors declare no competing financial interests.

How to cite this article: Gandin, V. *et al.* Targeting kinases with anilinopyrimidines: discovery of *N*-phenyl-*N*′-[4-(pyrimidin-4-ylamino)phenyl]urea derivatives as selective inhibitors of class III receptor tyrosine kinase subfamily. *Sci. Rep.* **5**, 16750; doi: 10.1038/srep16750 (2015).